INFORMATION TO USERS

This manuscript has been reproduced from the microfilm master. UMI films the text directly from the original or copy submitted. Thus, some thesis and dissertation copies are in typewriter face, while others may be from any type of computer printer.

The quality of this reproduction is dependent upon the quality of the copy submitted. Broken or indistinct print, colored or poor quality illustrations and photographs, print bleedthrough, substandard margins, and improper alignment can adversely affect reproduction.

In the unlikely event that the author did not send UMI a complete manuscript and there are missing pages, these will be noted. Also, if unauthorized copyright material had to be removed, a note will indicate the deletion.

Oversize materials (e.g., maps, drawings, charts) are reproduced by sectioning the original, beginning at the upper left-hand corner and continuing from left to right in equal sections with small overlaps. Each original is also photographed in one exposure and is included in reduced form at the back of the book.

Photographs included in the original manuscript have been reproduced xerographically in this copy. Higher quality 6" x 9" black and white photographic prints are available for any photographs or illustrations appearing in this copy for an additional charge. Contact UMI directly to order.

UMI®

Bell & Howell Information and Learning
300 North Zeeb Road, Ann Arbor, MI 48106-1346 USA
800-521-0600

Design and Energy Analysis of a Hybrid Electric Natural Gas Vehicle

Achilles Nikopoulos

A Thesis

in

The Department

of

Mechanical Engineering

Presented in Partial Fulfilment of the Requirements
for the Degree of Master of Applied Science at
Concordia University
Montreal, Quebec, Canada

April 1997

National Library
of Canada

Acquisitions and
Bibliographic Services

395 Wellington Street
Ottawa ON K1A 0N4
Canada

Bibliothèque nationale
du Canada

Acquisitions et
services bibliographiques

395, rue Wellington
Ottawa ON K1A 0N4
Canada

Your file Votre référence

Our file Notre référence

0-612-40218-5

Canada

ABSTRACT

Design and Energy Analysis
of a
Hybrid Electric Natural Gas Vehicle

Achilles Nikopoulos

The main goals of this thesis research were to provide a simple concept and to simulate the energy requirements of a hybrid electric vehicle, i.e. to design a very efficient power assist hybrid electric natural gas vehicle without compromising the vehicle space, weight, and comforts. It is recognized that HEV's represent new areas of research, where demonstration projects are also required to find out which modes of energy conversion would best suit the society.

A simple simulation procedure is introduced that is practical, can be used as an initial analytical approach for hybrid vehicle energy analysis, and can be easily validated. Two scenarios consisting of a 0-60-0 km/h and a 0-100-0 km/h cycle were established to demonstrate the highway and city mode driving situations. The energy efficiency and equivalent fuel consumption were determined for the specific hybrid powertrains. A comparison with established SAE drive cycles was effected to illustrate the feasibility of the proposed simulation processes. The hybrid powertrain is ideal for short commuting in the city where the use of the electric motor is advantageous, with a fuel economy that can range from 4.04 *l*/100

km to 2.90 l/100 km (58-81 mpg_{US}). The engine provides the means to extend vehicle range for inter-city or highway driving requirements.

By introducing a new AC induction electric drive system with energy recuperation capabilities, the vehicle performance and fuel economy can be improved and sustained for longer periods. With this modified powertrain, there is about a 29% improvement in energy efficiency over the current hybrid powertrain. The use of energy regeneration and its effect on vehicle braking and battery charging was also discussed.

A power assist hybrid electric natural gas vehicle is a feasible solution for commuting within a polluted city environment. An effective design requires that the hybrid powertrain is matched well for all vehicle speed ranges in terms of performance and fuel economy.

ACKNOWLEDGMENT

The author is deeply indebted to Dr. T. Krepec and Dr. H. Hong, his two supervisors, for their invaluable support, guidance and understanding throughout the course of this work.

Furthermore, the author greatly appreciates the support of his colleagues and friends. Special thanks are extended to the colleagues, throughout the years, at the Concordia University Fuel Control Laboratory.

The author also wishes to express his gratitude to Luciano Martin and Angela Vogas for additional editing and to Peter Kremmydiotis for his computer graphics assistance.

Most of all, the author expresses the deepest gratitude to his father Kostas, mother Helen, and brother Dimitrios Nikopoulos, for their encouragement and understanding throughout the course of this work.

The author also thanks, Chrysler Corporation, the U.S. Department of Energy, Natural Resources Canada, and the Natural Sciences and Engineering Research Council of Canada for the project sponsorship and their financial support.

TABLE OF CONTENTS

Page

LIST OF FIGURES

LIST OF TABLES

NOMENCLATURE

A	-	Distance from vehicle center of gravity to rear wheel, m
A_f	-	Frontal area, m^2
a	-	Vehicle deceleration, m/s^2
b_e	-	Engine specific fuel consumption approximation
C_d	-	Coefficient of drag
$C(i)$	-	Mass factor constant, i=1,..,5
E_{bat}	-	Energy available from the battery, kWh
EN_{ICE}	-	Energy consumed by intenal combustion engine, kJ
EN_{MOT}	-	Energy consumed by electric motor, kJ
Eng_{TRQ}	-	Torque developed at the engine, Nm
F_{aero}	-	Aerodynamic drag force, N
F_{cl}	-	Inclination force, N
F_{mdw}	-	Motive force available at the drive wheels, N
F_{mdwMAX}	-	Maximum motive force due to road adhesion limitation, N
F_{ro}	-	Rolling resistance force, N
F_{tot}	-	Total resistive force, N
$F_{tractive}$	-	Available force surplus, N
FS	-	Battery box safety factor
FS_{sf}	-	Shear stress safety factor on battery box bolts
g	-	Gravitational acceleration, m/s^2
H_{CG}	-	Height of the center of gravity, m
I	-	Battery discharge current, A
I_{max}	-	Peak current, A
L	-	Wheel base length, m
M_{eff}	-	Effective vehicle mass, kg

M_{fuel}	-	Mass of fuel, kg
$Melec_{TRQ}$	-	Torque produced by electric motor on transmission driveshaft, Nm
$Motor_{TRQ}$	-	Torque developed by the electric motor, Nm
m_{tray}	-	Mass of one battery box including the batteries, kg
m_V	-	Vehicle mass, kg
N_f	-	Differential ratio
$N_{gf\,(i)}$	-	Overall drive ratio, $N_i N_f$
N_i	-	Transmission gear ratio, i=1,..,5
N_n	-	Electric drive reduction ratio
N_{na}	-	Motor drive sprocket size; driving, 29 tooth
N_{nb}	-	Motor drive sprocket size; driven, 17 tooth
N_s	-	Electric drive ratio, $1/N_n = N_{nb} / N_{na}$
P_{bat}	-	Power available from the battery, kW
P_{ICE}	-	Power output from the internal combustion engine, kW
P_{req}	-	Desired battery power, kW
Q_{LHV}	-	Natural gas lower heating value, MJ/kg
r	-	Wheel radius, m
sfc	-	Engine specific fuel consumption, g/kWh
t	-	Time required to accelerate vehicle, s
t_W	-	Aluminum angle wall thickness, cm
V_{DOD}	-	Battery voltage at an 80 % depth of discharge, V
V_{fuel}	-	Volume of fuel, m^3 @ 20.7 MPa, 21° C
V_{HEV}	-	Vehicle velocity, m/s
V_{nom}	-	Nominal battery voltage, V
V_W	-	Wind velocity, m/s
Wh_{TRQ}	-	Drive torque developed at the wheels, Nm

GREEK SYMBOLS

η_e	-	Electric motor and controller efficiency
η_m	-	Mechanical drivetrain efficiency
θ	-	Angle of road inclination, degrees
μ_{ro}	-	Coefficient of rolling resistance
μ_{st}	-	Coefficient of road adhesion
μ_{cst}	-	Constant for the coefficient of rolling resistance
ρ_{Air}	-	The density of air, kg/m^3
ρ_{NG}	-	The density of natural gas, kg/m^3
σ_B	-	Bearing stress of aluminum angle, MPa
τ	-	Shear stress on battery box bolts, MPa
ω_e	-	Electric motor speed, rad/s

ABBREVIATIONS

APU	-	Alternate or Auxiliary Power Unit
CARB	-	California Air Resources Board
CNG	-	Compressed Natural Gas
DOD	-	Depth of Discharge
EV	-	Electric Vehicle
GV	-	Gasoline Vehicle
HEV	-	Hybrid Electric Vehicle
ICE	-	Internal Combustion Engine
NHEV	-	Neon Hybrid Electric Vehicle
PNGV	-	Partnership for a New Generation of Vehicles
SOC	-	State of Charge
ULEV	-	Ultra-low Emissions Vehicle
ZEV	-	Zero Emissions Vehicle

1. INTRODUCTION

Society's concern with energy conservation and pollution caused by vehicles, has accelerated the research for cleaner and more efficient powerplants. In some parts of the United States, government legislations have placed the automotive industry in a precarious position, by mandating the requirement for selling some percentage of zero emission vehicles (ZEV) by the end of this decade [1]*.

Research for vehicles on alternative fuels has been going on for decades, but the low range of operation on natural gas and electricity and the prohibitive cost of some of the key components, made the mass-production of such vehicles difficult. Thus, student design competitions sponsored by United States and Canadian government agencies, along with the three major automotive manufacturers (Ford, GM, Chrysler) have been geared to demonstrate the feasibility of incorporating present-day technology into existing vehicle platforms in order to produce less-polluting and more fuel efficient vehicles.

Even though electric vehicles address the zero emission requirement, their cost versus performance ratio is still relatively high as compared to the gasoline powered vehicles that are now readily available. As a mid-step solution, the combination of an electric drive with a smaller and more efficient engine is more promising than a pure electric design. Hybrid electric vehicles (HEVs) are thus

---

* Numbers in brackets designate references located at the end of this Thesis

seen as the stepping stone to electric vehicles. It is believed that the introduction of HEVs to the marketplace will help to familiarize the consumer with this new technology and will help to reduce pollution in populous city centers. In areas where electric energy is generated from "clean sources," like hydro-power and nuclear power plants, overall pollutant emissions are negligible. However, while an electric car itself does not produce any emissions, fossil fuel plants that are used to generate electricity, emit pollutants. Using pollution regulated power plants to generate electricity significantly reduces overall emission output; thus, if overall air-quality and power generation derived pollution is taken into account, it has been suggested that "...natural gas HEVs can be considered to be equivalent to electric 'ZEVs' if (for example) California's power mix is used " [2].

Compressed natural gas (CNG) has, already for a long time, demonstrated the potential of being a better fuel than liquid hydrocarbons, i.e. providing less polluting emissions and improved fuel economy. Many vehicles and industrial power plants have already been adapted and optimized to operate with CNG or liquefied natural gas (LNG). To further advance the development of CNG hybrids, the California Air Resources Board (CARB) has proposed regulations that would permit low emitting hybrid vehicles to receive full-credit as electric vehicles and, consequently, could be known as EZEVs, (equivalent-zero-emission vehicles) [2]. On the economic scale, natural gas is an inexpensive and abundant fuel that is readily available in North America with a fuel distribution infrastructure that has

already been developed in many areas of Canada and the USA.

The hybrid electric design allows the flexibility in the choice of various power units and drive configurations that would otherwise not be used in dedicated electric vehicles. The different types of HEV designs can be grouped into two distinct categories: charge-sustaining or charge-depleting vehicles.

i) A charge sustaining design uses a small internal combustion engine coupled with an electric generator to maintain the battery charge so as to have the possibility of continuously using the electric drive. A dedicated control scheme permits the engine to operate within its low fuel consumption limits and only when the battery state of charge drops below a specific charge level which is pre-determined by the vehicle manufacturer.

ii) A charge-depleting design does not allow for recharging of the battery while the vehicle is in motion. In this case a small low emission auxiliary power unit (APU) is used to supplement the driving capabilities of the electric motor. The APU is managed by a control strategy that provides the most optimum and efficient combination of each of the two powerplants. Batteries can be recharged by regenerative braking that can be implemented as part of the electric drive design. The batteries can be fully recharged from an electrical outlet when the vehicle is stationary.

A hybrid electric vehicle is used differently in "stop and go" traffic, as compared to the constant driving conditions encountered during highway driving.

Considering that pollution problems are abundant within the city center, a HEV design that caters to these concerns is of utmost importance. It is also required that a hybrid electric vehicle, that provides to the user the comforts expected of today's vehicles, can be utilized for several short-haul trips within the city, and would also be capable of an extended range on longer trips.

This research work will concentrate on the overall design of a hybrid electric vehicle, converted from a mass production vehicle, without effecting drastic structural changes, and with established technology that is available at a minimal cost. Simulated drive cycles will examine the feasibility of the proposed HEV and further analysis of the drivetrain will allow to look into the benefits of modifying the integral parts of the powertrain. It is important to investigate the different configurations of HEV design so that information can be accumulated and effectively applied to future vehicle research and development.

2. LITERATURE REVIEW

As electric and hybrid electric vehicle designs and control strategies have progressed in recent years, a general consensus to effectively meet consumer and government demands has yet to be reached. Various propulsion schemes have emerged from the design and engineering groups of the major automotive manufacturers. It has been understood that hybrid electric vehicles would be a transition phase for the transportation industry that would eventually result in mass-produced vehicles that will functionally meet zero emissions vehicle (ZEV) regulations in conjunction with vehicle comfort and consumer accessibility [3].

Examining the benefits of hybrid electric vehicles (HEVs) versus pure electric vehicles (EVs), Mason and Kristiansson [4], concluded that the cost of most HEVs would be less than that of EVs. HEVs tend to make up for deficiencies in battery technology and EVs would require great efforts for getting their weight reduced. Thus, it is logical for the automotive industry to focus on producing cost-effective HEVs which would then help to advance the vehicle technology, and in turn, result in technological breakthroughs that could lead to the development of better and less expensive EVs.

2.1 Electric and Hybrid Electric Vehicle Advancements

The interest in electric and hybrid electric vehicles, by more and more people today, is not something that will disappear. Different combinations of

alternative fuels, including electric power, are still being evaluated for their feasibility in a hybrid electric drivetrain. Although hybrid vehicle research programs are aimed at developing vehicles with high fuel economy and low emissions, it has been understood that the vehicle acceleration performance and a reasonable powertrain cost are also key factors [5]. Even though there are still no clear winners that have emerged from this research, automobile makers worldwide are establishing their own electric and hybrid electric vehicles and are preparing to sell them in meaningful quantities [3]. Currently, hybrid propulsion systems are aimed primarily to overcome the range limitations of pure electric vehicles powered by batteries alone [6].

After decades of electric and hybrid electric vehicle advancements, the 1990's have shown many types of vehicle forms other than the conventional spark ignition (SI) or compression ignition (CI) powered vehicles. Around the world, today's technology has provided the means to produce and to bring to the market the electric or hybrid electric vehicles. In 1994, Bill Powers of Ford's Research Laboratories [7], said that the industry is already moving toward hybrid-drive technology. In 1995, the Swedish firm Solon AB manufactured and offered to the public a four passenger HEV [8]. Major automotive manufacturers, have delved into experimental and theoretical analyses of hybrid electric vehicle design configurations and conversions. In 1991, Volkswagen AG was developing and testing hybrid drive vehicles in their Volkswagen and Audi Group. According to

Kaberlah [9], the vehicles with hybrid drive systems are more flexible than electric vehicles and have far more potential applications than electric drives that are limited by current battery technology. Fiat launched an electric truck in 1991 to complement their 1989 electric car. Both of these vehicles were designed specifically for European city driving [10]. The near term prospects are very positive of having hybrid vehicles that are road-worthy and efficient.

Utilities are also developing HEVs, especially with an increased emphasis on the reduction of vehicle emissions. The San Diego Gas & Electric (SDG&E) Company, in partnership with Unique Mobility, developed a hybrid electric powertrain with a natural gas fueled engine and placed it into a Dodge Caravan body [11]. SDG&E's goals in designing this hybrid prototype was to preserve the driving characteristics of the original vehicle. The intent of having a hybrid drive was to minimize the penalty of using available battery technology in a fully electric vehicle without giving up the benefit of low vehicle emissions [12]. Natural gas as a vehicular fuel has shown to be more environmentally friendly and cleaner burning than gasoline or propane and thus, was the best fuel available for the internal combustion engine.

Concerning the use of natural gas as a vehicle fuel, the Public Service Company (PSC) of Colorado has certified ANG1 natural gas retrofit kits for vehicles and stated that the best reason to convert to natural gas vehicles was for the improvement of the air quality [12]. Emissions information collected by the

company, showed an average reduction in pollutants of 97% in CO, 24% in CO_2, 39% in NO_x and 72% in reactive hydrocarbons. The PSC contends that a 5% conversion of transportation to natural gas operation would result in a yearly savings of 500 000 barrels of crude oil, which for the U.S. market, is a major import reduction.

In 1988, at the University of California-Davis, Mark DeLuchi et al [13], projected the feasibilities of various alternate fuels and their possible implementation in the U.S. market. It was concluded that a near term transition to natural gas would create a gaseous fuel infrastructure which would be beneficial to assist in the future implementation of a cleaner gaseous fuel such as hydrogen. Christopher Weaver at Sierra Research in Sacramento, California [14], reviewed natural gas vehicles and concluded that the use of natural gas possesses numerous advantages as a clean fuel for motor vehicles, having demonstrated considerable emissions benefits.

In 1991, at the Institute of Transportation Studies (University of California-Davis), Wang and DeLuchi [15] analyzed the impact of electric vehicles on petroleum consumption. They concluded that the use of EVs would reduce per-mile petroleum consumption by over 90% when the electricity is generated from non-petroleum fuels or by 65% if the electricity is generated from petroleum.

HEVs can be designed to satisfy various operational objectives: to extend the range of an electric vehicle, to directly replace a conventional vehicle, or to be

a combination of both. The addition of complex power and energy control strategies requires a more extended analysis, as it is discussed by Duoba et al [16]. These strategies are deemed necessary in maintaining an efficient and economical hybrid operation over any driving schedule or situation that could be encountered. By examining the results of prototype vehicles built for HEV Challenges by North American university and college student teams, a real look into the operation of different designs was possible and also provided the opportunity to display the capabilities of current technology. One of the most important conclusions that was derived from these results is that the level of sophistication in power control strategy can be directly related to the vehicle efficiencies. The diversity in HEV types witnessed at the competitions revealed that a classification system based on only three HEV types (range extender, fueled engine-electric, dual mode) was not feasible, since these systems do not encompass all the possible designs. Also, future testing procedures for emissions regulations need to accommodate the complexity that is becoming evident in HEVs.

Mastronardi and Doyle [17], at Thermo Power Corporation incorporated their vast natural gas and propane automotive experience into the development of engines sized for hybrid vehicle use. According to Thermo Power Corp. these engines are excellent alternatives to gasoline engines because of their lower tailpipe emissions and their use of a readily available and inexpensive domestic fuel. As for the gasoline engines, the CNG engines have a much higher power

density and energy density than batteries. Thus, they can readily be used in hybrid vehicles to improve the range and performance when compared to pure electric vehicles. Currently, natural gas and propane are the only alternative fuels that have a significant infrastructure in place to supply the fuel nationally in the U.S and Canada.

Given the current limitations of EV batteries, the most important technical parameter for electric vehicles is the overall vehicle efficiency. Individual components have been made more efficient but it has been seen that the whole system has to be also made efficient. By using the electric driveline as a generator when the conditions warrant, vehicle kinetic energy can be recovered, helping to increase the efficiency of the system. Hence, the use of regenerative braking systems combined with innovative ways for climate control will help reduce energy demands. Other methods of energy savings are associated with reducing the vehicle aerodynamic drag and rolling resistance. With the progression of electric and hybrid vehicles, all of the considered energy reduction techniques are being further emphasized in vehicle designs [18].

Mason and Kristiansson [4], compared the efficiency of EVs and HEVs. The vehicles that operated on energy that was primarily obtained from the electrical grid had an overall efficiency of 0.69. For the range extending series and parallel types of HEVs, with the initial EV mode powered from the grid, the efficiencies were at 0.40 and 0.34 respectively. Vehicles in HEV mode that were

never plugged-in, whether series or parallel drivetrains, had an efficiency of 0.20 or 0.11 respectively. With these various efficiency results the following was concluded: EVs and HEVs operating in an EV mode with power derived from the grid, were three times as efficient as HEVs operating in EV mode where the power was generated from the alternate power unit (APU).

Wyczalek and Wang [19], examined the opportunities of recovering vehicle kinetic energy. By developing a mathematical model of regenerative braking they evaluated some braking concepts for electric vehicles. Frequent starts and stops were the most beneficial conditions in returning energy to the battery pack. It was seen that there can be up to 20% of energy saved in a low speed urban drive setting. It was concluded that high regenerative power recovery levels are necessary. To achieve the most effective braking, (i.e. maximize the energy recovered), it was suggested that regenerative braking be split into three modes: service braking, a programmable braking based on battery life and emergency braking.

Giorgetti et al [20], at BREMBO Kelsey-Hayes, took regenerative braking one step forward by combining the braking control of the motor/generator and the hydraulic brake unit into one complete system activated by the brake pedal. Thus, the driver would not have to handle additional controls to initiate the generator mode for the electric driveline. This approach aimed to maximize the use of the generator every time the brake pedal is depressed and to have the hydraulic brakes

used only when the required deceleration is inadequate.

Energy recovery is a feasible process that could be incorporated into any electric or hybrid vehicle design. The next concern is the ability of the batteries to handle the energy charging rate from this system. It was realized by Edward Bass et al [21], at the Southwest Research Institute, that over-charging of the batteries during the energy recuperation modes was evident and could have adverse affects on the powertrain by limiting the future power and energy capabilities of the batteries. The authors deemed it necessary to recommend additional investigations into battery charging, relating to the effects of high current and high frequency charging on the battery life.

2.2 Evaluating Hybrid Vehicle Designs

The Idaho National Engineering Laboratory (INEL) has tested many electric vehicles and battery systems and developed a program to simulate the results on a computer. Outlined by Burke in an 1989 publication [22], the ELVEC simulation program was designed to facilitate the performance studies of electric and hybrid electric vehicles. The program was run on a SUN workstation and had limited simulation capabilities. By comparing the program predictions with dynamometer test results, it was seen that general energy consumption and range values agreed to within 10% of the measured and simulated values. It was concluded, that the ELVEC program needed further development to provide

greater accuracy for battery modeling at low states of charge, and more realistic motor power output modeling at high RPM.

To evaluate different hybrid vehicle designs, Burke [6] used the SIMPLEV software, also developed at INEL, to obtain results on vehicle performance and energy use. This software gave him the flexibility to simulate vehicles on a variety of Federal and California state driving cycles. It was also possible to simulate a different type of electric driveline without a battery pack, using instead an ultracapacitor unit that acted as a load leveler to an APU. At the time of his simulation, the SIMPLEV software was limited and could only simulate series HEV configurations. It did not have the capability to simulate parallel hybrid operation.

Moore and Lovins [23], used parameter spreadsheets and the SIMPLEV program to model vehicle performance, fuel economy and emissions. The objective was to present a vehicle design approach for a marketable, high-performance production automobile that would meet the goals established by the Partnership for a New Generation of Vehicles (PNGV). The goal of having a three times better fuel economy was seen as very unlikely if only small changes had to be made to conventional technologies. By combining new materials with the car platform design improvements and optimized hybrid drive systems, the PNGV goals could easily be reached [24].

In 1996, Aceves et al [2], at the Lawrence Livermore National Lab.

modeled compressed natural gas (CNG) series hybrid vehicles. They used a vehicle evaluation code, together with an optimizer program to determine the parameters that would give optimum vehicle fuel economy. Using SUPERCODE, a programmable shell coupled to a constrained optimization package, the user had the flexibility to specify an optimization problem and was also able to apply the new bounds of constraints to do a sensitivity analysis. Two vehicles, one stoichiometric and one lean-burn, CNG series hybrids, were optimized for high fuel economy and their results were compared. Even though both vehicles exhibited high fuel economies, the lean-burn engine was 4% more fuel efficient. It was also expected that the lean-burn engine would be able to achieve the California Air Resources Board (CARB) ultra-low emissions vehicle (ULEV) regulations. With eight independent variables and two inequality constraints, it would have been very difficult to come to the conclusions presented in this publication if the sophisticated optimization software had not been used.

In a 1993 publication, Burke [25] examined the on-off engine operation that could be incorporated in HEVs. It was seen that the "on" time of the engine will vary depending on the control strategy, the driving cycle and the use of the vehicle. A parallel-hybrid vehicle (HTV-1) utilized a complex control strategy that was vehicle velocity dependent. The engine driveline would be turned on at higher speeds only if the power demanded was greater than the capabilities of the electric driveline. By using existing vehicle technologies, improved emissions

and vehicle efficiencies could occur with an elaborate control system.

Merriman et al [26], performed analytical trials (using a numerical simulation), and experimental tests (using an engine dynamometer), on a series HEV design. By combining the results, they evaluated the effect of the APU on the performance of a series HEV. The most common control strategy for such a design was to have the APU turn "on" or "off" depending upon the battery state of charge (SOC). This research focused on the APU on/off operation and how it related to the vehicle fuel consumption and emissions for the particular series design detailed in the paper.

Cuddy [27], evaluated the accuracy of two HEV performance simulation programs, namely, CarSim 2.5.4 written by AeroVironment Inc. of Monrovia, California and SIMPLEV 3.0. The validation process was effected by using data compiled from two hybrid vehicles among the group of HEVs that participated in the 1994 HEV Challenge. The speed profiles, battery power and energy usage were collected with the aid of two data acquisition systems connected to the vehicles. Given the same inputs, both simulation programs predicted identical power and energy usage. The programs agreed within a 5% difference of each other and were within the uncertainty levels of the measured data. The author recommended that a simulation code needed to be carefully validated by using accurate characterizations of each HEV component before trusting the output results.

In a 1997 publication by Cuddy and Wipke [28], at the National Renewable Energy Lab (NREL), an analysis of various HEV drivetrains was performed with a primary focus on fuel economy. Using data from the literature and the industry with the Advanced Vehicle Simulator (ADVISOR), the charge-sustaining hybrids and an internal combustion engine vehicle (ICEV) were compared. Considering the main issue of fuel economy, the series hybrid defined in the paper was 18% more fuel efficient than the ICEV. The parallel hybrid was 24% more fuel efficient than the ICEV and 4% more fuel efficient than the series hybrid. The parallel hybrid control strategy was defined by the following: the heat engine never idles and it will always provide the necessary tractive power; the electric motor will provide additional torque when requested by the engine; the motor will always charge the batteries at any state of charge (SOC); the electric motor will also accept any extra torque from the heat engine to charge the batteries, if this torque is not required to meet the driving schedule.

2.3 Progression to Feasible Future Vehicle Designs

In 1995, following several successful alternate fuel competitions and two hybrid electric vehicle contests, the Concordia University Society of Automotive Engineers student branch added another hybrid vehicle to their fleet by converting a 1995 Chrysler Neon to a natural gas hybrid electric vehicle. The vehicle consisted of the following components: a DC series wound electric motor, a BMW

internal combustion engine converted for natural gas and a heating and air-conditioning system. The drivetrain arranged in a parallel configuration was selected to provide a ZEV operation in multiple urban excursions with a range extension available for sub-urban driving. The electric motor would be used to drive the vehicle in the city or as a supplement to the engine during peak power demands, (acceleration) on the highway. Having the capabilities of an EV drive, for a short duration, enables operation of the vehicle in city zones without increasing the pollutants and smog that are the direct result of conventional vehicles. The requirement for a climate control system, imposed another constraint in the vehicle design and illustrated the difficulties that are encountered in trying to produce a hybrid vehicle that has amenities and comforts already present in current vehicles. The feasibility of this parallel design was demonstrated at the 1995 HEV Challenge, having the engine operating over a prolonged period of time during the range event [29,30].

HEV and EV technology is leading towards an efficient economical 'supercar'. The U.S. government introduced the FutureCar concept under the PNGV program in cooperation with Chrysler, Ford and General Motors [31]. The objective for the automotive industry is to move the new technologies into high volume at a low production cost.

General Motors introduced the fully electric EV1 and the Chevy S-10 EV pickup to a selected segment of the California and Arizona market in 1996 [32].

These vehicles integrate several technologies that are close to meeting the goals proposed by the PNGV group for future vehicles. The EV1 combines a lightweight structure, an advanced electric regenerative braking system, highly efficient electric motors and a maintenance-free lead acid battery pack. By having these vehicles going into production and driven by consumers will provide valuable data that will aid in validating the new technology being used.

Chrysler unveiled a technology demonstrator vehicle, the Dodge Intrepid ESX [31], at the 1996 North American International Auto Show in Detroit. Constructed of a 100% aluminum unibody, this vehicle uses a hybrid-diesel electric/generator powerplant with advanced lead-acid batteries to drive twin electric motors placed in the rear wheel hubs.

Ford Motors unveiled the Ford Synergy 2010 concept car [31], at the same automotive show and will use this vehicle as a test bed to explore new fuel efficient technologies. The Synergy is a hybrid electric vehicle with two power sources in a series configuration. An efficient CI engine/generator unit produces electricity for motors placed in the wheels, with the excess engine and braking energy collected by a flywheel.

In 1996, Concordia University students successfully completed the first year of the FutureCar Challenge and placed fifth overall [33]. A Dodge Intrepid was converted to a hybrid vehicle with a very efficient direct injection diesel engine and a highly efficient brushless permanent magnet electric motor. In this

parallel charge-sustaining design, a hybrid control strategy enables the motor to operate as a generator when there is an excess of power from the engine or from deceleration. The goals of the two year competition project paralleled those of the PNGV, mainly to design and build a mid-size passenger automobile capable of achieving up to 80 mpg_{US}. By using the vehicle simulation process outlined in this thesis, preliminary fuel and energy consumption parameters were established for the FutureCar HEV design. This enabled the design team to quickly perform changes to the system setup and control strategy without having to undergo major vehicle alterations. They were also able to validate the analytical results by effecting simple vehicle tests on nearby roadways and highways [34].

3. THESIS OBJECTIVES AND METHODOLOGY

The Concordia University Society of Automotive Engineers (SAE) student branch has been participating in alternate fueled vehicle challenges since 1989. Recently, Concordia University has fielded teams that have successfully completed the 1993 and 1994 Ford Escort conversion class Hybrid Electric Vehicle (HEV) Challenges. The competition was extended for a third year to allow for the entrance of new vehicles, namely, the Chrysler Neon conversion class. A proposal was submitted to the organizing committee that awarded Concordia, along with 11 other North American Universities, a 1995 Chrysler Neon and the privilege to compete in the 1995 HEV Challenge. This competition was organized and sponsored by the U.S. Department of Energy (DOE), the Chrysler Corporation, Natural Resources Canada (NRC) and SAE. The competition objective was to convert the Neon to a power-assist compressed natural gas HEV that would also have an operational heating and air-conditioning system. This chapter outlines the objectives and methodology of the research work, which was performed in the frame of the Neon conversion.

3.1 Research Objectives

The Neon HEV competition consisted of several steps. The first was to convert the Chrysler Neon to run as a compressed natural gas (CNG) HEV with heating and air-conditioning capabilities. The next step was to attend the HEV

Challenge competition. The present step is to optimize the HEV design for the next HEV Challenge competition. This will entail the analyses of the vehicle's performance, to establish the vehicle's energy consumption during different driving trials and to suggest improvements relating to its dynamic performance and fuel efficiency. The main objective of this thesis research is to describe the conversion of the vehicle design and to perform the aforementioned analyses. The Neon HEV is already considered as a validated model, whose purpose is to confirm the feasibility of the technology being used. With computer simulations and basic optimization techniques, the vehicle design changes can be examined and improvements can be proposed.

3.2 Research Outline and Methodology

Six main chapters will present this thesis research. The design modifications of the vehicle and the components required for the conversion will be analyzed. Computer simulated results will be examined and the most feasible approach to improve the vehicle's capabilities will be determined. Each of the vehicle's systems will be described and modifications that might be deemed useful will be suggested.

In Chapter 4, the requirements for the hybrid powertrain will be discussed. A dynamic vehicle analysis will be performed and vehicle performance will be simulated and assessed from two perspectives: acceleration and fuel economy.

In Chapter 5, the vehicle will be introduced and specifically described from the point of view of the design concept. The internal combustion engine and electric motor selection will be outlined, and the vehicle control strategy will be discussed.

In Chapter 6, the electric energy storage system will be described. An experimental comparison of lead-acid batteries will be presented and the charging process of the system will be explained.

In Chapter 7, a modified driving strategy will be proposed and validated with analytical results from the simulation techniques that were used in Chapter 4. Specific drive cycles will be proposed and simulated to illustrate energy consumption and fuel economy for the Neon HEV. A comparison of the existing Neon conversion and the proposed modifications will be shown. The evolution to a charge sustaining hybrid vehicle will be outlined.

In Chapter 8, an experimental investigation of the Neon heating system will be performed. The results will be used to assess the feasibility of this setup and to propose a modified version of the system.

In Chapter 9, the hybrid electric economy will be discussed and the results from Chapter 4 and Chapter 7 will be compared.

In Chapter 10, a thesis summary will be presented, conclusions will be drawn and recommendations will be outlined to further improve the Neon hybrid electric vehicle.

4. VEHICLE DYNAMIC ANALYSIS

To adequately assess the requirements for the hybrid electric propulsion system, a vehicle dynamic analysis had to be performed. Since, the vehicle will be operated mainly in city type driving conditions, the design would reflect this type of driving behavior. Considering that the Neon HEV Challenge competition was organized for a two year period, the conversion goal for the Concordia HEV entry was to have a vehicle that would be in running condition for the first year of the competition. The second year would entail a modification to the vehicle design to improve the performance over that of the first year. The initial powerplant design goals were as follows:

- to have a vehicle that is operational in two modes (electric and hybrid drive),
- to ensure a hybrid electric acceleration of 0-60 km/h within 10 seconds,
- to attain a low specific fuel consumption and to maximize the total energy efficiency during driving cycles,
- to ensure low exhaust emissions.

4.1 Vehicle Force Analysis

From the point of view of the time available for the conversion, it was deemed prudent to maintain the original vehicle's manual five-speed transmission. This selection would pertain to the first phase of the design competition and the decision would be reassessed for the second year design. It was realized that the

most effective and simple solution for a hybrid powerplant was to combine both electric and engine drives into a single drive that would be connected to the existing transmission. Thus, depending upon the electric motor operating voltage and the motor's gear ratio, the two drive units would work in tandem to achieve the best performance at low velocities. With this design configuration, the powerplants can also individually operate the vehicle, which was one of the competition requirements. It was important, though, to determine at what conditions the optimal performance would occur. By examining different powerplants, it was realized that there were some other physical constraints to the design: the space that was available in the engine bay, and the components' availability. The drive components used in this project are described in Chapter 5.

The required power for the hybrid drivetrain was calculated by using a basic vehicle dynamic force analysis. Listed in Table 4.1 are the nominal parameters that were used in the analysis.

Table 4.1 Nominal Parameters used in the Analysis.

r	- Wheel radius (m)	0.3073
m_V	- Vehicle mass (kg) [weight: vehicle + 2 people + cargo]	1477.4
μ_{cst}	- Constant for the Coefficient of rolling resistance	0.008
g	- Gravity acceleration (m/s^2)	9.81
ρ_{Air}	- Density of air (kg/m^3)	1.202
C_d	- Drag coefficient	0.30
A_f	- Vehicle frontal area (m^2)	1.914
μ_{st}	- Coefficient of friction (from tire to ground)	0.85
η_m	- Drivetrain mechanical efficiency	0.95

The mathematical model used to calculate the acceleration and loads acting on the vehicle is described below. The fundamental forces that act in resisting the vehicle motion, equations 4.1, 4.2 and 4.3 respectively, are: aerodynamic drag, rolling resistance, and climbing resistance. The total resistive force is the summation of all the forces acting on the vehicle in motion, as it is outlined in equation 4.4.

$$F_{aero} = \frac{1}{2}\rho_{air} C_d A_f (V_{net})^2, \qquad (4.1)$$

$$\text{where: } V_{net} = V_{HEV} \pm V_w.$$

$$F_{ro} = \mu_{ro} m_V g \cos(\theta), \qquad (4.2)$$

$$\text{where: } \mu_{ro} = \mu_{cst} + \frac{(0.0015 \cdot V_{HEV})}{27.7}. \quad [35,36]$$

$$F_{cl} = m_V g \sin(\theta) \qquad (4.3)$$

$$F_{tot} = F_{aero} + F_{ro} + F_{cl} \qquad (4.4)$$

The total drive torque that is available at the wheels (by both the engine and the motor) and, thus, denoted as the total motive force at the wheels is shown in equations 4.5 and 4.6.

$$Wh_{TRQ} = (Melec_{TRQ} + Eng_{TRQ}) \cdot N_{gf} \qquad (4.5a)$$

$$Melec_{TRQ} = Motor_{TRQ} \cdot N_n \qquad (4.5b)$$

$$F_{mdw} = \frac{Wh_{TRQ}}{r} \cdot \eta_m \tag{4.6}$$

The motive force is used to overcome the total resistive force in order to maintain the vehicle at the driving speed. The force surplus is used to help in vehicle acceleration (equation 4.7), but the maximum force that can be attained is limited by road adhesion, (equation 4.8). Using the free-body diagram in Figure 4.1, an analysis of the aforementioned forces acting on the vehicle can be performed.

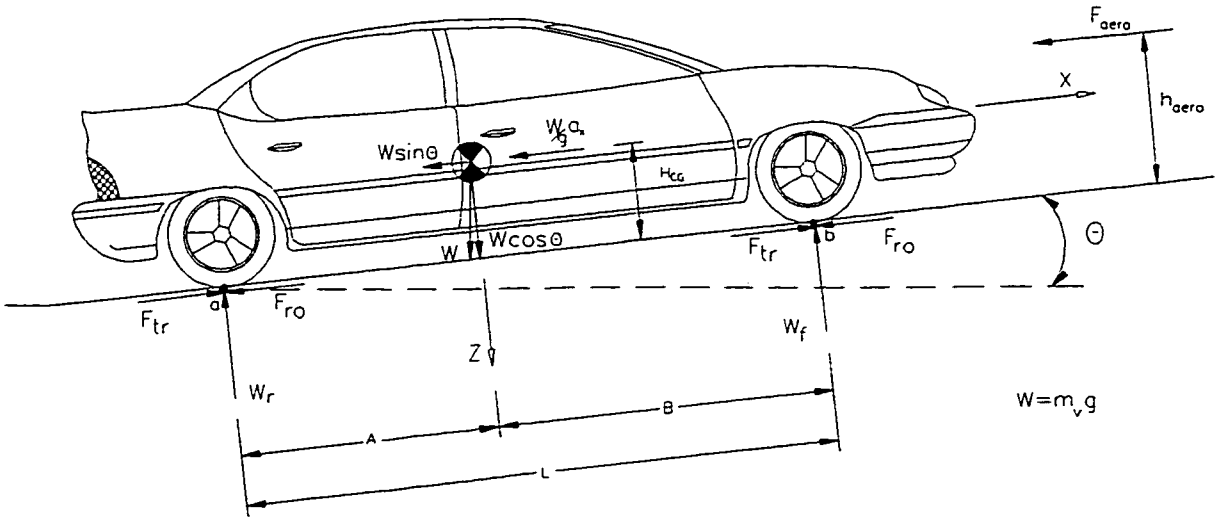

Figure 4.1 Neon HEV Free Body Diagram.

$$F_{tractive} = F_{mdw} - F_{tot} \tag{4.7}$$

$$F_{mdwMAX} = \frac{\frac{A\mu_{st}W}{L}}{1+\frac{\mu_{st}H_{CG}}{L}}, \quad [37] \tag{4.8}$$

The values for the parameters that are used in Equation 4.8 and illustrated in Figure 4.1 are listed in the following table.

Table 4.2 Parameters used for the Road Adhesion Limitation.

L	-	Wheelbase Length (m)	2.64
H_{CG}	-	Center of Gravity Height (m)	0.508
μ_{st}	-	Road Adhesion Coefficient	0.85
A	-	Length as shown in Figure 4.1 (m)	0.56 • L
Based on a weight distribution of front/rear: 56/44%			

The vehicle acceleration time can be calculated by using numerical integration techniques and the following expression:

$$t = M_{eff} \int_{V_1}^{V_2} \frac{dV}{F_{tractive}} \tag{4.9a}$$

The effective mass (M_{eff}), which takes into account the rotational inertia of the drivetrain is expressed in equation 4.9b. It is calculated by using the vehicle mass and a mass factor constant that varies with the final drive ratio [37,38].

$$\begin{aligned} C(i) &= 1 + 0.04 + 0.025(N_{gf(i)})^2 \\ M_{eff} &= C(i) \cdot m_V \end{aligned} \tag{4.9b}$$

In the sections that follow, the drive system characteristics are expanded upon.

4.2 Hybrid Drive System Development and Analysis

The Neon HEV is a prototype design. The vehicle will be classified as city oriented, also, having the capabilities of prolonged driving (highway driving) when required. The compressed natural gas fueled engine is the primary drive unit that can be assisted by an electric motor for short periods of time during specific drive situations. Thus, this powerplant configuration can be denoted as being parallel power assist, which is considered to be charge depleting.

Using the information that was outlined in section 4.1, the Neon drive system requirements and specifications can be determined. Design time and experience, along with budget constraints, were the compromising factors that lead to the choice of the CNG engine and electric drive units (detailed specifications are found in Chapter 5). In Table 4.3, the power and torque characteristics for the electric motor and the engine are summarized.

Table 4.3 Drive Component Manufacturer Ratings.

		Ratings	
	Drive Unit	**(Power - kW)**	**(Torque-Nm)**
Engine (gasoline)	BMW K75 3-Cylinder I.C. Engine	@ 8500 rpm: 56	@ 6750 rpm: 68
Electric Motor	Advanced DC Series X-91 4001 6.7" @ 96 Volt	Peak @ 2050 rpm: 27 Continuous: 9	@ Stall: 128

Both drive units had to be capable of transferring power to the front wheels through the Neon transaxle. An extension shaft was fabricated (Figure 4.2) to join the BMW engine to the transaxle. Power from the electric motor was transferred

to a sprocket located on the extension shaft. The sprocket diameter ratio, N_s, was determined by mating the two propulsion systems so that neither one would be spun beyond its rated top speed. The BMW engine's top speed is at 8900 rpm with peak power occurring at 8500 rpm. The Advanced DC motor cannot be spun at a higher speed than 5500 rpm, otherwise the windings could be damaged. Also, between 5000 and 5500 rpm the torque value approaches zero. By using the engine at 8500 rpm and the motor at 5000 rpm speed as a baseline, the following calculation determined the sprocket ratio that would be used to connect the electric motor to the drivetrain (see Figure 4.2).

$$N_s = \frac{N_{na}}{N_{nb}} = \frac{29}{17} = \frac{Engine\ RPM}{Motor\ RPM} = \frac{8500}{5000} = 1.7 \qquad (4.10)$$

where: N_{na} is the electric motor sprocket and N_{nb} is the driveshaft sprocket.

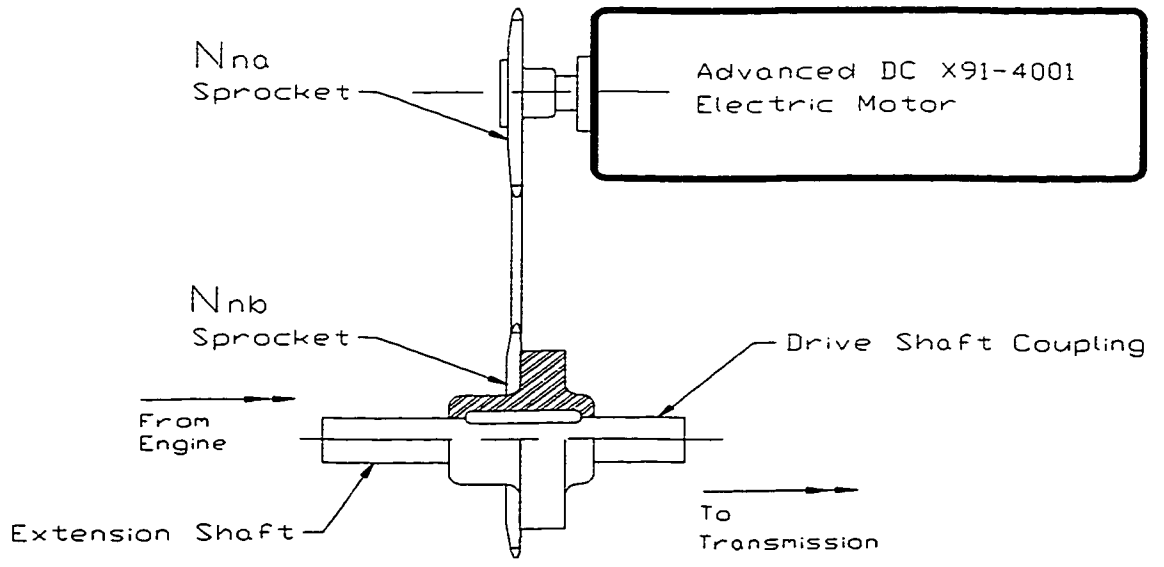

Figure 4.2 Electric Motor Sprocket Drive Schematic.

Since the engine peak torque occurs at 6750 rpm and the peak power occurs at 8500 rpm, it was essential to harness the engine capabilities at the higher speed range; hence, the engine has been connected directly to the transmission. To connect the electric motor, though, a reducing sprocket ratio was used ($N_n = 1/N_s$); the electric motor torque was equivalently reduced at the drive input to the transaxle. Thus, the power available to move the vehicle has been achieved through a compromise of both the engine and the motor capabilities.

The sprockets that were used provided an actual electric drive ratio of 1.706, that closely matched the calculated ratio. Thus, electric motor torque that is available at the driveshaft will be reduced by a factor of 1.706 and, consequently, the electric motor will be spinning 1.706 times slower than the engine.

The Advanced DC and the compressed natural gas BMW individual torque curves at their associated shaft outputs, are shown in Figure 4.3. Also, illustrated in this figure is the resulting combined torque of both units that is available at the transaxle drive shaft input, after taking into account the electric motor sprocket reduction.

The available torque and drive force at the wheels is calculated by using the combined torque that is available at the driveshaft input to the transaxle. Depending on the gear selected, the vehicle will be accelerated accordingly.

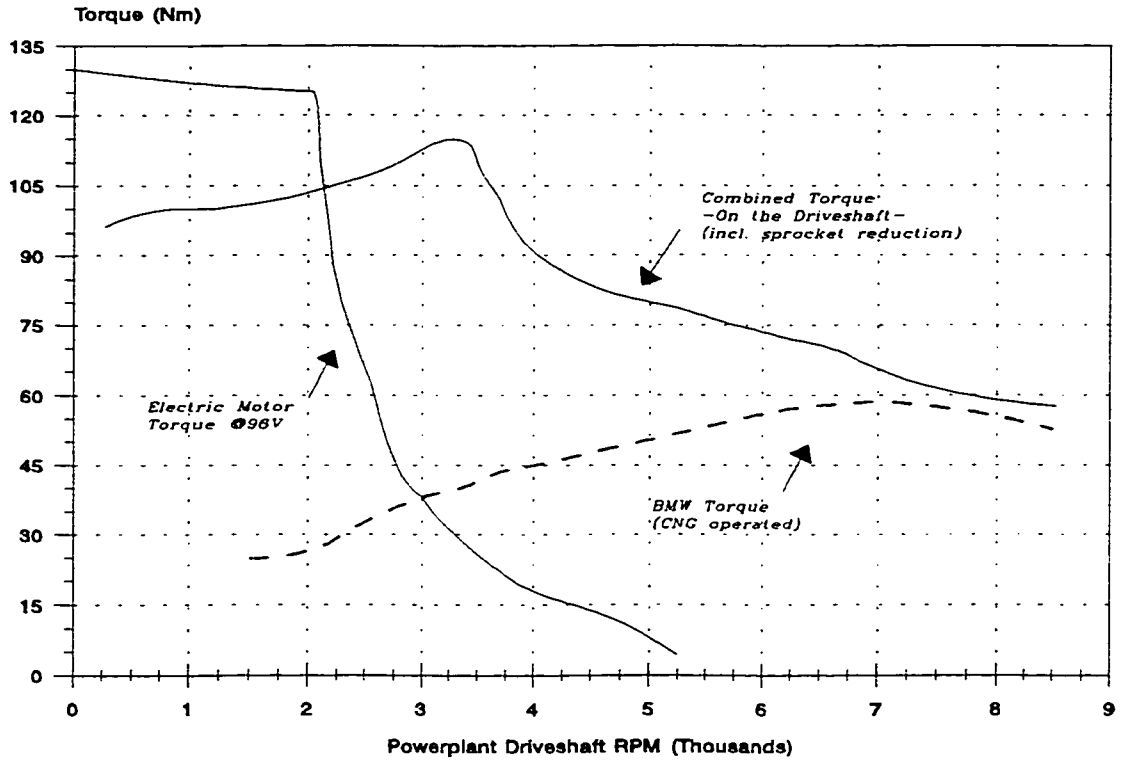

Figure 4.3 Individual Powerplant Torque Curves that are Superimposed (including the sprocket reduction) to Provide the Combined Torque.

A summary of the ratios for the engine, electric motor drive and the Neon five speed transaxle is shown in Table 4.4.

Table 4.4 HEV Drive Ratios and the Neon Five Speed Transaxle.

Transmission		**Overall Drive Ratio**	
Gear		Engine	Electric Motor
First	3.54	12.57	7.37
Second	2.13	7.56	4.43
Third	1.36	4.83	2.83
Fourth	1.03	3.66	2.14
Fifth	0.72	2.56	1.50
Final Drive	3.55		
Sprocket Reduction	0.586		

To determine the best vehicle acceleration response, various gear shift possibilities are examined, since this response cannot clearly be determined by just examining the individual powerplant characteristics. With this hybrid drivetrain, the electric motor is being operated over a wide speed range; between 2200-5500 rpm motor speed the motor torque does not remain constant. Due to this occurrence, the optimal shift speed determined for the best HEV acceleration, will not be the same when determining the best HEV economy shift speed.

One of the main objectives was to ensure a HEV acceleration to 60 km/h in under 10 seconds, since the focus is to have a city oriented HEV. The vehicle will not be sluggish during "stop and go" situations, typically occurring during city driving. Using the parameters listed in Table 4.5, the best acceleration time was determined by examining at what engine rpm the gearshifts would occur. The results are graphically represented in Figure 4.4. It could be seen that the best acceleration time of 9.51 seconds is obtained by using only two gears, with the shifting occurring at a drivetrain speed of 4250 rpm.

Table 4.5 System Response Parameters.

Vehicle Mass, m_V (vehicle weight + driver weight)	1397 kg
Battery Nominal Voltage	96 V
Drive Mode	HEV
Road Incline	Level Surface
Electric Drive Sprocket Reduction	0.586

A similar analysis was performed to determine the best acceleration time for two other conditions of 0-89 km/h and 0-100 km/h. These results are shown

in Figure 4.5 along with the top speed that could be obtained during acceleration at the respective rpm shifts.

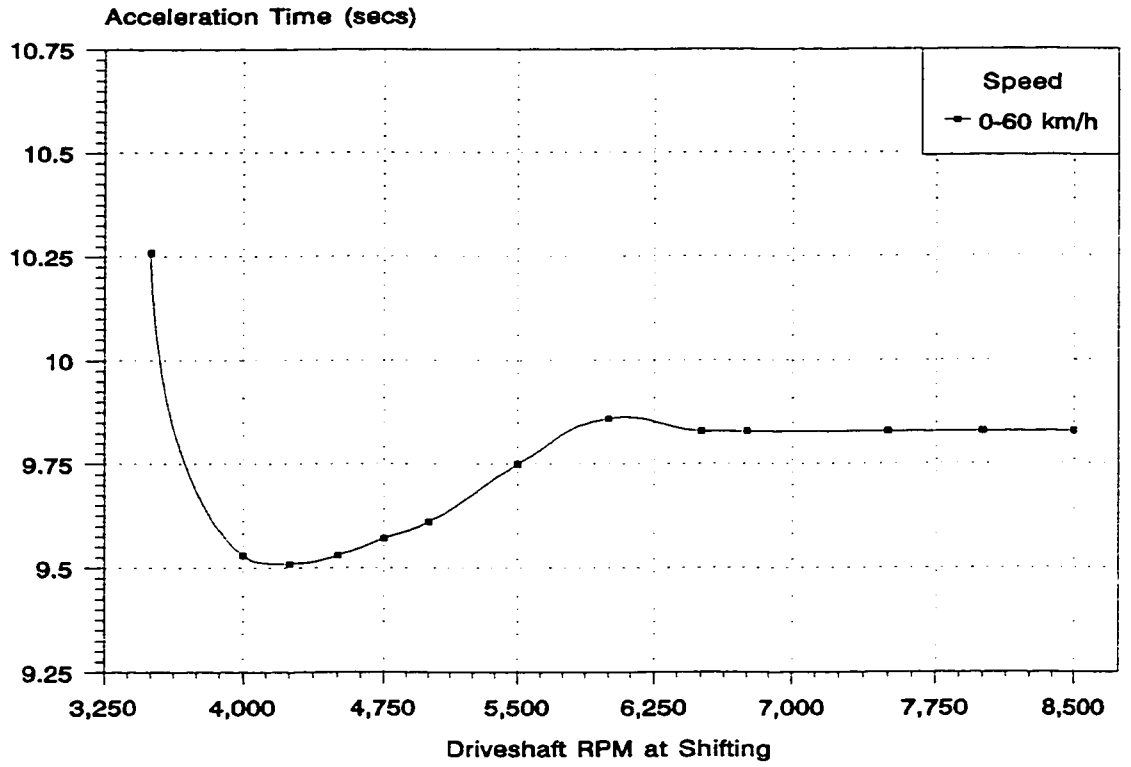

Figure 4.4 Time versus Shift RPM for Acceleration from 0-60 km/h.

It can be seen that the shift rpm for the two latter conditions is not at the same shifting value as for the 0-60 km/h condition. There is a minimum result at 4250 rpm but a 'global' minimum that occurs at 8500 rpm, also provides the highest result obtained for the top acceleration speed. These results illustrate that the electric motor, due to the sprocket reduction, does not contribute to acceleration as effectively as it would at lower speeds. At the higher drive speeds, it is the engine impact that provides the best result. The results for the two shift points and for an intermediate point of 6750 rpm are summarized in Table 4.6.

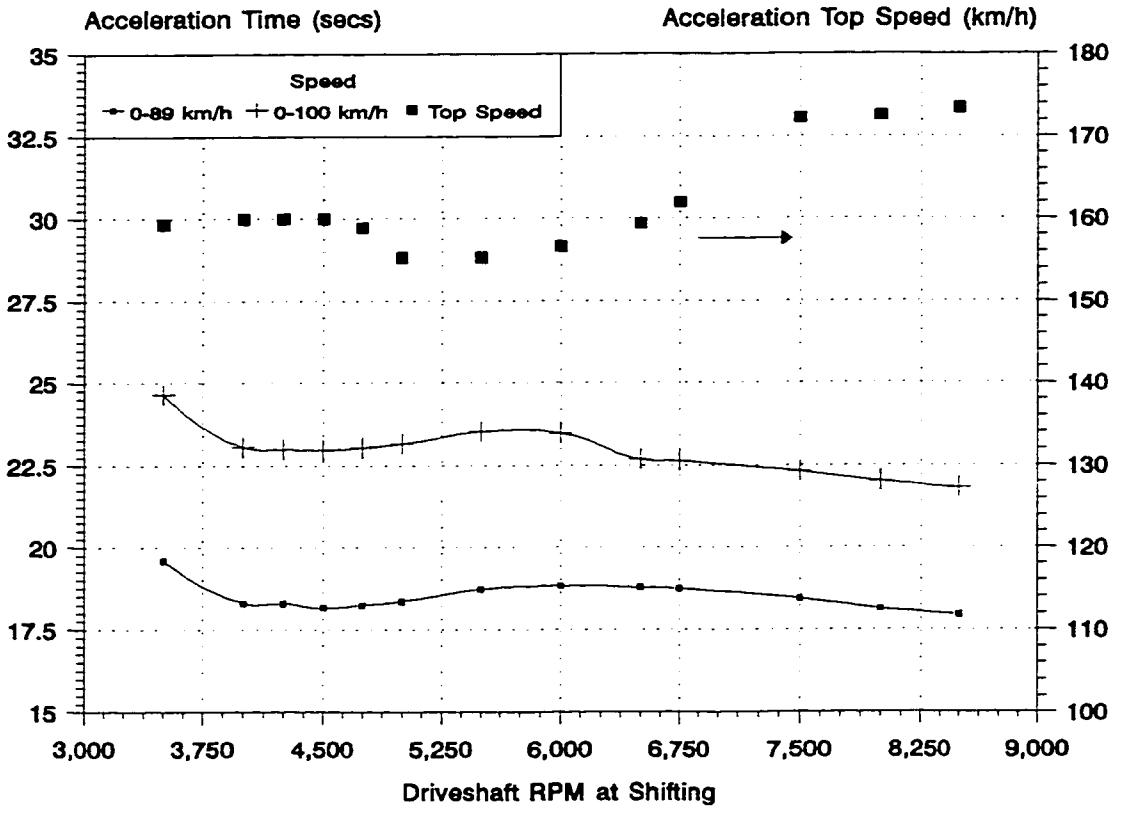

Figure 4.5 Time versus Shift RPM for Acceleration from 0-89 km/h and 0-100 km/h, as well as the Top Speed versus Shift RPM.

Table 4.6 Acceleration Result Summary.

Engine RPM Shift Point	**Time to Accelerate (seconds)**		
	0-60 km/h	0-89 km/h	0-100 km/h
4250	9.51	18.16	22.96
6750	9.83	18.74	22.63
8500	9.83	17.94	21.83

Another shift analysis was performed by varying the gear shift point to see if there would be an improvement in acceleration times. The shift from first to second gear was performed at 4250 rpm but the subsequent shift from second to third was performed at 8500 rpm. The results are shown in Table 4.7.

Table 4.7 Acceleration Result Summary II.

Engine RPM Shift Point	**Time to Accelerate (seconds)**		
	0-60 km/h	0-89 km/h	0-100 km/h
4250/8500	9.51	18.47	22.35

As the results illustrate, there is no significant improvement in the acceleration times, between shifting at 4250 and 8500 rpm. Gear shifting will occur at 4250 or 8500 rpm, to achieve the best acceleration times, depending upon the end speed (60 km/h or 100 km/h) required. In section 4.4, more favourable gear shifting will be determined from the point of view of fuel economy.

The acceleration time versus speed for the selected hybrid electric drive configuration is illustrated in Figures 4.6 and 4.7. In Figure 4.6 the best 0-60 km/h condition is plotted in terms of time and distance; hence, after attaining 60 km/h in 9.51 seconds the vehicle has traveled a distance of 121 m.

In Figure 4.7 a similar graph depicts the results that are obtained for the higher speeds. The gear-shifting is performed at 8500 rpm so that 89 km/h and 100 km/h can be attained as quickly as possible. Thus, the $^1/_4$ mile or 402 m can be achieved within 18.65 seconds at a speed of 91.96 km/h. To expand upon this response time analysis, superimposed on the total resistive forces of aerodynamic drag, rolling resistance and climbing resistance, a plot of the total wheel force available to accelerate the vehicle is shown versus vehicle speed in Figure 4.8.

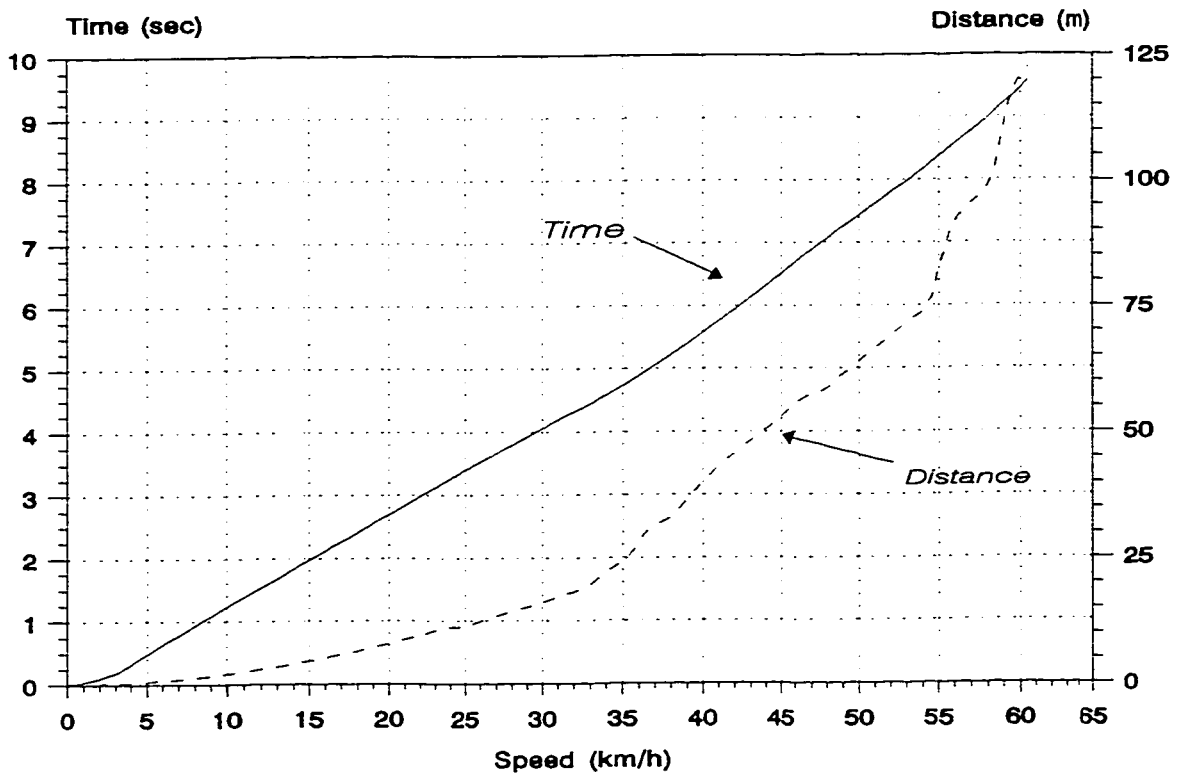

Figure 4.6 Acceleration Response for Low Speed Conditions.

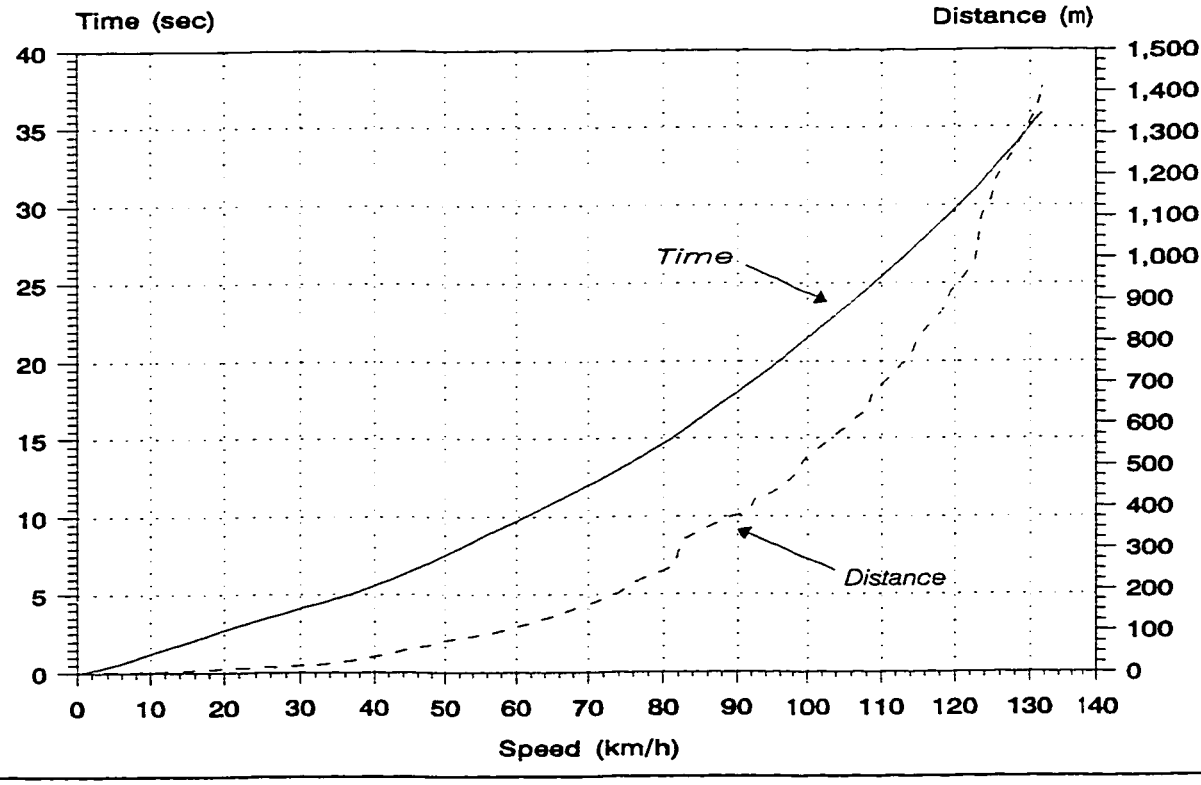

Figure 4.7 Acceleration Response for High Speed Conditions.

At higher speeds, aerodynamic drag is a major factor in reducing the vehicle response time. In this analysis the climbing resistance is examined for different conditions consisting of level ground and grades that vary from 1.75 % to 8.7%. The effect of driving over such slopes will be examined later during the analysis of energy consumption.

It can be seen again that only the first two gears are required to achieve a quick acceleration to either 60 km/h or 100 km/h and that the shifting at 8500 rpm will give a top speed of 173.5 km/h.

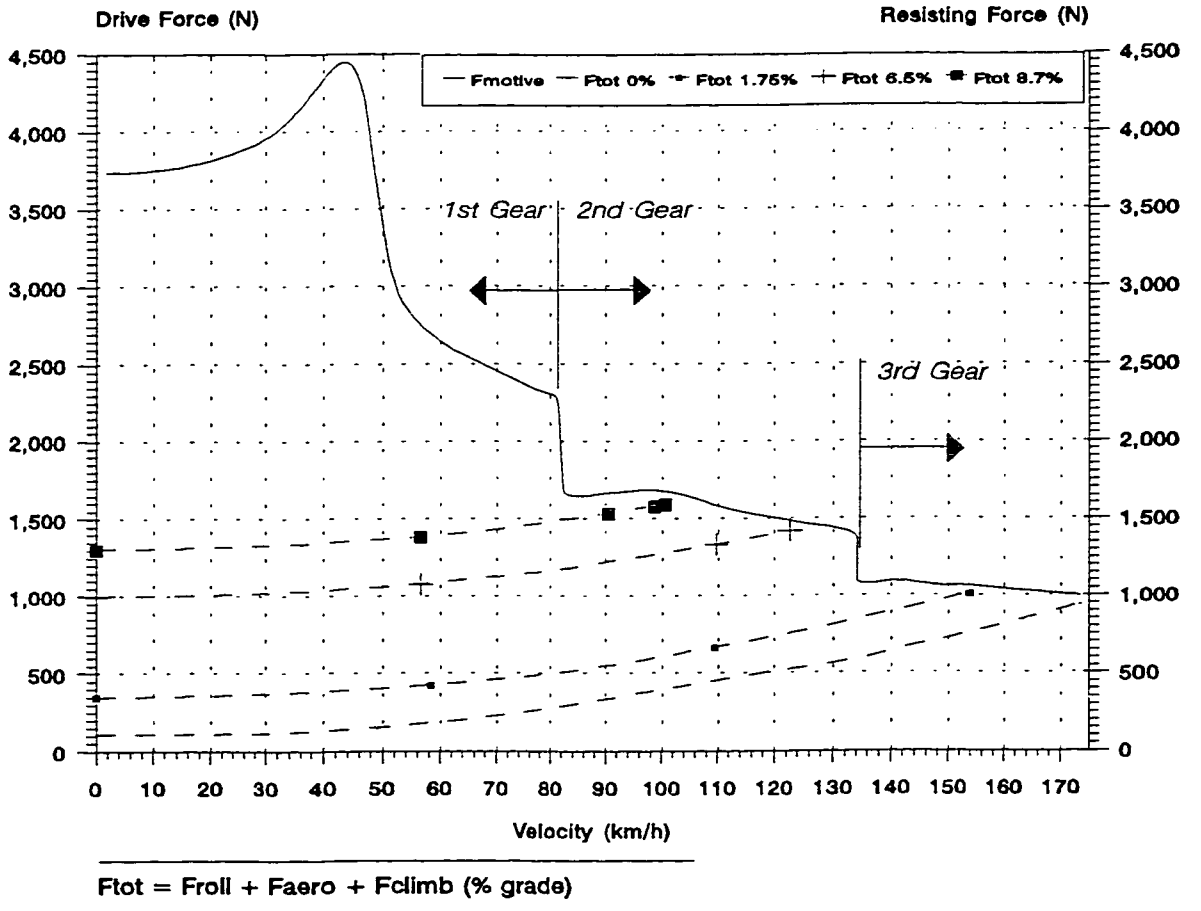

Figure 4.8 Drive and Resisting Forces vs. Vehicle Velocity.

Illustrated in Figure 4.9a is the drivetrain torque and drivetrain rpm versus time depicting an acceleration with three gears, (shifting occurring at 8500 rpm). A comparison of vehicle acceleration and top speed is again performed using four gears and a lower shift speed of 4250 rpm, (illustrated in Figure 4.9b). With this shifting, the top attainable speed is 160 km/h.

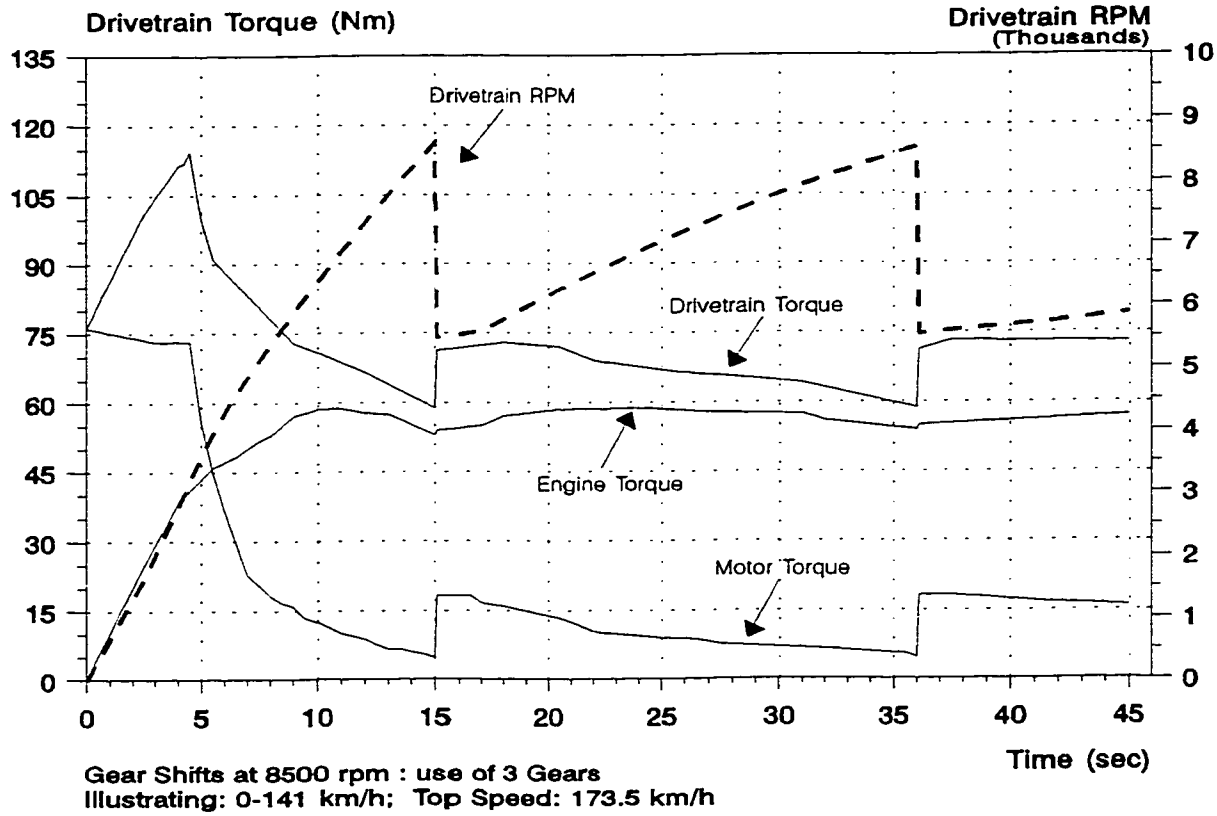

Figure 4.9a Drivetrain Torque and Drivetrain RPM vs. Time (Three Gears).

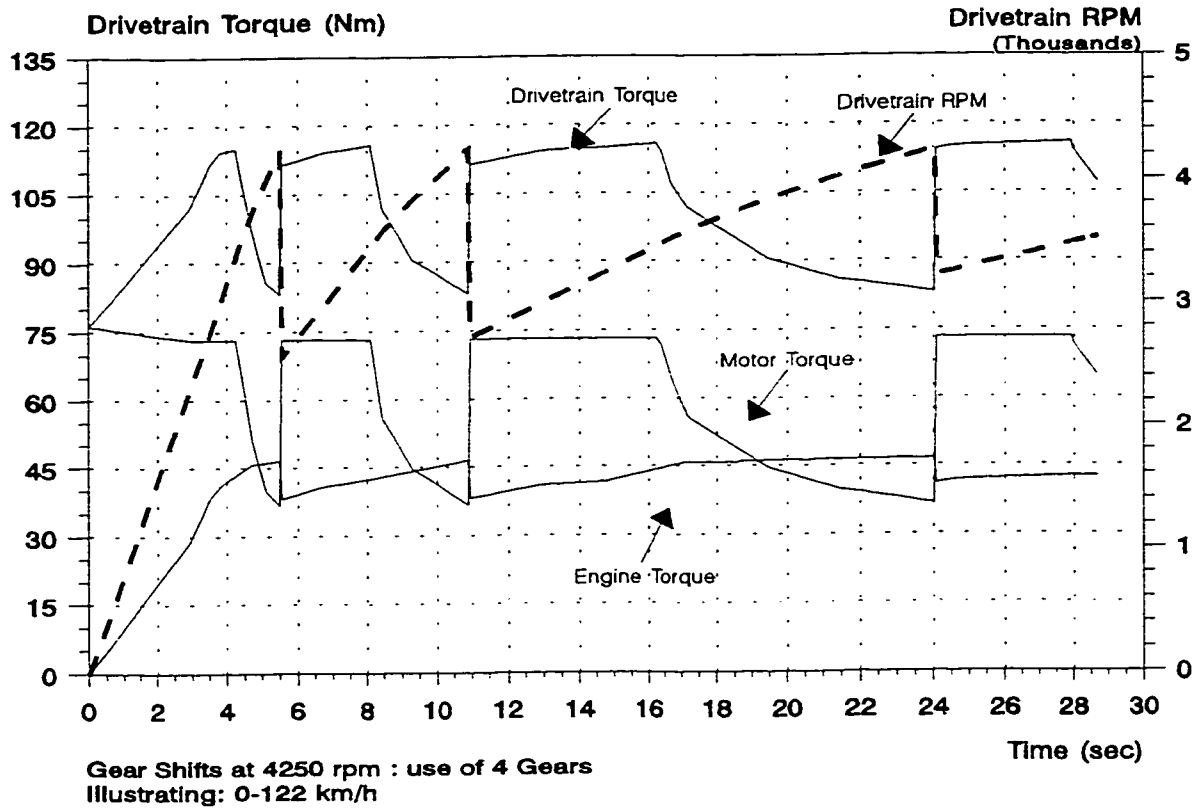

Figure 4.9b Drivetrain Torque and Drivetrain RPM vs. Time (Four Gears).

In this section it has been shown that the goal of 0-60 km/h within 10 seconds was achieved. This design also enables the vehicle to be operational for short durations as a purely electric vehicle. This is discussed in the following section. Having established the vehicle drive characteristics and the vehicle response for the hybrid drivetrain, an analysis of the electric vehicle operation will follow.

4.3 Electric Drive Analysis

It was required by the HEV Challenge regulations that the Neon hybrid electric vehicles have: a dedicated minimum electric range of 8 km at a constant speed of 48 km/h. The description and the selection process of the chosen motor and the batteries are discussed in the next chapters.

Since the drivetrain has basically been designed for hybrid operation, in an electric drive mode, the vehicle's performance will be different. The electric drive performance was also determined for certain acceleration conditions that would occur during city driving scenarios.

The best acceleration responses for two conditions of 0-48 km/h and 0-60 km/h, as well as the top speed attained, is illustrated in Figure 4.10 and summarized in Table 4.8. The results are based upon the engine rpm, since the driveshaft input is at the same rpm as the engine and the motor output is altered by the 1.706 sprocket reduction.

Table 4.8 Electric Drive Acceleration Response Summary.

Drivetrain RPM Shift Point	**Equivalent Motor RPM**	**Time to Accelerate (seconds)** 0-48 km/h	0-60 km/h	**Top Speed** (km/h)
3000	1758	11.38	17.08	120.0
3500	2052	10.72	15.45	123.0
3750	2198	10.67	15.10	124.3
4500	2647	11.55	16.05	105.6
6000	3517	14.65	25.74	89.9

It is seen from Table 4.8, that to achieve the best acceleration time, the gear shifting should occur at the drivetrain speed of 3750 rpm. Accelerating to 48 km/h requires the usage of the first two gears, whereas, three gears are used to accelerate to 60 km/h. The acceleration response for the electric drive is depicted in Figure 4.11. After attaining 48 km/h, it is seen that in electric mode the Neon will pass a distance of 95.5 m. It has been shown that the vehicle performance in an electric mode is acceptable and that the vehicle can be operational solely with an electric drive.

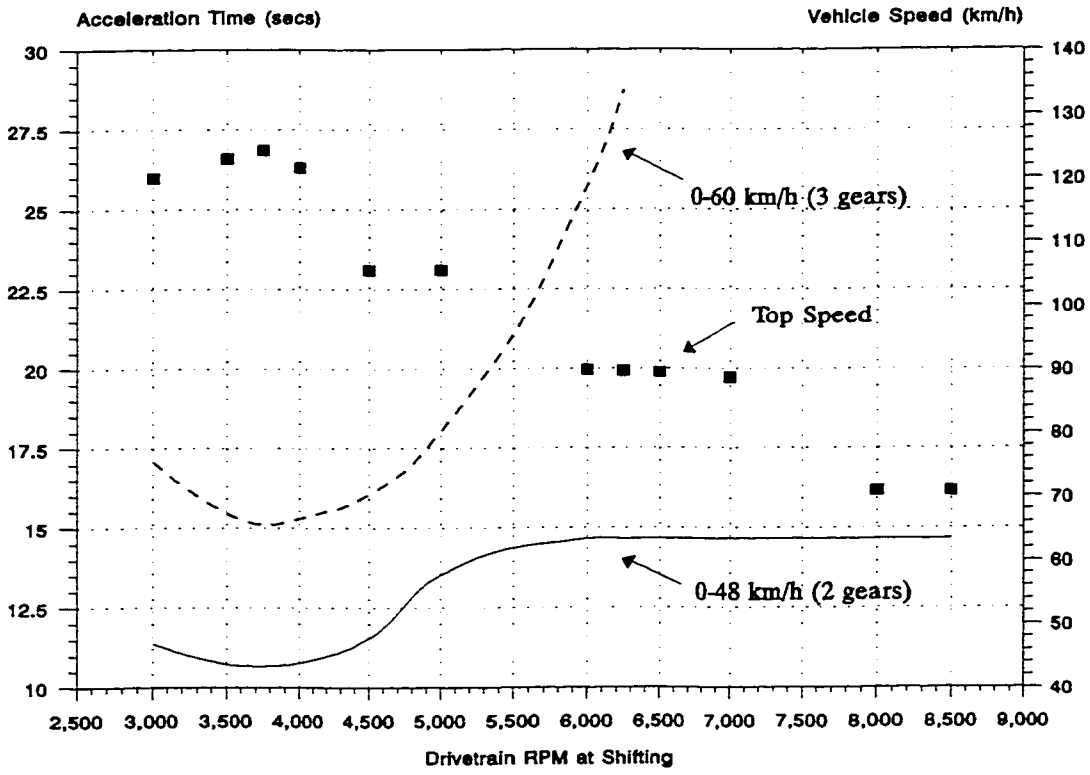

Figure 4.10 Acceleration Time & Vehicle Speed vs. Drivetrain RPM at Gear Shifting for the Electric Drive.

The gear shifting points can be recognized, particularly on the distance versus speed graph in Figure 4.11.

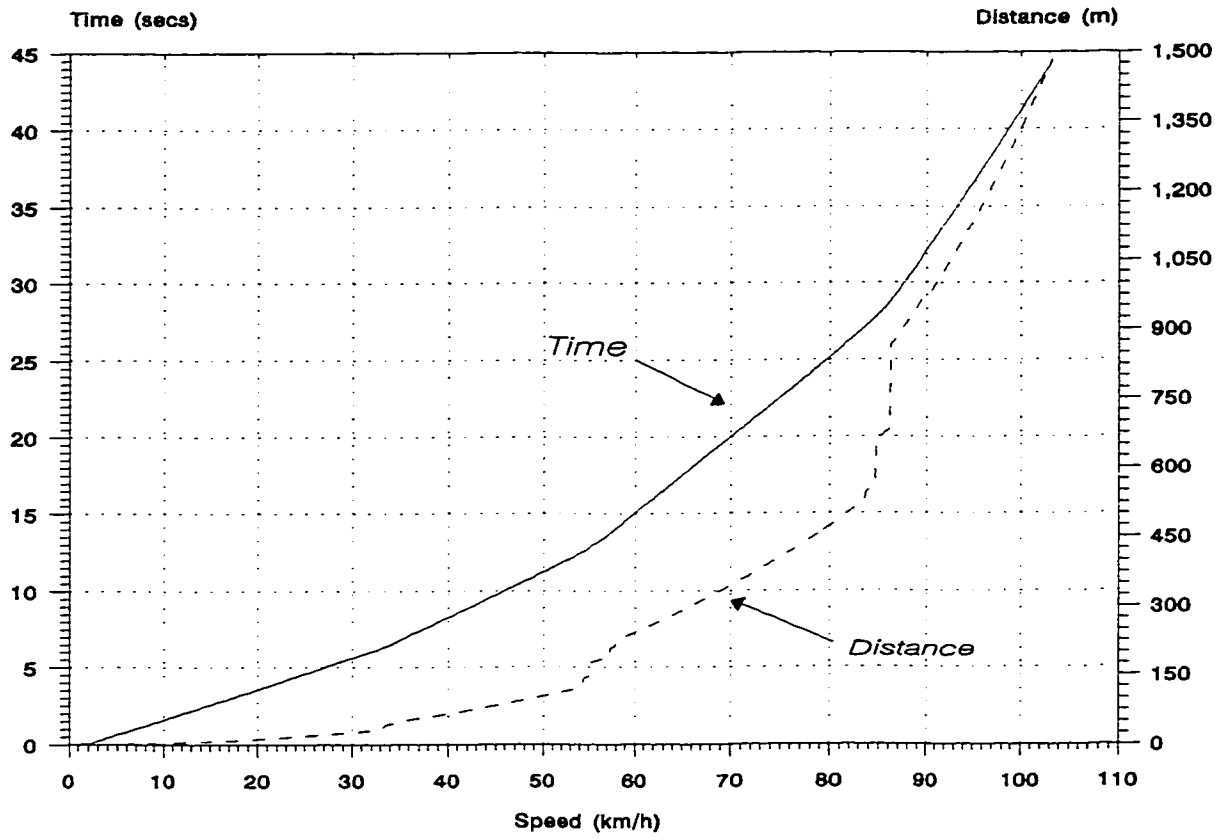

Figure 4.11 Electric Drive Acceleration Response.

4.4 Fuel Economy Analysis

The performance results of the hybrid and electric drives, in terms of achieving the best acceleration times, have been determined in the previous sections. Consequently, in this section the operating conditions that would lead to the most efficient use of the Neon HEV will be analyzed.

The vehicle drive configuration does not change. The driver's concern though, is not to achieve the best acceleration but rather to minimize energy use and to, subsequently, extend the vehicle range. This situation will be referred to as economy mode. Due to the combined motor and engine characteristics, two conditions of 0-60 km/h and 0-100 km/h are examined. The best fuel economy is determined by simulating two drive circuits over distances of 1 km, 4 km and 10 km and consisting of a 0-60-0 km/h cycle and a 0-100-0 km/h cycle. The optimal shift speed for economy driving is realized by examining when the largest energy efficiency (km/kWh) rate would occur. The drive cycles can be divided into three different phases: acceleration, steady state and braking. During the acceleration portion of the cycles the electric motor is used in conjunction with the engine. For the steady state portion, only the engine is on. During the deceleration portion of the cycle both powerplants are off; the brakes are used to slow down the vehicle and fuel is conserved. A typical cycle is illustrated in Figure 4.12. The proposed cycle makes vehicle road testing feasible without requiring the use of a vehicle

dynamometer at a standardized driving cycle. A comparison with standardized cycles is performed later in the analysis.

Energy consumption is calculated for the hybrid drivetrain by examining the amount of energy that is supplied to each individual powerplant. To calculate the consumption of electrical energy, the electric power, supplied to the motor by the controller, is calculated over a specific time range and then adjusted for the battery and electric motor/controller efficiency as it is shown in Equation 4.11.

$$EN_{MOT} = \sum \left(\frac{Motor_{TRQ} \cdot \omega_e}{\eta_e} \cdot \Delta t \right) \tag{4.11}$$

The knowledge of the fuel consumption characteristics of the engine, (Figure 5.6) enables the calculation of energy consumed by the engine over a specific period of time (Equation 4.12). The lower heating value (Q_{LHV}) of natural gas is assumed as being 47.8 MJ/kg [39].

$$EN_{ICE} = \Sigma \left(\frac{sfc}{3600} \cdot P_{ICE} \cdot Q_{LHV} \cdot \Delta t \right) \tag{4.12}$$

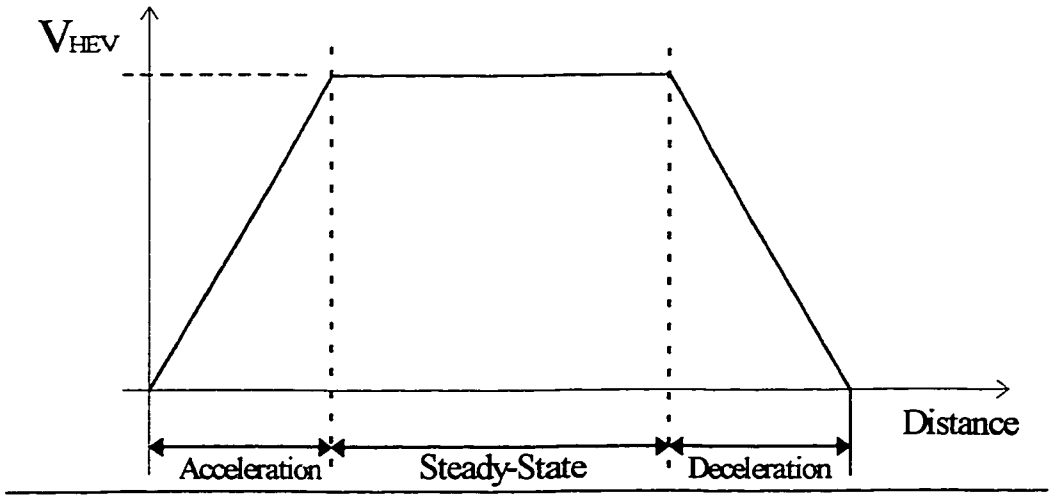

Figure 4.12 A Simulation Drive Cycle.

During the acceleration portion of the cycles, both powerplants are used so that the cruise speed of 60 km/h or 100 km/h can be reached quickly and efficiently. After reaching the designated speed, the electric motor operation is not required anymore (especially on a level road) and it is turned off. During the deceleration portion of the cycle, the fuel system will be completely shut-down. Thus, there will be no energy consumption from either powerplant. However, with the electric motor and drivetrain configuration used there is no possibility of energy recovery during decelerations.

4.4.1 Determination of Optimum Conditions and Drive Cycle Simulations

As it was shown in the previous sections of this chapter, a similar simulation is performed to determine the optimal conditions that will produce the best overall fuel economy. Drivetrain speed at shifting is varied to determine the greatest driving distance achieved with the least amount of powerplant energy.

The energy consumption for the economy mode acceleration of 0-60 km/h, with the shifting occurring at the optimal speed of 2000 rpm, is illustrated in Figure 4.13a (Total: 688 kJ). The drivetrain data also accounts for the drag forces. The steady state phase will be performed while in fourth gear. As a comparison, the energy consumption for the performance mode acceleration to 60 km/h is shown in Figure 4.13b (Total: 822 kJ).

a)

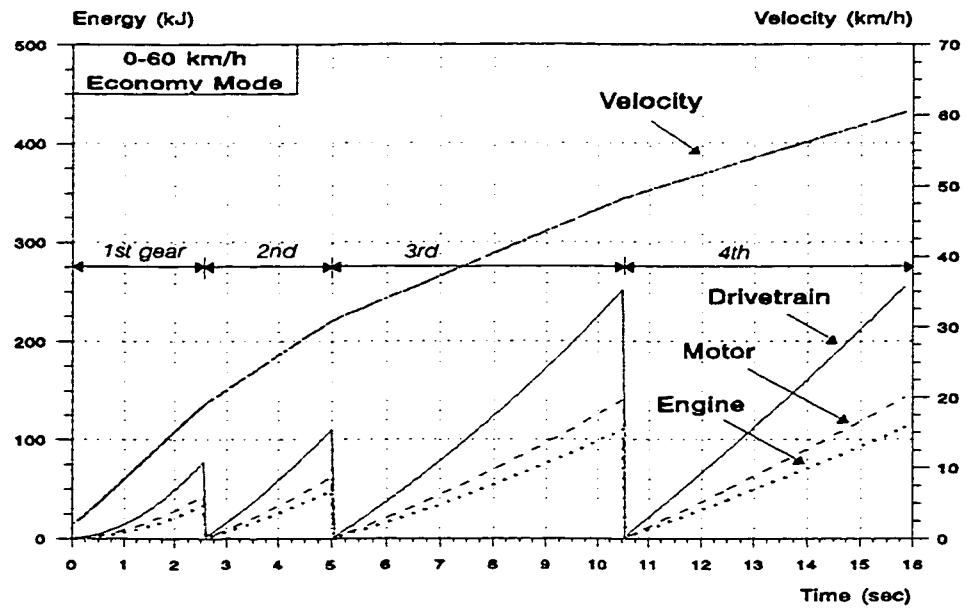

b)

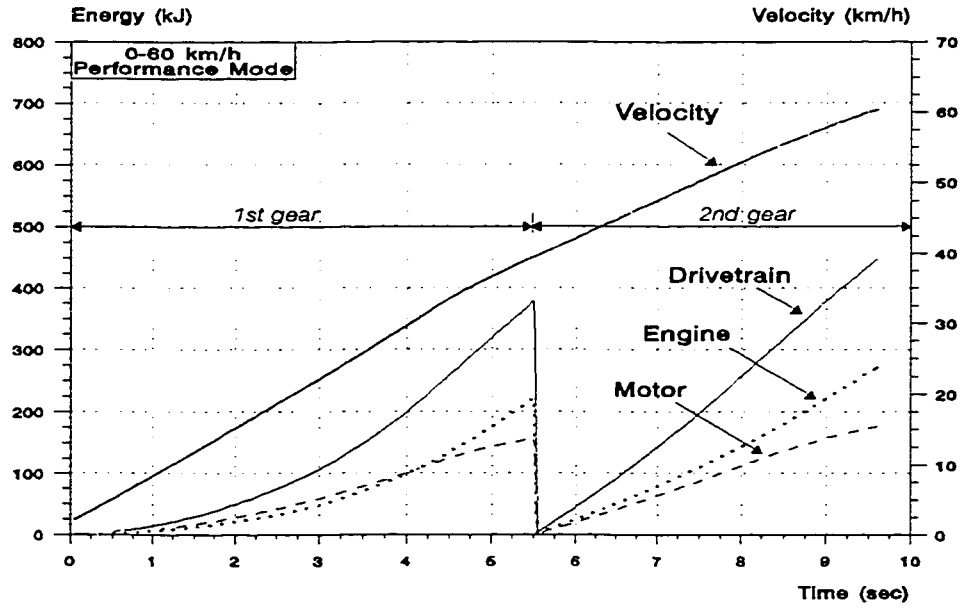

Figure 4.13a&b Energy Consumption for Acceleration to 60 km/h.

It is seen that the smallest combined energy consumption occurs when the gear shifting is performed at a low speed of 2000 rpm. With this shifting pattern, the acceleration portion of the cycle is long and there is a minimal energy consumption by the powerplants. The length of the steady-state portion of the

cycle is comparatively short and the engine is operated for only a short period during this portion. The engine is also operating in a region of low specific fuel consumption. The results are summarized in Table 4.9 and shown in Figure 4.14.

Table 4.9 A Summary of the 60 km/h Drive Cycle Simulation.

	Energy Efficiency Distance/Energy - (km/kWh)		
Drivetrain RPM at Shifting	**1 km cycle**	**4 km cycle**	**10 km cycle**
2000	2.80	3.89	4.23
2500	2.66	3.85	4.23
3000	2.61	3.83	4.22
3500	2.56	3.80	4.21

The 1 km cycle is a typical situation that would be encountered when driving within a city; whereas, the 4 km and 10 km cycles would be typical of driving on major arteries within a city and its suburbs. Highway driving will be examined for the 0-100-0 km/h cycle.

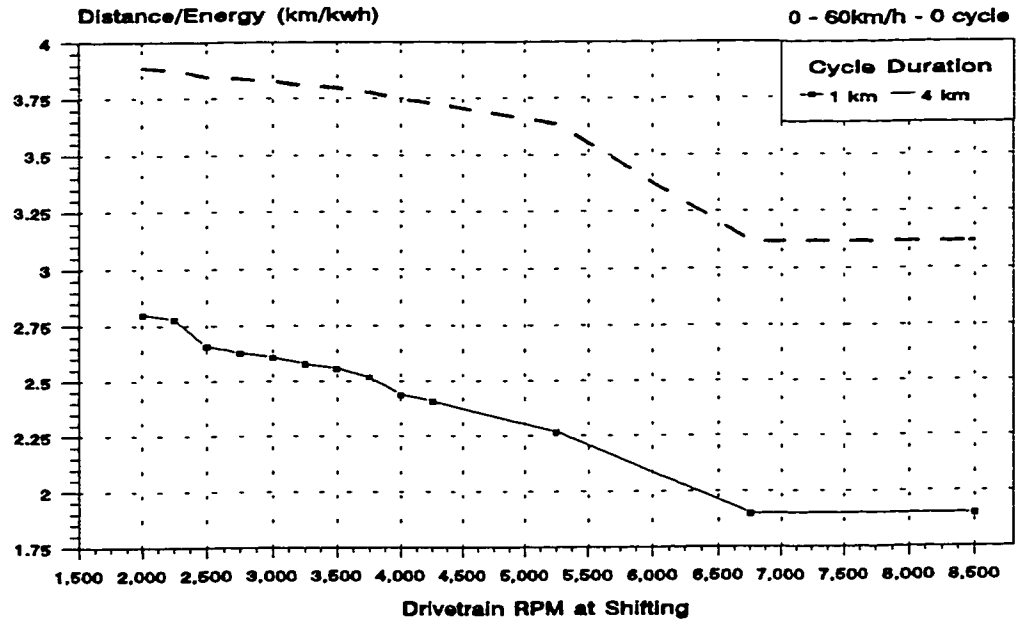

Figure 4.14 Determination of Optimal Energy Efficiency for a 0-60-0 km/h Cycle.

An analysis for highway driving is similarly performed. Drivetrain speed at shifting is varied to determine the optimal conditions to accelerate and to subsequently cruise at 100 km/h. The deceleration portion of the cycle is effected similarly as in the 0-60 km/h analysis. The results for the 0-100 km/h drive cycle simulation are summarized in Table 4.10 and illustrated in Figure 4.15.

Table 4.10 A Summary of the 100 km/h Drive Cycle Simulation.

	Energy Efficiency Distance/Energy - (km/kWh)	
Drivetrain RPM at Shifting	**4 km circuit (Highway - Cruise)**	**10 km circuit (Highway - Cruise)**
3000	2.50	2.49
3150	2.52	2.50
3500	2.14	2.34
3750	2.13	2.34
4250	2.10	2.31

The 4 km and 10 km cycles at 100 km/h, simulate commuting between suburb and urban locales using highways. It is seen that the optimal drivetrain shift speed required to accelerate and to subsequently cruise at 100 km/h is 3150 rpm. As it is illustrated in Figure 4.15, the energy efficiency in this cycle peaks at the 3150 rpm shift point, but drops drastically beyond this shift point. This occurrence is due to the duration of the steady state phase of the cycle. The energy consumption for the economy mode acceleration of 0-100 km/h, with the shifting occurring at the optimal speed of 3150 rpm, is illustrated in Figure 4.16. It is seen that all five gears are required to accelerate to 100 km/h.

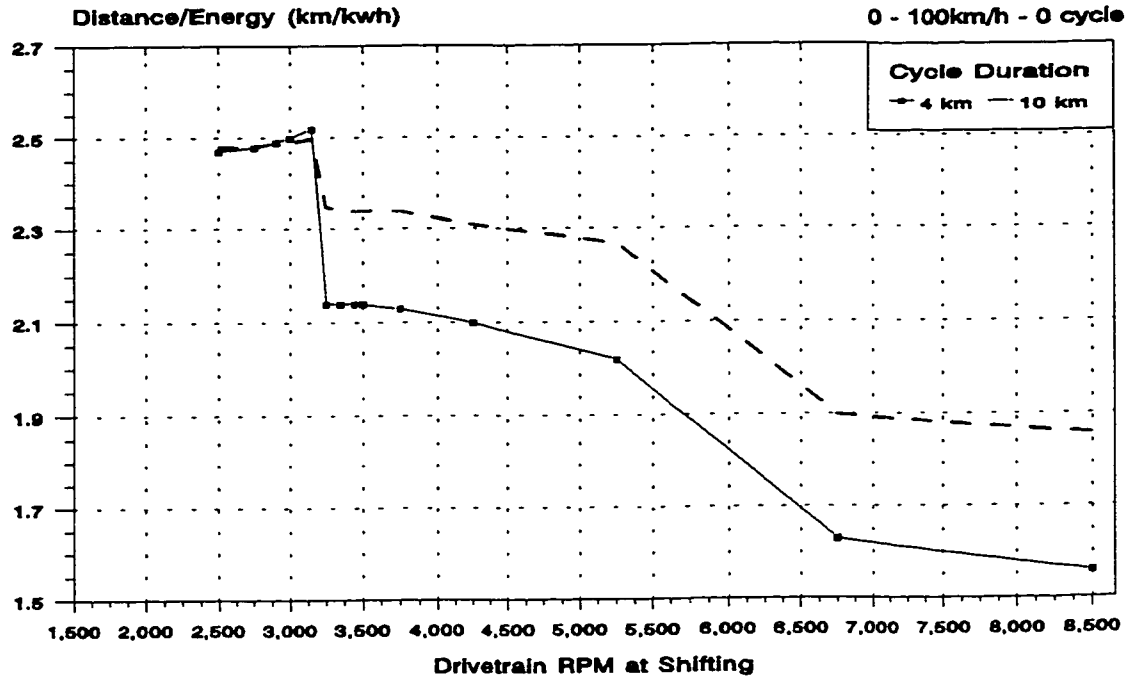

Figure 4.15 Determination of Optimal Energy Efficiency for a 0-100-0 km/h Cycle.

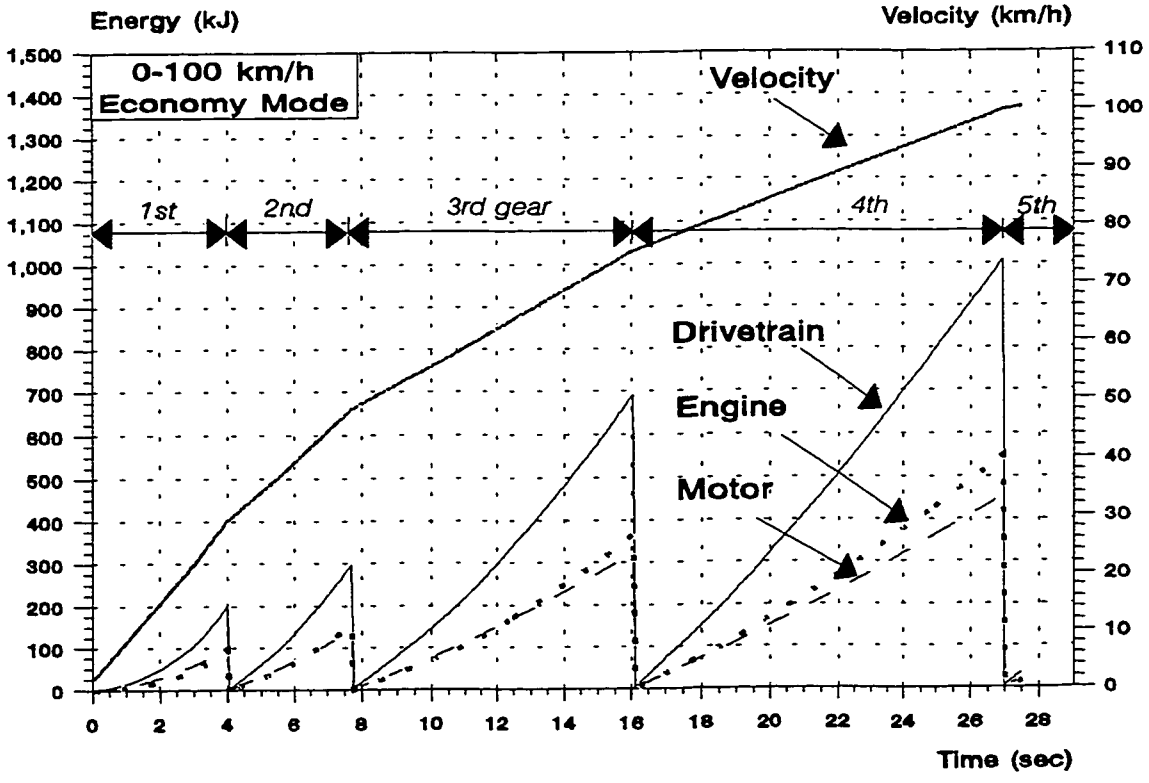

Figure 4.16 Energy Consumption for Economy Mode Acceleration of 0-100 km/h.

The results for the 0-60-0 km/h and the 0-100-0 km/h cycles can be redefined to reflect energy consumption that is equivalent to a gasoline powered vehicle. An equivalent gasoline fuel economy can be determined knowing that the energy content of gasoline for 1 U.S. gallon is 120 600 kJ [40]. It is also known that 1 kWh of energy is equivalent to 3600 kJ. Thus, the Neon HEV fuel economy for the specific drive conditions that were examined in this chapter, is summarized in Table 4.11. The calculated energy consumption (ℓ /100 km) might seem quite low but it should be realized that the battery state of charge is not taken into account and that the vehicle is cruising at either a constant 60 or 100 km/h. Eventually, repeated use of the electric drive will diminish the available electric energy and vehicle performance will also diminish. These results provide a good analysis of short duration trips having the batteries recharged at home or at work, while the vehicle is stationary.

Table 4.11 Economy Mode Fuel Consumption Simulation Summary.

Condition / Cycle	**Energy Efficiency (km/kWh)**	**Equivalent Fuel Consumption ℓ /100 km (mpg$_{US}$)**
Cycle: 0-60-0 km/h		
1 km cycle	2.80	4.04 (58.2)
4 km cycle	3.89	2.90 (81.0)
10 km cycle	4.22	2.67 (87.9)
Cruise @ 60 km/h	4.48	2.52 (93.2)
Cycle: 0-100-0 km/h		
4 km cycle	2.52	4.48 (52.5)
10 km cycle	2.50	4.52 (52.0)
Cruise @ 100 km/h	2.49	4.54 (51.8)

Other drive cycles that incorporate driving over slopes have also been examined. Two conditions consisting of a 1.75% and a 6.5% grade, are analyzed in terms of energy consumed during cruising in economy mode. The results for 60 km/h and 100 km/h are listed in Table 4.12. It can be seen that there is a decrease in energy efficiency of approximately 38-80%, as compared to the level surface, depending upon the road inclination and the cruise speed. A total fuel economy for various conditions can be developed by combining the results of Tables 4.11 and 4.12.

Table 4.12 Energy Efficiency and Fuel Economy for Driving over Slopes.

	Energy Efficiency (km/kWh)			**Equivalent Fuel Consumption ℓ/100 km (mpg$_{US}$)**		
Condition	**Grade of Surface**			**Grade of Surface**		
	0%	**1.75%**	**6.5 %**	**0%**	**1.75%**	**6.5 %**
Cruise @ 60 km/h	4.48	2.16	0.89	2.52 (93.2)	5.23 (45.0)	12.70 (18.5)
Cruise @ 100 km/h	2.49	1.54	0.77	4.54 (51.8)	7.34 (32.1)	14.67 (16.0)

4.4.2 Advanced Fuel Economy Simulation

The fuel economy analysis was further advanced with the use of a commercial vehicle simulation package. The *Eagles v.1.1 - An Electric and Gasoline Vehicle - Fuel Efficiency* software package was supplied by Argonne National Laboratory [41]. A gasoline vehicle (GV) or an electric vehicle (EV) analysis can be performed for fifteen different driving profiles. Unfortunately, this software is not sophisticated enough to perform a simulation for a hybrid electric vehicle. Since, in the Neon HEV the engine is the primary drive unit, (the electric

motor being used occasionally) the GV simulation was used for the fuel economy analysis. The GV input variables were modified to reflect the Neon HEV's drive design, using the combined torque of Figure 4.3. The input variables and associated data are listed in Table 4.13.

Table 4.13 *Eagles v.1.1* Gasoline Vehicle Input Data for NHEV Simulation Analysis.

Software Variables	Input Data Set
curb wt. w/o battery (kg), cwnb	1267.0
payload (kg), pLw	130.0
accessory power demand (kW), pacc	0.00
drivetrain eff. (Fraction), effd	0.95
rolling res. coeff., (--), k0	0.008
frontal area, (m^2), farea	1.914
drag coeff., (--), cd	0.30
grade, (%), grade	0.0
engine displacement, (liter), vdisp	0.750
N/v, (rpm/mph), rpmmph	51.16
number of cylinder, (--), cyl	3
engine ind. power eff. (--), eta	0.408
engine friction factor (kJ/rev/ℓ), fk	0.220
cold start friction multiplier, (--), fcold	1.07
idle friction multiplier, (--), fidle	1.16
engine idle speed, (rpm), nidle	850
engine rpm at max. torque, (rpm), nt	3400
engine torque @ nt, (ft-lb), tmax	83.8
engine rpm at max. power, (rpm), np	8500
engine torque @ np, (ft-lb), tpmax	41.9
number of gears, (--), LGEAR	4
shift schedule (mph, gear ratio) pairs	0/3.54, 21.7/2.13, 36.0/1.36, 56.0/1.03

The engine and motor characteristics were combined and the maximum torque and power values are indicative of the combined hybrid-power drive peak

values, as it was illustrated in Figure 4.3. The input data values for top speed/rpm ratio, along with the number of gears and shift schedules are obtained from the economy mode analysis. For the input data set, the output from the 0-60 km/h acceleration, determined in section 4.4.1, was used.

Four driving profiles representing city type conditions were used to complete the simulation. The drive profiles that are illustrated in Figures 4.17a & 4.17b are: the SAEj227ad Cycle, the EPA New York City Cycle (NYCC), the EPA Urban Dynamometer Driving Cycle (FUDS), and the Los Angeles City Cycle (LA-92). The resulting simulation output for each cycle is summarized in Tables 4.14a and 4.14b.

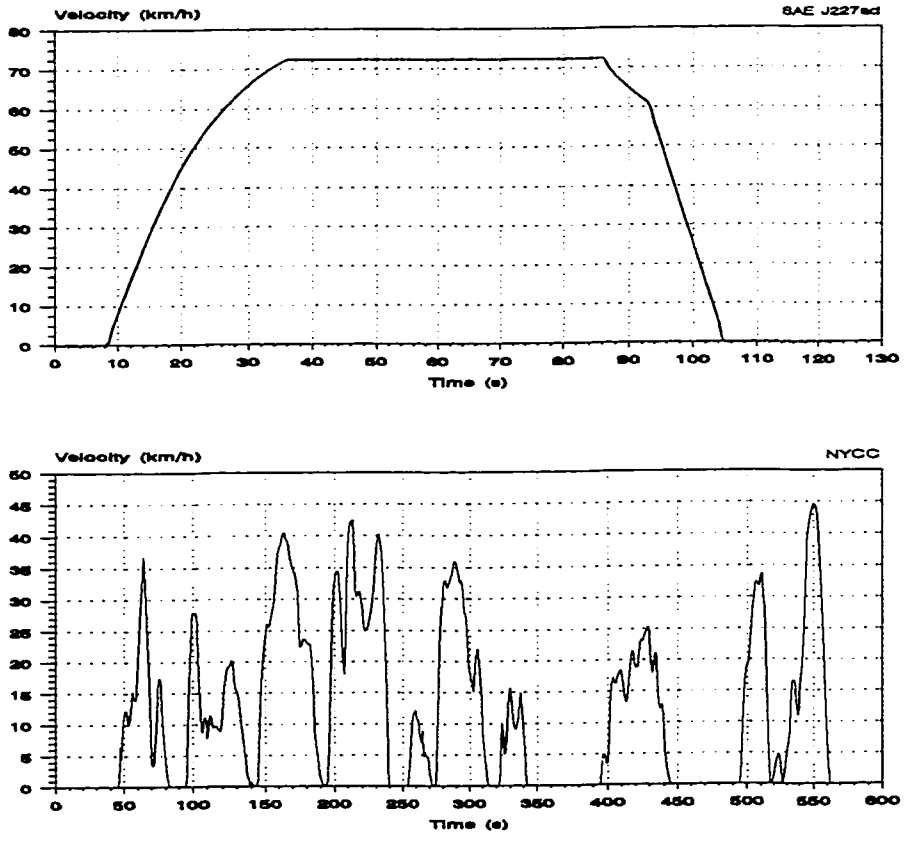

Figure 4.17a Drive Profiles: SAEj227ad and NYCC.

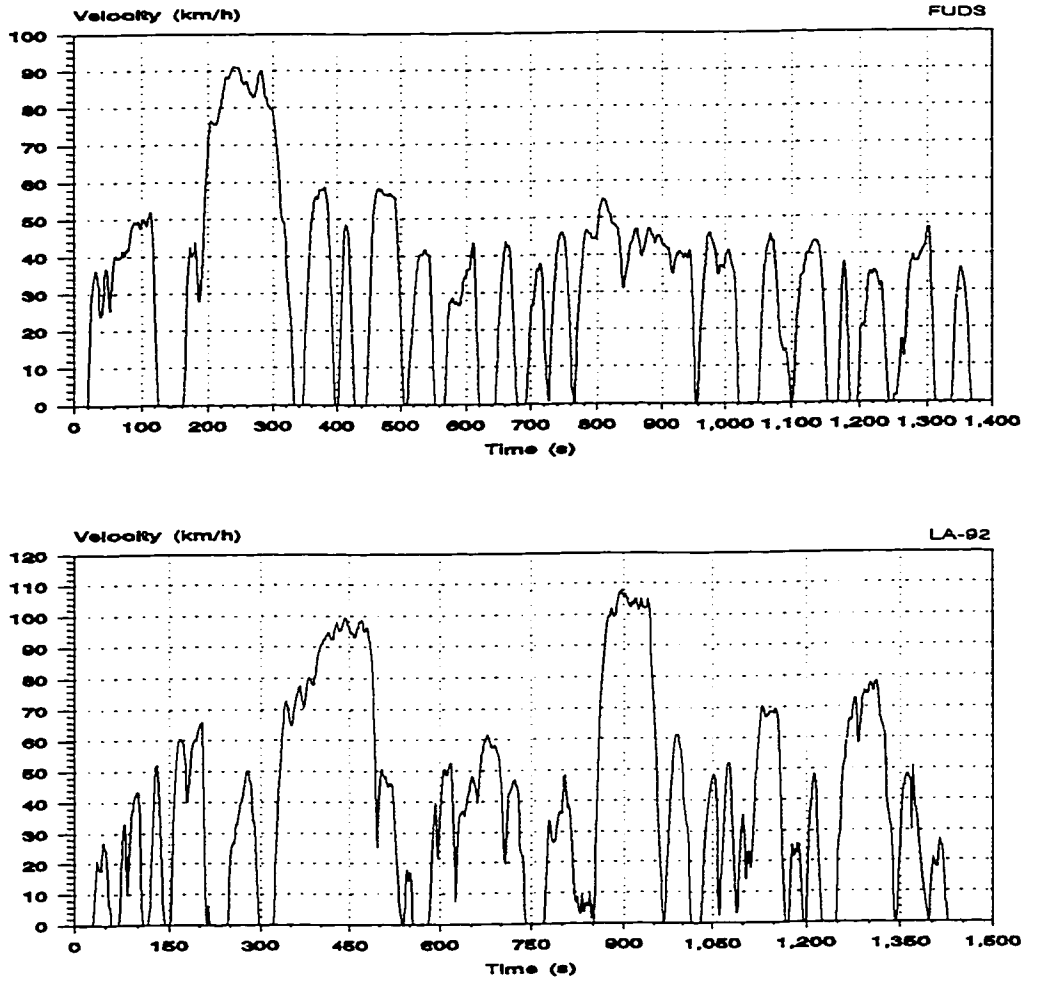

Figure 4.17b Drive Profiles: FUDS and LA-92.

Table 4.14a *Eagles v.1.1* Fuel Economy Output -- Data Set 1 (SAEj227ad & NYCC).

Output Results	SAEj227ad Cycle	NYCC
Fuel Consumption , kJ/m	1.445	2.479
Fuel Efficiency, *l*/100 km (mpg_{US})	4.54 (51.86)	7.74 (30.24)
Cycle Driving Distance, km	1.589	1.897
Cycle Duration, s	122.0	600.0
Vehicle Standing Time, s (%)	25.0 (20.49)	218.0 (36.33)
Vehicle Running Time, s (%)	97.0 (79.51)	382.0 (63.67)
Vehicle Acceleration Time, s (%)	28.0 (22.49)	181.0 (30.17)
Vehicle Deceleration Time, s (%)	19.0 (15.57)	190.0 (31.67)
Maximum Vehicle Speed, km/h	72.40	44.57
Cycle Average Speed, km/h	46.89	11.38
Average Running Speed, km/h	58.97	17.88

Table 4.14b *Eagles v.1.1* Fuel Economy Output -- Data Set 2 (FUDS & LA-92).

Output Results	FUDS Cycle	LA-92 Cycle
Fuel Consumption , kJ/m	1.517	1.694
Fuel Efficiency, *l*/100 km (mpgus)	4.76 (49.42)	5.32 (44.26)
Cycle Driving Distance, km	11.990	15.794
Cycle Duration, s	1371	1431
Vehicle Standing Time, s (%)	243.0 (17.72)	213.0 (14.89)
Vehicle Running Time, s (%)	1128.0 (82.28)	1218.0 (85.11)
Vehicle Acceleration Time, s (%)	545.0 (39.75)	549.0 (38.69)
Vehicle Deceleration Time, s (%)	477.0 (34.79)	490.0 (34.24)
Maximum Vehicle Speed, km/h	91.20	108.12
Cycle Average Speed, km/h	31.48	39.73
Average Running Speed, km/h	38.27	46.68

The aforementioned cycles are representative of city testing on vehicles performed by the EPA. Sharp peaks and descents during the cycle indicated acceleration and deceleration phases experienced in the 'stop and go' city traffic. Even though the NYCC and LA-92 cycles are similar in nature they are indicative of city driving in two populous American cities.

Even though the output data does not provide a true complete representation of the Neon HEV electric drive characteristics, the vehicle's performance over varying conditions can easily be examined with this simulation package. Having a breakdown of the vehicle running, standing, acceleration and deceleration times provides a basis to further optimize the hybrid drive control strategy and to improve upon energy efficiency. During the standing time period, the CNG fuel system can be shut-off to reduce unnecessary fuel consumption. The electric motor will be used to supplement the engine power only during the acceleration

time period. Also, as it will be discussed in Chapter 7, during the deceleration time period the propulsion batteries can be recharged through the regenerative braking using the electric motor/controller with the ability for energy recuperation.

The drive cycle simulations examined in section 4.4.1 provide results that are indicative of ideal driving situations. It can be seen that the standardized city cycles (FUDS, LA-92, etc..) provide a better representation of everyday driving situations. But, as a first step analysis without resorting to dynamometer tests, the drive cycle simulation proposed in this thesis provides a good initial overview of energy consumption; in effect, it gives an upper bound on the maximum fuel economy that can be achieved during ideal conditions. The SAE j227ad cycle has a similar profile as with the proposed cycle in this thesis research. A comparison of the 0-60-0 km/h and the 0-100-0 km/h cycle with the SAE cycle, detailed in Table 4.15, illustrates that it is feasible to use the simulated cycles, as proposed in this thesis, for a quick determination of a vehicle's energy consumption.

Table 4.15 Simulation Cycle Comparison.

Output Results	0-60-0 km/h	0-100-0 km/h	SAE j227ad
Cycle Driving Distance, km	1.0	4.0	1.589
Cycle Duration, s	70.0	130.0	122.0
Maximum Vehicle Speed, km/h	60.0	100	72.4
Energy Efficiency, (kJ/m) km/kWh	(1.287) 2.80	(1.428) 2.52	(1.445) 2.49
Fuel Consumption ℓ/100 km (mpg_{US})	4.04 (58.2)	4.48 (52.5)	4.54 (51.86)

4.4.3 Experimental Fuel Economy Results

Examining data from the 1995 HEV Challenge [30], the experimental

results can be used to compare with the simulated data. At the Challenge, the Neon HEV was driven for 145 km on a 2.89 km test track. The average lap speed ranged from a minimum of 64.4 km/h to a maximum of 88.5 km/h, with speed limits to adhere to the track banks and straight-ways, (a schematic of the track is shown in Appendix 1). A malfunction with the electric drive required that the course would be driven with the CNG engine only. The amount of CNG that was supplied, was equivalent to 11 liters of gasoline fuel. The vehicle's fuel consumption was thus 13.2 km/*l*. In a separate event, when the electric drive was still operational, 4.34 km were driven on the same track solely with electric power. This resulted in 0.3 kWh of electric energy consumed. A combined Neon HEV fuel consumption is extrapolated using the experimental results that were obtained from the engine and electric only conditions. A summary of these results and calculations is shown in Table 4.16.

Table 4.16 HEV Challenge Fuel Consumption Results.

Condition / Event	**Energy Efficiency km/*l* (km/kWh)**	**Equivalent Fuel Consumption *l* /100 km (mpg$_{US}$)**
Neon HEV- 145 km [solely engine drive]	13.2 (1.49)	7.58 (31.0)
Neon HEV - 4.34 km [solely electric drive]	(14.47)*	----------
Neon HEV- Calculated [combined 149.34 km]	(1.87)*	6.04* (38.9)*
Stock Neon Car [specifications]	12.3 (1.39)	8.13 (28.9)
* Not Corrected for the Battery State of Charge		

These competition data are not representative of a HEV drive with

corrected data for the battery state of charge, but it gives a real world analysis of the behaviour of two different powerplants. Using the simulated results in section 4.4.1 and from Table 4.12, a HEV fuel consumption can be simulated given a breakdown of the track speeds and grades. Thirty-five percent of the drive is over a 0 % grade at a maximum speed of 84 km/h. Thirty-seven percent of the drive is over an approximate 1-2 % grade at an average speed of 48 km/h. Twenty-eight percent of the drive occurs over a banked surface at an approximate 6.5 % grade at a maximum speed of 80 km/h. Interpolating for these speeds and for the specific grades, an approximate theoretical *maximum* attainable fuel economy (5.06 *l*/100 km) can be derived for a lap on the track; the data is listed in Table 4.17

Table 4.17 Simulated Fuel Consumption for Test Track Conditions.

Track Grade and Respective Speeds	**Portion of Drive on Track Section**	**Interpolated Fuel Consumption for Portion of Track (mpgUS)**
0% : 84 km/h	35%	70 mpg * 35% = *24.5 mpg*
2% : 48 km/h	37%	46.5 mpg* 37% = *17.2 mpg*
6.5% : 80 km/h	28%	17.3 mpg* 28% = *4.8 mpg*
Totals	100%	5.06 *l* /100 km or 46.5 mpg

The procedure summarized in Table 4.17 illustrates how the simulated drive cycles can be applied to the test track to obtain a general fuel consumption result, without having to use expensive and time consuming procedures. It is difficult to compare the simulated numbers with the experimental ones, since the vehicle was not operating at its designed capacity and peak performance levels.

4.5 Summary

It was shown that the design and analysis of a hybrid electric drive requires a thorough examination of the vehicle performance and fuel economy. The hybrid drive system was developed for a five speed transaxle configuration. The intricacy of the proposed system required a performance analysis for both low and high speed scenarios. Available transaxle gear shifting was examined and the optimal gear shifting was determined for different operating modes. A simple drive cycle simulation was proposed, to offset the problems encountered in determining the vehicle's energy consumption, when sophisticated dynamometer equipment and software programs are not available. Using commercial vehicle simulation packages as a comparison, it was shown that the proposed simulation is a good tool that can be used for a quick initial understanding of a hybrid vehicle's energy efficiency.

5. HYBRID ELECTRIC NEON CONVERSION DESIGN CONCEPT

In this chapter, the particular components used in the vehicle conversion and their incorporation in this vehicle design will be discussed. In the sub-sections that follow, there will be a specific description and an analysis of the design pertaining to each area of the vehicle. The topics discussed are as follows: the vehicle design configuration, the vehicle handling, the internal combustion engine (ICE) conversion to compressed natural gas (CNG), the fuel system design, the fuel delivery strategy, the electric motor selection, the drive strategy, and the heating and cooling systems.

5.1 Vehicle Design Configuration

The design configuration for the Neon conversion was set within the parameters that were outlined for the HEV 1995 Challenge competition. A parallel power-assist configuration was deemed an appropriate interpretation of the competition rules. Thus, this vehicle can be operated in two distinct drive modes: as a zero emissions vehicle (ZEV) and as a hybrid electric vehicle (HEV). In ZEV mode, the vehicle will be used for short trips, primarily in city driving conditions. In HEV mode, the internal combustion engine is the main power unit that receives assistance from the electric motor only when an increased demand for driving power is required. The control scheme illustrating this configuration is shown in Figure 5.1.

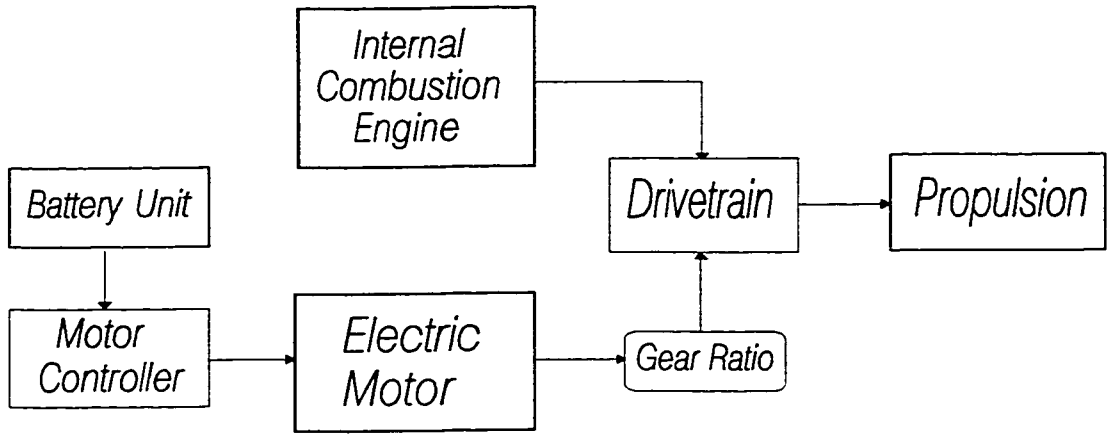

Figure 5.1 Hybrid Electric Neon Drive Configuration.

5.1.1 The Arrangement of the Neon HEV Components

A Chrysler Neon (1995) was converted into a hybrid electric vehicle, taking into consideration the hypothetical future possibility of the mass production of such a vehicle. The objective was to minimize changes to the existing Neon platform so that the cost to implement the conversion would not be a prohibitive factor for the manufacturer. The conversion components were chosen with an emphasis being placed on their commercial availability, performance, cost and shipping lead-time.

The Neon HEV (NHEV) power-assist design combines the ICE with the electric motor drive into a single unit which, in turn, is coupled to the original front wheel drive Neon five-speed transaxle. The energy storage systems, the battery packs and the CNG tank are located towards the rear of the vehicle, since their placement is constrained by the weight and volume of the associated

components. The vehicle structure, except for the area reserved for mounting of the battery pack, was kept intact. There were no modifications to the vehicle's exterior; thus, the vehicle's original aerodynamic characteristics were retained. The location of the larger components was arranged such that the weight was distributed as equally as possible over the front and rear vehicle axles. It was important to minimize vehicle weight in order to retain the vehicle handling capabilities. It was also important to retain the carrying capacity of four adult passengers and therefore, the vehicle interior was not modified.

Ancillary electrical components that belong to the electric propulsion system were located in the spare-tire wheel well. The space saver spare-tire was relocated and positioned vertically behind the rear seats; it is now accessible from the inside of the car by invoking the 60/40 split folding seat back.

Vehicle safety has not been compromised but rather enhanced with the multitude of features that will interrupt power and/or fuel delivery in the event of a mishap. As a competition requirement, there is a fire extinguisher that was installed which, if desired, can be permanently kept in the vehicle.

The addition of a heating and air-conditioning system invoked a few more constraints relating to component placement, as well as to the vehicle's performance characteristics; it is analyzed in later chapters.

A detailed vehicle schematic, along with a description of the major components, is shown in Figure 5.2.

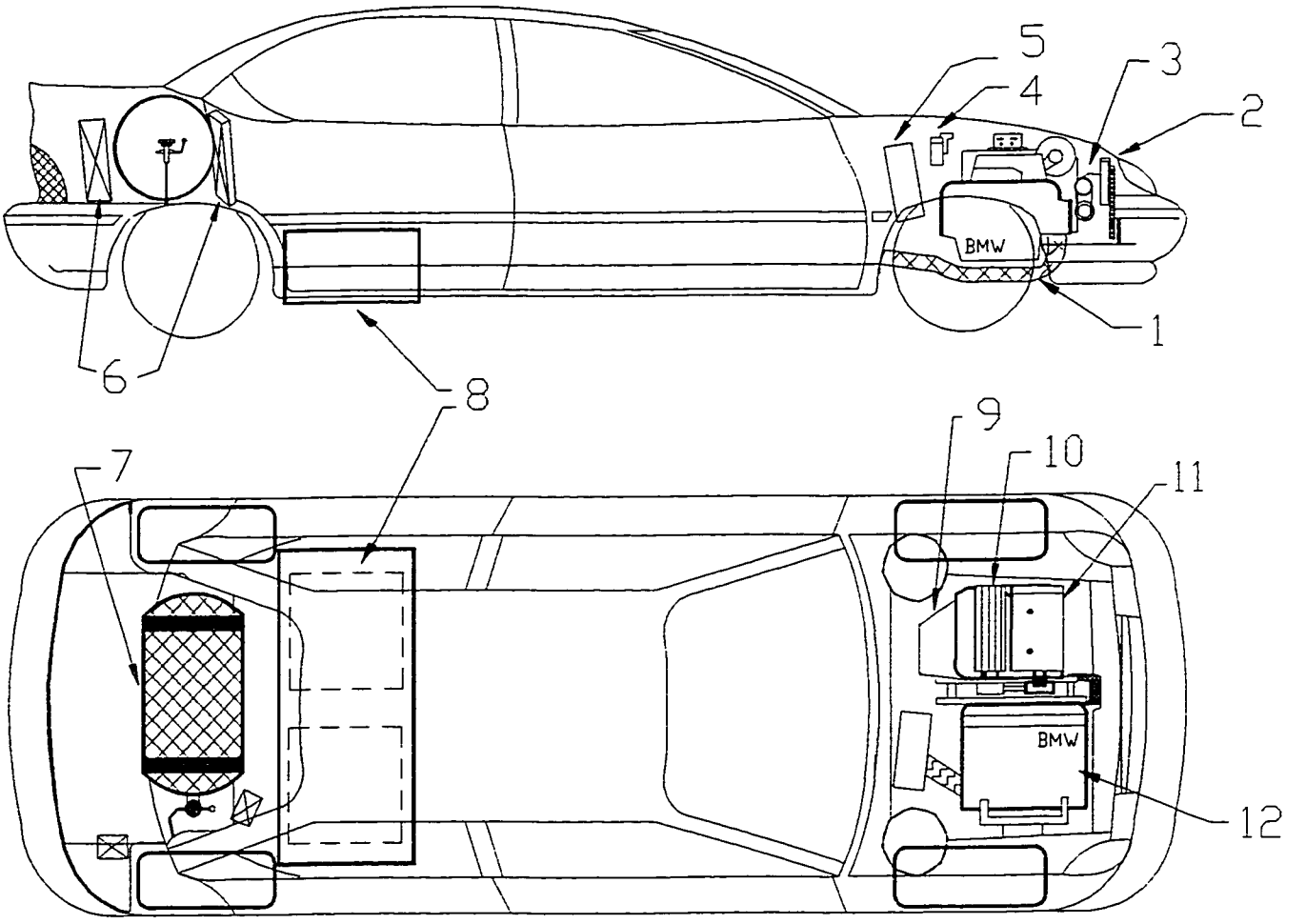

1. BMW Exhaust
2. Radiator and Condenser
3. Electric Motor & A/C Compresor
4. Electric Vacuum Brake Pump
5. Electric Heater
6. Battery Chargers
7. CNG Cylinder (EDO Literider)
8. Battery Containers
9. Neon Five-Speed Transaxle
10. Motor Controller
11. Electric Drive Motor
12. ICE - BMW 750cc

Figure 5.2 The Concordia Neon HEV Layout.

5.1.2 HEV Powertrain Design

The Advanced DC electric motor and the BMW K75 engine are jointly coupled to the original Neon five-speed transaxle. An extension shaft is connected

to the existing Neon flywheel and the dry clutch unit. A second half-shaft is attached to the original BMW clutch assembly. Power from the electric motor is transmitted through a chain driven sprocket by a collar joining the two half-shafts. The Neon half-shaft is supported by a sealed deep groove ball bearing that is placed in a cover plate fastened to the transaxle outer surface. The BMW engine half shaft is installed in another similar bearing, that is located in a cover plate fastened to the engine bell-housing. Three high strength bolts (one inch diameter) join the two cover plates. Two supports, the bearing and the existing Neon flywheel, ensure that the Neon half-shaft is kept aligned. The collar transmits the power and also acts as a locator for the BMW shaft.

A solid shaft instead of two half-shafts could have been used in this design. This would have ensured a simpler design, but assembling the power units with the drivetrain would have been very difficult. Thus, the need for occasional mounting and disassembling of the units justified the half-shaft design.

The NHEV drive is a dual clutch unit that provides the driver with the means to operate the vehicle at two propulsion modes that are denoted as the HEV mode and the ZEV mode. The driver will operate the Neon clutch as it is in a regular car, whereas, the BMW clutch is a part of the components that are used in the driving mode selection process.

HEV mode is always the primary mode of operation. When ZEV mode is required (operation solely by the electric motor) the BMW clutch is disengaged,

thus disconnecting the ICE from the main drive. The assembly of the drive unit is illustrated in Figure 5.3. Depending upon the required drive mode, the BMW clutch functions as a mechanical switch for on-off situations (see the detailed layout in Figure 5.5).

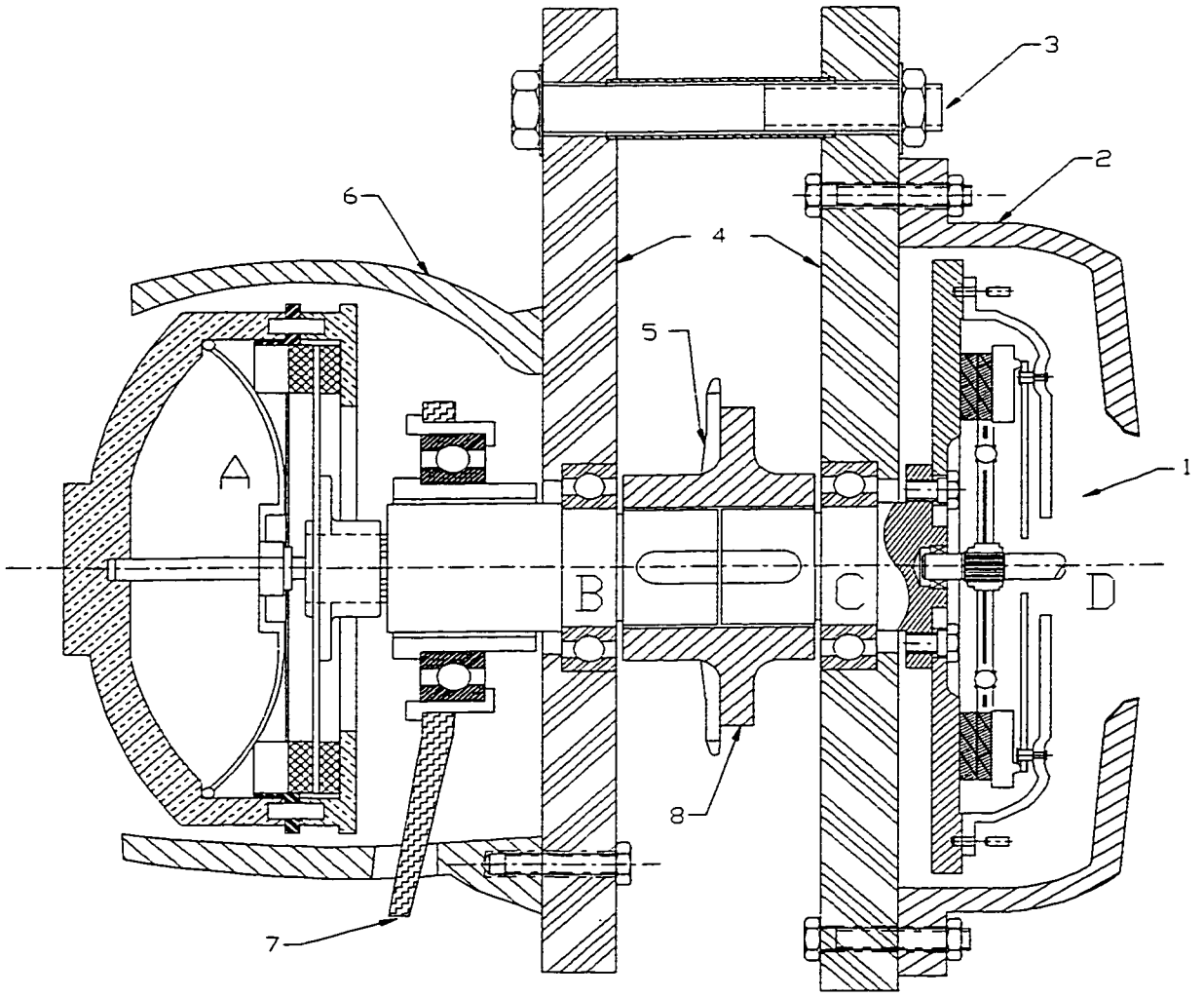

1. Neon Clutch/Flywheel Assembly
2. Neon Transaxle Housing
3. Connecting Bolt
4. Housing Cover Plates
A. BMW Clutch/Spring Assembly
B. BMW HAlf-shaft
5. Motor Sprocket
6. BMW Bell Housing
7. BMW Clutch on/off Lever
8. Half-shaft Hub
C. Neon Half-shaft
D. Neon Transaxle Drive Shaft

Figure 5.3 Powertrain Unit Assembly.

Shown, in Figure 5.4, is a top view of the drive bay with the complete powertrain consisting of the engine and electric motor.

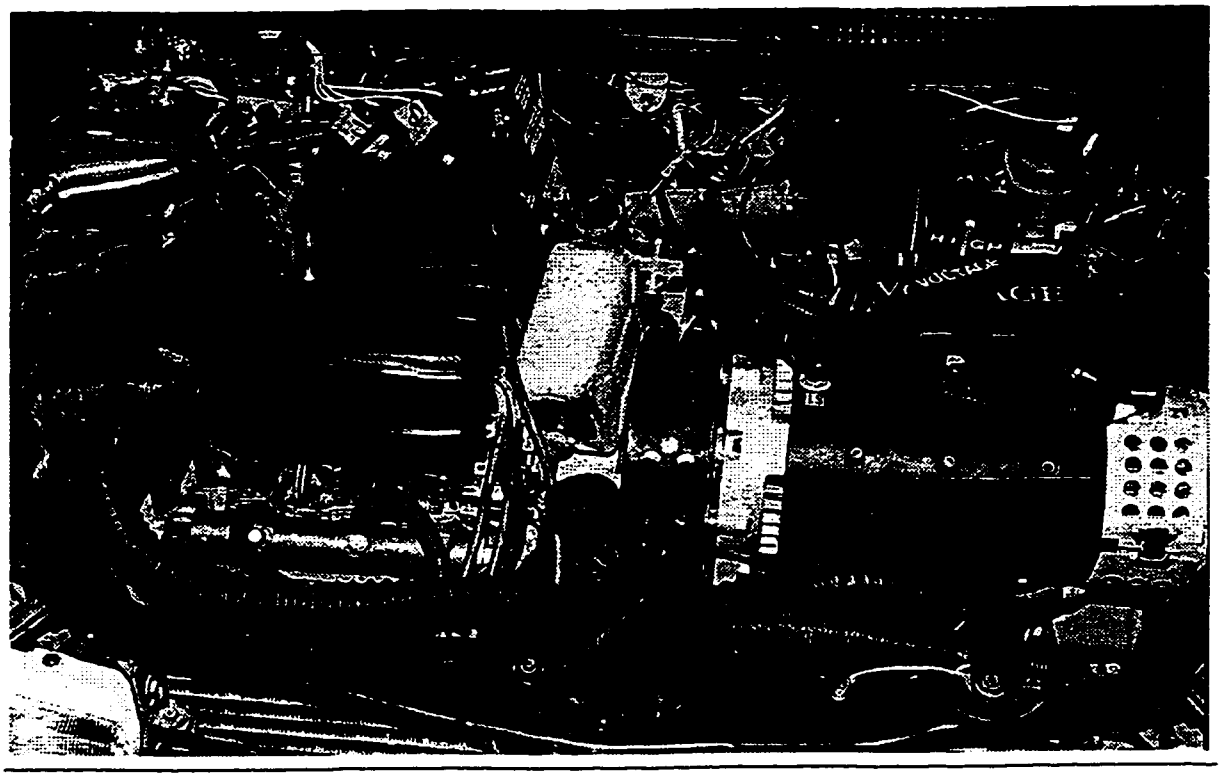

Figure 5.4 Drive Bay Top View.

5.1.3 HEV Mode - BMW Clutch Design

The original BMW clutch was adapted to run in the NHEV drivetrain. As it was shown in Figure 5.3, the BMW clutch and spring assembly were retained. The mechanism's function was not altered but rather adapted to the drive design. The BMW clutch is activated after the force applied to the hand-lever (item-7 in Fig. 5.3) is transmitted through a shaft that is located in the center of the clutch spring. This pin has a maximum stroke of 8 mm. The resulting thrust against the clutch spring disengages the BMW clutch disk.

Referring to Figure 5.3 there are two bearings that are incorporated in this assembly. The force that is applied on the lever acts on a collar that is attached to the outer race of the ball bearing. The inner race is attached to a collar that rotates with the drive shaft. A deep groove ball bearing is used (since it is rated for high speeds), which is sealed and can also handle the required axial load; a typical thrust bearing could not accommodate the aforementioned requirements. Initiated by the lever motion, the collar will slide freely on a journal bearing, depressing the clutch pin. In Figure 5.5, a cross-section view of the BMW clutch-pin assembly is shown. The clutch assembly housing (8) is attached to the engine crankshaft. The pin is inserted in the clutch spring that is attached to the clutch disk. The bearing ensures that the pin rotates freely. When the pin (7) is depressed by the lever, it will in turn depress the inner race of the clutch spring bearing (6), whereas the outer race is fixed to the insert (5).

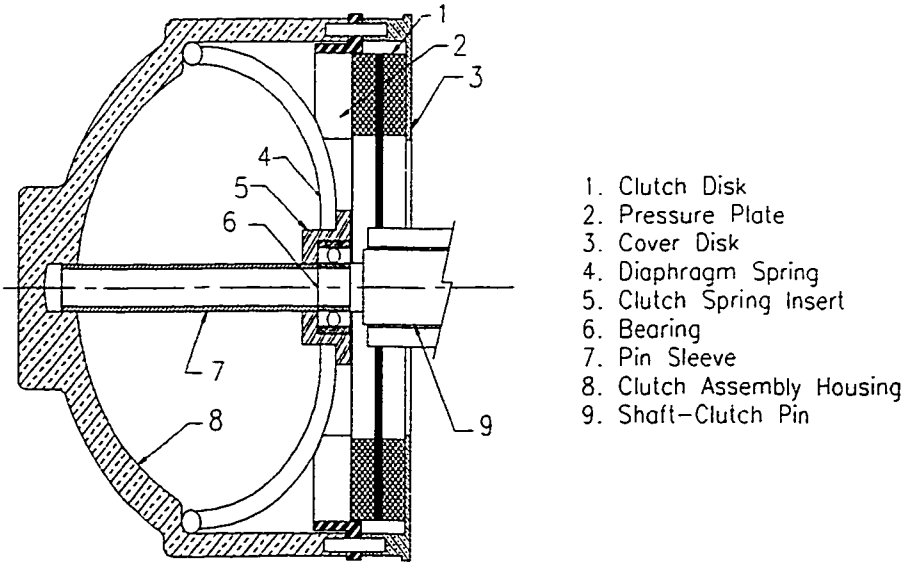

Figure 5.5 BMW Clutch Pin and Bearing Detail.

This assembly was designed to ensure that any small misalignment with the drive shaft would not cause the pin to become stuck in the clutch disk. With the bearing in place, any possible friction that could occur between the disk and the pin is avoided.

The axial load required to disengage the clutch disk was calculated to be approximately 33.7 N (150 lbs). A thrust bearing that is sealed, small enough to fit in the disk and capable of handling the required load was not available. Instead, a deep groove sealed ball bearing (6) was chosen. This bearing is typically used in aerospace applications and is manufactured by Barden Precision Bearings [42] (specifications in Appendix 2). It is rated for a basic dynamic radial load of 31.5 N (140 lbs) and a thrust load of 25.2 N (112 lbs). Since this clutch would be operated only for short periods, this bearing was deemed adequate for this application. Also, according to the manufacturer, the listed load ratings may be exceeded for short time periods.

5.2 Vehicle Handling

The driveability characteristics of this HEV have not been significantly altered, as compared to the production Neon car. There are only minor modifications to the suspension, due to a small increase in the overall vehicle weight. The effect of this increased weight is discussed in the following sections.

5.2.1 Weight Distribution

To ensure vehicle stability and to avoid major structural changes, it was necessary to maintain the weight of the fully loaded NHEV below the gross vehicle weight rating plus 10% (GVWR+10%). This rating was established by the competition organizers and had to be strictly adhered to. It was also required that the maximum front and rear axle weights were not exceeded and that the side-to-side weight distribution was kept within 5%. In Table 5.1 the parameters are listed along with the final loaded NHEV weight and its distribution. The allocated weight parameters are the maximum limits that are set by the vehicle manufacturer. In order to maintain the road worthiness and safety of the existing vehicle, the NHEV design had to respect these limits. For these calculations a loaded vehicle is referred to as a vehicle that includes a driver and a passenger with 10 kg of cargo.

The loaded NHEV weight of 1477.4 kg is well below the maximum allowable vehicle weight. Since, it was required that the NHEV retains a four

passenger capability, it was necessary that with four passengers the weight limit not be exceeded. Thus, at 1477.4 kg there is a reserve of over 200 kg that can be allocated to the rear passengers or for additional cargo.

Table 5.1 Vehicle Weight Analysis.

Allocated Weight Parameters	**Vehicle Weight Results**
GVWR+10% - 1686 kg	Curb Weight - 1090.2 kg
Max. Front axle - 904 kg	Front Axle (loaded) - 828.3 kg
Max. Rear axle - 782 kg	Rear Axle (loaded) - 649.1 kg
Max. Side-to-Side Weight Ratio: 1.05	Side-to-Side Weight Ratio - 1.04
Initial Neon Weight (loaded) -1268.6 kg	**NHEV Weight (loaded)** - 1477.4 kg
Front/Rear Distribution (%) - 62.54 / 37.46	56.06 / 43.94
Left/Right Distribution (%) - 50.20 / 49.80	50.97 / 49.03

5.2.2 Suspension Modifications

To compensate for the decrease in ride height, the coil springs were stiffened by adding rubber spring inserts. Two of these inserts were placed in each coil in the front and in the rear. The result was an increase in vehicle height by 5 cm. Suspension testing was performed using the *Test Lane* computerized product of the **John Bean Company** [43] (Appendix 2). The results are shown in Figure 5.6. It should be noted that the vehicle weight during the test was 1395 kg, which included one person sitting in the driver's position. The compressed natural gas cylinder was half-full and the tire pressures were set at 275 kPa (40 psi).

The suspension test is a drop test performed on all four corners of the car

from a height of 5 cm. The settling time of each vehicle corner is shown in the figure, and it can be seen that the oscillation damping is quick and vehicle motion is terminated within 0.7 seconds. These results revealed that it was not necessary to further alter the original Neon suspension.

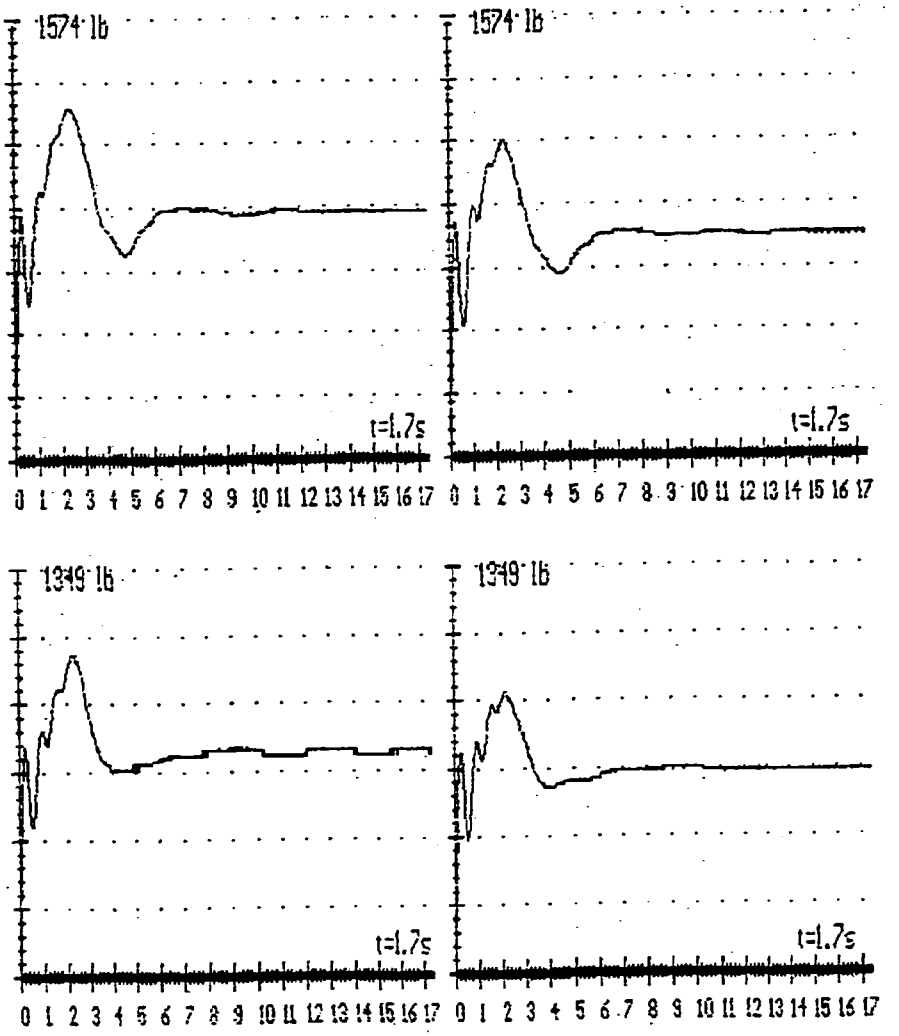

FRONT LE : OK
WEIGHT : 882 lb

93 % IMBAL: 0 % 93 %

FRONT RI : OK
WEIGHT : 793 lb

REAR LE : OK
WEIGHT : 738 lb

93 % IMBAL: 0 % 93 %

REAR RI : OK
WEIGHT : 461 lb

TOTAL WEIGHT : 3075 lb

Figure 5.6 Suspension Characteristics - Test Results.

5.2.3 Low Rolling Resistance Tires

To improve vehicle performance and to reduce fuel consumption, it is important to considerably reduce energy losses. One step of achieving this goal is to reduce vehicle rolling losses by using newer compound low rolling resistant tires. The important features in tires for electric and hybrid electric vehicles are:

- a large diameter; there are fewer revolutions per kilometer thus, higher mileage,
- a narrow profile; gives a smaller contact area with the road surface,
- a hard compound; provides the least possible amount of internal friction, and
- the capability of increasing the inflation pressure; in effect this makes the tire harder and rolling resistance is decreased.

The tires being used on the Neon HEV are manufactured by **GoodYear Inc.** and the specifications for both the original and the new tires are listed in Table 5.2. Even though the original tires have good characteristics, the low rolling resistance tires are instrumental in decreasing the vehicle fuel consumption and the larger diameter helps to improve the vehicle ride.

Table 5.2 Tire Specifications.

	NEW	**ORIGINAL**
Manufacturer Model/Type	GoodYear Inc. Invicta GR/ P185/70R14	GoodYear Inc. Invicta GS/ P185/70R13
Coefficient of Rolling Resistance	0.008	0.010
Wheel-Tire radius (m)	0.3073	0.2946
Max. Inflation Pressure (kPa/psi)	300 / 44	300 / 44

5.3 The Internal Combustion Engine (ICE)

Among the various engines that were investigated, the BMW K75 motorcycle engine was considered to be the best choice for this design application. The K75 unit is a 0.75 ℓ engine that originally has a peak power output of 56 kW (75 hp). It is a flat three cylinder four stroke in-line engine, with a multi-port electronic fuel injection. Also, with a compression ratio of 11:1, it is better suited for combustion of natural gas. Another reason that this motorcycle engine was chosen is that it features a water-cooled system. With these specifications there was no need to perform major modifications to the engine, except for the fuel supply, so as to enable the CNG operation. The fuel system and engine mounting will be detailed in the sections that follow. The engine characteristics with CNG as fuel are shown in Figure 5.7. Operating with CNG reduces the torque, power and specific fuel consumption by 10-15% of the original values [2,14]; the engine key characteristic values are listed in Table 5.3.

Table 5.3 A Summary of the Engine Characteristics.

Parameters	Original	CNG Modified	@ Engine RPM
Peak Torque (Nm)	68	58	6750
Peak Power (kW)	56	47	8500
Minimum (g/kWh) Specific Fuel Consumption	303	257	3500

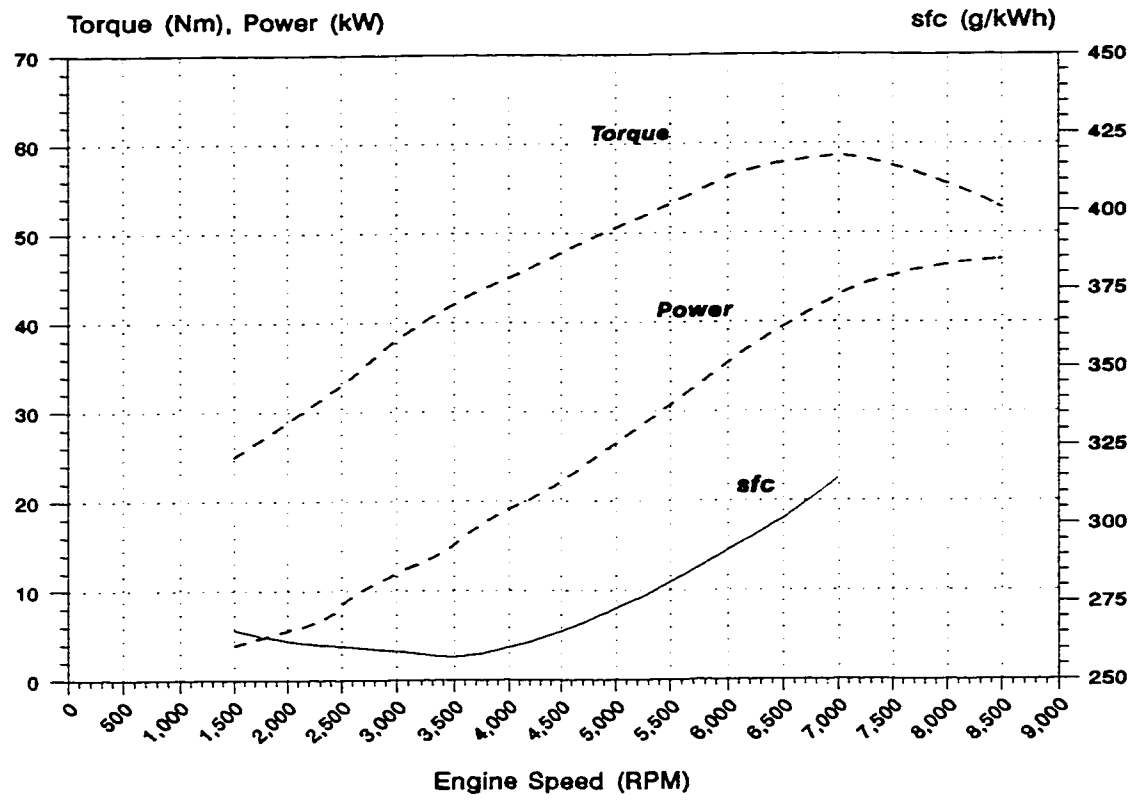

Figure 5.7 Torque, Power and Specific Fuel Consumption vs. Engine Speed for Natural Gas Operation.

5.3.1 ICE Mounting

BMW K-series engines are designed so that the engine block and the transmission casing are two separate units. These two units are coupled via a bell housing that contains the clutch, starter and alternator. This bell housing (Figure 5.8a) was used as the anchor point to attach the engine to the Neon drivetrain.

From the installation perspective, the BMW K75 was compact enough to be located in the Neon engine bay. The powertrain's length increase due to the electric motor drive incorporation did not cause a problem. Hence, it was not

necessary to perform any structural modifications to the Neon engine bay. This engine was easily adaptable to the existing Neon transaxle because the drive output of this engine was counterclockwise, and a complex gear drive was not required to connect the engine to the transmission.

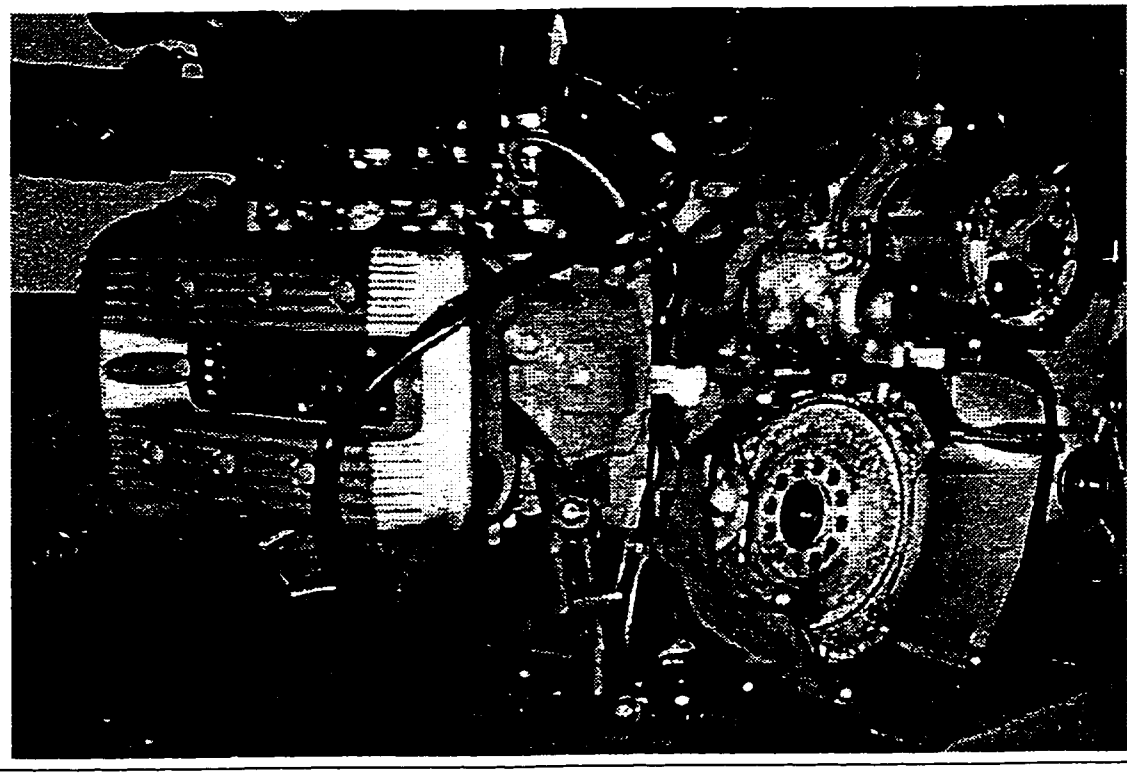

Figure 5.8a The BMW K75 Engine and Bell Housing.

The engine is rigidly attached to the drivetrain so that all the components move in the rubber mounts together as a single unit. All the original Neon mounts were incorporated into the drive design. The original mounting points were also retained so that the vehicle's monocoque structure was loaded in the locations that were designed to handle these loads. In Figure 5.8b, the engine mounting position is depicted.

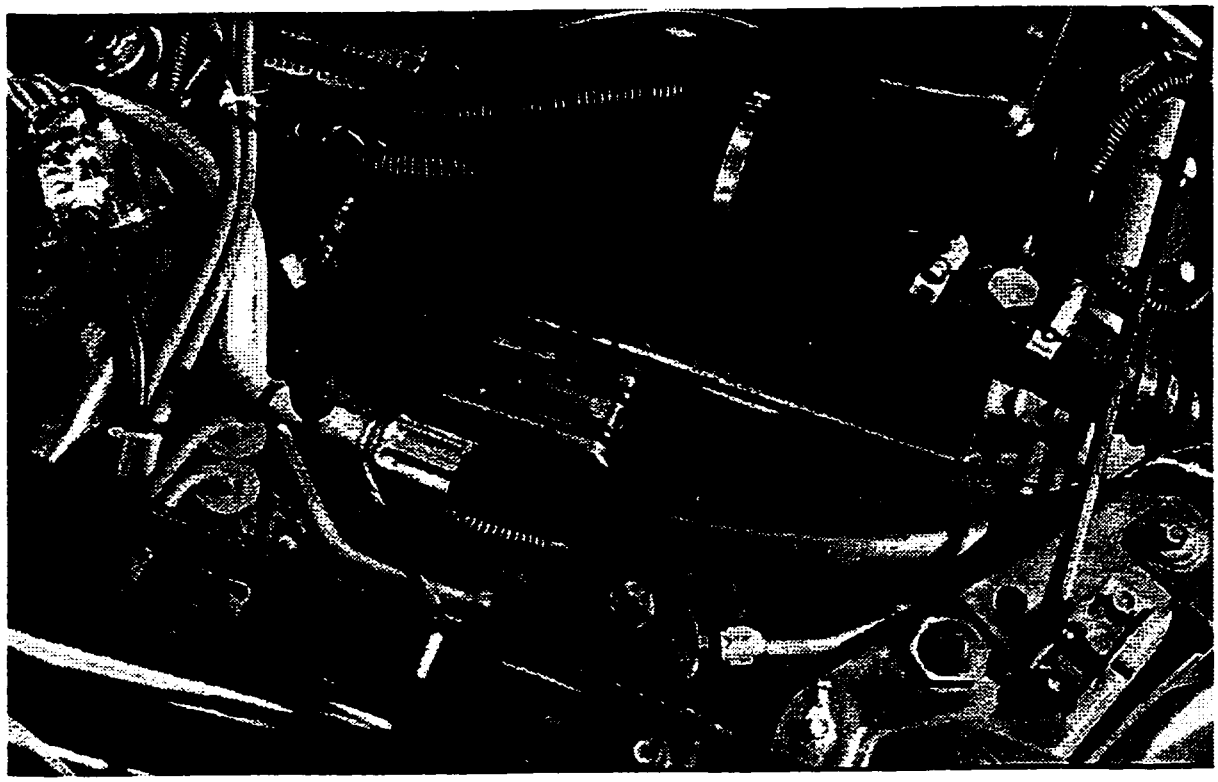

Figure 5.8b Engine Mounting Detail.

5.3.2 ICE Power Requirements

In the hybrid mode of operation, the vehicle had to be driven at a minimum average cruising speed of 89 km/h. In this mode, both the engine and the electric motor power had to be sized accordingly. The sizing of the engine was thus determined with the assumption that a failure of the electric motor would not impede the vehicle operation; the engine should solely be capable of maintaining the average cruising speed. The basic calculations with the drivetrain efficiency, being denoted as η_m, are shown in the following equations. The power to maintain 89 km/h on a level surface was calculated as follows:

$$P_{ICE} = \frac{V_{HEV} \cdot (F_{aero} + F_{ro})}{\eta_m}$$
$$P_{ICE} = \frac{(24.7 \frac{m}{s}) \cdot (135.6\,N + 210.9\,N)}{0.95} = 9\,kW \quad (5.1)$$

While driving on an inclined road consisting of a 1.75% grade, the power to maintain 89 km/h is:

$$P_{ICE} = \frac{V_{HEV} \cdot (F_{aero} + F_{ro} + F_{cl})}{\eta_m}$$
$$P_{ICE} = \frac{(24.7 \frac{m}{s}) \cdot (135.6\,N + 210.9\,N + 253.6\,N)}{0.95} = 15.6\,kW \quad (5.2)$$

The resistive force calculations are based on the vehicle model introduced in Chapter 4, using the nominal parameters from Table 4.1 with a maximum vehicle weight of 1477.4 kg. If the vehicle at 89 km/h was to be driven in second gear, the engine would be operating at 5800 rpm, that would result in a CNG engine power output of approximately 34 kW. In third gear the engine output would be 17 kW at 3700 rpm. These preliminary findings show that the CNG modified engine can adequately sustain the power required for the aforementioned driving conditions.

5.4 ICE Natural Gas Conversion

Engine fuel delivery components were the only ones to be changed for the BMW engine. The fuel rail was redesigned to accommodate the usage of compressed natural gas. It was constructed from a brass tube that was as large as possible in volume for the space that was available (3.8 cm OD, 3.2 cm ID, 23 cm long). A large tube was recommended by Jim Cohen of **Siemens Automotive** [44] so that pressure fluctuations caused by the injection pulses could be minimized. The new fuel rail is pictured in Figure 5.9.

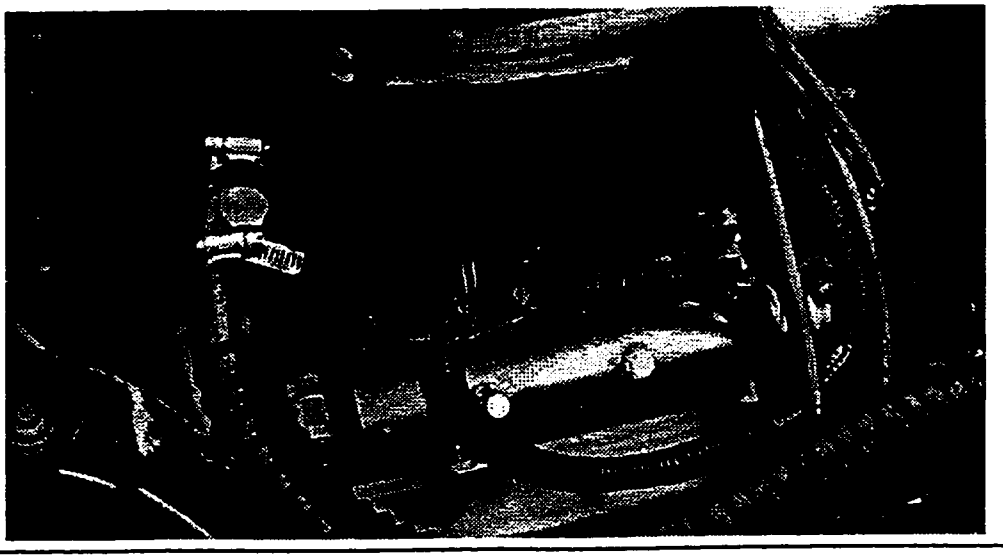

Figure 5.9 Natural Gas Fuel Rail Fabricated for the BMW K75.

The fuel was delivered to the intake manifold through three **Siemens** Deka I natural gas injectors (see Figure 5.10). From the flow data that were provided by Siemens Automotive Inc., the injector fuel dose for different pulse widths was calculated. The results were plotted in Figure 5.11 for the three fuel temperatures of: -20°C, 0°C, and 20°C.

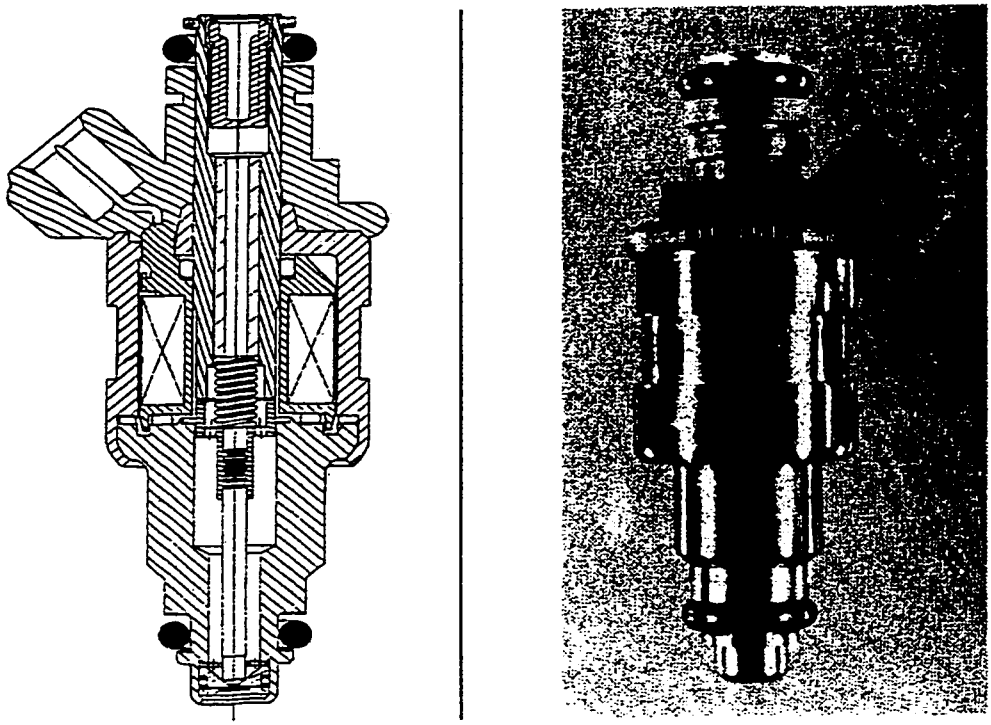

Figure 5.10 Siemens Deka I Injector [45].

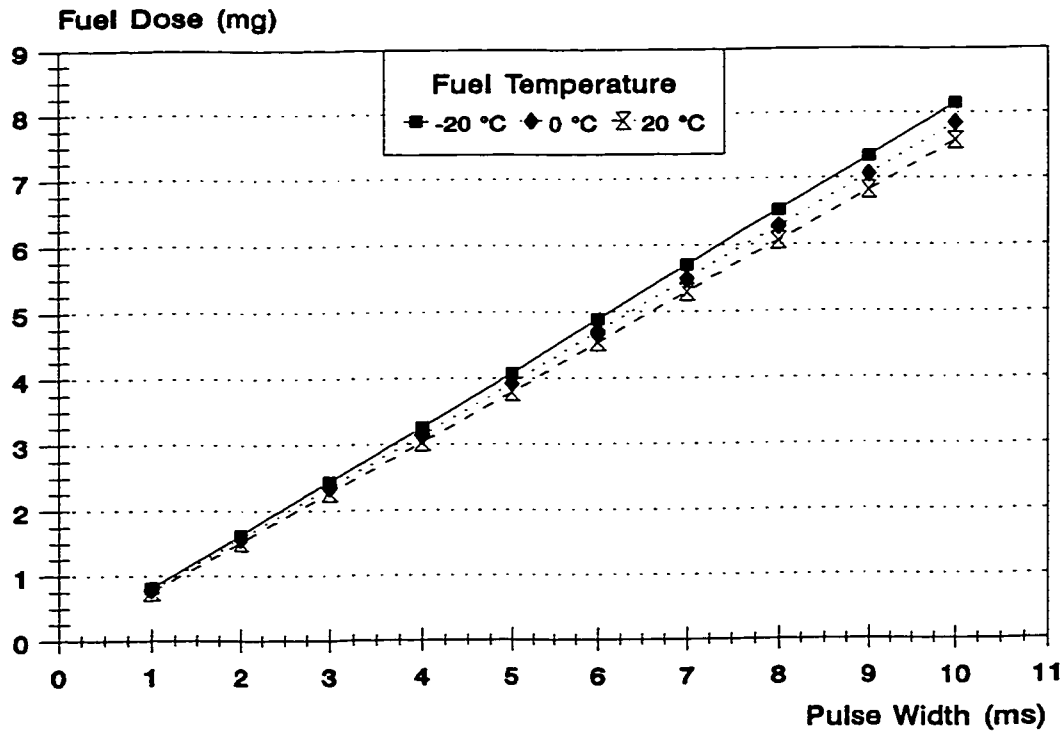

Figure 5.11 Injector Fuel Dose vs. Pulse Width.

5.4.1 CNG Fuel System

The compressed natural gas is stored in an all-composite cylinder, that is manufactured by **EDO-Literider** and is certified according to the ANSI-AGA-NGV2 standards. This cylinder has a 100% carbon fiber outer shell and a seamless, leak-proof thermoplastic inner liner. In Table 5.4 the cylinder parameters are listed. In contrast to other available cylinders, this cylinder is light-weight and also very compact; it occupies a portion of the trunk space with a sufficient amount of protective clearance from the vehicle's interior sides.

Table 5.4 CNG Cylinder Description.

CYLINDER	**EDO All-Composite**
Physical Dimensions	40.6 cm x 84.8 cm
Empty Weight (kg)	24.5
Max. Operating Pressure	24.8 MPa or 3600 psi
Interior Volume (liters)	75.5
Equivalent US Gallon$_{gasoline}$ (liters) @ 20.7 MPa (3000 psi) @ 24.8 MPa (3600 psi)	 5.8 (21.95) 6.6 (24.98)

As an added safety precaution, the interior of the trunk was sealed from the passenger compartment with a polyweave flame retardant tarpaulin, which was attached to a 0.32 cm thick polyethylene sheet.

The fuel supply system is sized to operate at up to 24.8 MPa (3600 psi) and has many safety features incorporated in the design. There are two shut-off

solenoid valves; one for the low pressure side and one for the high pressure side, which will disable the fuel flow when the engine is not in operation. The solenoids will only be activated after the engine is started. A pressure relief device, along with a manual shut-off valve, is pre-installed on the cylinder by the manufacturer. A pressure transducer is placed in the fuel line exiting the cylinder and a temperature sensor is attached on the opposite end of the cylinder. The high pressure fuel line is a 0.64 cm (1/4 in.) O.D. stainless steel tube that is sized for a burst pressure of 35.1 MPa (5100 psi). Using the cylinder as the starting point, the fuel line exits the trunk into the rear passenger wheel-well and connects to the fuel filler receptacle. A pressure gage, a back-check valve and a quarter-turn valve are also joined at this location. Continuing towards the front of the vehicle, the fuel line is routed along the path of the original Neon gasoline fuel line. To prevent any leaks from multiple elbow fittings and unions, a one piece formed tube is routed under the vehicle to the engine compartment. For added protection from road debris or stones, the fuel line was passed through a 0.8 cm ($^5/_{16}$ in.) polyethylene hose. Once in the engine compartment, the high pressure line is attached to a high pressure **RACOR-Parker** CNG filter. The natural gas is subsequently brought down to a lower pressure by a **GFI** pressure regulator, which is connected to the engine fuel rail by a flexible stainless steel braided hose. The layout of the fuel system can be fully understood by examining Figure 5.12.

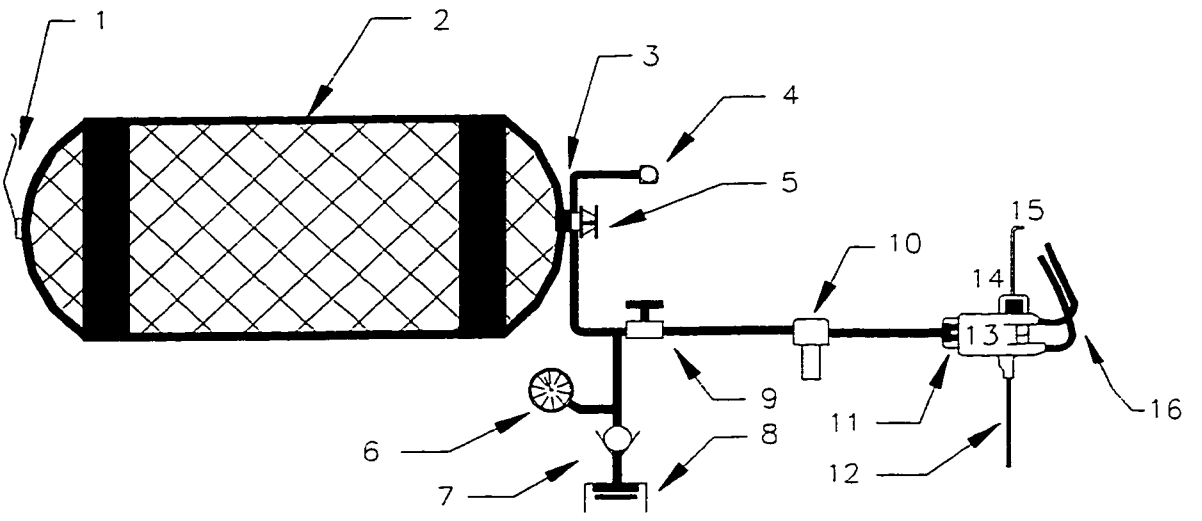

1. Temperature Sensor
2. CNG Cylinder
3. Pressure Relief Device
4. Pressure Transducer
5. Manual Shut-Off Valve
6. Pressure Gauge
7. Back Check Valve
8. Fuel Filler Receptacle
9. Quarter Turn Shut-Off Valve
10. High Pressure Filter
11. High Pressure Solenoid
12. Pressure Relief Tube
13. Pressure Regulator
14. Low Pressure Solenoid
15. Low Pressure Line to Fuel Rail
16. Coolant Lines - Supply & Return

Figure 5.12 Compressed Natural Gas Fuel System Layout.

5.4.2 Natural Gas Pressure Regulator

Natural gas is stored in a gaseous compressed phase and the pressure to the engine fuel rail is dropped to a level that can be handled by the injectors. The GFI pressure regulator provides a fuel rail pressure of approximately 690 kPa (100 psi), within an accuracy of 5-15 psi. The regulator is heated with engine coolant to prevent it from freezing during the pressure drop from the cylinder. The direction of coolant flow in the regulator is not relevant. In case of any problems resulting in excessive tank pressure, there is a pressure relief port that is vented to the outside of the engine compartment.

5.4.3 CNG Cylinder Mounting

Placed in the NHEV trunk, the CNG cylinder was positioned as far forward as possible and it was located equidistantly between the vehicle's rear strut towers. There were no structural changes that would be required for the installation of this cylinder. Using the manufacturer supplied brackets, the cylinder was bolted onto aluminum angles that were attached to the trunk floor.

Steel plates (0.64 cm / $^{1}/_{4}$ in. thick) were fabricated and placed as shims at the points where the interior trunk mounting surface was not flat. To complete the cylinder attachment to the floor, steel plates and C-channels were installed underneath the vehicle. The vehicle's sheet metal floor was in effect sandwiched between two steel plates - one on the inside of the trunk and one on the outside. The two aluminum angles that were placed on the floor, bridged the spare-tire opening; thus a surface for bolting the cylinder brackets was created. The cylinder brackets were mounted on the angles that were affixed on top of the sandwiched structure. The mounted cylinder is shown in Figure 5.13.

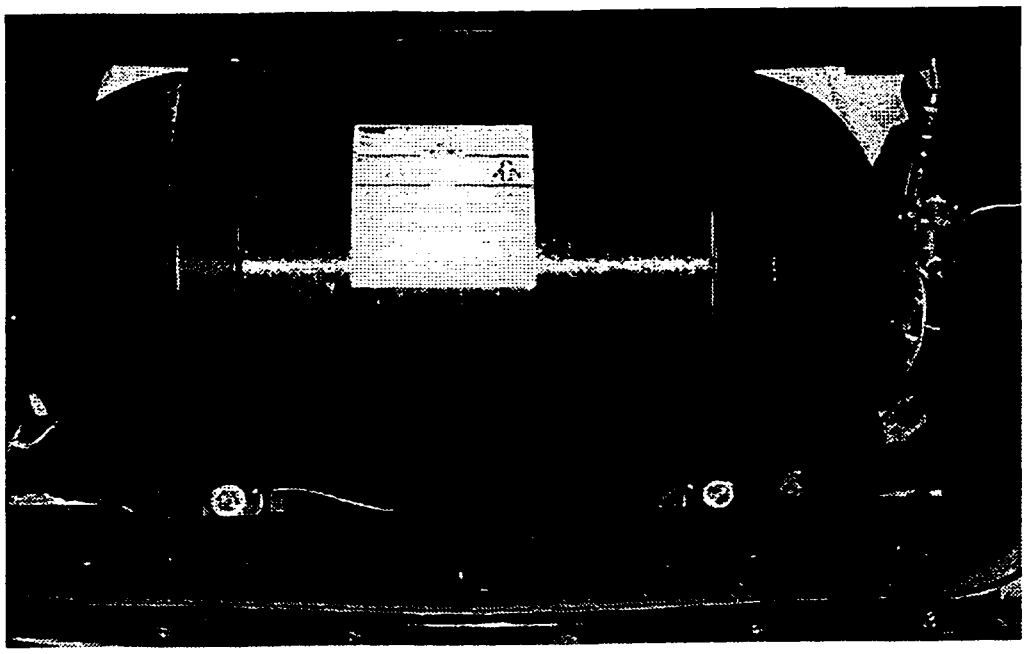

Figure 5.13 CNG Cylinder.

5.4.4 CNG Volume Sizing

Fuel consumption and the vehicle target range had to be projected so that the correct cylinder size could be chosen. The following parameters were used in the calculation of the required cylinder capacity:

- a design range of 280 km (minimum requirement for the HEV Challenge),
- a design pressure of 20.7 MPa and 21 ^{0}C,
- a compressibility factor of 259.7, at a natural gas density of 0.83 kg/m^{3},
- an engine specific fuel consumption of approximately 300 g/kWh.

The calculations are made for a steady state hybrid mode operation, at a constant speed of 89 km/h, over a level driving surface. The required energy is calculated by equation 5.3 using results from equation 5.1.

$$Energy = \frac{Power \cdot Range}{V_{HEV}}$$
$$Energy = \frac{9\ kW \cdot 280\ km}{89\ km/h} = 28.3\ kWh \quad (5.3)$$

The mass and volume of fuel needed are calculated by equations 5.4 and 5.5.

$$M_{fuel} = b_e \cdot Energy$$
$$M_{fuel} = 300\ \frac{g}{kWh} \cdot 28.3\ kWh = 8.49\ kg \quad (5.4)$$

$$V_{fuel} = \frac{M_{fuel}}{\rho_{NG}} = 10.23\ m^3 \quad (5.5)$$

The fuel capacity of CNG required to achieve a 280 km driving range is defined as:

$$Water\ Capacity = \frac{V_{fuel} \cdot 1000\ \ell/m^3}{Compressibility\ Factor} = 39.4\ \ell \quad (5.6)$$

The EDO-Literider model 80 cylinder outlined in Table 5.4 has a water capacity of 75.5 liters. Taking into account various road conditions and driving speeds, there is enough reserve of fuel in the cylinder to accommodate a much longer driving range. The theoretical driving range at an 89 km/h speed on a level surface was calculated to be 536.5 km.

5.5 Fuel Injection Strategy

The existing electronic engine management system on the BMW K75 was replaced with an after-market system. This replacement was necessary since the engine was converted to CNG and there was no possible access to the engine's electronic control unit (ECU), so as to change the fuel delivery settings. Adjustments were required to operate the engine efficiently with the much higher volumetric flow of natural gas, so that a precise amount of fuel would be delivered to the engine for all operating conditions.

A TEC2 fuel injection and ignition control system by **Electromotive Inc.** was used to control the engine. This unit was also equipped with high energy ignition coils, which helped to initiate combustion of the fuel/air mixture. Natural gas has a higher ignition temperature and a slower flame propagation speed as compared to gasoline. The TEC2 inputs and outputs for engine operation are listed in Table 5.5.

Table 5.5 TEC2 Engine Inputs and Outputs.

TEC2 Inputs	TEC2 Outputs
Manifold Absolute Pressure (MAP) or Mass Air Flow (MAF) Sensor	Fuel Injector Pulse Width
Crank Angle Magnetic Position & Speed Sensor	Ignition Spark Advance
Throttle Position Sensor (TPS)	High Pressure Solenoid Shut-Off
Coolant Temperature Sensor	Low Pressure Solenoid Shut-Off
Fuel Temperature Sensor (FTS)	
Heated Exhaust Gas Oxygen Sensor (EGO)	
Battery Voltage Meter	

Engine operating parameters can be optimized through MS-DOS computer software from Electromotive Inc. There are features such as the fuel and ignition control that can be adjusted for eight speeds and load ranges. A 3-D spark advance table (RPM, MAP, Advance degrees) allows the advance settings to be mapped over the entire engine operating range. There is also a coolant advance table that allows the advance to be increased for lower engine temperatures, as well as fuel flow rate correction for fuel temperature, battery voltage, cold starts, warm-up and for acceleration and deceleration modes of operation.

Illustrated in Figure 5.14 is the fuel delivery system that consists of a closed-loop, multi-point gaseous injection system operating on the MAF concept.

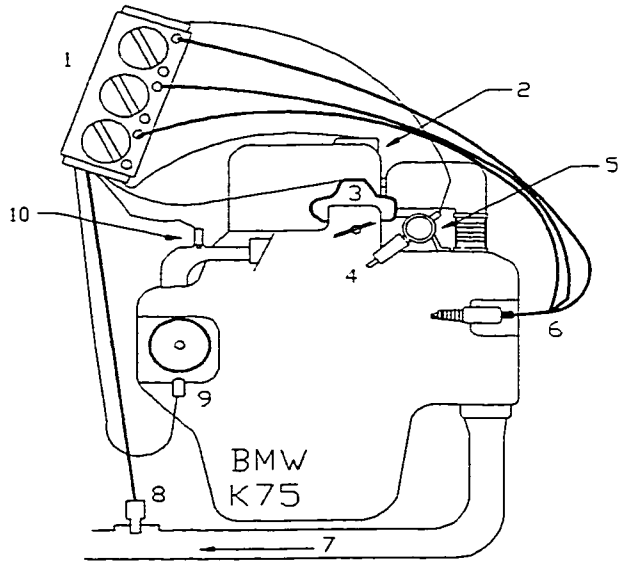

1. TEC2 Unit
2. Mass Air Flow (MAF) sensor
3. Throttle Position Sensor (TPS)
4. Fuel Injector
5. Fuel Rail and Fuel Temperature Sensor (FTS)
6. Spark Plugs and Wires
7. Exhaust Route
8. Exhaust Gas Oxygen (EGO) Sensor
9. RPM - Magnetic Pick-Up
10. Coolant Temperature Sensor

Figure 5.14 Fuel Control System Schematic.

Initially, the engine calibration was performed using the speed density approach (i.e. the manifold pressure (vacuum) is measured along with the air

temperature in the manifold and a value of mass air flow is computed by the TEC unit). The fuel temperature sensor was installed on the fuel rail and connected to the Manifold Air Temperature (MAT) sensor input. It was concluded that the MAT sensor input can only make the mixture leaner (shorten the injector pulse width) while as the air temperature increases, the density decreases and thus less fuel can be burned. Using the fuel temperature sensor, the injector pulse width had to increase with an increase in fuel temperature. A longer pulse width would then be required to inject the same mass of fuel. This resulted in a loss of resolution and accuracy in the engine calibration process.

Other problems were also encountered during the calibration process. The Electromotive manual stated that the manifold absolute pressure (MAP) value should be around 30-35 kPa at idle and just over 100 kPa at full load. In the NHEV case, the minimum MAP value was never less than 65 kPa. This also resulted in a loss of resolution and accuracy in the engine calibration process. The reasoning for these problems can be explained by the following two factors:

- the engine has a large exhaust and intake valve overlap, causing a high MAP value during idling, and
- the motorcycle engine intake is not made in the same way as is a car engine intake manifold.

Any changes to the engine valve-train were not feasible but there was an attempt to solve the intake manifold problem. A balancing tube was attached to

each vacuum port located under each throttle-butterfly opening. The small orifice diameter on these ports created a large restriction, which, in turn caused high and unstable MAP readings. This problem caused the engine to have a poor transient response. Finally, to correct this problem it was decided to divert from the speed density system to the air mass flow approach. Thus, the MAP sensor was replaced with a MAF sensor (originally present on the BMW engine). The advantage of using this sensor is that it measures the quantity of air entering the engine regardless of the engine's volumetric efficiency or the air density. With this change, a very noticeable improvement occurred in the engine operation. A stable engine idle was achieved and the transient response problems were minimized.

For closed loop control and to reduce the tailpipe emissions, a **BOSCH** heated exhaust gas oxygen (EGO) sensor was incorporated with a three-way catalytic converter. To reduce the cold-start emissions and to quickly initiate the catalyst reaction, the whole exhaust system was isolated with a fiberglass wrap. The catalyst supplied by **Johnson Matthey** [46] was composed of Palladium coated elements (specifications in Appendix 2). It was placed at approximately 100 cm distance from the BMW engine exhaust ports. The original engine crankcase ventilation system has been maintained to control the evaporative emissions. There were no evaporative emissions resulting from the fuel storage, since the usage of CNG was within a closed system.

5.6 Electric Motor

In this hybrid electric vehicle, the electric motor that is incorporated in the powertrain design, is being used as a power assist unit; however, the option of driving the vehicle with only electric power has also been made available. The main criteria for the selection of the electric drive system were:

- the motor and controller efficiencies,
- the cost of the components,
- a robust and road-worthy construction.

Realizing that the vehicle's main powerplant would be the BMW engine and the electric motor would be just an auxiliary system, it was concluded that an expensive and technologically advanced electric drive would not be justified in this phase of the design. Robust, compact and inexpensive series wound motors have been widely used in heavy duty applications such as forklifts, thus, motor selection was focused in that direction. Although a permanent magnet motor would be a better alternative, the prohibitive cost was the final deciding factor. The minimal vehicle range requirements did not justify the motor expense. Recently introduced to the electric vehicles, alternating current (AC) motors require expensive control components; thus, these motors were also not considered. An inexpensive series wound DC motor manufactured by **Advanced D.C. Motors Inc.** [47] (manufacturer information in Appendix 2), was selected for the electric propulsion system and the data for this motor are listed in Table 5.6.

Table 5.6 Electric Motor Information.

Manufacturer - Type/Model	Advanced D.C. Motors Inc. Series Wound DC/ X91-4001
Operating Voltage	96 Volts
Power - Peak **- Continuous**	27.0 kW (36 hp) 9.05 kW (12 hp)
Dimensions (cm)	Length: 38.94 Diameter: 17.0
Weight	37 kg
Cost/Power	48 $/kW

The motor torque characteristic for a 96 Volt application is illustrated in Figure 5.15. This electric motor can achieve a peak power of 27 kW at 2050 rpm and its stall torque, almost constant until 2000 rpm, is 128 Nm approximately.

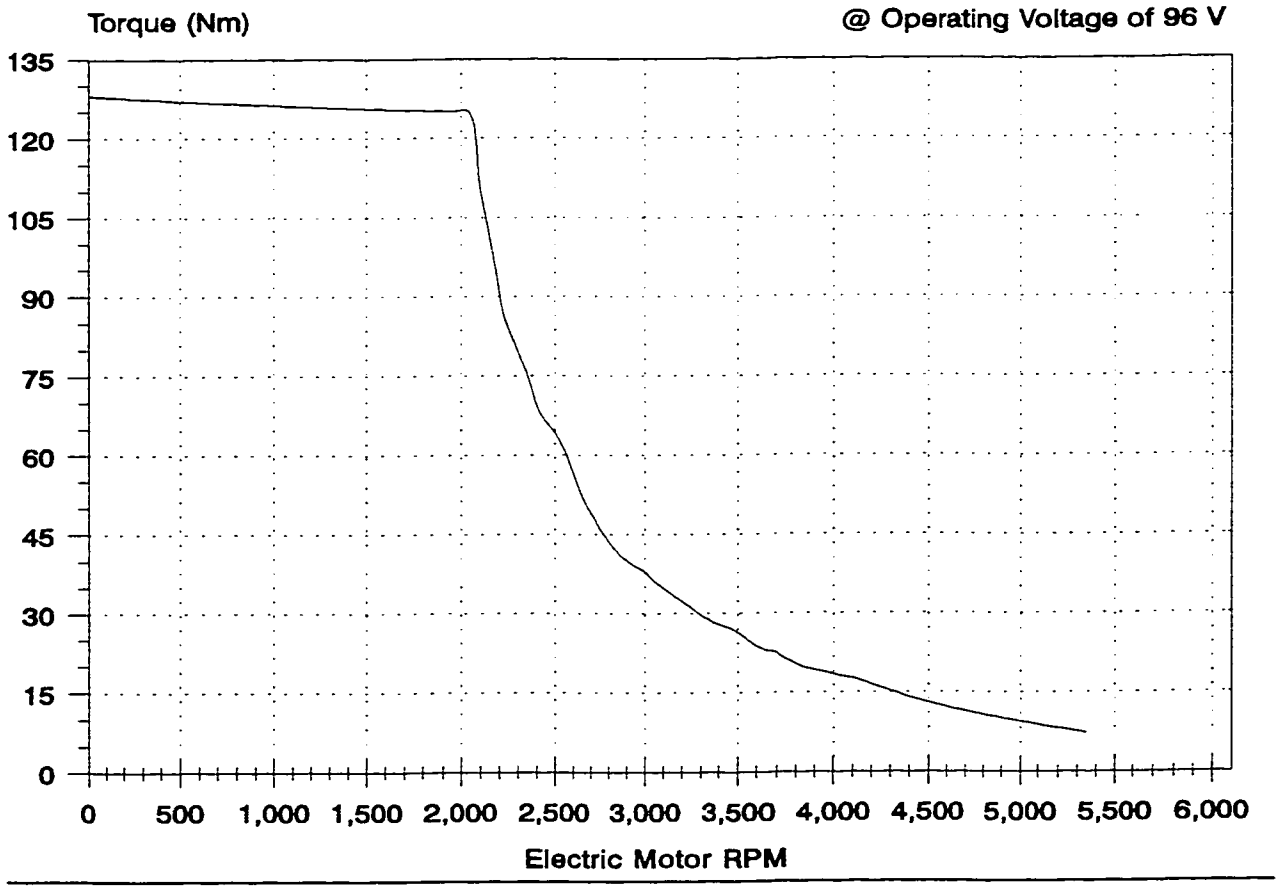

Figure 5.15 Advanced DC X91-4001 @96 V - Torque vs. Motor RPM.

The minimum electric drive requirement for the HEV challenge is to maintain a speed of 48 km/h for a range of 8 km. A higher design range of 10 km was selected to determine the battery energy required (see Chapter 6) and using the resistive forces (rolling, aerodynamic and climbing), the power demanded by the electric motor was calculated. Driving over: *1)* a level surface, *2)* a 1.75% grade and *3)* a 6.5% grade at 48 km/h, would respectively require 2.5 kW, 6.0 kW and 16 kW. Thus, with a peak power of 27 kW and a continuous rating of 9 kW this electric motor could be used for short time durations in a daily driving scenario and the speed and range requirements would be sufficiently met.

As it was explained in section 5.1, the motor is in parallel coupled to the original Neon transaxle and to the BMW engine using a sprocket and chain ensemble. The control strategy for the electric drive is analyzed in the following section. The motor and controller are illustrated in Figure 5.16a.

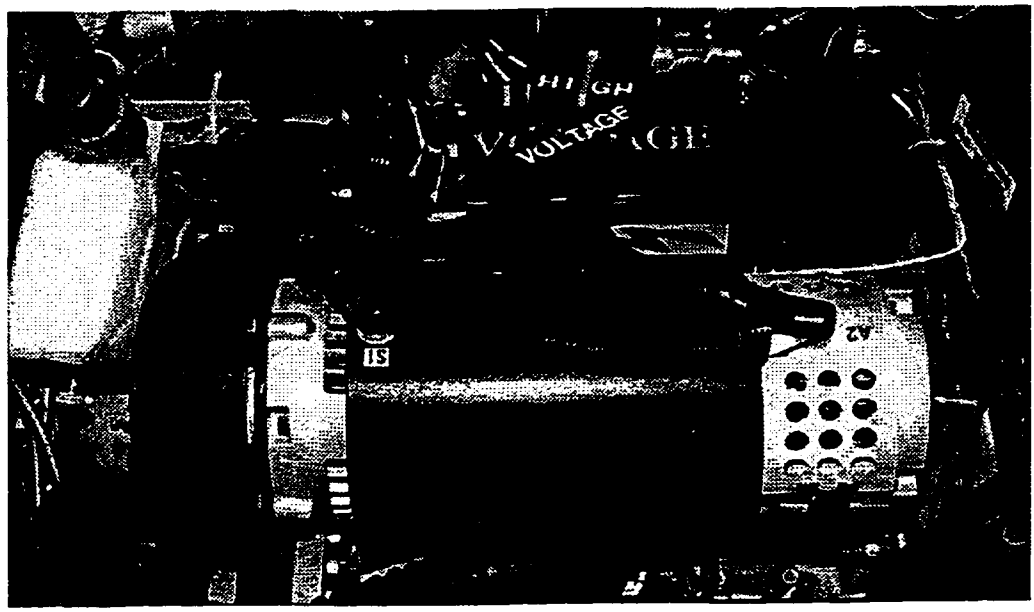

Figure 5.16a A View of the Electric Motor and Controller.

5.7 HEV Control Strategy

An electric motor controller and two control units are the backbone of the HEV control strategy, which enables the driver to select the appropriate driving mode. The high and low voltage grids are also an important portion of the propulsion system and the key individual components are described in the sub-sections that follow.

5.7.1 Motor Controller Unit

The operation of the Advanced DC motor is provided by the use of a 1221B-74 **Curtis** controller. This controller uses an efficient pulse width modulation (PWM) control strategy. An important feature of this controller is that the MOSFets are operated at a high frequency of 15 kHz, thus, the unit can supply the motor with low ripple current (Appendix 2). The motor stall current can then be kept close to the controller current limit until 2000 rpm. Also, the Curtis unit has a sturdy construction and is capable of operating in extremely harsh driving environments.

The controller supply voltage capabilities are matched well with the Advanced DC motor characteristics of 72-120 Volts. The motor can also be supplied with a maximum of 400 amps (two minute rating) and 150 amps continuous (one hour rating). The supply current to the controller will depend upon the batteries used in the propulsion battery pack. A more detailed

description of the controller's circuitry, construction and operation is discussed in reference [48].

To properly synchronize the motor operation with the engine, the throttle position is sensed by a 5kΩ potentiometer. It is incorporated into an automotive pedal position sensor that is attached to the existing throttle pedal. Using a simple voltage divider setup, as the pedal is depressed, the value of the potentiometer is varied, thus enabling the controller to adjust the power requirements that are demanded by the driver. The potentiometer must indicate zero ohms, when the accelerator pedal is at rest and when the ignition is engaged, otherwise the controller will be inoperable. This feature prevents the vehicle from accidentally moving when the ignition is being turned on. The combined electric motor and controller efficiency will vary relative to torque. An efficiency of 87% can be attained if the motor operation is maintained between 2500-3500 rpm. The Advanced DC/Curtis Controller efficiency map is depicted in Figure 5.16b.

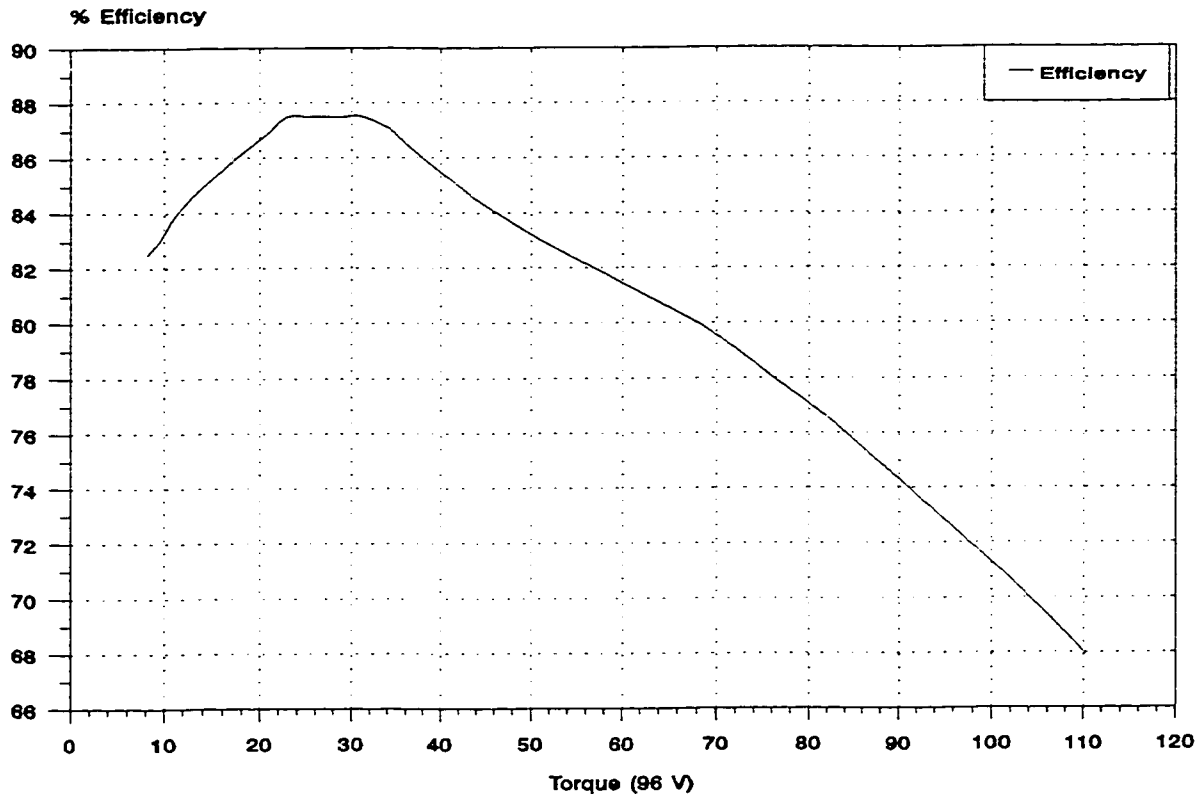

Figure 5.16b Advanced DC Motor and Controller Efficiency Map.

5.7.2 Electric Components

The electric propulsion drive is energized by a network of power conductors, fuses and main contactors. These components work in tandem to provide a safe and efficient means of transferring electric power to the motor controller. A DC-DC converter uses a high voltage grid to supply power to the low voltage systems. The on-board battery chargers enable the user to easily recharge the high power system from any available electrical outlet. In Figure 5.17 the locations of all the components are outlined and are subsequently described in the following sections.

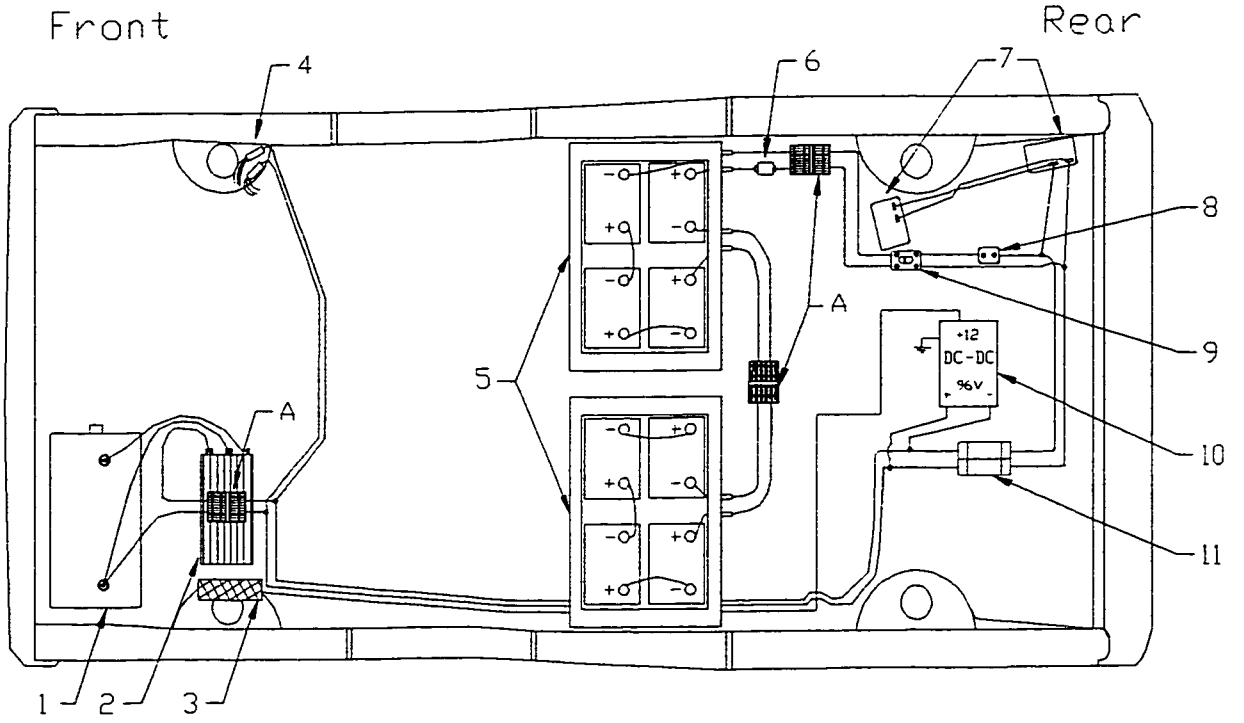

1. Advanced-DC Traction Motor
2. Curtis 1221B Controller
3. 12V Fuse Box
4. High Voltage Distribution Blocks
5. Battery Boxes
6. 400 Amp Time Delay Fuse
7. Battery Chargers
8. 500 Amp, 50mV Shunt
9. Circuit Breaker
10. DC-DC Converter (96V-12V)
11. Main Contactors

A. Quick Disconnects

Figure 5.17 High Voltage Conductors and Electric Propulsion Components.

5.7.2.1 High Power Conductors

All of the conductors of the electric drive system are completely isolated from the vehicle chassis and protected from the possibility of road debris. High voltage conductors were selected with an insulation rating of 600 volts, which is five times higher than the peak reference voltage (110 V). The wire gage required for the conductors was calculated using peak current equations (I_{max}). The batteries forming the propulsion battery unit are interconnected with a wire that is

capable of handling a current of 600 Amps (1.25 times greater than I_{max}). The wire gage standard tables in Appendix 2 were used to select the appropriate wire gage.

$$I_{max} = (Max.\ Controller\ Current) + (Max.\ Current\ Heater\ /\ Air\ Cond.\ System).$$
$$I_{max} = 400\ Amps + 80\ Amps = 480\ Amps.$$

The high power conductors were each placed in individual flexible plastic tubings that were routed on the driver's side underneath the vehicle. A **Buss** fuse rated for 400 Amps is placed on the high voltage line to protect the batteries from being damaged if any of the conductors should short. A circuit breaker, manufactured by **Square D**, is placed between the fuse and the main system contactors. The breaker is rated for a maximum rupture of 10 000 Amps at 120 Volts and it can also be used to manually shut-off the high power electrical system. The manufacturers' specifications for the aforementioned components are included in Appendix 2.

5.7.2.2 Main Contactors

To energize the electric drive system, **Albright** SW-200B contactors are incorporated in the system (Appendix Figure A.2). The contactors that operate from a 12 Volt source are primarily used to isolate the user from all high voltage lines. The contactors have the capability of tripping a fault current of up to 1500 amps. The circuit breaker will trip and the fuse will blow well before the contactor rating is reached. The units can handle a 450 amp draw for brief periods

of time, that could occur when the vehicle is being accelerated from rest. The continuous rating of 250 amps is about four times the amount required to maintain elevated cruising speeds.

To operate the vehicle, all that is required is to turn the ignition key to the *on* position, which will activate the 12 Volt grid. When the 12 Volt electrical system is activated, the contactors are automatically energized rendering the vehicle operational.

5.7.2.3 The DC-DC Converter

The internal combustion engine is not equipped with an alternator, hence, to maintain the 12 Volt system active throughout every vehicle mode of operation, a DC-to-DC converter was installed. A **Sevcon** 330 Watt unit is placed on the NHEV and connected to the electrical network (Appendix Figure A.2). This device operates within a nominal input range from the propulsion batteries of 72-128 Volts and provides a constant regulated output of 13.5 Volts. The many features of this unit are outlined in Appendix 2. A small 12 V auxiliary battery is also placed in parallel with the converter. This connection ensures that the converter is not damaged if there would be any instantaneous high loads. The schematic that is supplied by the distributor of the unit (Figure 5.18) illustrates the load leveling setup that is used on the NHEV. This setup ensures that occasional large current peaks can be handled, since the converter output rating is 25 amps.

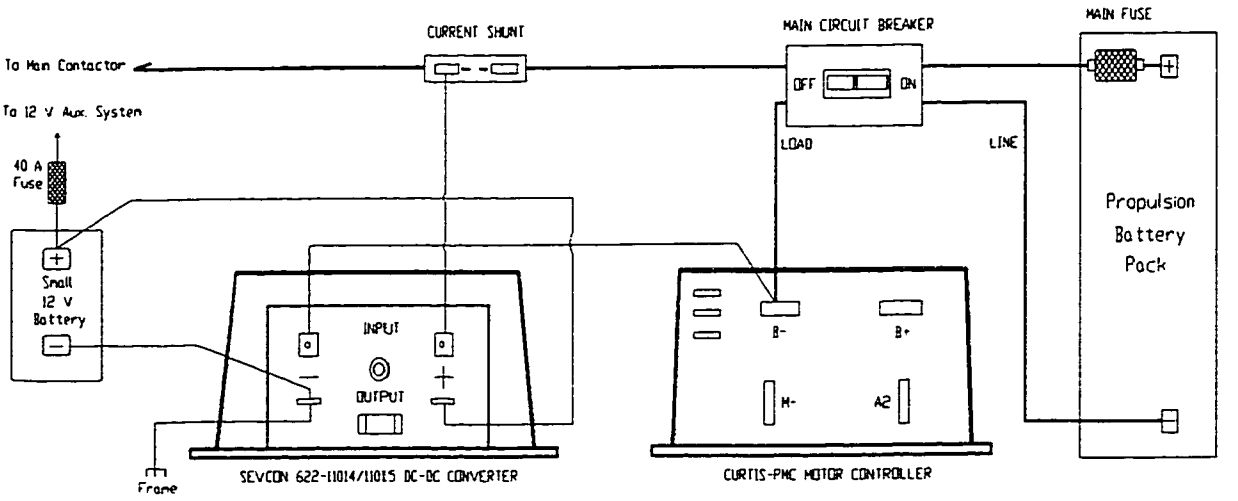

Figure 5.18 DC-DC Converter Setup - Load Leveling.

5.7.3 Modes of Operation

As it has been previously stated, the NHEV has two basic modes of operation that can be identified as Hybrid Electric Vehicle (HEV) and Zero Emissions Vehicle (ZEV). Only one mode can be active at any time and can be engaged at the driver's discretion.

The primary operating mode will always be HEV, where the ICE is the main propulsion unit and the electric motor will assist when there is an increased demand for power. Initial start-up will be in HEV mode and by raising or lowering the mode selector lever there can be a change in the operation mode.

To ensure a proper vehicle operation during start-up, there are certain steps that need to be followed. To drive the vehicle in hybrid mode, the driver must ensure that the lever is positioned in the HEV mode. In this case HEV mode is determined when the lever is lowered, i.e. placed at rest on the vehicle floor.

Upon confirmation of the lever's position one has to start the car by turning the ignition key, and drive away just like in any conventional vehicle. By turning the key to the start position, the electric motor rotates and starts the ICE. The original starting relay was reconfigured so that the motor controller would sense a small resistance (500 ohms), which would get the motor to spin at approximately 300 rpm thus, acting as a starter.

In Figure 5.19, an overhead view of the driver's position outlines the location of the various controls that would be required while driving. The fire extinguishing system will be fully described in a subsequent section.

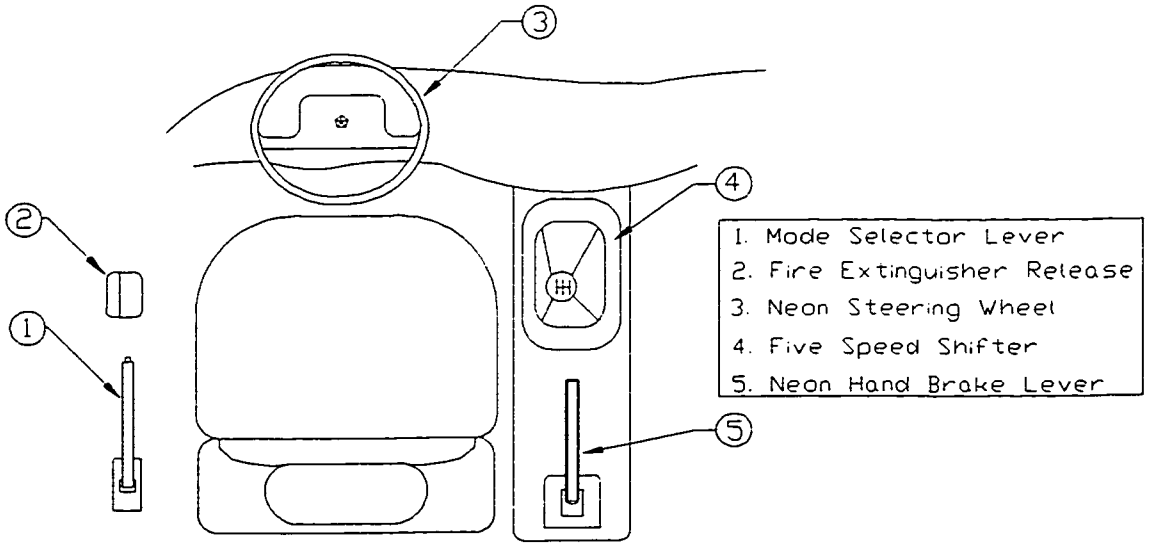

Figure 5.19 Bird's Eye View of the Controls Layout on the Driver's Side.

To commence the operation in ZEV mode, the selector lever needs to be raised. This procedure can be performed at any time during the driving period, whether the vehicle is in motion or at rest. Placing the vehicle into ZEV mode,

initiates the following operations:

- a deactivation of the engine's clutch,
- a shut-down of electric power to the engine's ECU and to all the fuel solenoids,
- the vehicle's battery indicator on the dash will be lit, indicating that the NHEV is in 'battery' operation, i.e. in ZEV mode.

If the driver is operating the vehicle in ZEV mode and wishes to return to HEV mode, then all that is required is to drop the lever into the HEV mode position. While the vehicle is in motion, the rotation of the electric motor will cause the ICE to start.

Two control units consisting of relays and switches complete the design. One unit is used to initiate the required mode configuration to match the driver's selection. The other unit is used to inhibit the creation of a high voltage spark. Prior to the closing of the main contactors, the motor controller is charged and upon vehicle shut-down it is discharged. The same unit is also responsible in activating the DC-DC converter and the battery tray ventilation fans. The control unit schematics are included in Appendix 2.

5.8 Heating, Ventilation and Air Conditioning System Design

The inclusion of a heating, ventilation and air-conditioning (HVAC) system in the vehicle design was deemed necessary if the driver and passenger comfort requirements were to be met. Heating is necessary, especially for vehicles being driven in the northern winter climates. Air-conditioning is also required for the warmer climates. To adhere to the HEV Challenge competition rules, it was required that the HVAC system be operational during both of the vehicle propulsion modes, (HEV or ZEV). Also, while in the ZEV mode, the system had to adhere to the zero emission requirements. These requirements posed a challenge to the type of systems that could be used in this design.

5.8.1 Heating System Design

In the NHEV the complete heating system design will be deployed over two phases. In the first phase of the design, the heating system consists of a combined two *dual-element* electric heater which is attached to the existing heater core. As it is illustrated in Figure 5.20, engine coolant is used as the working fluid for the heater. Supplied from the propulsion battery pack at 96 Volts, the heater can provide up to 5 kW of heat. This unit is a 3.2 kg self-contained system that consists of a solid state controlled all copper heat exchanger. A pump that operates at 12 Volts is used to circulate the coolant through the original heater core ducting. This system is isolated from the engine coolant and it incorporates its

own coolant reservoir. Thus, irrespective of the drive mode, there will always be heating available to the passenger compartment.

1. Electric Heater Unit
2. Coolant Pumped to Heater Core
3. Vehicle Heater Core
4. Coolant Reservoir and Overflow
5. Coolant Return to Heater
6. 12V Pump for Coolant Circulation

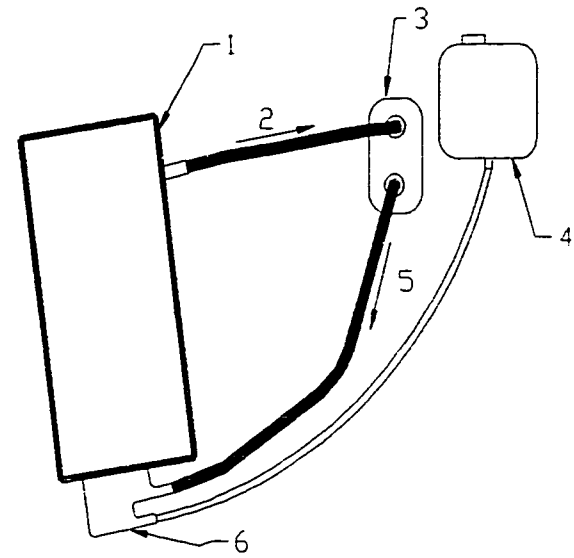

Figure 5.20 Heating System Configuration.

The use of a 5 kW heater ensures that the passenger compartment becomes heated quickly and that the propulsion batteries are not depleted very fast. The heater unit is operated under an "on/off" control. When the coolant temperature reaches approximately 79°C (175°F) the elements will turn off so that the internal components will not overheat. To operate the heater, it is required that the 12 V pump is energized, and the original dash-operated controls are used to that effect. Heating ventilation and defogging is maintained with no visible alterations to the controls. By turning the heater knob to the heat (red) position, the driver or passenger can start the heating. Turning the knob back to the cool position will turn the heater off. Whether the vehicle is stationary or in motion, the heating system will always be functional and it can be used as per the driver's discretion.

Operation of this system necessitates that the driver considers the amount of energy left in the propulsion batteries. By extended usage of heating, the vehicle's electric drive range and performance capabilities can be much affected; thus, heating must be used prudently, particularly on cold winter days.

The second phase considered for this system, consists of placing the electric heater in parallel with the engine coolant system. This modification will be described in the heating test result section.

5.8.2 Air-Conditioning System

An air-conditioning (A/C) system has also been maintained in the NHEV. The components that were already installed in the Neon have been used in the new design. The original air-conditioning compressor, illustrated in Figure 5.21, is to be driven by an auxiliary electric motor that draws power from the propulsion battery pack.

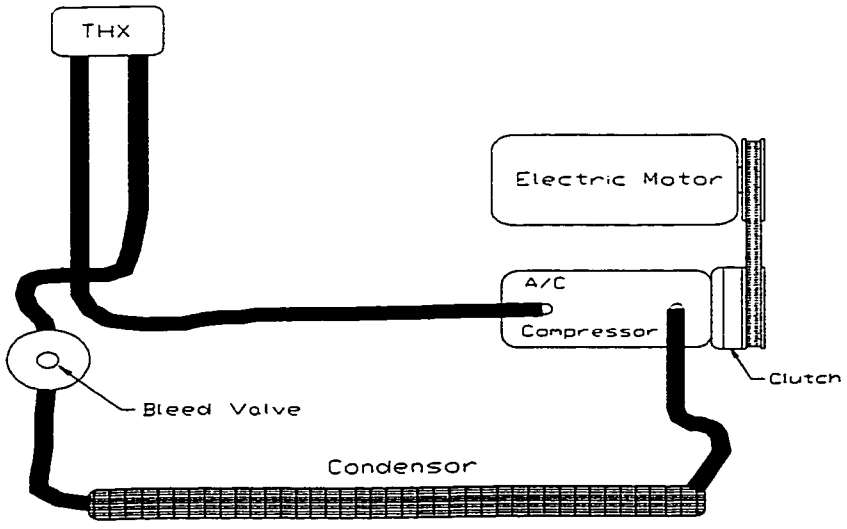

Figure 5.21 Air-Conditioning System Layout.

The original sensor and dash controls are used to operate the cooling system and, as in a regular car, the driver just has to rotate the heating/cooling knob to the cold (blue) position to start the cooling. The standard low and high pressure cut-off switches, as well as the A/C dash selector position, are the inputs that will determine the on-off cycling of the electro-magnetic clutch.

Technical information concerning the compressor power consumption, cooling capacity and volumetric efficiency is included in Appendix 2. The operating speed of the electric motor is selected by choosing the optimum speed that the compressor will be operated at. Regardless of the vehicle's speed or operation mode and even when the vehicle will be at rest, the A/C compressor will sustain a continuous speed of operation.

5.8.3 Ventilation System

The vehicle's ventilation fans and ducting were retained in their original form and their function has not been altered. By adjusting the appropriate knob, the heating and air-conditioning can be changed to the defogging or economy modes. The cooled or heated air can be directed to the panel, floor or window vents. Additional openings were cut into the rear floor, next to the rear seat cushions, so that interior air-circulation is enhanced, since the trunk area (housing the CNG cylinder) has been sealed from the passenger compartment.

5.9 Ancillary Systems and Safety Features

To ease safety concerns that a consumer would have during the operation of a hybrid electric vehicle, many safety features have been installed during this conversion. Vehicle driveability and ergonomic features have been retained as close as possible to the original vehicle specifications. Minor additions to the vehicle interior are the only indicators that this vehicle has been modified. The goal is to provide a potential consumer with a safe and roadworthy vehicle.

To ensure that all high voltage lines are isolated from the occupants, the conductors were routed on the outside of the vehicle and all of the other components were placed in the rear wheel well.

5.9.1 Instrumentation

The original instrument cluster has been kept and three additional gages have been added to the panel surface. A battery state of charge meter, a tachometer and an ammeter were required for this design. The battery state of charge meter or 'fuel gage' by **Curtis Instruments** is a one piece unit with a digital LED display that is designed for lead-acid battery powered vehicles. Existing dash signals were also incorporated in the control strategy. The alternator/battery light is used to indicate to the driver when the vehicle is in the electric mode. The check engine light uses the BMW computer code output to flash trouble codes. All of the stock gages such as the speedometer, fuel gage and

temperature gage remain as part of the design.

5.9.2 Fire Extinguishing System

To comply with the HEV Challenge regulations, a fire extinguisher has been installed and it is operable by the driver in the case of an emergency. It would be up to the driver to decide when to use the system. The trunk release lever, located on the floor of the driver's right side, has been used as the extinguisher release handle. The extinguisher that is mounted in the trunk is attached to the trunk release cable. The nozzle has been extended with copper tubing, which is routed to all the critical areas on the car, namely the battery boxes and the engine bay. Even though the vehicle is safe to drive without the need of a fire extinguishing system, it was a competition requirement. If the extinguisher would become a permanent fixture on the vehicle, then a second handle next to the trunk release lever would be used for the activation of the system.

5.9.3 Emergency Switches

There are many precautionary measures that have been taken to ensure that the vehicle occupants are always safe. The vehicle can not be operated, driven, started, etc. if certain switches have not been engaged. An emergency shut-off switch is placed behind the fuel filler door. If the door is opened during fuel filling and battery recharging, the 12 V system is put off-line, thus the ignition can not be turned on and vehicle operation is disabled. When the door is closed firmly

the switch is again engaged and vehicle operation is possible. The circuit breaker on the high voltage grid has to be switched to the *on* position or else the vehicle cannot be operated. Also, this vehicle requires a key in the ignition to be placed in the *on* position so that the vehicle can be driven. If any of the aforementioned conditions are not satisfactorily met, then one cannot operate this HEV.

The Neon HEV is equipped with shut-off controls operated by solenoid valves that will disrupt fuel delivery and electric power in the event of an emergency. When the fuel filler door is opened, high and low pressure fuel solenoid valves are deactivated. Opening the fuel filler door also cuts electric power to the control units and deactivates the main contactors. Placed in series with the fuel filler door switch is an inertia sensor supplied by **First Inertia Switch**. This sensor is designed to shut off power to the fuel line solenoid valve and to the electrical contactors, following a crash.

5.9.4 CNG Filler and Battery Charging Receptacles

The Neon original gasoline filling area and hinged-panel have been retained. Housed behind the panel is the electric male charger outlet and the CNG refueling assemblage. To initiate battery charging, one end of the power cord is plugged into the receptacle and the other into the appropriate wall outlet. During the fuel fillup, the fuel level is displayed on the pressure gage that is placed in the fuel line coming from the cylinder. A quarter turn valve is used to interrupt fuel

flow to the engine bay. A back check valve ensures that the fuel fillup is done safely and that there is no back flow into the filler pump. These "energy fill" receptacles are described in Figure 5.22 and illustrated in the Figure 5.23.

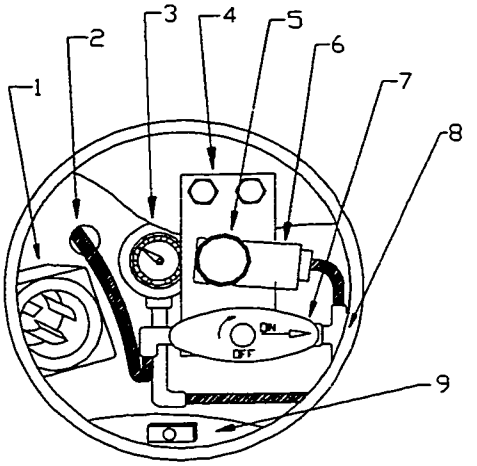

1. Electric Charging Outlet
2. High Pressure Fuel Line from Cylinder
3. Pressure Gauge & CNG Fuel Level Sensor
4. Metal Bracket
5. NGV-1 CNG Fuel Receptacle
6. Back Check Valve
7. Quarter Turn Shut-Off Valve
8. High Pressure Fuel Line to Pressure Regulator
9. Emergency Shut-Off Switch (when filler door is open)

Figure 5.22 Description of CNG and Charging Receptacles.

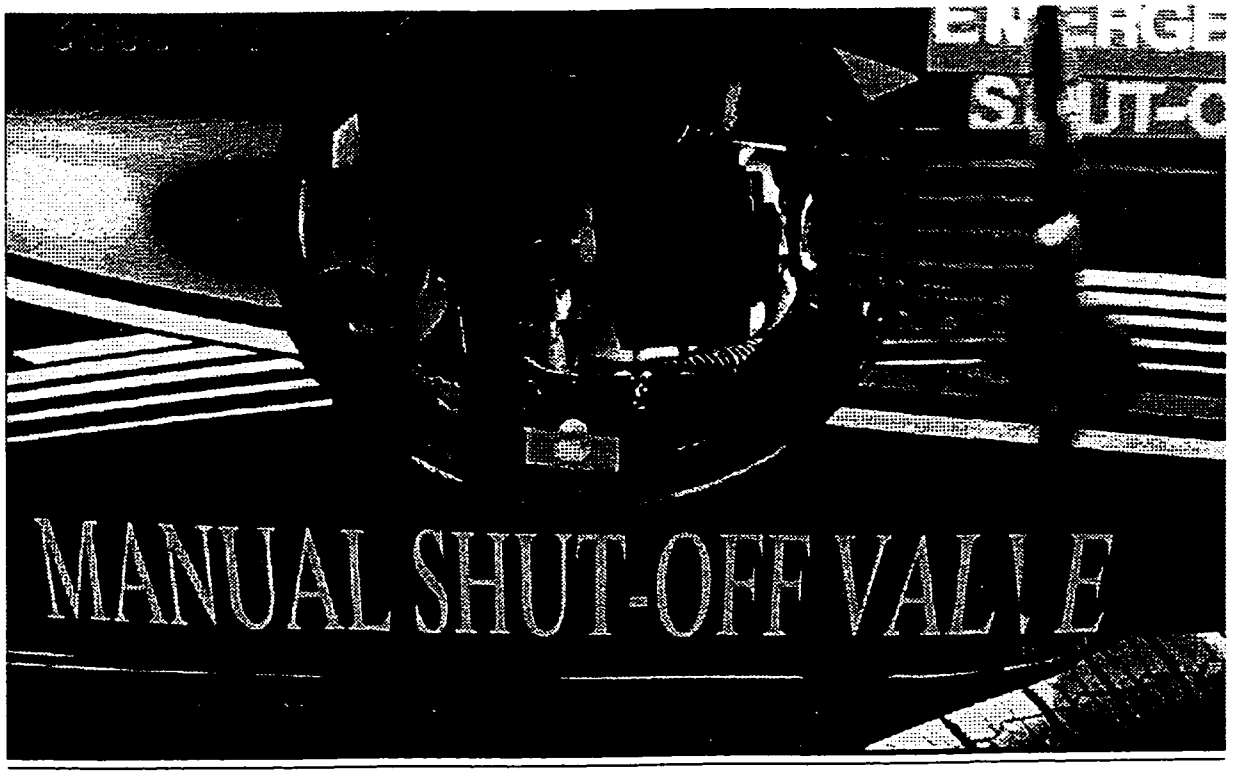

Figure 5.23 Illustration of Fuel Filler Opening.

5.9.5 Braking and Power Steering Modifications

In this design, there can be different modes of operation. In electric mode, since the engine is not operating, there is no hydraulic power or vacuum available to assist in the braking and power steering systems. To solve this problem it was decided to replace the power steering with manual steering that is a basic feature on certain Neon models. To replace the original power brake system, a separate electric vacuum pump with its own reservoir was installed (Figure 5.24). Even with a small vehicle weight increase, there is adequate braking available and the braking ability, as compared to the original vehicle, has not been affected.

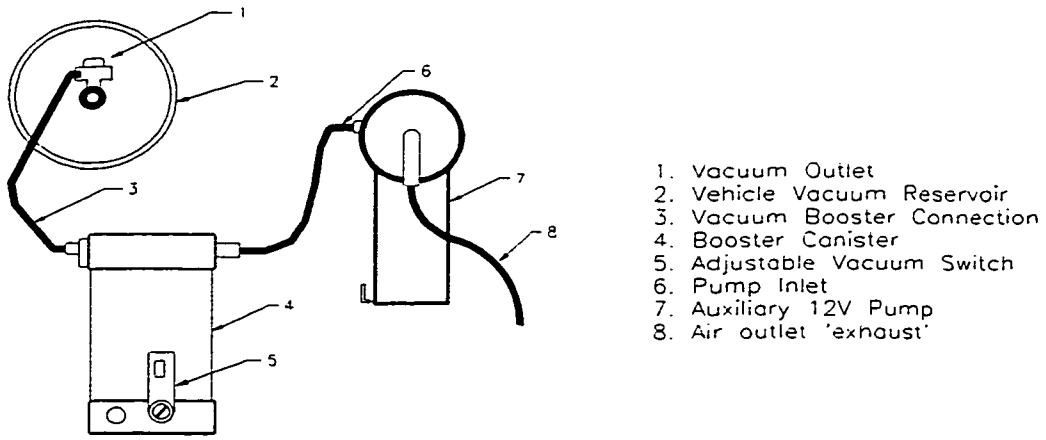

Figure 5.24 Electric Assist Brake System.

Braking tests without the electric assist system produced respectable results with the front brakes handling the majority of the load. A braking test result is illustrated in Figure 5.25. This test was conducted concurrently with the suspension test using the *Test Lane Products*. Wheel friction, applied braking force and axle deceleration is measured for both the front, rear and parking brakes.

The axle deceleration or amount of stopping force provided by the brake system should be greater than 0.5g as it has been established by industry standards [49]. Testing of the NHEV front brakes provided an axle deceleration of 0.66g when the wheels locked up. Using both the rear and front braking effect and the weight distribution, the vehicle deceleration was calculated to be 0.53g. With the addition of the electric assist system, braking will be better and the braking distances would be further reduced.

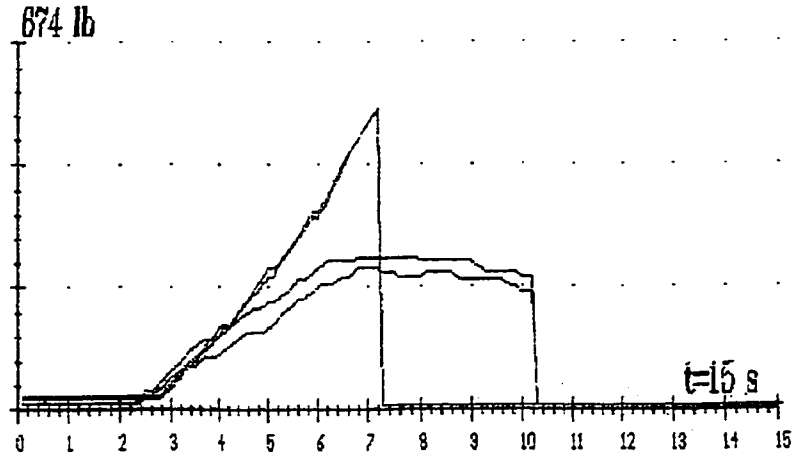

BRAKE TEST :		LE F.	RI	LE R.	RI	LE PB	RI
WHEEL FRICTION	lb	20	34	13	20	13	20
MAX. BRAKE FORCE	lb	560	553	256	277	411	418
BLOCK IMBALANCE	%	1		7		2	
MAX. IMBALANCE	%	10		29		30	
OVALITY	%	--		--	--	--	--
MAX.PEDAL PRESS.	lb	--		--		--	
PEDAL FORCE AMPLIF.*		--		--		--	
AXLE DECELERATION	g	1675 lb 0.66 g		1400 lb 0.38 g			

WEIGHT : 3075 lb DECEL.SBR : 0.53 g DECEL.PK : 0.27 g

FRONT TRACK VAL: -4.8 ft/mile REAR TRACK VALUE: -7.9 ft/mile

Figure 5.25 Brake Test Data.

5.10 Summary

The individual powerplants that are integrated to form the power-assist design for the Neon HEV have been described. An integral part of the mechanical aspect of the HEV mode - the BMW clutch design, was also detailed. Powerplant mounting and power requirements for each drive mode were also determined. The conversion to a CNG fuel system, ranging from fuel storage, fuel delivery and fuel control strategy was examined. Suspension and brake test results confirmed the handling and driveability of the modified vehicle. The hybrid electric control strategy was presented and discussed in terms of the high power, low power and auxiliary systems. Also, it was seen how heating, ventilation and air-conditioning systems were implemented in the HEV design. A description of the ancillary and safety systems in the modified vehicle followed.

6. PROPULSION BATTERY SYSTEM

The electric energy storage unit consists of an electro-chemical battery pack. In this thesis, the focus will be on the battery criteria relevant to the NHEV design. The battery selection process, battery charging, and the mounting and design of the battery boxes will be discussed in relation to the HEV Challenge competition requirements.

6.1 Battery Description and Selection Criteria

The electric propulsion unit on this vehicle is considered as mainly an auxiliary drive, therefore, it was not deemed necessary to install a massive battery system. The only prerequisite was that the vehicle acceleration and electric vehicle range would be satisfied. The selection criteria determining the battery choice were narrowed down to space, location, weight, performance and cost.

Considering the requirements for the 1995 HEV Challenge, it was realized that the only practical battery system commercially available, at an acceptable cost, consisted of lead-acid batteries. Experimental results from the NiCad battery system can be used as a comparison to illustrate the advantages of choosing a lead-acid battery [48]. The battery technology is still evolving; hence, the lead-acid battery system was chosen for simplicity, ease of operation and for the immediate satisfaction of the minimum competition requirements. The placement of the batteries also accommodates the possibility of any future changes and, if so

desired, the type of the energy storage system can be altered. Considering that the NHEV project is in its first design phase, automotive lead-acid batteries were seen as a simple and cost-effective solution for traction batteries. A detailed description of the batteries being used and the manufacturer specifications are listed in Table 6.1.

Table 6.1 Propulsion Battery Specifications.

Manufacturer/ Type	East-Penn / PowerSurge 26-525 SLA (Sealed Automotive Lead-Acid)
Number of 12 Volt units / Connection	Eight (8) / One (1) string in Series
Nominal Battery Pack Voltage	Ninety-Six (96) Volts
Battery Pack Capacity	1.95 kWh @ C/0.5 rate
12 V Cell Rating (Cell Capacity)	69 Ahr @ C/20 rate, 36 Ahr @ C/3 rate
Dimensions per 12 Volt unit (cm)	*Length*: 22.2 *Width*: 17.1 *Height*: 20.3
Cost per unit / Total Cost ($CDN)	$ 64.00 / $ 512.00
Battery Pack Weight	114.3 kg

The battery pack capacity of 1.95 kWh for a C/0.5 rate is calculated by using the experimental energy density data expanded upon in Tables 6.3 and 6.4. The 12V cell rating is supplied by the battery manufacturer.

6.2 Testing and Choosing the Lead-Acid Battery

Selection of the proper lead-acid battery for application to this design entailed an analysis of the electric drive performance. The design parameters of the 1995 HEV Challenge required that an eight (8) kilometer ZEV range be achieved at an average speed of 48 km/h. By determining the energy available from the propulsion batteries, the vehicle's performance during the ZEV range could be established. Knowing the system's current demands would also determine the maximum current available for quick accelerations. Using vehicle dynamic performance characteristics described in Chapter 4, the power required to propel the vehicle at a constant speed of 48 km/h on a level surface and on a 1.75% grade is calculated to be 2.5 kW and 6 kW respectively. Using an average power taken from these results, the power needed from the batteries is calculated in equation 6.1. Gradually, the nominal battery voltage will drop as a function of time. To calculate the current required to maintain the vehicle at the desired constant speed of 48 km/h, an average voltage is used. Shown in equation 6.2, an average is taken between the nominal and 80 % depth of discharge (DOD) voltage. The 80% DOD voltage is calculated by taking 80% of the no-load voltage, 108 V, from the 8 cell string at 13.5 V each.

$$P_{req} = \frac{Power}{\eta_e} = \frac{4.25\,kW}{0.86} = 4.94\,kW \qquad (6.1)$$

$$V_{avg} = \frac{V_{nom(96V)} + V_{DOD(86.4V)}}{2} = 91.2\ V \qquad (6.2)$$

Subsequently, the peak continuous current draw can be calculated by equation 6.3. Even though this is an average result, it is a good approximation and it can be used as a reference point for testing the capacity of prospective battery systems.

$$I = \frac{Power_{req.}}{Voltage_{avg.}} = 54.2\ A \qquad (6.3)$$

Two brands of batteries adequately met all of the selection criteria that were stated in section 6.1. These two batteries, manufactured by **East Penn**, the *PowerSurge Deep Cycle U1DC44* and the *PowerSurge SLA 26-525*, (Table 6.2) were rigorously tested. The results will be examined in the following pages.

Table 6.2 The Two Lead-Acid Batteries Tested.

Battery Type	*PowerSurge SLA 26-525*	*PowerSurge Deep CycleU1DC44*
Dimensions (cm) Length x Width x Height	22.2 x 17.1 x 20.3	19.7 x 13.0 x 18.4
Unit Weight (kg) [12 V cell]	14.3	10.4
Capacity (C/20 rate) (manufacturer specs.)	69 Ahr	44 Ahr

Since battery energy does not remain constant throughout the vehicle's operating envelope, due to the electro-chemical process, power discharge tests were performed to establish the battery performance characteristics over different applied loads. These tests would serve to quickly analyze each battery and see

which one is more appropriate for this project. Since the tests are a time consuming process of discharging and recharging, the discharge was performed at two starting power levels (565 Watts and 790 Watts). These levels, though, were not randomly chosen. By using the calculated constant current draw, equation 6.3, a constant power draw of 650.4 W is calculated for a 12 Volt cell (12V • 54.2A). It was realized that battery discharges at both, 565 W and 790 W rates would be valid tests, by bracketing around the 650.4 W calculation. The 790 W rate would examine battery behavior that could arise during harsher conditions such as cold weather, acceleration, and the overcoming of slopes. With the 565 W test, an analysis of battery performance under a lighter load can be performed. In the following figures the results for the discharge tests are illustrated for both batteries. The tests were performed several times and the mean results are used for analysis. In Figure 6.1 the test results are shown for both batteries that underwent the power discharges. Results obtained from both of these batteries, for the discharge at starting level of 565 W, are superimposed in Figure 6.2. The comparative data are summarized in Table 6.3. In terms of the time it took for the fully charged battery to undergo a total energy discharge to an 80% DOD, the PowerSurge 26-525 outperformed the other lead-acid battery. Further details of why the PowerSurge 26-525 battery was chosen to be used with this drivetrain are discussed in the following pages.

Table 6.3 Overview of the Discharge Tests.

PowerSurge SLA 26-525		PowerSurge Deep Cycle U1DC44	
Starting Load (W)	Time (min.)	Starting Load (W)	Time (min.)
565	31	565	19
790	18	790	12

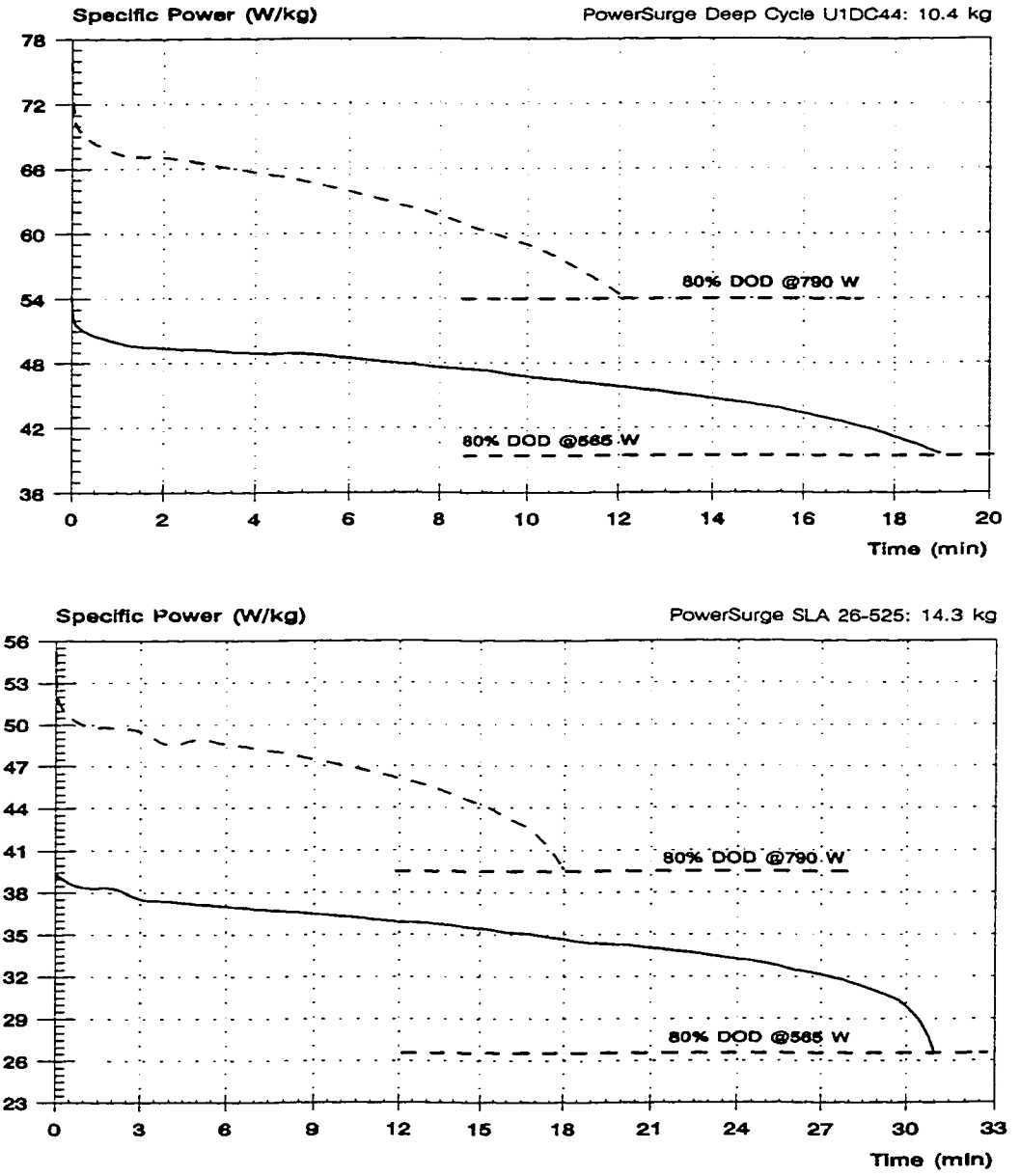

Figure 6.1 Power Discharges at the 565W and 790W Starting Levels for the PowerSurge Deep Cycle Lead Acid U1DC44 and the SLA 26-525 Batteries.

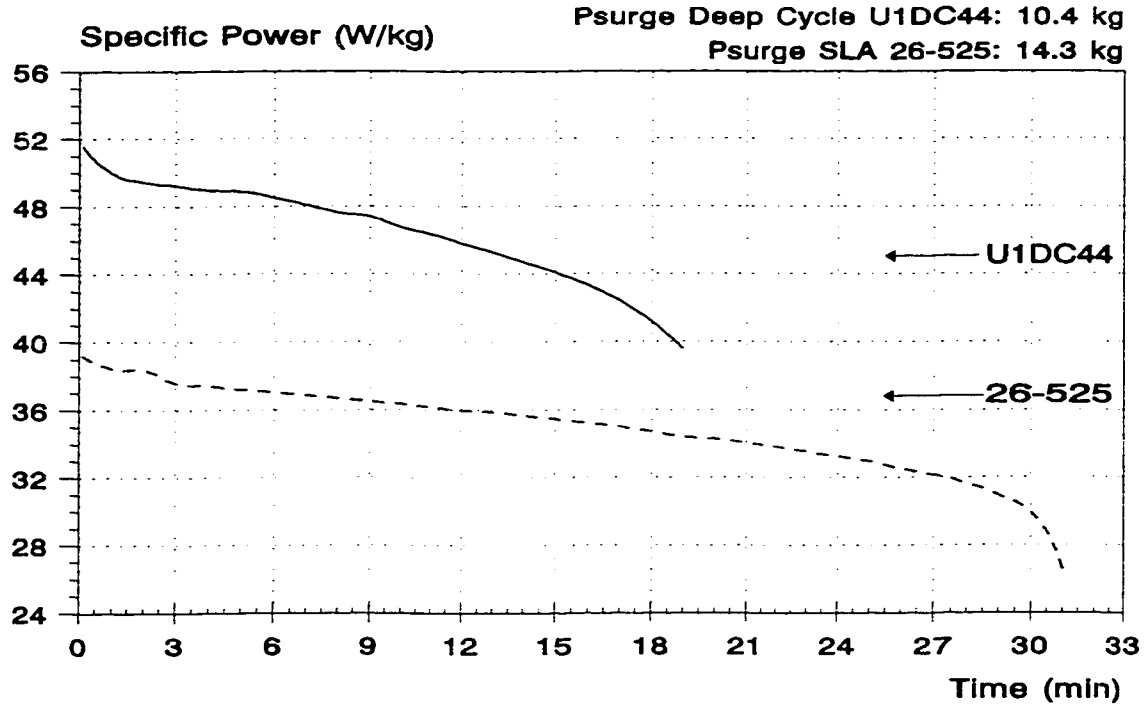

Figure 6.2 Comparison of the Two Batteries for the 565W Discharge Starting Level.

Using the information in Table 6.3, Figure 6.1 and the respective battery weights, the power and energy density for each unit can be calculated (Table 6.4). The battery energy can be calculated by equation 6.4. From these results, the PowerSurge SLA 26-525 was chosen.

$$E_{bat} = \int P_{bat}\, dt \tag{6.4}$$

Table 6.4 Battery Energy and Power Density.

	PowerSurge SLA 26-525		**PowerSurge Deep Cycle**	
Discharge Starting Level (W)	Energy Density (Whr/kg)	Average Power Density (W/kg)	Energy Density (Whr/kg)	Average Power Density (W/kg)
565	17.07	33.03	14.87	46.95
790	13.70	45.67	12.43	62.20

Even though the U1DC44 demonstrated a higher power density and has lower weight, the 26-525 battery has a greater energy density and lasted longer in terms of maintaining a voltage that was above 80 % DOD. The space that was allocated to the batteries also presented a physical limit as to which battery could be used. It was also important, that the battery be able to supply high currents that would be required by the electric drive. Even though the U1DC44 had a higher specific power, it could not supply the high instantaneous current draw that was required for the electric drive in the NHEV. Separate uncontrolled tests were performed with both batteries. They were used to crank a 3.8 V6 engine, the current drawn was measured for the initial starting period, to determine if they could supply an instantaneous high current draw (a max. of 400A) to the electric motor controller. The positive results of these tests, along with the greater energy density (compared to the U1DC44) of the 26-525 battery, were the determining factors. Since, the vehicle drive strategy does not allow for the regeneration of electric energy, it was not extremely important to have a deep cycle battery construction in this phase of the design.

With the design objective, a constant 48 km/h over a 10 km driving range, it could be seen that this trip would require approximately 12.6 minutes to complete. Using the average power required from the batteries of 4.94 kW (from equation 6.1), this 10 km trip would consume 1.04 kWh from the battery pack. Using the data for the 790 W power draw, at 12.6 minutes the battery specific power is 46

W/kg; thus, from the 114.3 kg pack, 5.26 kW would be required and 1.105 kWh would be consumed. Thus, using the C/0.5 rate, 56.7% of the available battery pack energy would be consumed.

The best case scenario and the maximum theoretical electric driving range can be established by using the data for the 565 W power draw. At the 12.6 minute mark, the battery specific power was 36.2 W/kg. For the 114.3 kg battery pack, 0.87 kWh would be consumed. Having reached the 80% DOD level at the 31 minute mark, 1.57 kWh would be consumed. With a required 12.6 minutes to travel 10 km, and after extrapolating the distance to the 31 minute time period, the maximum electric driving range of the vehicle can be evaluated at 18 km.

6.3 Battery Charging

The battery charging system located on-board the vehicle, provides the capability to charge the battery pack at any conventional electrical outlet. The two units that were chosen are manufactured to comply to strict industry standards and are UL listed and CSA approved.

Listed in Table 6.5 are the charger manufacturer specifications; the descriptive pamphlet is included in Appendix 3.

Table 6.5 Battery Charger Specifications.

Manufacturer/Type	Todd Engineering Sales Inc.- Power Source Battery Charger
Input: Voltage	100 - 130 VAC
Output per unit: Voltage	55.2 VDC from 0-Approx. 85% Load 48 VDC @ Full Load
Units/Connection/Location **Total Output Voltage**	2 units/Connected in Series/On-Board 110.4 VDC; 96 VDC @ Full Load
Unit Weight/Total Weight	5 kg / 10 kg
Unit Size (cm)	Width: 18.4 Length: 39.4 Height: 10.2

The two selected charging units were custom manufactured. Once installed and connected in the vehicle, in series, they provide a charging output of 110.4 VDC. This results in a 13.8 Volt charge to each propulsion battery, which is the ideal charging voltage for typical lead-acid batteries. These units are designed to be plugged into any conventional 15 A, 110 V household or industrial outlet. Battery charging is through a pure DC charger output that is regulated at 110.4 Volts. The charging operation is performed through a taper type charge, which

adjusts the current flow depending upon the voltage difference between the battery and the charger, until there is no current flow.

These units are compact and lightweight. They were placed close to the battery pack in unobtrusive areas and near the refueling/charging receptacle (Section 5.9). Illustrated in Figure 6.3, the two chargers (denoted by the letter A) are placed on the rear right side of the vehicle.

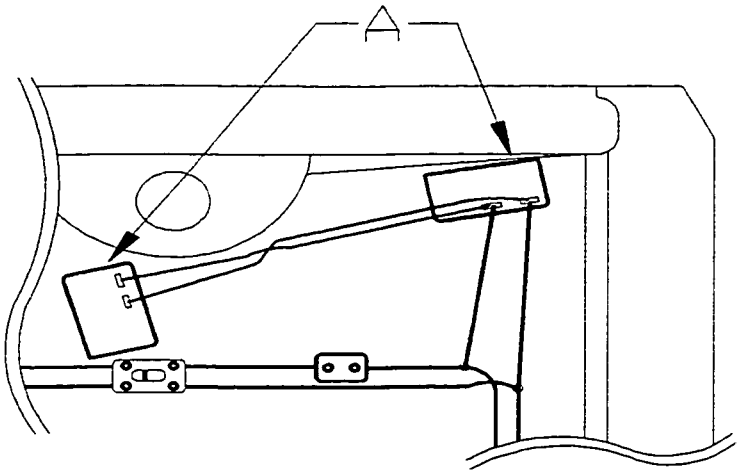

Figure 6.3 Vehicle Cut-Out View - Location of the Two Chargers.

To conform to the HEV Challenge the charging system was modified to be supplied from a 30A, 220-240 VAC outlet. The use of a 220-110 V transformer (off-board the vehicle) along with a timer in-line with the Neon charging units, enabled the charging process to be initiated through the supplied high voltage. By removing these extra components, battery charging can continue with the low voltage 110 V outlets. Typically, charging of the batteries will occur at the driver's discretion when an electrical outlet is available. To replenish this battery pack when it is at 75% depth of discharge, it will take approximately 6 hours using

the 110 V outlet.

A printout of the NHEV charging characteristics is shown in Figure 6.4. Battery charging was done through a 220V outlet and the 220-110V transformer, thus, having the input to the vehicle chargers set at 110 V. As it is shown in the figure, the total harmonic distortion (THD) is very high, however, these results can be attributed to the use of the transformer.

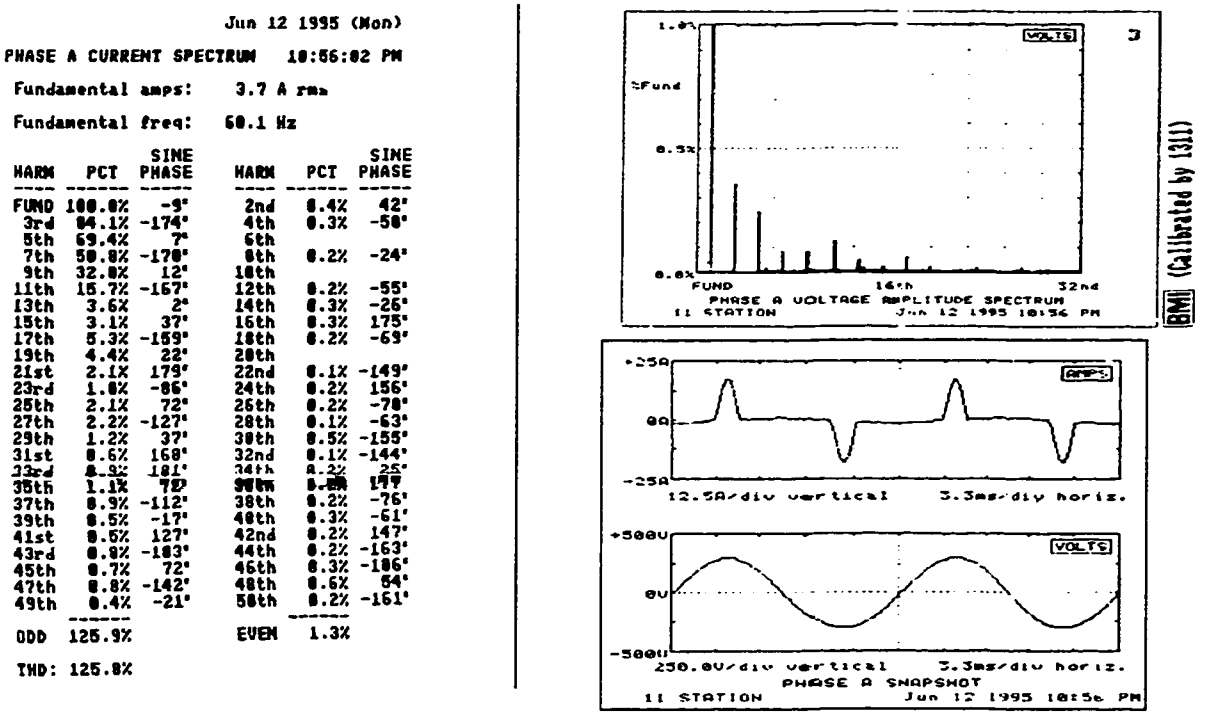

Jun 12 1995 (Mon)

PHASE A CURRENT SPECTRUM 10:56:02 PM

Fundamental amps: 3.7 A rms

Fundamental freq: 60.1 Hz

HARM	PCT	SINE PHASE	HARM	PCT	SINE PHASE
FUND	100.0%	-9°	2nd	0.4%	42°
3rd	84.1%	-174°	4th	0.3%	-58°
5th	69.4%	7°	6th		
7th	50.8%	-170°	8th	0.2%	-24°
9th	32.8%	12°	10th		
11th	15.7%	-167°	12th	0.2%	-55°
13th	3.6%	2°	14th	0.3%	-26°
15th	3.1%	37°	16th	0.3%	175°
17th	5.3%	-159°	18th	0.2%	-69°
19th	4.4%	22°	20th		
21st	2.1%	179°	22nd	0.1%	-149°
23rd	1.8%	-86°	24th	0.2%	156°
25th	2.1%	72°	26th	0.2%	-70°
27th	2.2%	-127°	28th	0.1%	-63°
29th	1.2%	37°	30th	0.5%	-155°
31st	0.6%	160°	32nd	0.1%	-144°
33rd	0.9%	101°	34th	0.2%	25°
35th	1.1%	72°	36th	0.2%	177°
37th	0.9%	-112°	38th	0.2%	-76°
39th	0.5%	-17°	40th	0.3%	-61°
41st	0.6%	127°	42nd	0.2%	147°
43rd	0.8%	-103°	44th	0.2%	-163°
45th	0.7%	72°	46th	0.3%	-186°
47th	0.8%	-142°	48th	0.6%	64°
49th	0.4%	-21°	50th	0.2%	-161°
ODD	125.9%		EVEN	1.3%	

THD: 125.8%

Figure 6.4 Charging Results - Graphs

With the present hybrid electric drive design for this first project phase, it is not possible to regenerate the mechanical energy while the vehicle is in motion. By modifying the electric drive system, the vehicle driving range can be increased and battery charging would not be limited to that supplied by an electrical outlet at stationary conditions.

6.4 Location of the Batteries

The vehicle space limitations and weight distribution requirement limited the choice of the areas that would fit the batteries and the respective enclosure. To minimize modifications to the vehicle structure, the CNG cylinder was placed in the Neon trunk. Thus, the batteries could only be located underneath the vehicle. It was important that the two energy systems, electric and CNG, were isolated from each other. It was also important that the electrical components (discussed in section 5.6.2) were near the batteries, minimizing the length of the high voltage lines. The placement of the batteries towards the vehicle's rear equalized the overall vehicle balance, giving a better weight distribution to the whole structure.

The battery area that was used previously housed the Neon stock gasoline fuel tank. Two indented sections of the vehicle rear sheet metal surface were cut out and a 0.32 cm (1/8") steel plate was welded along the edges. This modification provided a flat surface for the attachment of the battery box and gave the Neon structure more torsional rigidity. Also, the increased volume that was acquired with this change, allowed for the batteries to be placed higher up, which provided the same ground clearance that was originally available with the stock vehicle. The rear seats and seat belts fit in their original locations, since these areas were not affected by the modifications.

6.4.1 Battery Box Design and Mounting

The batteries were placed in two separate boxes that are located on either side of the exhaust pipe that is routed down the vehicle middle. Using structural aluminum angles that are welded together, a box-like container was formed and sealed by thin aluminum plates. Each box was sized to contain four PowerSurge 26-525 batteries, as it is shown in Figure 6.5. The boxes were designed as a modular system that simplified the connection to the vehicle's high voltage grid. It is not required to have both boxes installed to make the vehicle operational. The batteries were connected in series. Between the two boxes, the batteries were inter-connected with quick-disconnect *Anderson* connectors. The high voltage line outputs were connected to the vehicle's voltage grid by another *Anderson* connector.

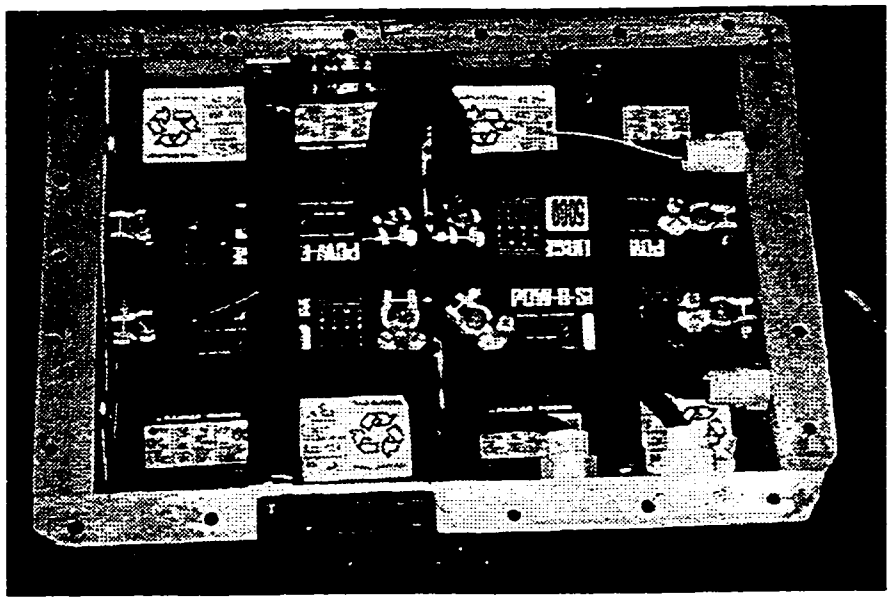

Figure 6.5 PowerSurge 26-525 Batteries Installed in One Battery Box.

Between the batteries and the inner surfaces of the boxes, and also between each battery, there is a 0.16 cm thick polyethylene plastic sheet. This sheet acts as a protective barrier between the aluminum walls and the battery posts, isolating any surfaces that can be involved in an electrical short. There also is a 0.32 cm thick polyethylene plastic sheet glued to the underside area of the metal vehicle plate. The aluminum battery boxes are, thus, not in direct contact with the steel plate when they are bolted to the vehicle. To complete the installation in each box, two insulated bars are placed over the batteries to clamp them down. A side cross-section view of one battery box and the mounting location is illustrated in Figure 6.6.

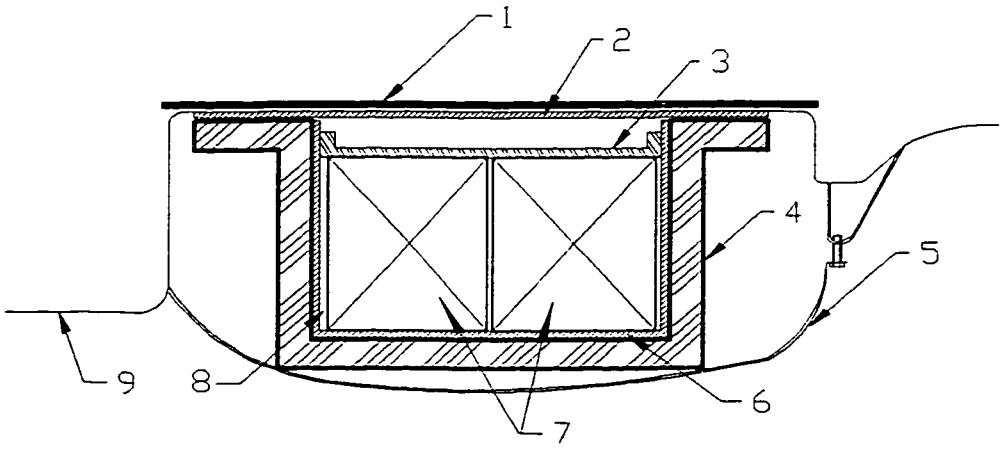

1. Inner Steel Plate - 0.32cm thick
2. Polyethylene Sheet - 0.32cm thick
3. Battery 'Clamp-Down' Bar
4. Aluminum Battery Box
5. Metal Strap
6. Polyethylene Sheet- 0.16cm thick
7. Batteries
8. Air-Gap
9. Vehicle Underbody - Sheet Metal

Figure 6.6 Side Cross-Section of a Battery Box.

The battery boxes that are mounted underneath the Neon HEV are held in place by high strength bolts. To spread the load across a larger area, each box is supported by a thin metal strap that is placed across the box's bottom surface. This mounting arrangement ensures that in case of an impact equivalent to a force of 30g, (see calculations in Appendix 3) the boxes will not separate from the attached surface.

6.4.2 Battery Box Ventilation

To ensure that there is no harmful buildup of hydrogen gas from the lead-acid batteries, the battery boxes are ventilated. The batteries in the boxes are resting on a polyethylene sheet, which in effect raises them by 0.16 cm. Thus, holes in the bottom of the boxes permit air to be drawn and to be circulated throughout the box. Fresh air, along with battery "exhaust air", is drawn out from the top of the boxes by brushless electric fans that are rated for 10 CFM (0.28 m^3/min) flow rate. Each box has its own fan, which is installed in a canister towards the rear of the box. The canister is attached to the battery box by two tubes and the air is exhausted through these tubes. The fans are always activated during the following conditions: when the vehicle's low voltage (12V) grid is active, when the vehicle is operating in any drive mode and also when the batteries are being charged.

6.5 Summary

The NHEV propulsion system criteria of space, location, weight, performance and cost were the determining factors in choosing the two East-Penn lead-acid batteries. Tests performed on these batteries, namely, the PowerSurge SLA 26-525 and the PowerSurge U1DC44 provided energy and power density data that were used to compare the two systems. From the tests and the analysis that followed, it was determined that the best battery to supply energy to the electric drive and to meet the minimum range requirements was the PowerSurge SLA 26-525. A description of the battery charging system followed. The placement of the batteries, the battery box construction and battery ventilation were also presented.

7. MODIFIED DRIVE STRATEGY ANALYSIS

The performance characteristics for the acceleration and economy modes of the converted Neon car were presented and discussed in Chapter 4. A detailed description of the vehicle components and the drive system followed in Chapters 5 and 6. In this chapter, a proposed drivetrain design modification, and simulation results of improved vehicle performance for the next competition will be presented.

It will be explained how the hybrid drivetrain could be improved in terms of driveability and how the vehicle economy could be enhanced in terms of regenerative driving. This section will thus illustrate the changes that would provide improved results regarding the established objectives, that are restated as follows:

- to improve hybrid vehicle and electric only vehicle driveability,
- to further decrease the acceleration time required to attain speeds of 60 km/h and 100 km/h and,
- to improve the overall vehicle fuel economy.

The simplified driving cycle simulation, proposed in Chapter 4, will be used again to explore how energy consumption can be minimized using an electric motor that allows for energy recuperation during deceleration and hill descent.

7.1 Hybrid Drive System Changes

By replacing the present electric drive with a more sophisticated and advanced system, electric energy regeneration can be achieved. The vehicle's kinetic energy at deceleration and potential energy during down-hill driving can be harnessed, converted to electric energy, and stored in batteries through the use of an electric motor with regeneration capabilities and an adequate battery pack. This will also minimize energy losses through braking. The updated electric drive would have to be compact enough to replace the existing drive without entailing additional modifications to the vehicle.

The electric drive that was chosen to replace the present one, consists of a high-efficiency AC Induction motor combined with a controller that features smooth and powerful regenerative braking. In Figure 7.1, a size comparison is depicted for both the motor and controller systems.

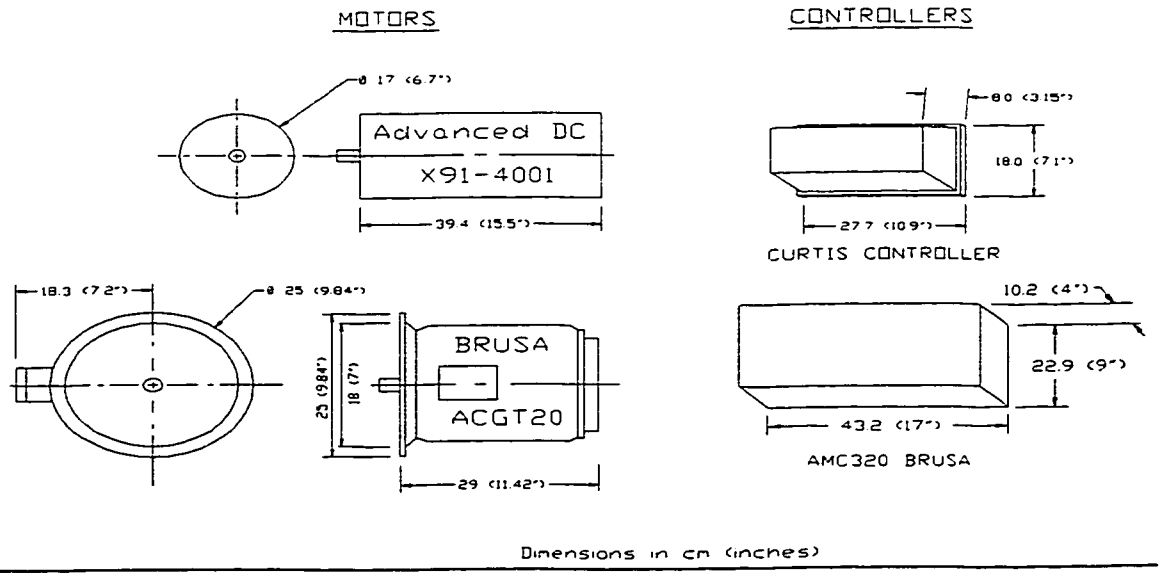

Figure 7.1 Motor and Controller Dimensions.

It can be seen that the new electric drive will be able to fit in the space that is occupied presently by the existing motor and controller. The basic characteristics for both, the present and the proposed electric systems, are listed in Table 7.1.

Table 7.1 Electric Motor and Controller Characteristics.

Electric Motor Manufacturer/Type	Advanced DC Motors Inc. Series Wound DC /X91-4001	Brusa Elektronik AC Induction / ACgt20
Operating Voltage	96 Volts	144 Volts
Power -Nominal	9 kW (12 hp)	12 kW (16 hp)
-Maximum	27 kW (36.2 hp)	28 kW (37 hp)
Torque -Nominal	N/A	20 Nm
-Maximum	128 Nm	74 Nm
Maximum Speed	5500 rpm	13000 rpm
Motor Controller Manufacturer/Type	Curtis Instruments Inc. Curtis PMC Model 1221B-74	Brusa Elektronik AC Controller / AC320
Electrical Power -Maximum	N/A	35 kW
-Nominal	N/A	19 kW
Voltage -Nominal	72-120 Volts	108-144 Volts
(Safe Operating Range)	> 48 Volts	92-173 Volts
Current -Max. Motor	400 Amps	240 Amps rms
-Max. Battery	400 Amps	240 Amps
Efficiency -Nominal Power	N/A	98%
-Full Load	Combined with Motor : 86%	96%
Energy Regeneration	NO	YES
Weight : Motor/Controller	37 kg / 5 kg	30 kg / 9 kg
($US) Motor/Controller: Total	$960 / $750 : $1710	$1800 / $5885 : $7685
Total Cost/Max. Motor kW	$63.3 / kW	$274.5 / kW

The most efficient motor/controller system that provides energy regeneration and is commercially available for electric vehicle applications, is the brushless permanent magnet (or AC synchronous) motor. AC induction motors are similar to brushless permanent magnet motors, but have coils for the rotor poles instead of magnets, what is slightly reducing their overall efficiency. The

AC induction motors though, have less rotational losses due to magnetic hysterisis. They can be operated safely at high rotational speeds, extending their operational envelope. They do not contain expensive and heavy magnets that reduces the cost to manufacture the motor. AC induction motors are ideal for applications which can expect a broad range of operating conditions, such as for vehicles that are exposed to urban driving with plenty of acceleration and deceleration [50].

The changing of the electric drive system also requires that the drive ratio be adjusted and the battery system increased to a 144 Volt supply. Since the AC induction motor can be rotated up to 13000 rpm, the maximum torque to the drive wheels could be increased, by matching the engine and motor speeds with an increasing drive ratio. By matching the engine at 8500 rpm and the motor at 13000 rpm speed, the sprocket drive ratio can be determined by equation 7.1.

$$N_s = \frac{Engine\ RPM}{AC\ Motor\ RPM} = \frac{8500}{13000} = 0.654 \qquad (7.1)$$

In this case, the sprockets that will be used will provide an increased electric drive ratio of 1.529; ($N_n = 1/N_s$). Thus, the electric motor torque that is available at the driveshaft will be increased by a factor of 1.529 and consequently the electric motor will be spinning 1.529 times faster than the engine. By properly adjusting the sprocket ratio in the NHEV, the proposed induction motor could easily be implemented. By comparing the *Advanced-DC* series wound motor and the *Brusa* AC induction motor peak torque values, as they are adjusted for the

NHEV drivetrain (Table 7.2), it can be seen that the Brusa motor will actually increase the vehicle's performance.

Table 7.2 Electric Motor Torque Comparison.

	Electric Motor	
	Advanced DC	**Brusa AC**
Sprocket Ratio	0.586	1.529
Motor Speed (rpm) @ Peak Power	2050	4000
Drivetrain Speed (rpm)	3500	2615
Peak Motor Torque (Nm)	128.0	74.0
Adjusted Peak Torque (Nm)	75.0	113.2

An AC induction motor and controller manufactured by **Brusa Electronik** (specifications in Appendix 4) [51] and distributed in North America by **Solectria Corp.**, were chosen for their following characteristics:

1. The motor is a compact and sealed unit with no brushes or magnets and it has a very low electrical resistance with ultra-low rotating losses.
2. The controller provides smooth regenerative braking (with incorporated overload protection) and is capable of a high peak power capacity. The controller efficiency ranges between 95-99%.
3. The vehicle performance will be improved and, with energy recuperation, the vehicle will become more energy efficient.

The motor torque characteristic at a 144 Volt application, (the drive ratio is not included) is shown in Figure 7.2. A peak power of 28 kW is achieved at 4000 rpm and the stall torque remaining almost constant until 4000 rpm, is 74 Nm.

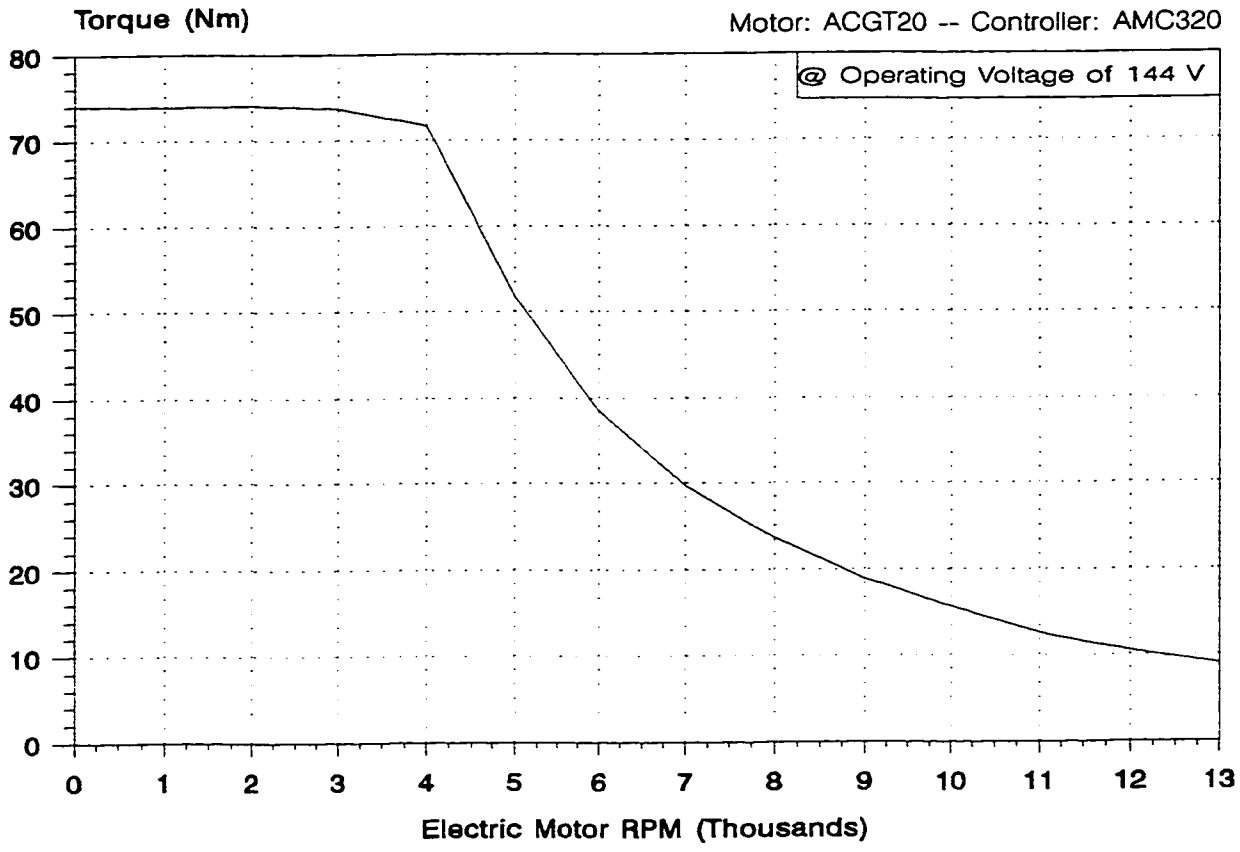

Figure 7.2 Brusa AC Induction ACgt20 Motor @144 V -Torque vs. Motor RPM.

To accommodate the new electric drive characteristics, the batteries have to be changed. Examining the operation of the new electric drive system, the determining factors for the batteries are the following:

- the capability to supply a maximum battery current of 240 Amps,
- a battery pack nominal voltage of 144 Volts,
- a deep cycle battery construction to enhance the recharging process during energy recuperation and,
- a compact battery unit that would fit in the existing location allocated to the current battery system.

Re-examining section 6.2, Testing and Choosing of the Lead-Acid Battery, it can be seen that the East-Penn *PowerSurge Deep Cycle U1DC44* battery would satisfy all of the aforementioned requirements. In this case, the U1DC44 does not have to supply an instantaneous high current draw of 400A (only 240A), as was the case with the Advanced DC system. To operate at 144 Volts, twelve - 12V batteries will be connected in series and placed in the same location occupied by the current batteries. The change of batteries will only add an extra 10.4 kg to the overall vehicle weight. The existing battery trays will each contain five batteries. A separate enclosure can be constructed adjacent to the trays, to accommodate the remaining two batteries. In Figure 7.3, a schematic of the battery tray is shown along with an outline depicting the old and the new battery placement. If it were so desired, new trays could be specifically designed to be mounted in the same location to hold the new batteries.

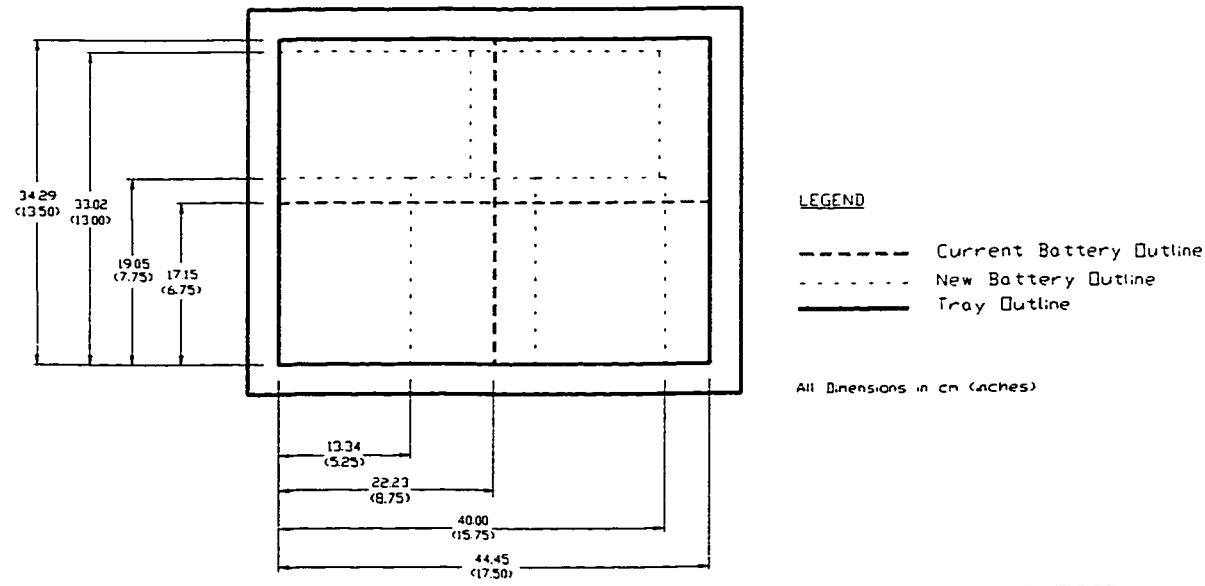

Figure 7.3 Schematic of One Battery Tray with Present and New Battery Outlines.

The proposed changes to the drive system entails an adjustment to the vehicle parameters that will be used in the vehicle performance and energy economy analyses. The nominal parameters listed in Table 4.1 remain the same except for the vehicle mass, which changes to 1487.8 kg. This includes the weight of the vehicle, two people and cargo. Listed in Table 7.3, are the system response parameters that are used to determine the best acceleration and energy consumption results.

Table 7.3 Modified System Parameters.

Vehicle Mass, m_V (vehicle weight + driver weight)	1407.4 kg
Battery Nominal Voltage	144 V
Drive Mode	HEV
Road Incline	Level Surface
Electric Drive Sprocket Ratio	1.529

7.2 Performance Mode Analysis

Using the modifications that were outlined in the previous section, the vehicle performance can be re-examined. The available drive force and torque at the wheels is once again calculated by using the combined torque available at the transaxle driveshaft input. A summary of the drive ratios with the Neon five speed transaxle is shown in Table 7.4.

Table 7.4 Modified HEV Drive Ratios and the Neon Five Speed Transaxle.

Transmission		**Overall Drive Ratio**	
Gear		Engine	Electric Motor
First	3.54	12.57	19.22
Second	2.13	7.56	11.56
Third	1.36	4.83	7.39
Fourth	1.03	3.66	5.60
Fifth	0.72	2.56	3.91
Final Drive	3.55		
Sprocket Ratio	1.529		

A quick examination of the different possible gear shifts is performed. It is seen that the best HEV acceleration time is achieved when the gear shifting occurs at the drivetrain speed of 8500 rpm. A summary of these results is shown in Table 7.5. At 8500 rpm the engine is producing 48 kW of power and 54 Nm of torque. At this engine speed, the electric motor is spinning at 13000 rpm and is still providing a peak 12 kW of power and 9 Nm of torque, which translates to a torque of 13.8 Nm at the transaxle driveshaft input.

Table 7.5 Acceleration Result Summary.

Engine RPM Shift Point	Time to Accelerate (seconds) 0-60 km/h	0-100 km/h	Acceleration Top Speed (km/h)
4500	8.20	20.35	162
5500	8.17	19.92	184
6500	8.05	18.62	184
8500	8.05	18.07	184

The simulated acceleration response for this modified hybrid electric drive is illustrated in Figure 7.4. The gear shifting is performed at 8500 rpm and the best acceleration for both 0-60 km/h and 0-100 km/h conditions is plotted in terms of time and distance. For attaining 60 km/h in 8.05 seconds the vehicle has to travel 94 m. The $^1/_4$ mile or 402 m distance can be achieved within 17.51 seconds at the end speed of 98.23 km/h.

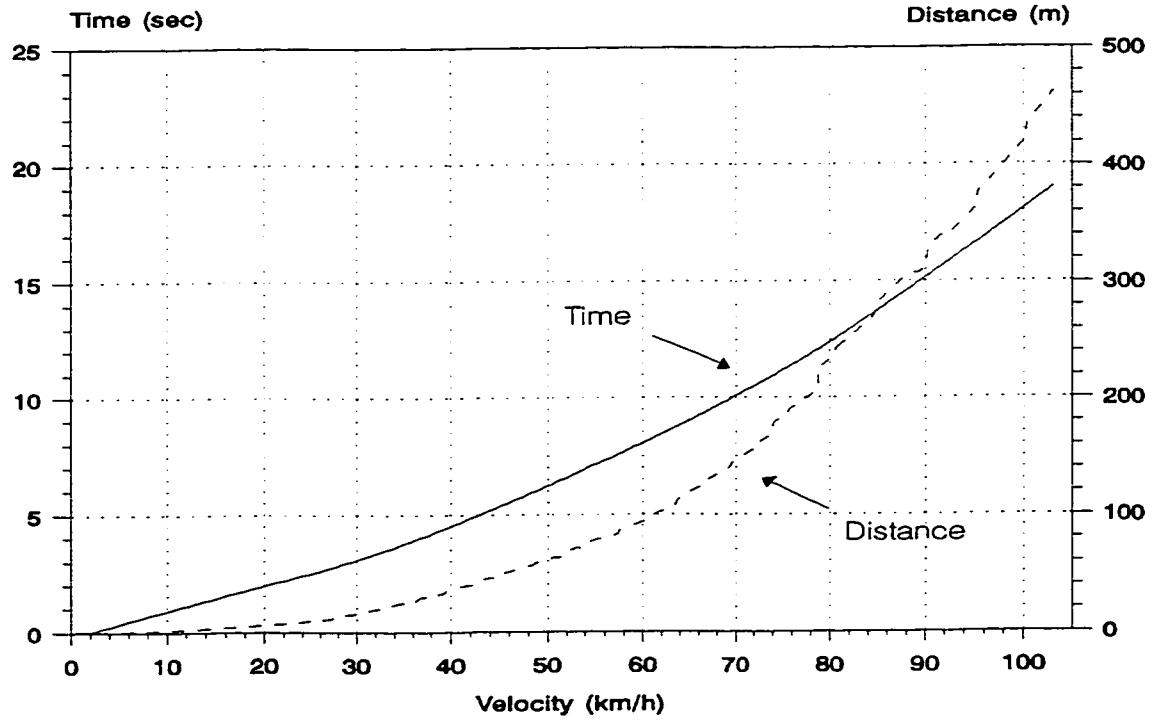

Figure 7.4 Acceleration Response for the Modified HEV Drive.

A plot of the simulated drive force available to accelerate the vehicle is shown in Figure 7.5. It can again be seen that only the first two gears are required to accelerate to either 60 or 100 km/h, with the third gear being used to accelerate to a top speed of 184 km/h. Thus, in a performance mode, only three gears are required to operate the vehicle.

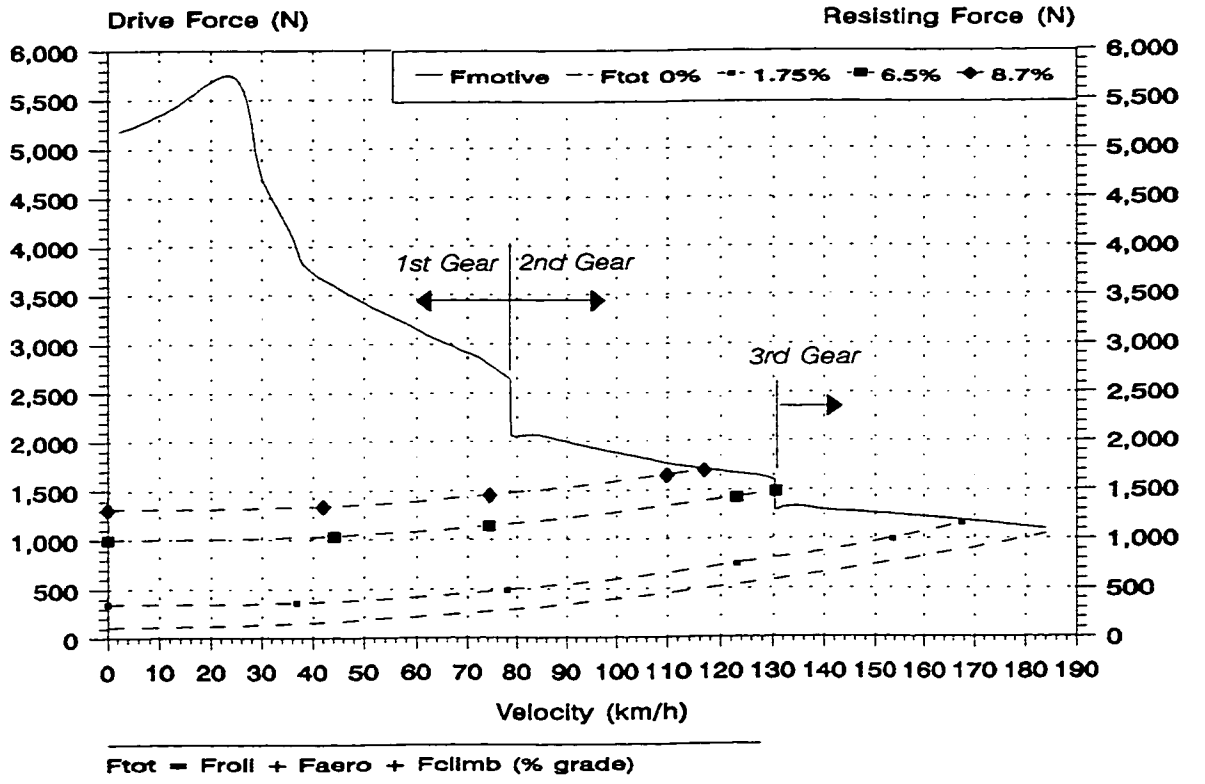

Figure 7.5 Drive and Resisting Forces vs. Vehicle Velocity (Modified Drivetrain).

Also, illustrated in Figure 7.6 are the simulated drivetrain torque and drivetrain rpm versus time for this performance mode acceleration, where the gear shifting is occurring at 8500 rpm. It can be seen that at this shift point, the engine torque is almost constant from 5700 rpm onwards. Since the engine is designated as the vehicle's main powerplant, it is desired (for performance oriented situations)

to operate the engine at its maximum output point. As it is shown in Figure 7.6, the engine produces a continuous maximum torque, with the additional torque from the electric motor being used to further improve the acceleration times.

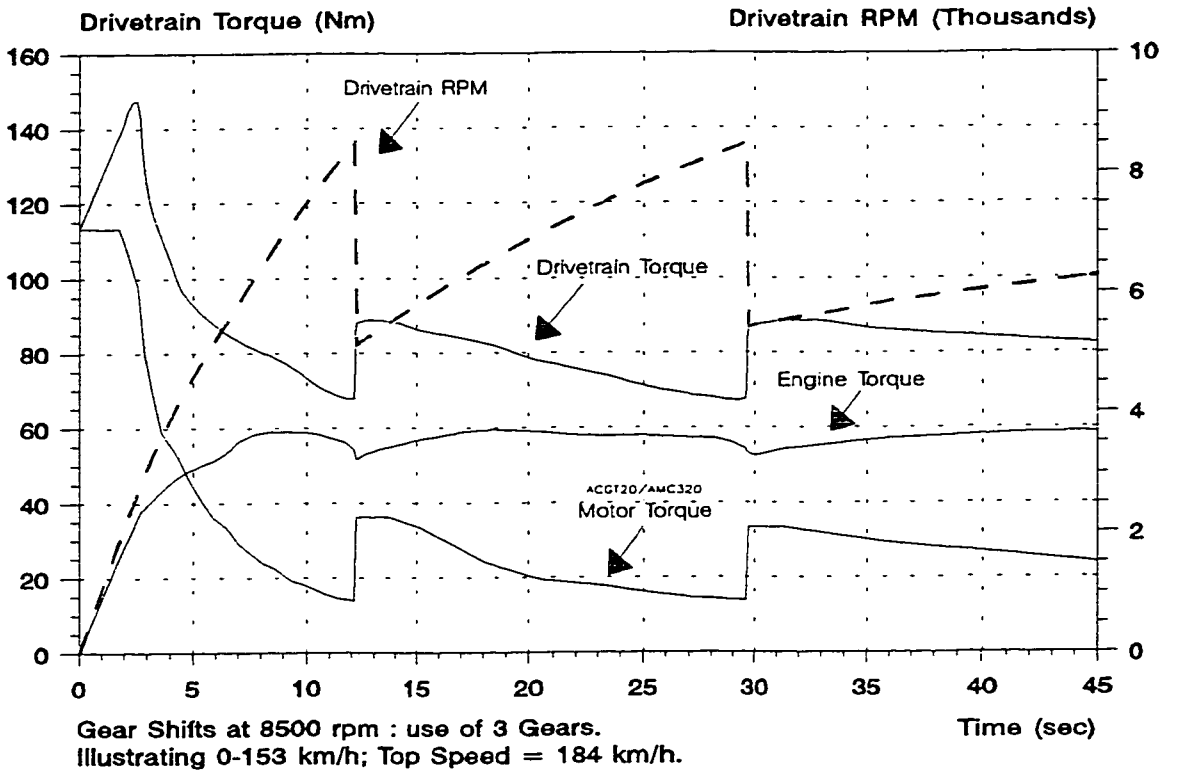

Figure 7.6 Drivetrain Torque and Drivetrain RPM vs. Time (Modified Drive).

A comparison of the performance mode acceleration results with the old and new drivetrain configurations is presented in Table 7.6. In terms of performance driveability the AC Induction drivetrain provides a considerable improvement and sufficiently satisfies the acceleration objectives.

Table 7.6 Performance Mode Comparison.

	Best Acceleration Time (seconds) 0-60 km/h	0-100 km/h	**Acceleration Top Speed** (km/h)
New: **AC Induction Drivetrain**	8.05	18.07	184.0
Old: **Advanced DC Drivetrain**	9.51	21.83	173.5
% Improvement	18.0 %	21.0 %	5.7 %

The performance improvement during the HEV operation can also be applied to the vehicle EV operation. The vehicle's economy mode performance and the use of the AC Induction energy recuperation capabilities will be discussed in the following section.

7.3 Fuel Economy Analysis for NHEV with the AC Induction Drivetrain

Having examined the driveability performance of the modified vehicle design, by focusing upon the vehicle's acceleration capabilities, the analysis will be expanded to examine vehicle energy consumption and energy recuperation. As it was discussed in section 4.4, the vehicle driveability will be examined from the perspective of minimizing the energy consumed, with the operation of the two powerplants during different phases of a simplified drive circuit.

Two drive cycles are again used in the simulation (0-60-0 km/h and 0-100-0 km/h cycles) and the optimal shift speed to achieve the largest energy efficiency rate is again determined. In the following table, (in conjunction with Figure 4.12), the simulation setup is re-stated and summarized.

Table 7.7 Simulation Circuit Description.

Drive Cycles	0-60-0 km/h, 0-100-0 km/h
Distances	1 km, 4 km, 10 km
Cycle Phases	Acceleration, Steady State, Deceleration
Phase I - Acceleration	Hybrid Mode : Engine + Motor
Phase II - Steady State	Engine Mode : Engine Only
Phase III - Deceleration	Electric Mode : Motor Only (Regeneration)

Equations 4.11 and 4.12 can again be used to calculate the energy consumed by the electric drive and the engine, respectively. During the deceleration phase the vehicle will be in electric mode. In this phase the electric motor functions as a generator. Thus, the energy recuperating properties of the electric drive system can be used to convert the vehicle's kinetic energy into

electric energy and, subsequently, slow the vehicle without the use of brakes. If it would be desired to further decrease the stopping distance, the brakes could be applied to slow down the vehicle; however, a part of the vehicle's kinetic energy would be dissipated.

7.3.1 Determination of Optimum Conditions for Maximum Energy Efficiency

By shifting gears at various drivetrain speeds, the best conditions are determined for the least amount of overall energy consumed. With the modified electric drivetrain, there can also be an accounting for the most energy that could be recovered during deceleration. Each phase of the 0-60-0 km/h and 0-100-0 km/h drive cycles is discussed in detail in subsequent sections. A summary of the drivetrain shift speed and corresponding overall energy efficiency is presented in Tables 7.8a and 7.8b. The energy efficiency is calculated by summing the energy consumed during the acceleration and steady state phases and the energy recovered during the deceleration phase.

Table 7.8a A Summary of the 60 km/h Simulation - Modified Drivetrain.

	Energy Efficiency Distance/Energy - (km/kWh)		
Drivetrain RPM at Shifting	**1 km circuit**	**4 km circuit**	**10 km circuit**
2500	3.81	4.33	4.45
3000	3.90	4.35	4.46
3500	3.94	4.37	4.47
4500	3.79	4.34	4.47

The most energy efficient condition exists when the 0-60-0 km/h drive cycle is

performed with the gear shifting occurring at a drivetrain speed of 3500 rpm. For the 0-100-0 km/h cycle, the most energy efficient condition occurs when the gear shifting is at a drivetrain speed of 3000 rpm.

Table 7.8b A Summary of the 100 km/h Simulation - Modified Drivetrain.

	Energy Efficiency Distance/Energy - (km/kWh)	
Drivetrain RPM at Shifting	**4 km circuit**	**10 km circuit**
2500	2.87	2.63
3000	2.96	2.66
3500	2.87	2.64
4000	2.89	2.65
4500	2.86	2.64

7.3.2 Phase I of the Simulation Drive Cycle - Acceleration

For economy mode operation, the vehicle acceleration is performed similarly as for the performance mode. Both powerplants are being used with the goal of having adequate acceleration and at the same time of minimizing the energy consumption. This phase of the drive cycle is illustrated in Figure 7.7.

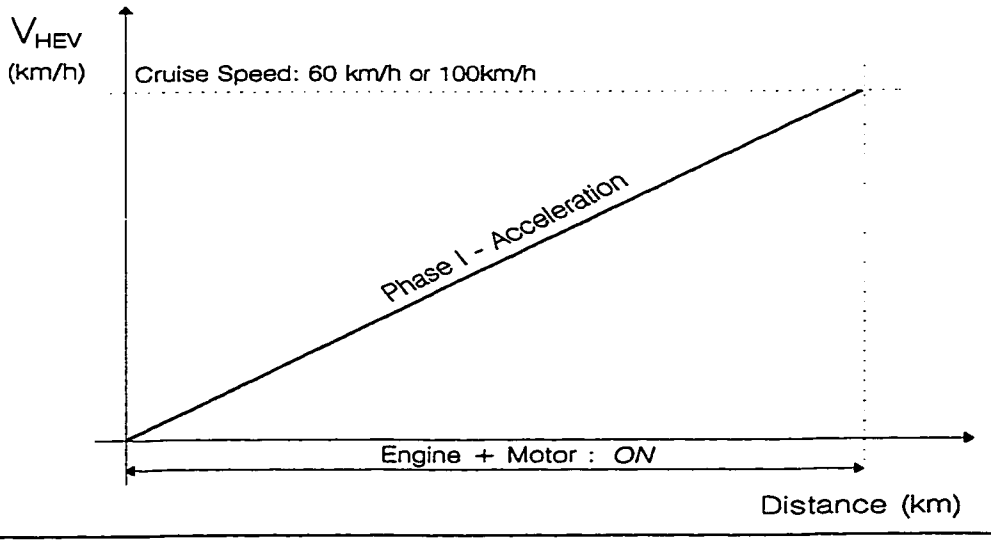

Figure 7.7 Drive Cycle - Acceleration Phase.

For acceleration to 60 km/h, during the performance mode operation, one gear was required to achieve 60 km/h within 8.05 sec., traveling a distance of 94 m. Whereas, for the economy mode operation, the gear shifting was performed at a drivetrain speed of 3500 rpm and three gears were required to achieve 60 km/h within 8.45 sec., traveling a distance of 111.6 m. The respective energy consumption graphs for both the performance and economy mode acceleration phases, to a speed of 60 km/h, are shown in Figures 7.8a and 7.8b.

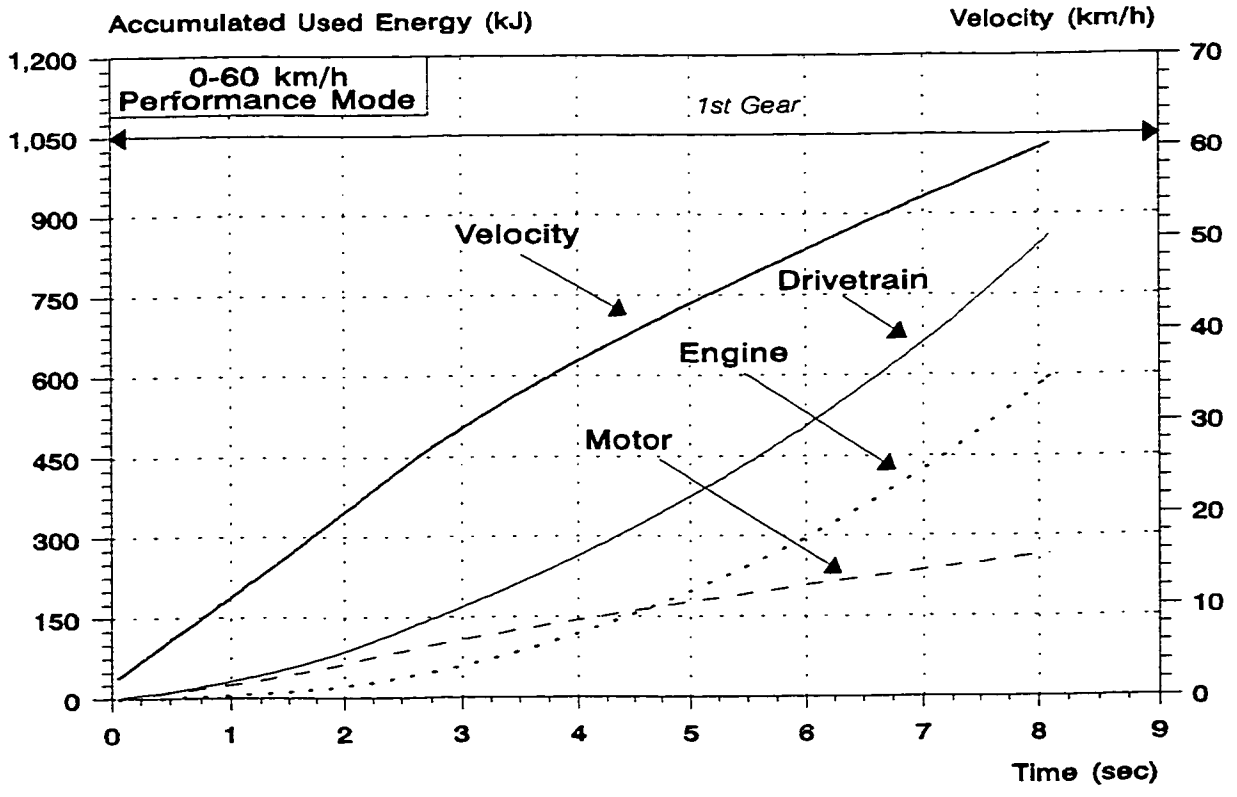

Figure 7.8a Performance Mode Energy Consumption for Acceleration of 0-60 km/h - Modified Drivetrain.

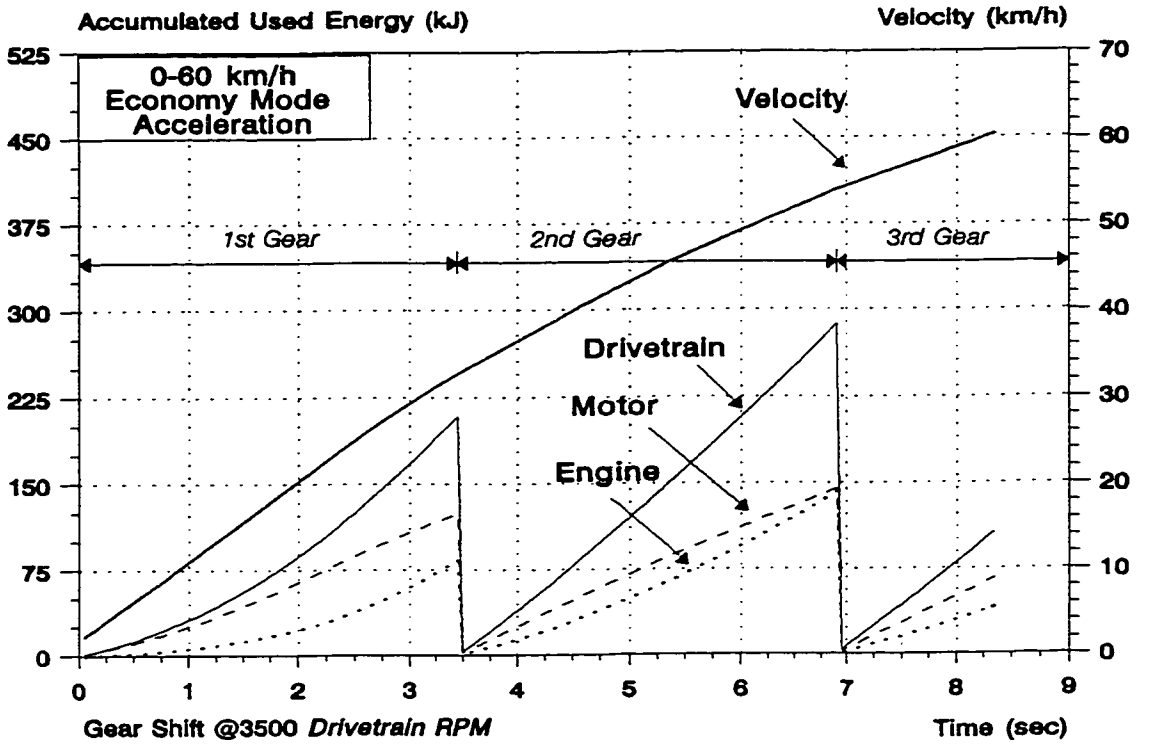

Figure 7.8b Economy Mode Energy Consumption for Acceleration to 60 km/h - Modified Drivetrain.

For acceleration to 100 km/h, a similar analysis was effected. During the performance mode operation, the gear shifting occurred again at a drivetrain speed of 8500 rpm. The first two gears were required to achieve 100 km/h within 18.07 seconds, travelling a distance of 418 m. For the economy mode operation, the gear shifting occurred at a drivetrain speed of 3000 rpm. In this mode, all five gears were required to reach 100 km/h; this was performed in 22.3 sec. over a distance of 820 m. The energy consumption for the 0-100 km/h economy mode acceleration is shown in Figure 7.9. Summarized in Table 7.9 is the total energy consumed for the different acceleration conditions, for both the 60 km/h and 100 km/h acceleration phases.

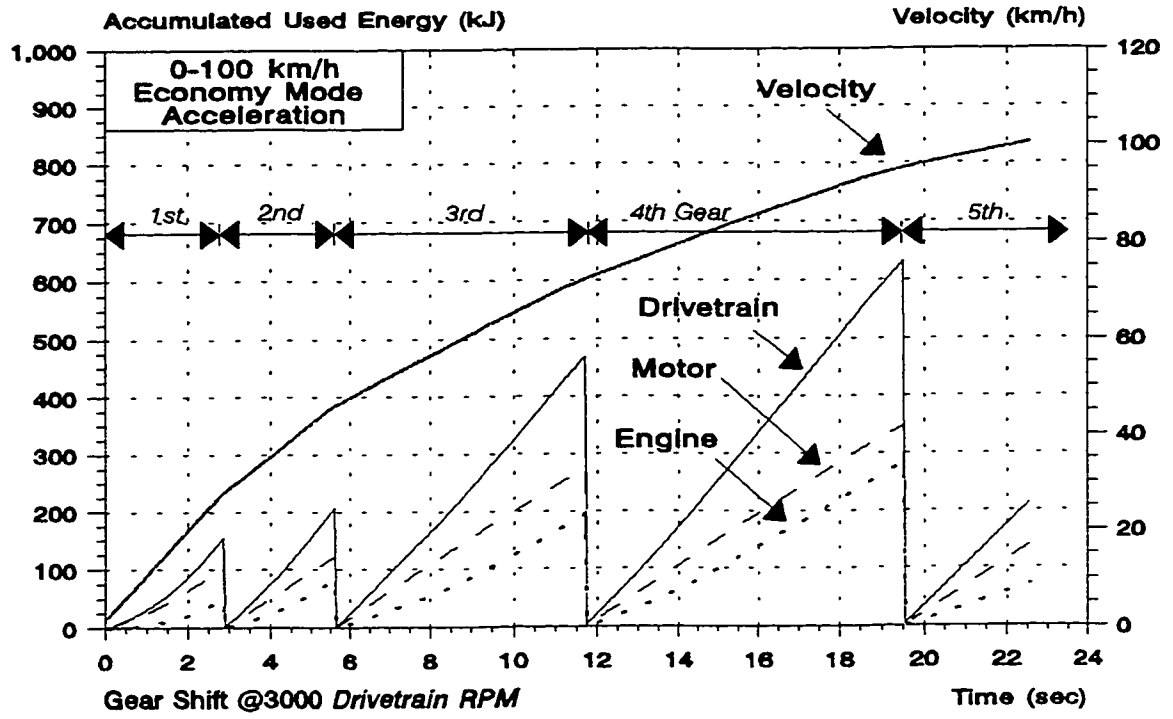

Figure 7.9 Economy Mode Energy Consumption for Acceleration to 100 km/h - Modified Drivetrain.

Table 7.9 Energy Consumption Summary for the Cycle Acceleration Phases.

	Acceleration Conditions			
	0-60 km/h		**0-100 km/h**	
Mode	*Performance*	*Economy*	*Performance*	*Economy*
Total Energy Consumed (kJ)	857.9	598.9	2757.9	1658.9
Gears Used	1	3	2	5
Time Required (s)	8.05	8.45	18.07	22.30
Distance Required (m)	94	111.6	418	820

7.3.3 Phase II of the Simulation Drive Cycle - Steady State

Having established the energy consumption during the acceleration phase of the drive cycles, the next step would be to examine the results during the steady state phase of the cycle. During this phase, the electric motor is shut-off since the power assist from the motor is not required to maintain the required constant speed. The engine is used, within its lowest specific fuel consumption (sfc) regime, to maintain the required steady state speed. Depending upon the drivetrain speed reached at the end of the acceleration phase, the appropriate gear is selected to maintain the engine in a low sfc range. Listed in Table 7.10 is the steady state gear and the drivetrain end speed once the steady speed of 60 km/h or 100 km/h was reached.

Table 7.10 Settings for Steady State Driving.

	Steady Velocity	
	60 km/h	**100 km/h**
Drivetrain Speed at Steady State (rpm)	2497	2204
Steady State Gear	3	5
Engine sfc in Final Gear (g/kWh)	261.0	261.5

It is seen that for both speeds of 60 km/h and 100 km/h the engine sfc at steady state is about 261 g/kWh. The complete simulation drive cycle would range from between a 1-10 km distance, thus, steady state portion of the cycle would vary accordingly. The final results are tabulated in Table 7.11.

Table 7.11 Steady State Data - Modified Drivetrain.

	Steady Velocity	
	60 km/h	**100 km/h**
	1 km Circuit	
Energy Consumed (kJ)	539.4	n/a
Steady State Gear	3	n/a
Driving Time (s)	40.75	n/a
Distance Covered (m)	679.24	n/a
	4 km Circuit	
Energy Consumed (kJ)	2921.8	3748.6
Steady State Gear	3	5
Driving Time (s)	220.71	93.23
Distance Covered (m)	3679.24	2589
	10 km Circuit	
Energy Consumed (kJ)	7686.6	12435.8
Steady State Gear	3	5
Driving Time (s)	580.64	309.29
Distance Covered (m)	9679.24	8589.02
Energy Efficiency (kJ/m)	0.794	1.448
Energy Efficiency (km/kWh)	4.53	2.49

7.3.4 Phase III of the Simulation Drive Cycle - Deceleration

Once the steady state phase of the cycle is completed, the vehicle will enter the deceleration phase of the cycle. At the end of the steady state phase, the engine's fuel delivery system will be turned off and the engine will be disconnected from the HEV drivetrain. The electric drive will remain connected but it will change to the electric generating mode and the energy recuperation phase will be enhanced by immediately shifting the transmission to the next lower gear. Having the electric motor in generator mode enables the use of the

regenerative braking feature available from this electric motor and controller. The drag forces (aerodynamic, rolling and grade) will also eventually slow down the vehicle. In conjunction with these forces, regenerative braking will decrease the stopping distance with minimizing the use of the vehicle brakes. Using the vehicle brakes would create a loss of energy through its dissipation. If it would be desired to further decrease the stopping distance, the brakes should be used. The deceleration phase of the drive cycle is shown in Figure 7.10.

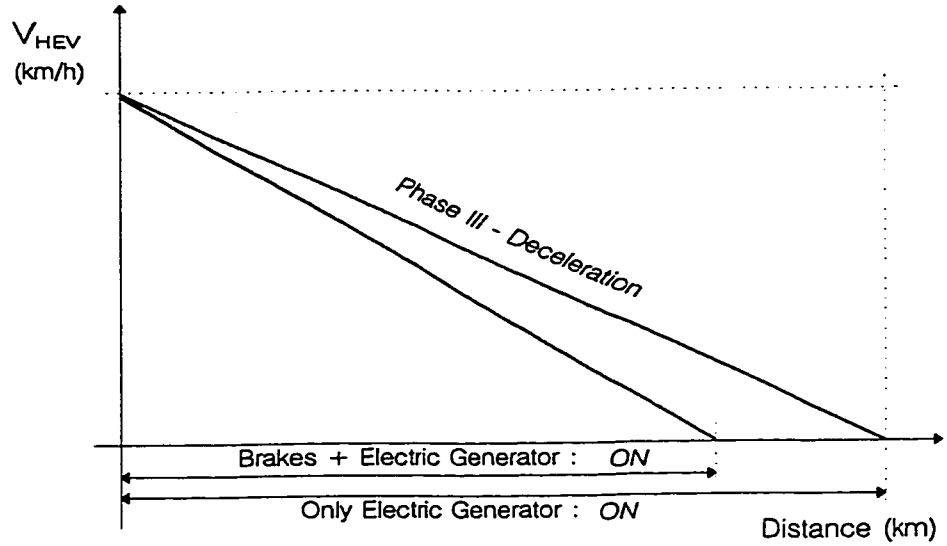

Figure 7.10 Drive Cycle - Deceleration Phase.

The steady state gear will dictate the downshift pattern that will be used to initiate the deceleration phase. If the steady state portion of the cycle were driven in third gear then a downshift to second gear would accompany the deceleration phase. Decelerating from 60 km/h required 209.2 m and 12.8 sec. to get the vehicle to come to a complete stop without the use of any other means of braking. Similarly, decelerating from 100 km/h required 591 m and 24.9 sec. Illustrated in

Figures 7.11a and 7.11b are the respective energy recuperation graphs for both the 60 km/h and 100 km/h deceleration phases.

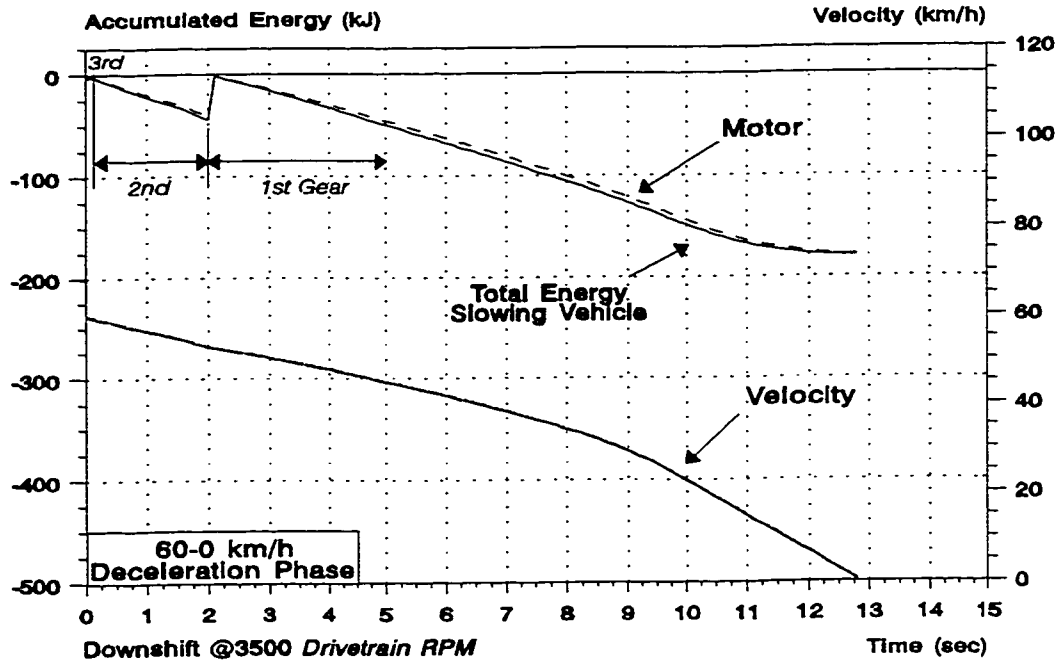

Figure 7.11a Energy Consumption for Deceleration of 60-0 km/h.

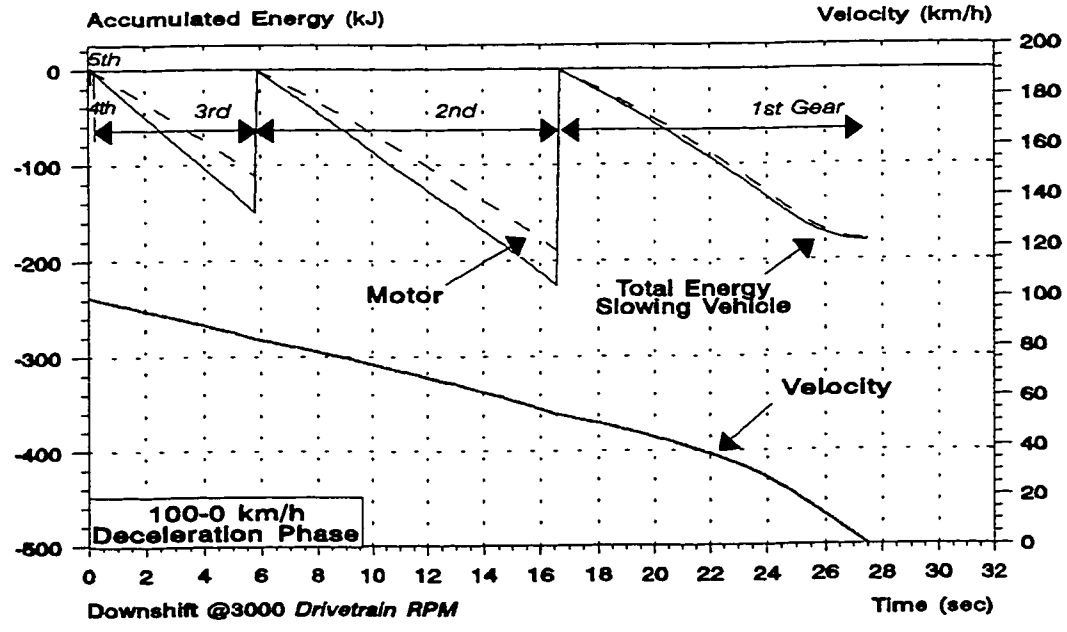

Figure 7.11b Energy Consumption for Deceleration of 100-0 km/h.

Listed in Table 7.12 is a summary of the results for the decelerations from 60-0 km/h and from 100-0 km/h.

Table 7.12 Energy Consumption Summary for the Deceleration Phase.

	Deceleration Conditions	
	60-0 km/h	**100-0 km/h**
Energy Recovered: Motor (kJ)	221.0	481.0
Energy Recovered: Total (kJ)	225.6	547.0
Steady State Gear	3rd	5th
Downshift Speed (rpm)	3500	3000
Time Required (s)	12.8	24.9
Stopping Distance (m)	209.2	591
Energy Recovered: Energy Efficiency (kJ/m)	1.08	0.93

From the simulation it was seen that during the 100-0 km/h deceleration phase a greater amount of energy could be recovered if the transmission were to be downshifted on every second gear. Illustrated in Figure 7.12, at the down shift speed of 3000 rpm, the shift from the steady state gear (fifth) was directly to the third gear and then to the first one. However, it could be seen that the stopping distance and time are longer as compared to the regular (gear by gear) downshift schedule. Thus, to decrease the stopping distance, the brakes would have to be used, which would reduce the gains achieved by the energy being recovered. A comparison of the data follows in Table 7.13. By examining the recovered energy efficiency value, it is understood that the regular downshift schedule should not be altered. The explanation can be given by comparing the two graphs in Figure

7.11b and Figure 7.2. It is now obvious that by increasing the electric motor/generator speed, lower torque is produced, thus decreasing the amount of electric energy produced by the generator.

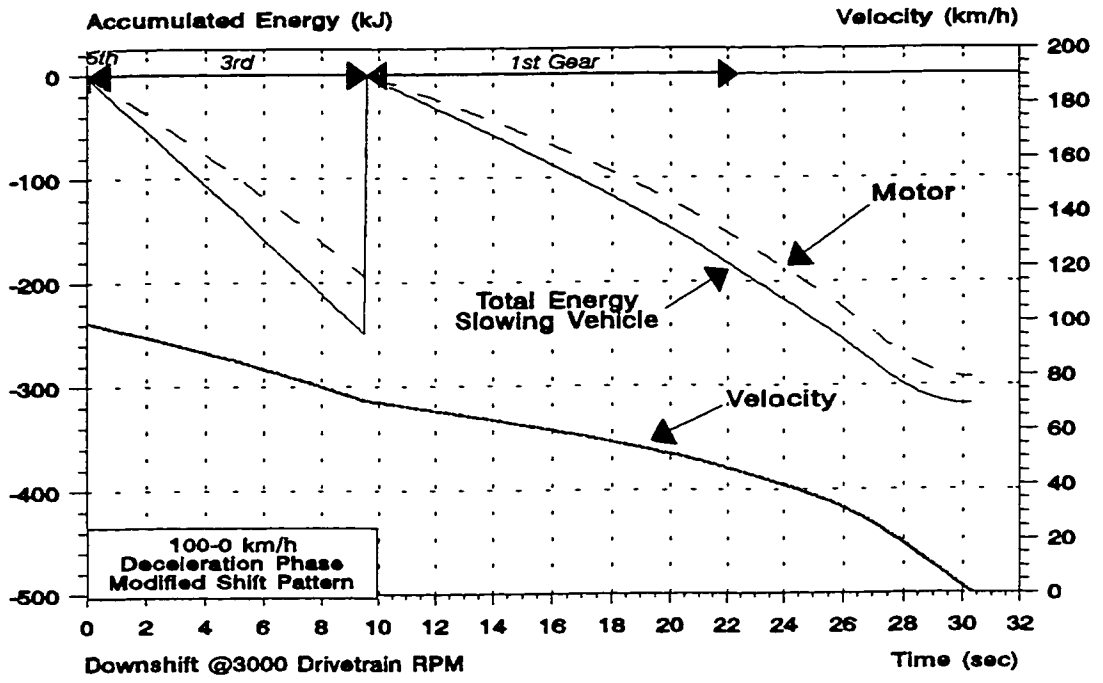

Figure 7.12 Energy Consumption for Deceleration of 100-0 km/h - A Different Shift Schedule.

Table 7.13 Deceleration Data Comparison for Two Downshift Patterns.

100-0 km/h	Downshift Schedule (Gears)	
Downshift Speed: 3000 rpm	**5-3-1**	**5-4-3-2-1**
Energy Recovered: Motor (kJ)	488.0	481
Energy Recovered: Total (kJ) (Motor + Drivetrain)	569.8	547
Time Required (s)	30.35	24.9
Stopping Distance (m)	744.9	591
Energy Recovered: Energy Efficiency (kJ/m)	0.76	0.93

7.3.5 Energy Efficiency and Fuel Consumption Simulation Summary

Having examined each phase of the drive cycle, the best overall conditions could be chosen that would produce the greatest cycle energy efficiency. These results could be next translated to the best fuel consumption that can be achieved for this modified drivetrain. In effect, this simulation, as shown in Chapter 4, determines an upper limit to the maximum possible energy efficiency that could be attained with the chosen components. With the modified drivetrain that provides for energy recuperation, the batteries would be recharged during any deceleration situation. This feature would greatly enhance the vehicle driveability and would help to extend the vehicle's electric range by maintaining the battery state of charge at a significantly higher level than with the previous drivetrain.

The calculated energy consumption using the proposed simulation drive cycle for the modified drivetrain also accounts for the energy recuperated during the deceleration phase. The results are summarized in Table 7.14a for the economy mode operation. Also shown in Table 7.14b are the results which incorporate the performance mode acceleration. A comparison of the previous and modified drivetrain results for the economy mode energy consumption is shown in Chapter 9.

Table 7.14a Fuel Consumption Summary - *Economy Mode* (Modified).

Condition / Cycle	Energy Efficiency (km/kWh)	Equivalent Fuel Consumption ℓ /100 km	(mpg_{US})
Cycle: 0-60-0 km/h			
1 km cycle	3.94	2.87	(82.1)
4 km cycle	4.37	2.59	(90.8)
10 km cycle	4.47	2.53	(93.0)
Cruise @ 60 km/h	4.53	2.49	(94.3)
Cycle: 0-100-0 km/h			
4 km cycle	2.96	3.81	(61.7)
10 km cycle	2.66	4.25	(55.3)
Cruise @ 100 km/h	2.49	4.54	(51.8)

Table 7.14b Fuel Consumption Summary - *Performance Mode* (Modified).

Condition / Cycle	Energy Efficiency (km/kWh)	Equivalent Fuel Consumption ℓ /100 km	(mpg_{US})
Cycle: 0-60-0 km/h			
1 km cycle	3.14	3.60	(65.4)
4 km cycle	4.10	2.76	(85.3)
10 km cycle	4.36	2.59	(90.8)
Cruise @ 60 km/h	4.56	2.48	(94.8)
Cycle: 0-100-0 km/h			
4 km cycle	2.35	4.80	(49.0)
10 km cycle	2.44	4.62	(50.9)
Cruise @ 100 km/h	2.51	4.50	(52.3)

7.4 Summary

The change of the vehicle's electric driveline to an AC induction electric drive system was shown to be feasible, in terms of component placement and vehicle performance requirements. The only disadvantage of such a system would be its relatively high cost. This electric drive system also has the capabilities of providing energy recuperation. The process of energy recovery was examined during vehicle deceleration. To take full advantage of the AC induction motor characteristics, the PowerSurge U1DC44 batteries were seen as a better energy source. It was shown that the existing battery boxes could be re-used. As in Chapter 4, simplified simulation drive cycles were used to determine the vehicle's energy consumption with the AC induction electric drive system. The use of the brakes during deceleration was also discussed.

8. HEATING SYSTEM ANALYSIS AND MODIFICATIONS

As described and illustrated in section 5.8.1, it is understood that repeated and prolonged use of the heating system would greatly reduce the battery energy available to power the electric drivetrain. The battery energy drain can be curtailed by minimizing the heater operation and by implementing a system that would also use engine waste heat for interior heating.

8.1 Heating Analysis

The current electric heating system employs an "on/off" set up that will automatically cycle the heater operation when the coolant temperature approximately reaches 79°C. Depending upon the battery voltage and battery state of charge (SOC), the heater will ensure the appropriate heating. If it is so desired, the vehicle's occupants could manually turn the heater off for a longer period of time and could turn it back on for short bursts of heat. In Figure 8.1, the current being drawn by the heater is depicted for the system operating over a 26 minute time period. The system was operated while the vehicle remained stationary and there was no intermediate recovery of energy through battery charging. Starting from approximately the 18 min. mark and onwards (after it was noticed that the battery voltage started to decrease faster) the heater "off" time was extended by manually turning off the heating for a short duration (0.5-1.5 minutes). It was also seen, if it were desired, this heating system would provide a simple means of

discharging the batteries to a specific SOC level. The power dissipated (for heating) from the battery pack over the same time period is illustrated in Figure 8.2.

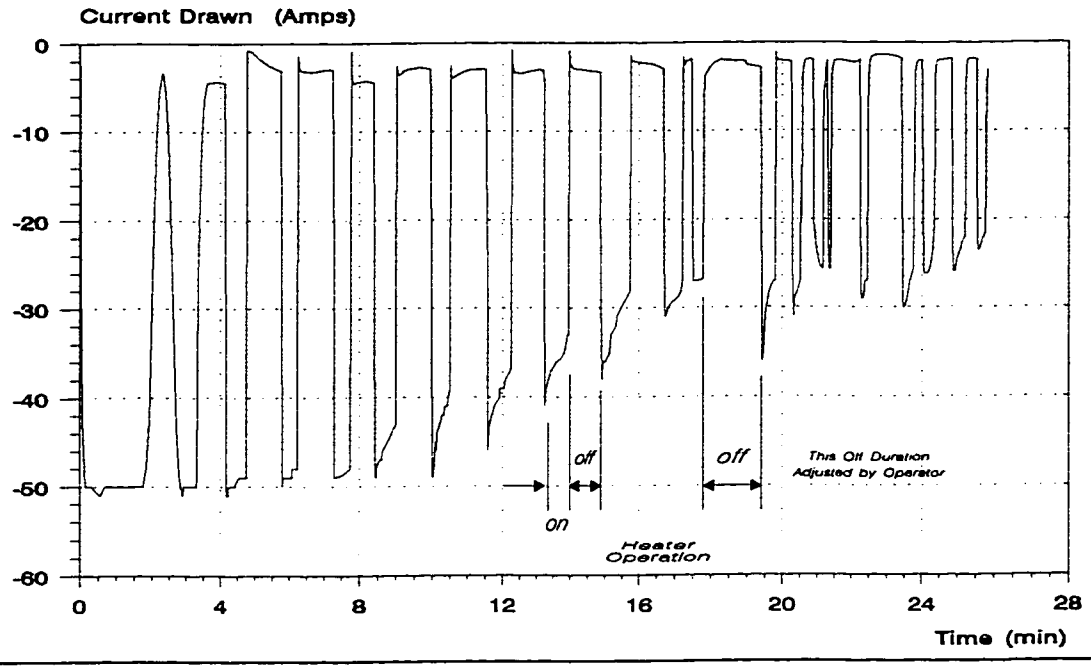

Figure 8.1 Heater Operation - Current Drawn vs. Time.

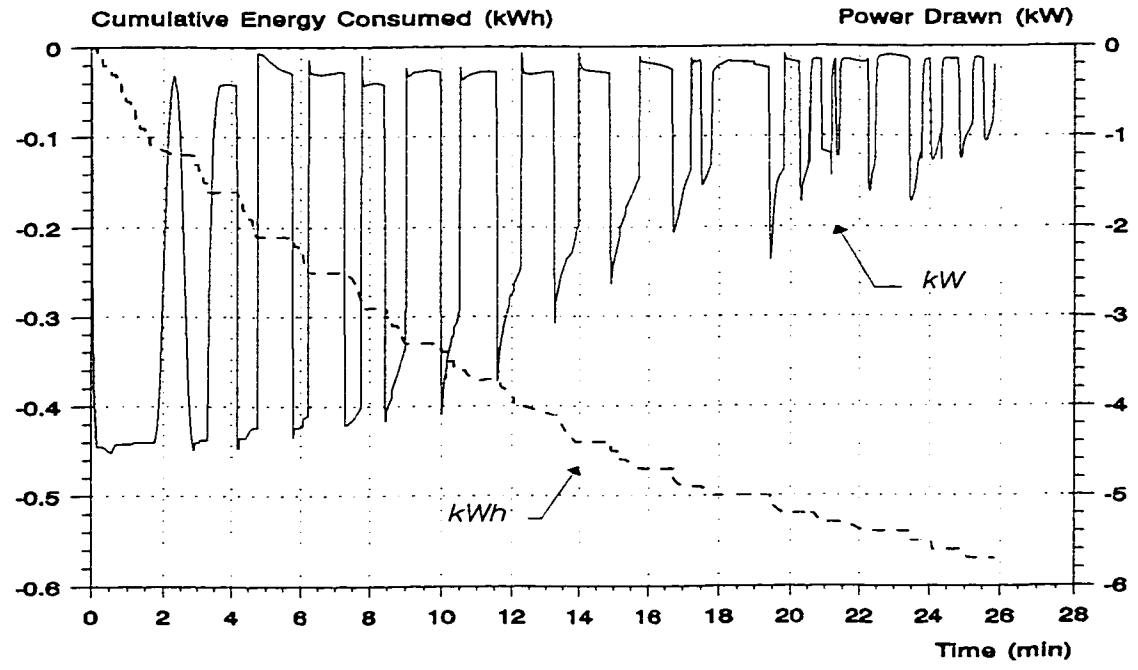

Figure 8.2 Power and Accumulated Energy Consumed vs. Time.

Also, illustrated in Figure 8.2, is the cumulative energy consumed by operating the heating system for the prescribed period. Some of the test data are presented in the following table.

Table 8.1 Selected Heater Test Results.

Time (sec)	Battery Level (Volts)	Current Drawn (Amps)	Power Dissipated (kW)	Cumulative Energy Consumed (kWh)	Cumulative Capacity Discharge (Amp-hrs)
1.0	95.50	- 2.30	- 0.22	0.00	0.00
90.0	88.00	- 50.0	- 4.40	- 0.10	- 1.10
250.0	87.50	- 44.0	- 3.85	- 0.16	- 1.80
505.0	85.50	- 27.0	- 2.31	- 0.29	- 3.30
740.0	86.50	- 3.40	- 0.29	- 0.40	- 4.80
1350.0	71.50	- 4.10	- 0.29	- 0.54	- 7.00
1550.0	64.50	- 3.00	- 0.19	- 0.57	- 7.60

Using a 100 km/h steady state condition from the 4 km circuit in Chapter 7, the vehicle would travel approximately 2.75 km in 99 seconds. If the heater were to be operated for 90% of the time, i.e. 90 sec., then 0.1 kWh would be consumed from the battery pack. Thus, the vehicle's energy consumption would be 2.30 km/kWh as compared to 2.51 km/kWh. This result translates to an 8.4 % decrease in energy efficiency. By applying a similar analysis to the steady state drive on the 10 km circuit, the energy consumption would be 2.36 km/kWh as compared to 2.51 km/kWh, which translates to a 6 % decrease. From these results it can be approximated that the operation of the heater during steady state driving will decrease the vehicle's energy efficiency by about 5 to 10 %.

8.2 Proposed Changes to the Heating System

A modification to the heating system could decrease the use of extra battery energy, without requiring a replacement of the heater. The ICE coolant flow could be redirected and connected in parallel with the heater coolant lines. By drawing the excess waste heat from the engine the passenger compartment could be heated as it is in conventional vehicles. This parallel heating arrangement would provide heating when the engine would not be running, while at the same time reducing the energy drain from the batteries when the engine would be running.

As it is illustrated in Figure 8.3, the ICE coolant system would be connected in parallel with the electric heater via a series of back-check valves. This connection permits coolant to flow in one direction from the electric heater, preventing the heating of coolant that is flowing towards the engine (one way valves *A* & *B*). Thus, when the engine would be off, the coolant flow could be kept within the electric heater 'zone'. Once the engine coolant has reached a temperature of 21°C the electric heater would automatically shut-off, and would only turn on again, if the temperature were to drop below this level.

Connecting the system in series would not be a feasible solution for the following two reasons:

i) the electric heater could not be used if the engine were off, and

ii) engine coolant could reach a higher temperature which could damage the heater's internal components.

The changes to the coolant lines between the heater and the engine are more evident when both illustrations in Figures 8.3 and 8.3a are compared. Figure 8.3a is a copy of Figure 5.20.

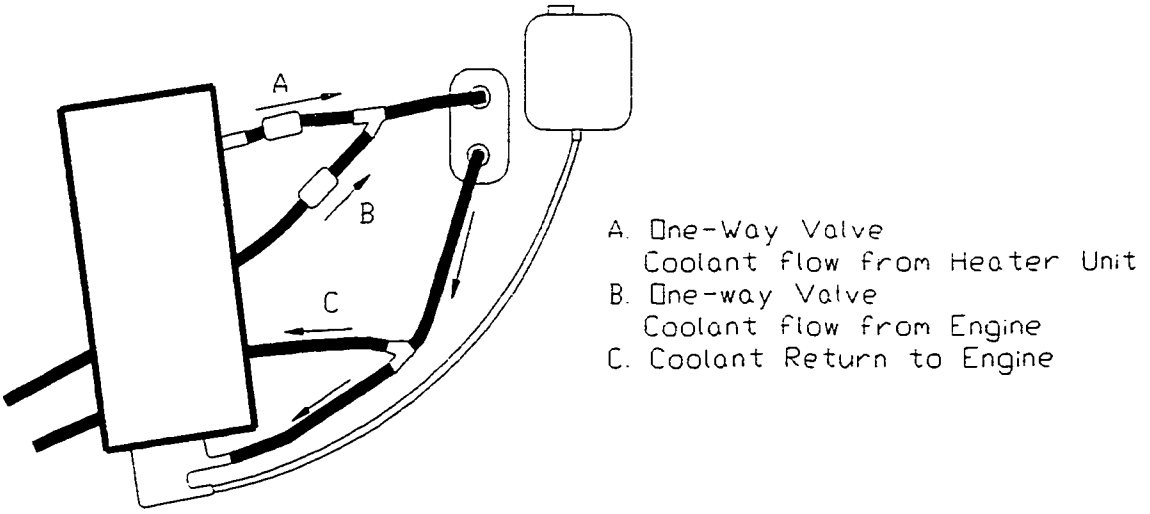

Figure 8.3 A Modified Setup for the Heating System.

1. Electric Heater Unit
2. Coolant Pumped to Heater Core
3. Vehicle Heater Core
4. Coolant Reservoir and Overflow
5. Coolant Return to Heater
6. 12V Pump for Coolant Circulation

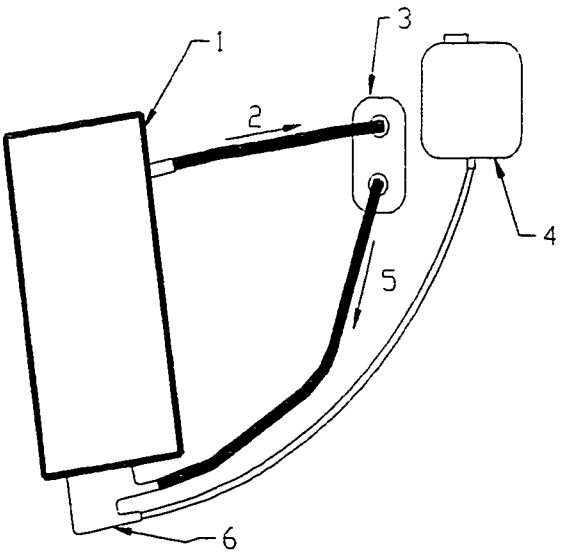

Figure 8.3a The Old Heating Configuration (first illustrated in Figure 5.20).

8.3 Summary

It was seen that the use of the electric heating system could reduce the vehicle's energy efficiency by 5-10%. By connecting the two separate coolant systems, from the engine and the electric heater, a combined heating system could be developed which would take advantage of the engine waste heat for heating. This parallel system would:

1) permit the use of the heater when the engine would not be operational,
2) use the engine waste heat for heating when the engine would be operational,
3) eliminate extra energy consumption from the batteries when the engine would reach its operational temperature.

9. ANALYSIS OF THE HYBRID ELECTRIC VEHICLE ECONOMY

The useful electric energy stored in the batteries allows only for a limited driving range, which is further reduced as power demand increases. The addition of more batteries to the propulsion battery pack would rectify the situation, but other constraints such as the increased weight would reduce the benefits of such a solution, by reducing the vehicle performance.

The simulation results obtained for both the existing and the proposed drivetrain systems were considered as the most efficient for each pertinent configuration. It was realized, though, that the energy recuperation rate depends upon the motor/generator size and the battery pack capacity. It came out that the most beneficial situation would be to use the energy recuperation to brake the vehicle in most cases without using the brakes, except in extreme cases.

In the proposed drivetrain configuration the electric motor/generator can only absorb a torque up to its maximum rated output at the respective speed. Examining Figure 7.2, between the 4000-13000 rpm region, shows that the motor torque is not constant and is decreasing with speed. Decelerating at this condition would require more use of the brakes to slow down the vehicle at a reasonable stopping distance; since, in this range of operation the energy recuperation capacity of the generator is drastically reduced and only a larger motor would be able to accommodate the vehicle kinetic energy available during the deceleration

phase. This would give improved braking and more effective energy recuperation results since such a greater motor would be operating in a higher torque range, particularly if the transmission would be simultaneously downshifted from fifth gear straight to the second or first gear.

Assuming that the motor would be sized to accommodate maximum of kinetic energy decrease then, the batteries should in turn be capable of absorbing such sudden energy input. However, it has been seen that, in majority the battery manufacturers and the research and development groups have not addressed this issue correctly. Still, as evidenced in recent publications, the authors assume that the battery will be able to absorb and store all of the energy being available at deceleration [4,26,28]. Research in new battery technologies has shown some interest in determining the battery charge acceptance rate, but there has not been much research effected pertaining to existing battery technologies [52].

The chemical structure and the state of charge (SOC) of the respective battery cell are key factors that would determine the energy rate that can be stored. During certain drive scenarios, the battery SOC will fluctuate and decrease depending upon the power demand. By not knowing the battery's *rate of charge acceptance*, and the total of the short bursts of energy the battery can accept, a complete analysis of energy regeneration cannot be made.

Even though the charging characteristics of the batteries are not known, a comparison of the simulation results presented in Chapters 4 and 7 of this thesis

could be used to illustrate the effectiveness of such a system. The energy efficiency and fuel economy simulation results provide an upper limit, regarding the highest possible energy recuperation conditions that could exist. Since the simulation approach was consistently applied to both drivetrain configurations, a direct comparison of the advantage of energy regeneration can be performed. Two data samples, taken from Chapters 4 and 7, are used to illustrate the benefits of regeneration only as it relates to the vehicle economy (see Tables 9.1 & 9.2).

Examining the data for a longer drive range, consisting of a 10 km circuit, it was established that the energy regeneration had a minimal effect on the vehicle's energy efficiency. Being in the steady state portion of the cycle for a longer period, it is the engine fuel economy that has a greater impact. Listed in Table 9.1 are the data used for this comparison.

The situation dramatically changes in a city operation where the acceleration and deceleration occurs much more often. As given by the simulation (Table 9.2), the results show an improvement in fuel economy of about 29%. Of course, these results can be much reduced regarding the limited ability of the electric generator and battery to absorb high energy rate. The results are indicative of ideal conditions which might not be prevalent in real driving situations. However, for inter-city driving (warranted by mail, courier, merchandise delivery, etc...) the investment seems to be much more justified.

Table 9.1 Comparison of Economy Mode Data for the 10 km Inter-City Cycle.

Economy Mode 10 km Cycle Data	**Current Drivetrain (Chapter 4)**	**Modified Drivetrain (Chapter 7)**	**% Improvement**
0-60-0 km/h Cycle			
Energy Efficiency (km/kWh)	4.22	4.47	5.6
Equivalent Fuel Consumption ℓ/100 km (mpg_{US})	2.67 (87.9)	2.53 (93.0)	
0-100-0 km/h Cycle			
Energy Efficiency (km/kWh)	2.50	2.66	6.0
Equivalent Fuel Consumption ℓ/100 km (mpg_{US})	4.52 (52.0)	4.25 (55.3)	

Table 9.2 Comparison of Economy Mode Data for the 1 km City Cycle.

Economy Mode 1 km Cycle Data	**Current Drivetrain (Chapter 4)**	**Modified Drivetrain (Chapter 7)**	**% Improvement**
0-60-0 km/h Cycle			
Energy Efficiency (km/kWh)	2.80	3.94	28.9
Equivalent Fuel Consumption ℓ/100 km (mpg_{US})	4.04 (58.2)	2.87 (82.1)	

10. THESIS SUMMARY AND RECOMMENDATIONS

The main goals of this thesis research were to provide a simple concept and to simulate the energy requirements of a hybrid electric vehicle, i.e. to design a power assist HEV without compromising the vehicle space, weight, and comforts. This research work allowed to propose a vehicle which would be much more efficient without compromising the driveability and comfort; because of greater efficiency it would also be less polluting.

It is recognized that HEV's represent new areas of research, where demonstration projects are also required to discover which modes of energy conversion would best suit the society. The U.S. Environment Protection Agency (EPA) vehicle testing requires the use of a chassis dynamometer and every researcher does not have such means; thus, modeling and simulation programs cannot be easily validated. An initial analytical approach that is practical and can easily be used is such that validation is possible by going onto a nearby highway. Thus, simplified simulation driving cycles have been developed to be used for HEV projects, so that the models could be validated based on existing means.

Two scenarios consisting of a 0-60-0 km/h and a 0-100-0 km/h cycle were established to demonstrate the highway and city mode driving situations. The energy efficiency and equivalent fuel consumption were determined for the specific hybrid powertrains. A comparison with established SAE drive cycles was

effected to illustrate the feasibility of using a simplified procedure to determine the HEV performance and economy results.

From the presented research, the following conclusions have been drawn:

1) A compact vehicle is not an obstacle in developing a hybrid drivetrain. It has been shown that it is feasible to convert a four passenger vehicle to a hybrid electric natural gas vehicle, retaining comforts and driveability available in present vehicles. By sacrificing extravagant performance and using available technology, an economical and fuel efficient vehicle can be developed. With the use of certain safety features, the HEV can be as safe as any of today's vehicles.

2) It is beneficial to use an alternative fuel such as natural gas to decrease polluting emissions. A major drawback is the reduction of trunk space due to the size and shape of the CNG cylinder.

3) The power-assist mode requires that an analysis should be performed at different driving conditions. The selection and matching of the engine with the electric motor affects the effectiveness of the hybrid operation. As drive components, the BMW K75 engine and Advanced DC motor when combined show evident drawbacks. To fully harness the engine power output, the hybrid powertrain must be operated in a high speed range. The electric motor though, will provide a high constant torque at a low speed range. An acceleration to 100 km/h requires almost 22 seconds, whereas attaining 60 km/h requires 9.5 seconds.

4) The hybrid powertrain is best for short commuting in the city where the use

of an electric motor is ideal, and as it was shown in Chapter 4, a high fuel economy can be achieved ranging from 4.04 - 2.90 ℓ/100 km (58 - 81 mpg_{US}).

5) The vehicle's electric range however, is limited by the low energy density of the batteries, thus by incorporating energy recuperation at deceleration the vehicle fuel economy and range can be increased. The change of electric motor to the Brusa Electronik AC induction motor showed a considerable improvement in vehicle performance and in fuel economy. With this hybrid powertrain there is about 29% improvement in energy efficiency over the previous setup. This motor, with the advantage of an increased sprocket ratio between the motor and the transaxle, can be operated in a higher speed range, thus enabling the full use of engine and motor peak torque and power.

6) One of the unknowns in using energy regeneration is derived from the inability of the industry to provide the researcher with the necessary data, regarding the energy absorption capabilities of the electric motor/generator to convert electrical energy from its mechanical form and of the batteries to absorb this energy at high rate, particularly at different states of charge. This makes an exact calculation of the benefits related to energy regeneration very difficult.

7) The proposed modified electric drive offers the following advantages: a better match between the engine and motor drivelines, regenerative braking and increased energy efficiency & fuel economy, as well as an increase in vehicle performance. The major disadvantage is the high system cost, which is about four

times higher per kW output, as compared to the current system used.

8) The current heating system could significantly reduce vehicle performance and fuel economy during very cold conditions that would require prolonged interior heating and window defrosting. Using the engine waste heat, in parallel with the electric heating system, could greatly reduce the electric energy consumption. This would also allow for a reduction in the electric heater size.

Based on the above conclusions drawn, the following recommendations are proposed for an improved HEV:

1) The high cost of the AC Induction drivetrain suggests that the next step to upgrading the HEV design would be to improve the engine characteristics. It would require a more efficient engine that would also permit for a better power match with the electric motor. The new generation compact high speed direct injection turbo-charged diesel engines, like the 1.9ℓ TDI engines recently introduced by Volkswagen [53], would provide the best near term solution to further improve the vehicle fuel economy

2) To fully take advantage of an electric system's regenerative capabilities and to decrease the deceleration distance without using brakes, a higher capacity energy absorbing system is needed; a larger electric motor/generator, which would provide a higher torque to decelerate. From the point of view of acceleration, the existing system is satisfactory, providing the necessary performance. However, from the point of view of economy, the brakes still need to be used to decelerate

within a shorter distance. If we want to achieve the improved economy results discussed in section 7.4, we need to pay for a larger electric motor/generator.

3) Even if a more powerful motor were to be used, there is no certainty that the batteries will be able to absorb all the electric power. An emphasis needs to be placed on effectively establishing the battery SOC which is a deciding factor in energy absorption rate, since a fully charged battery minimizes the current absorbed. To progress with a more intricate energy analysis, the following information, which is not currently available, would be required:

i. battery characteristics for the absorption rate of the electric current,
ii. current absorption rate data at different SOCs.

4) By neglecting the need for interior vehicle heating while in electric mode, the electric portion of the heating system could be eliminated, which would also reduce the complexity of the system. A possible additional solution would be to preheat the vehicle before the trip, while it is stationary and being charged before the trip.

In summary, this thesis research has shown that the use of a simplified driving cycle simulation can provide approximate energy consumption results that can be used to compare the hybrid drivetrains with or without energy regeneration. A power assist natural gas HEV is a feasible solution for commuting within a polluted city environment. An effective design requires that the hybrid powertrain is matched well for all vehicle speeds in terms of performance and fuel economy.

REFERENCES

1. U.S. Department of Energy, "The Clean Air Act: What it means for Municipal Fleets," U.S. DOE Pamphlet, DE9216426, March 1993.

2. Aceves, S.M., Smith, J.R., Perkins, L.J., Haney, S.W., and Flowers, D.L., "Optimization of a CNG Series Hybrid Concept Vehicle," SAE Paper No. 960234.

3. Riezenman, Michael J., "Electric Vehicles," IEEE Spectrum, November 1992, pp. 18-21.

4. Mason, Jr., W.T., and Kristiansson, U., "Hybrid EVs versus Pure EVs: Which Gives Greater Benefits?," SAE Paper No. 94C017.

5. Anderson, C., and Pettit, E., "The Effects of APU Characteristics on the Design of Hybrid Control Strategies for Hybrid Electric Vehicles," SAE Paper No. 950493.

6. Burke, A.F., "Hybrid/Electric Vehicle Design Options and Evaluations," SAE Paper No. 920447.

7. Keebler, Jack, "Research on hybrid drive attracts all the big guys," Automotive News, June 6, 1994, pg. 50.

8. Riezenman, M.J., and Wouk, V., "EV Watch: California considers hybrid EVs," IEEE Spectrum, September 1995, pp. 72-75.

9. Kaberlah, A., "Electric Hybrid Drive Systems for Passenger Cars and Taxis," SAE Paper No. 910247.

10. Fleming, A., and Rowand, R., "Fiat Launches Electric Truck," Automotive News Insight, November 25, 1991, pg. 2i.

11. Nelson, T.T., "A Hybrid Natural Gas Vehicles," SAE Paper No. 901497.

12. The Clean Fuels Report, June 1990, pp. 126-133.

13. DeLuchi, M.A., Johnston, R.A., and Sperling D., "Methanol vs. Natural Gas Vehicles: A Comparison of Resource Supply, Performance, Emissions, Fuel Storage, Safety, Costs, and Transitions," SAE Paper No. 881656.

14. Weaver, C.S., "Natural Gas Vehicles - Review of the State of the Art," SAE Paper No. 892133.

15. Wang, Q., and DeLuchi, M.A., "Impacts of Electric Vehicles on Primary Energy Consumption and Petroleum Displacement," Energy, Vol. 17, No. 4, 1992, pp. 351-366.

16. Duoba, M., Larsen, R., and LeBlanc, N., "Design Diversity of HEVs with Example Vehicles from HEV Competitions," SAE Paper No. 960736.

17. Mastronardi, R., and Doyle, E., " Natural Gas Engines for Hybrid Vehicle Systems," SAE Paper No. 941812.

18. Riezenman, Michael J., "Electric Vehicles," IEEE Spectrum, November 1992, pp. 22-24.

19. Wyczalek, F.A., Wang, T.C., "Regenerative Braking Concepts for Electric Vehicles - A Primer," SAE Paper No. 920648.

20. Giorgetti, A., Cavestro, L., and Rampazzo, M., "Design of a Lightweight Braking System for Electric Cars," SAE Paper No. 920649.

21. Bass, E., Mabrito, B., Kong, H., and McAlwee, G., "A Competition Hybrid Electric Vehicle," SAE Paper No. 921544.

22. Burke, A. F., "Comparison of Simulation and Test for Electric Vehicles of Recent Design," SAE Paper No. 890818.

23. Moore, T.C., and Lovins A.B., "Vehicle Design Strategies to Meet and Exceed PNGV Goals," SAE Paper No. 951906.

24. Mendler, C., "Taking a new look at hybrid electric vehicle efficiency," Automotive Engineering, February 1997, pp. 67-70.

25. Burke, A.F., "On-Off Engine Operation for Hybrid/Electric Vehicles," SAE Paper No. 930042.

26. Merriman, C., Gerpen, J.V., Luecke, G., "The Effects of Engine Performance and Engine Starts on Series HEV Operation," SAE Paper No. 970288.

27. Cuddy, M., "A Comparison of Modeled and Measured Energy Use in Hybrid Electric Vehicles," SAE Paper No. 950959.

28. Cuddy, M., and Wipke, K.B., "Analysis of the Fuel Economy Benefit of Drivetrain Hybridization," SAE Paper No. 970289.

29. Nikopoulos, A., Theofanopoulos, J., Martin, L., Martini, R., "The Concordia University 1995 - Chrysler Neon Hybrid Electric Vehicle," SAE Special Publication No. SP-1170.

30. LeBlanc, N., Larsen, R., Duoba, M., "The 1995 HEV Challenge: Results and Technology Summary," SAE Paper No. 960741.

31. Dateline 2000, United States Council for Automotive Research (USCAR), Vol. 1, Issue 4, Winter 1995.

32. Dateline 2000, United States Council for Automotive Research (USCAR), Vol. 2, Issue 1, Spring 1996.

33. Nikopoulos, A., Metrakos, G., Monahan, D., et al, "The Concordia University 1996 - FutureCar Hybrid Electric Vehicle," SAE Special Publication No. SP-1234.

34. Nikopoulos, A., Hong, H., Krepec, T., "Energy Consumption Study for a Hybrid Electric Vehicle," SAE Paper No. 970198.

35. Adler, U., Bosch Automotive Handbook, 3rd edition, Society of Automotive Engineers, Inc., Warrendale, PA, 1993, pg. 325.

36. Gillespie, T.D., Fundamentals of Vehicle Dynamics, Society of Automotive Engineers, Inc., Warrendale, PA, 1992, pg. 118.

37. Gillespie, T.D., pp. 27-42.

38. Frantzeskakis, P., Krepec, T., and Sankar, S., "Specific Analysis on Electric Vehicle Performance Characteristics with the Aid of Optimization Techniques," SAE Paper No. 940336.

39. Stone, Richard, Introduction to Internal Combustion Engines, 2nd edition, Society of Automotive Engineers, Inc., Warrendale, PA, 1992.

40. Ross, M., and Wu, W., "Fuel Economy Analysis for a Hybrid Concept Car Based on a Buffered Fuel-Engine Operating at an Optimal Point," SAE Paper No. 950958.

41. EAGLES Version 1.1: An Electric and Gasoline-Vehicle Fuel-Efficiency Software Package, Center for Transportation Research, Energy Systems Division, Argonne National Laboratory, Argonne, Illinois, 1995.

42. Barden Precision Miniature and Instrument Bearings, "Barden Engineering Data," Catalog, Concordia University Mechanical Engineering.

43. John Bean Company, "Test Lane Products", Pamphlet, Automotive Service Equipment Division, Conway, Arkansas, 1996.

44. Conversations with Jim "Turbo" Cohen, Actuators & Fuel Systems Components Division, Siemens Automotive, Virginia, 1995.

45. DeGrace, L.G, and Bata, G.T., "The Bendix DEKA Fuel Injector Series - Design and Performance," SAE Paper No. 850559.

46. Johnson Matthey, "Catalyst Specifications," Product Sample Group, Michigan, 1995.

47. Advanced D.C. Motors, Inc., "Advanced DC Technical Specifications," Syracuse, NY, 1995.

48. Frantzeskakis, P., "Experimental and Analytical Investigation on Hybrid Electric Vehicles," Thesis - Master of Applied Science, Mechanical Engineering, Concordia University, 1994.

49. Adler, U., Bosch Automotive Handbook, 3rd edition, Society of Automotive Engineers, Inc., Warrendale, PA, 1993, pg. 600.

50. Solectria Corporation, "Electric Vehicle Components," Pamphlet, Arlington, MA, 1994.

51. Brusa Electronik, "AC Induction Electric Drive Specifications," Switzerland, 1996.

52. U.S. Department of Energy, "Annual Automotive Technology Development Customers' Corodination Meeting," Preprints: Vol. I-III, Dearborn, Michigan, October 28-November 1, 1996.

53. Volkswagen, "Volkswagen TDI," Pamphlet, 1995.

54. Curtis Instruments Inc., "Curtis PMC Data," Pamphlet, Mt. Kisko, NY, 1991.

55. Bussman Copper Industries, "SPD Electrical Protection Handbook," Bridgeton, MO, 1992.

56. KTA Services Inc., "Electric Vehicle Components & Publications Catalog," Upland, CA, 1994.

57. Nippondenso America, "Compressor 10PA17 Specifications," Michigan, 1995.

58. Todd Engineering Sales Inc., "Power Source: Battery Charger/Power Supply," Pamphlet, Tucson, AZ, 1995.

APPENDIX 1

Specifications and Information Relative to Chapter 4

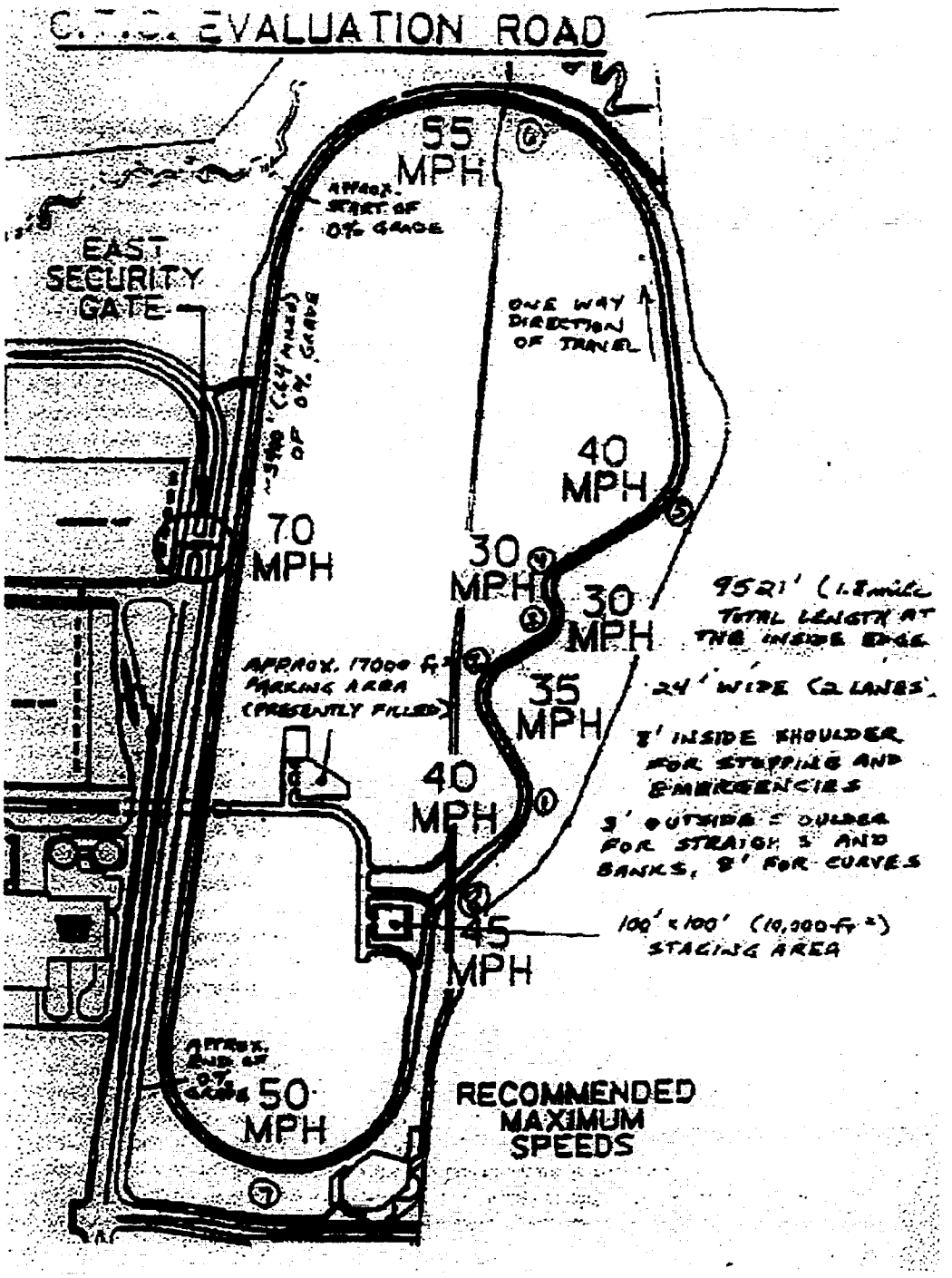

Figure A.1 Schematic of 1995 Challenge Test Track [30].

APPENDIX 2

Specifications and Information Relative to Chapter 5

LOW TORQUE
LOW TO HIGH SPEED
DEEP GROOVE
PRESSED STEEL RETAINERS

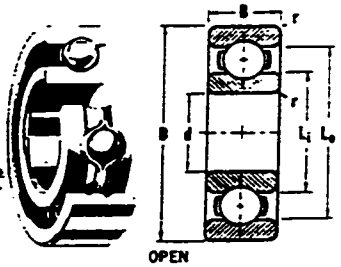

OPEN

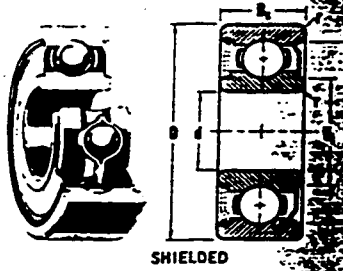

SHIELDED

AVAILABILITY. All sizes listed are normally available from stock in stainless steel. • Sizes also available in chrome steel; specify by omitting prefix S, as R3K, etc.

DIMENSIONS BORE, O.D., WIDTH—inches d	D	B	B_i	MAX. FILLET RADIUS inches r	BASIC ORDERING NUMBER STANDARD RETAINER Open	Single shield	Double shield	"W" RETAINER Open	Single shield	Double shield	OTHER DIMENSIONS inches L_i	L_o	B_i	B_o	APPROX. WEIGHT pounds	DATA REFERENCE NUMBER Standard retainer	"W" retainer
.1562	.3125	.1094	.1250	.005	SR155K	SR155S	SR155SS	SR155W	SR155SW	SR155SSW	.222	.280	.222	.284	.001	R156	R156W
.1575	.6299	.1969	.1969	.012	•S34K	•S34S	•S34SS	•S34W	•S34SW	•S34SSW	.295	.492	.256	.547	.01	34	34
.1875	.3125	.1094	.1250	.005	SR156K	SR156S	SR156SS	SR156W	SR156SW	SR156SSW	.222	.280	.222	.284	.001	R156	R156W
.1875	.3750	.1250	.1250	.005	SR166K	SR166S	SR166SS	SR166W	SR166SW	SR166SSW	.235	.325	.235	.341	.002	R166	R166
.1875	.5000	.1094		.005	SR186X1			SR186WX1			.235	.325			.004	R166	R166
.1875	.5000		.1094	.005					SR186SWX3				.235	.341	.004		R166
.1875	.5000		.1562	.005		SR186SX2	SR186SSX2		SR186SWX2	SR186SSWX2			.235	.341	.006	R166	R166
.1875	.5000	.1562	.1960	.012	•SR3K	•SR3S	•SR3SS	•SR3W	•SR3SW	•SR3SSW	.276	.412	.252	.430	.005	R3	R3W
.1875	.5694	.1960	.1960	.012	SR3X31	SR3SX31	SR3SSX31	SR3WX31	SR3SWX31	SR3SSWX31			.252	.430	.008	R3	R3W
.1875	.7435	.1960	.1960	.012	SR3X37	SR3SX37	SR3SSX37	SR3WX37	SR3SWX37	SR3SSWX37			.252	.430	.02	R3	R3W
.1875	.7500	.1960	.1960	.012	SR3X8	SR3SX8	SR3SSX8	SR3WX8	SR3SWX8	SR3SSWX8	.252	.430	.252	.430	.02	R3	R3W
.1875	.7717	.1960	.1960	.012	SR3X62	SR3SX62	SR3SSX62	SR3WX62	SR3SWX62	SR3SSWX62			.252	.430	.02	R3	R3W
.1875	.8685	.1960	.1960	.012	SR3X60	SR3SX60	SR3SSX60	SR3WX60	SR3SWX60	SR3SSWX60			.252	.430	.03	R3	R3W
.1875	.8750	.1960	.1960	.012	SR3X23	SR3SX23	SR3SSX23	SR3WX23	SR3SWX23	SR3SSWX23	.252	.430	.252	.430	.03	R3	R3W
.1969	.6299	.1969	.1969	.012	•S34-5K	•S34-5S	•S34-5SS	•S34-5W	•S34-5SW	•S34-5SSW	.295	.492	.256	.547	.01	34	34
.1969	.7480	.2362	.2362	.012	•S35K	•S35S	•S35SS				.383	.596	.342	.646	.02	36	
.2362	.7480	.2362	.2362	.012	•S36K	•S36S	•S36SS				.383	.596	.342	.646	.02	36	
.2500	.3750	.1250	.1250	.005	SR168K	SR168S	SR168SS				.284	.343	.284	.347	.002	R168	
.2500	.5000	.1250	.1875	.005				SR188W	SR188SW	SR188SSW	.330	.420	.310	.436	.005		R188
.2500	.6250	.1960	.1960	.012	•SR4K	•SR4S	•SR4SS	•SR4W	•SR4SW	•SR4SSW	.365	.512	.322	.547	.01	R4	R4
.2500	.7500	.2188	.2812	.016	•SR4A	•SR4AS	•SR4ASS				.386	.596	.342	.646	.02	36	
.2500	1.0480		.1960	.012		SR4SX35	SR4SSX35		SR4SWX35	SR4SSWX35			.322	.547	.04	R4	R4
.2756	.8661	.2756	.2756	.012	•S37K	•S37S	•S37SS				.463	.692	.415	.744	.03	38	
.3150	.8661	.2756	.2756	.012	•S38K	•S38S	•S38SS				.463	.692	.415	.744	.03	38	
.3750	.8750	.2188	.2812	.016	•SR6K	•SR6S	•SR6SS				.520	.744	.472	.784	.03	38	
.5000	1.1250	.2500	.3125	.016	•SR8K	•SR8S	•SR8SS				.736	.972	.682	1.013	.05	R8	
.6250	1.3750	.2812	.3438	.031	•SR10K	•SR10S	•SR10SS				.895	1.153	.835	1.215	.08	103	

APPLICATIONS. Gyro gimbals, stable platforms, synchros, motors, generators, servomechanisms, computer gear systems, recording devices, optical systems, potentiometers, control mechanisms and other low torque, low to high speed applications.

DESCRIPTION. Low torque deep groove bearings for smooth, quiet operation with minimum vibration; support radial loads and thrust in either direction. Many sizes (suffix X) are narrow width or large O.D. for synchro and small motor use.

Standard ball retainers are one-piece in smaller sizes, two-piece in larger. Barden-developed "W" retainer is two-piece "antiwindup" type designed to prevent retainer lock, reduce torque peaks and increase bearing life.

Close clearance shields protect against contamination and lubricant loss; precision snap wire shield retention avoids outer ring distortion. Shields and snap wires are removable.

MATERIAL. Rings and balls: corrosion resistant AISI 440C stainless steel; many sizes also available in SAE 52100 chrome bearing steel. Retainers: one-piece—hardened pressed stainless steel; two-piece—pressed stainless steel. Shields and snap wires: stainless steel. Further data on page 48.

LUBRICANTS NORMALLY SUPPLIED. Oil: MIL-L-6085A (Barden code O-11) for low torque operation, open or shielded bearings, low speed only. Grease: MIL-G-3278 (Barden code G-2) for open or shielded bearings, moderate to high speed. Further data on page 66.

PRELOADED PAIRS. Most sizes listed may be obtained in DB or DF duplex pairs with controlled axial preload. Further data on page 52.

FURTHER DATA. Tolerances, page 46. Radial and axial play and yield, page 49. Shaft and housing shoulders and fits, page 68. Calibrated bearings, page 72.

LOW TORQUE
LOW TO HIGH SPEED

BORE .1562"—.625
O.D. .3125"—1.375

PERFORMANCE DATA

AVERAGE RUNNING TORQUE. Torque values below are for code 5 radial play range. They apply to clean bearings lubricated with light instrument oil and operated below 25 rpm at normal temperature. Starting or peak torques may reach approximately double these values. Further data on page 56.

THRUST LOAD

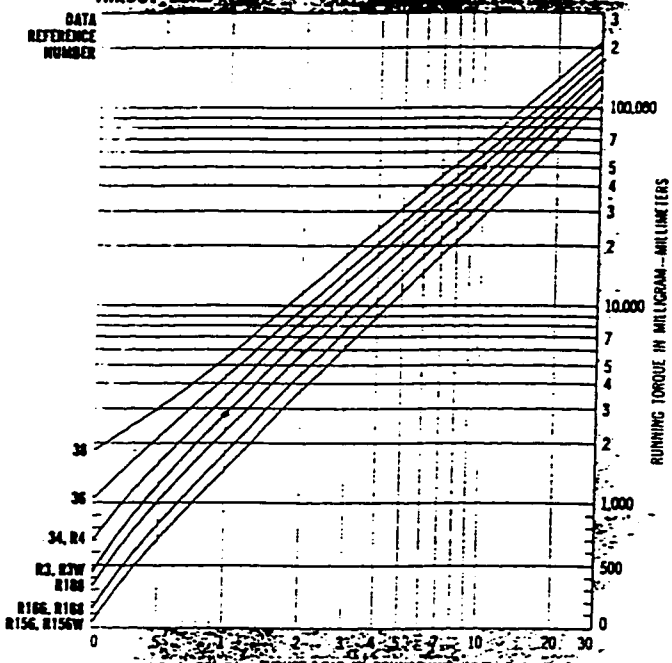

RADIAL LOAD

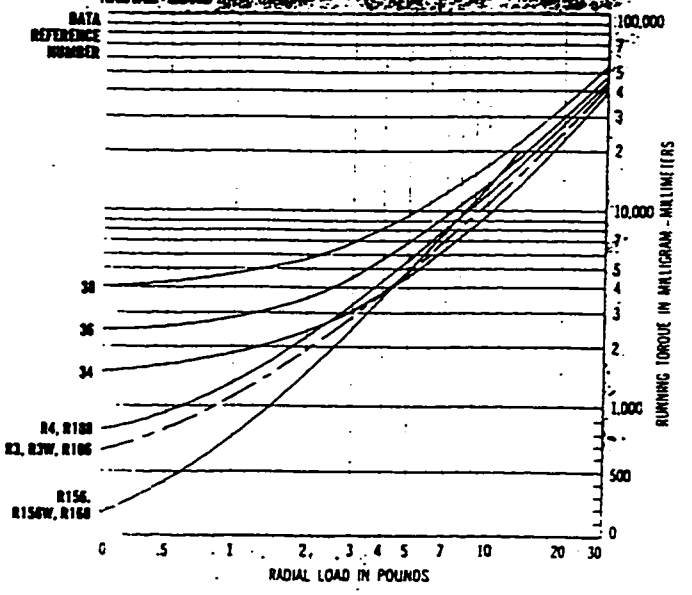

STATIC LOAD RATINGS. Static ratings are shown below for radial play ranges normally supplied. These values indicate peak loads that can be sustained by bearings without permanent effect on smoothness or low torque performance. Further data on page 60.

DATA REFERENCE NUMBER	STATIC LOAD RATINGS—pounds: THRUST LOAD—T_o: RADIAL PLAY RANGE: Code 2 .0001"-.0003"	Code 3 .0002"-.0004"	Code 4 .0003"-.0005"	Code 5 .0005"-.0008"	Code 6 .0008"-.0011"	RADIAL LOAD C_o
R156	25	27	29	32	36	15
R156W	31	33	36	40	44	18
R166	54	56	60	64	72	34
R3	90	91	95	105	112	60
R3W	77	78	81	90	96	51
34	138	144	147	150	162	88
36	174	180	186	192	210	114
R168	31	33	36	40	44	18
R188	75	77	81	88	94	46
R4	108	112	116	125	132	70
38	252	259	266	273	287	167
R8	1450	1200	1180	900	580	508
103	2100	2300	2325	2350	1700	730

DYNAMIC LOAD RATINGS. Radial load ratings below are for 500-hour design life, or 2500-hour average life, with proper mounting, lubrication and protection of bearings. Use value C_s for fatigue life computation procedure on page 62.

- ○ Normal speed limit for bearings with one-piece standard retainers.
- □ Normal speed limit for bearings with two-piece standard retainers or "W" retainers.

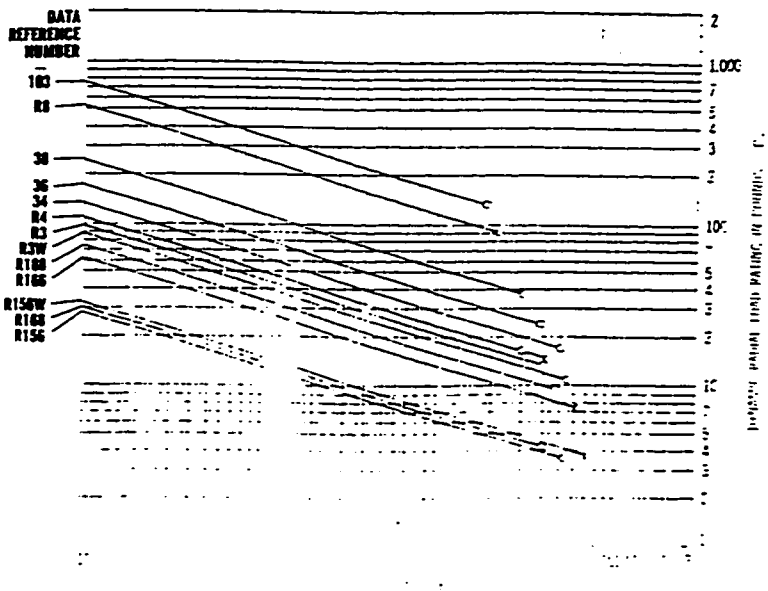

COMPUTERIZED SUSPENSION TESTER

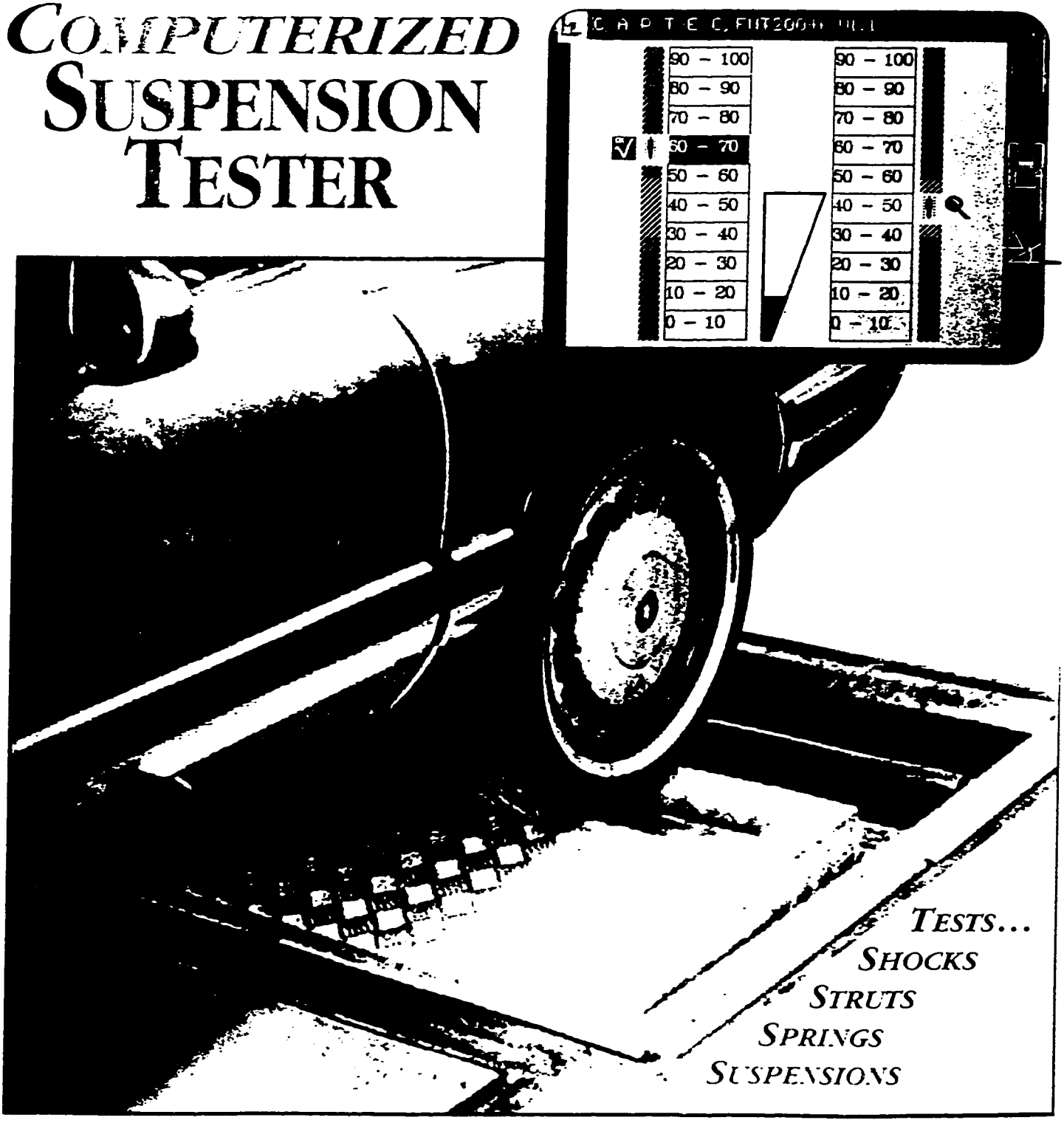

TAKING THE GUESSWORK OUT OF VEHICLE INSPECTIONS

Computerized Reliability – Shock / Strut / Suspension Testing

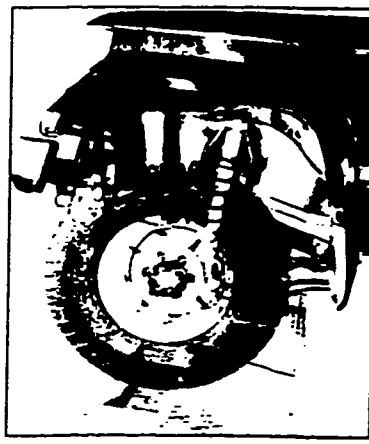

FAST... Checks performance of shocks, struts and under-car suspension and provides the analysis in less than 60 seconds.

EFFECTIVE ... Computerized analysis provides clear indications of poor/bad suspension parts with customer printouts. Pinpoints problems which are difficult to measure manually.

EASY TO USE ... Drive vehicle onto drop ramp. Push remote control button. Computer does the rest.

CREDIBILITY ... Establishes customer confidence for repair recommendation.

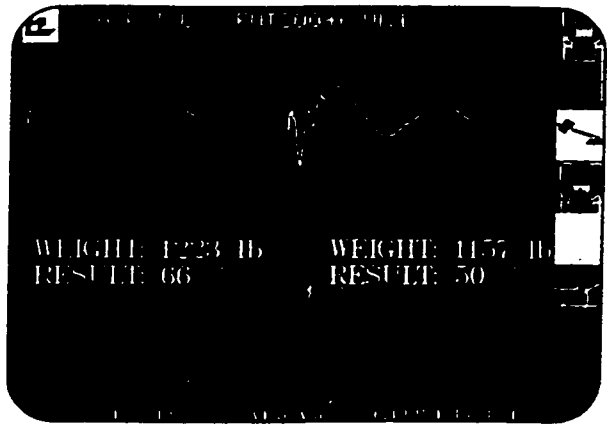

MEASURES AND DISPLAYS

- Rate of suspension dampening after 2" drop test
- Compares relative dampening effectiveness to new vehicle standards

SPECIFICATIONS

Max. axle weight	4,000 lbs.	Length	98" (2450 mm)
Temperature range	-20°C up to 70°C	Height	100" (205 mm)
Test speed	5 to 15 km/h	Width	31" (775 mm)
Power Requirements	220 V/60 Hz	Weight	704 lbs. (330 kg)
	110 V/60 Hz	Console	FMC 14" or 19" mobile computer console

FWT-2000
Suspension Tester

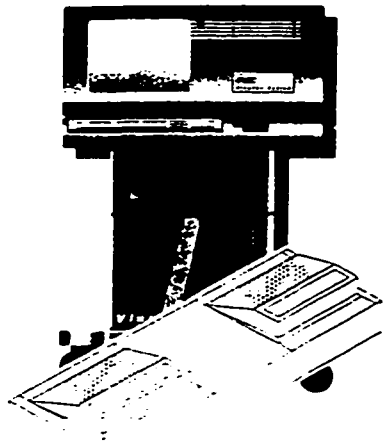

STANDARD EQUIPMENT

- Fall method FWT 2000 system testing unit
- Integrated weight scale unit
- Connecting cables
- Deluxe Mobile Console, PC, keyboard, hard drive, 3.5" floppy drive
- 14" or 19" SVGA color monitor, 9 pin printer, control system
- IR remote control
- Graphic display of front and rear suspension activity
- Database system

NOTE: The Deluxe Mobile Console can be used with other test lane products and/or upgraded to perform complete 4-wheel alignment.

John Bean

The Products...The People...The Pride... Wheel Service Equipment Since 1925
Automotive Service Equipment Division – Conway, Arkansas 72032
1-800-FMC-TEAM **FAX (501) 450-1585**

NEW! ROLLER BRAKE TESTER

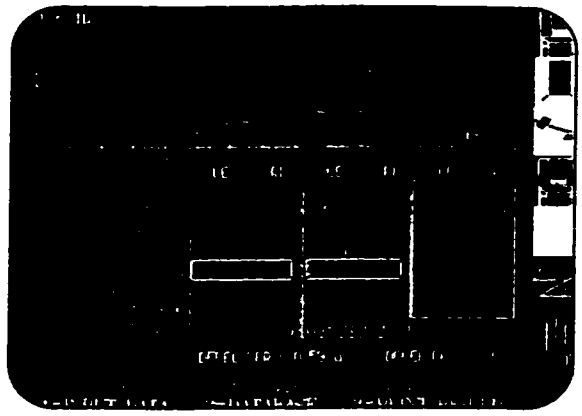

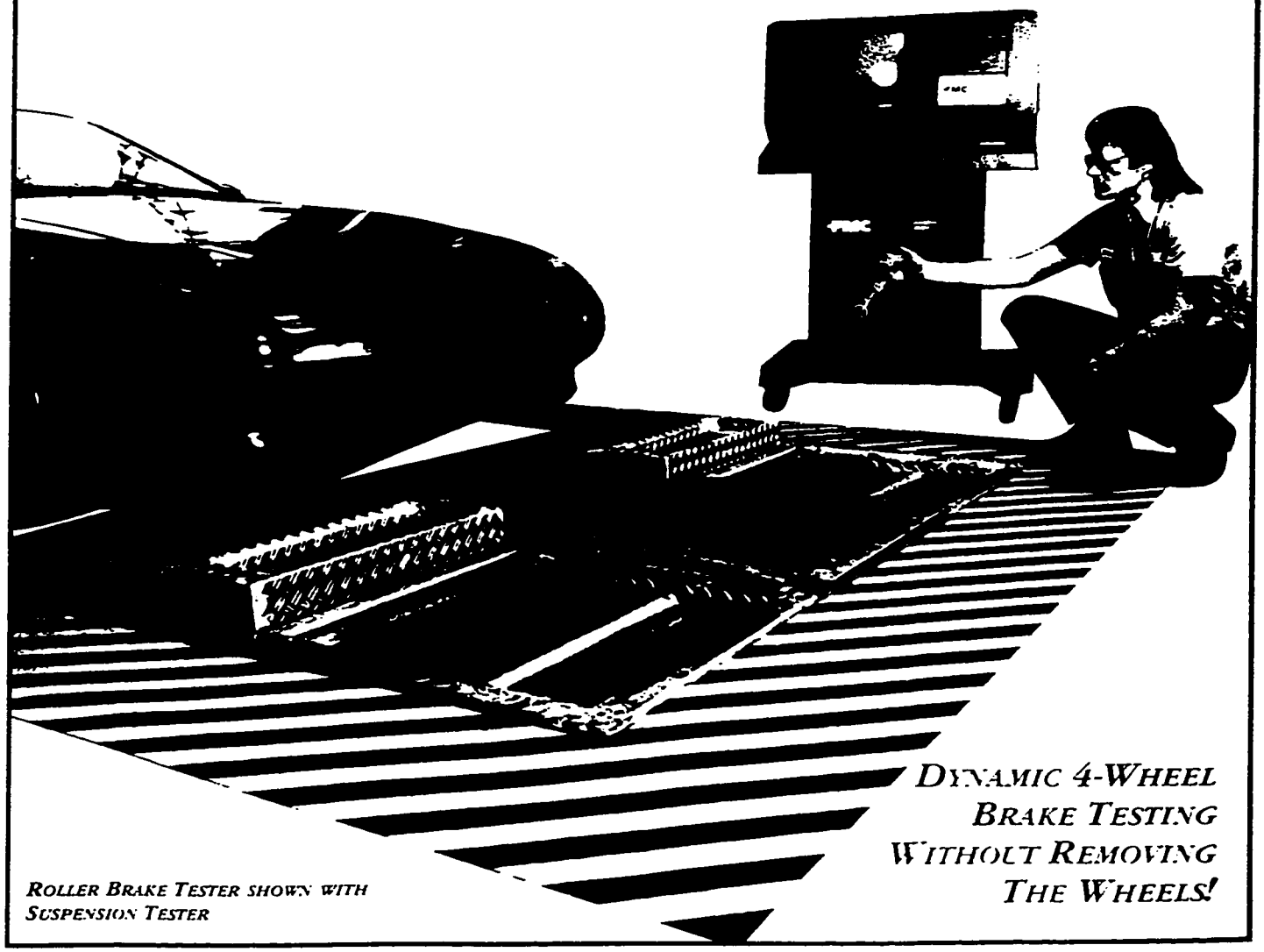

DYNAMIC 4-WHEEL BRAKE TESTING WITHOUT REMOVING THE WHEELS!

ROLLER BRAKE TESTER SHOWN WITH SUSPENSION TESTER

TAKING THE GUESSWORK OUT OF VEHICLE INSPECTIONS

The New Standard in Dynamic Brake Testing

FAST... Checks front, rear and parking brake performance in less than 3 minutes without removing the wheels.

EFFECTIVE ... Automatically tests vehicle braking system performance. Checks each individual wheel. Identifies even hidden hydraulic problems.

RELIABLE ... Repeatable readings. Retested vehicles after repairs show improved results.

EASY TO USE ... User friendly computer screens and handy remote control for easy to learn operation. Simple to understand results complete with computer printouts.

PROFITABLE ... More thorough inspections result in increased sales and profits and higher customer satisfaction.

MEASURES AND DISPLAYS

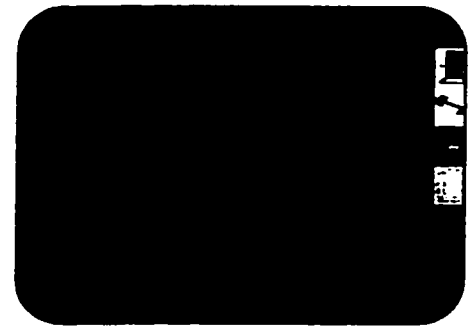

Wheel Friction	Initial force required to start turning the wheel. Helps to detect seized caliper or defective wheel cylinders, over-torqued wheel bearings and defective wheel axles.
Maximum Brake Force	The maximum stopping forces encountered during the test.
Block Imbalance	Difference in brake force between the left and right wheels.
Maximum Imbalance	The largest difference between the left and right wheel encountered during the test.
Ovality	The amount in percentage of out-of-round. Indicates a pulsating pedal.
Axle deceleration	The amount of stopping force provided by the brake system. Front, rear and parking brake deceleration are measured.

SPECIFICATIONS

Model IBDE2005KS ... Roller Brake Tester for cars & trucks up to 3 tons/axle load. Remote Control Operation with choice of 14" or 19" mobile computer consoles.

Length	92.125" (2340 mm)	Roller Diameter	7.874" (200 mm)	Reduction Gear Ratio	40/1
Width	27.5" (700 mm)	Roller Length	27.559" (700 mm)	Footprint	16 sq. ft.
Height:	10" (250 mm)	Roller Offset	.984" (25 mm)	Power Regulation	230V/3ph/3 amps
Weight	814 lbs. (370 kg)	Motor	5 hp (3.7 kw)		

STANDARD EQUIPMENT

Roller type brake tester • Connecting cables • Deluxe console, PC, keyboard, hard drive, 3.5" floppy • 14" or 19" SVGA color monitor, 9 pin printer, control system • IR remote control • Graphic display of brake force and imbalance, left and right front, left and right rear, deceleration percent. • Database system • Weighing unit

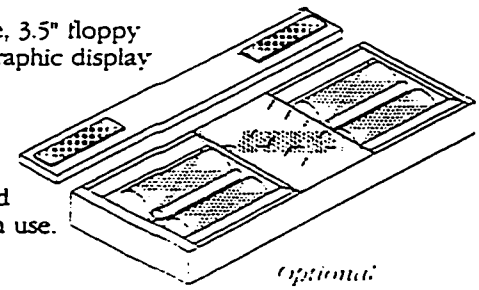

Optional

CONSTRUCTION

Zinc coated steel construction for durability. Waterproof electric motors for safety, epoxy and quartz sand embedded rollers for performance. Hinged roller covers for storage when not in use.

INSTALLATION

Above-ground or in-ground installations available.

John Bean

The Products...The People...The Pride... Wheel Service Equipment Since 1925
Automotive Service Equipment Division – Conway, Arkansas 72032
1-800-FMC-TEAM FAX (501) 450-1585

JOHNSON MATTHEY - PRODUCTION SAMPLE GROUP

Order Type:	CONCORDIA UNIVERSITY	Catalyst System:	0:1:0/JM102CK/141.4
Customer Order No.:	NOT AVAILABLE	PM Used/Ratio:	PD ONLY
JM Order No.:	091-5-0038 #1	Substrate Type:	E/500
No. Pcs. Shipped:	4	Substrate Size:	98.4 X 100
Date Shipped:	5/26/95	Substrate Volume:	46.36

LOT DATA	AVERAGE	RANGE
Washcoat Loading (g/in3)	2.13	2.11 - 2.14
Precious Metal Loading (g/ft3)	131.8	130.1 - 133.2

QUALITY CONTROL DATA

Platinum Metal Loading (g/ft3)	0.00	0.00 - 0.00
Palladium Metal Loading (g/ft3)	131.22	127.57 - 134.87
Rhodium Metal Loading (g/ft3)	0.00	0.00 - 0.00
BET Surface Area Fresh (m2/cm3)	N/A	N/A
Visual Defects Inspection	PASS	
Precious Metal Gradient (%)	N/A	

JMI ORDER #: 091-5-0038 #1

	TAG NO.	WCL	PGM LOADING
OM	60420	2.11	131.7
OM	60425	2.14	132.1
OM	60426	2.14	133.2
OM	60431	2.14	130.1
	R-HIGH	2.14	133.2
	R-LOW	2.11	130.1
	AVERAGE	2.13	131.8
QC			
OM	60427	2.11	134.9
OM	60367	2.07	127.6
RETAIN			
OM	60428	2.14	130.0

Advanced D.C. Motors, Inc.

ELECTRIC VEHICLE APPLICATIONS
S-2 THERMAL DATA PER ISO STANDARDS
X91-4001 6.7" DIA. MOTOR

75 - .03I
96 - .03I

Voltage Curves

Class - H Temperature

Time On	*Volts*	*Amps*	*RPM*	*H.P.*	*KW*
		75 Volts			
5 Minutes	68.0	235	1940	17.0	12.85
15 Minutes	69.0	186	2200	14.6	11.00
30 Minutes	70.5	151	2400	12.4	9.35
1 Hour	71.0	135	2480	11.1	8.40
Continuous	71.5	121	2600	10.0	7.55
				Peak H.P. - 29	
		96 Volts			
5 Minutes	90.0	200	2700	20.20	15.25
15 Minutes	91.0	156	3250	16.10	12.20
30 Minutes	92.0	132	3520	14.10	10.65
1 Hour	91.5	120	3650	12.85	9.70
Continuous	93.0	110	3800	12.00	9.05
				Peak H.P. - 39	

Test performed with fully seated brushes **Date: 2/21/92**

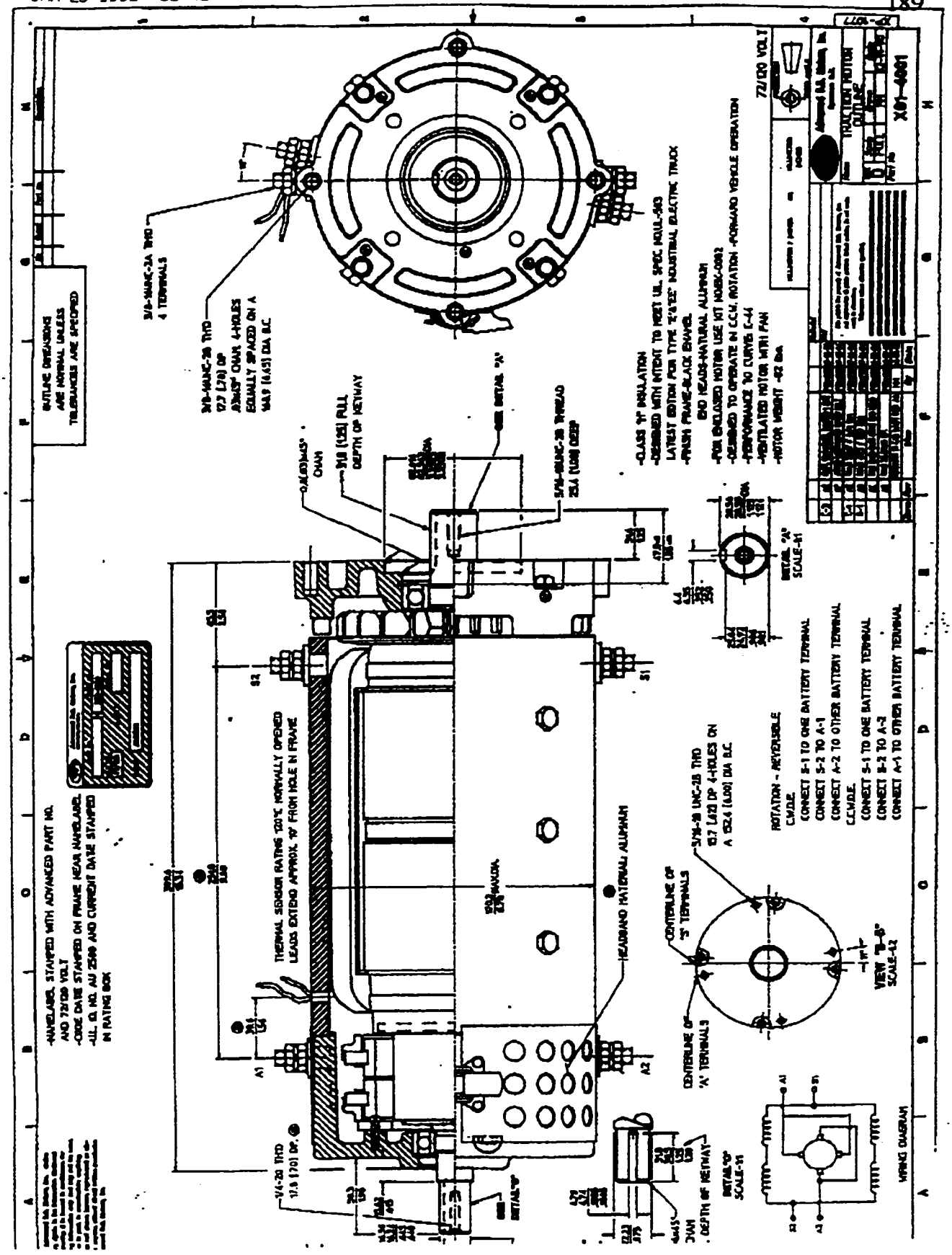
X01-4001
72/100 VOLT
TRACTION MOTOR OUTLINE
-CLASS 'H' INSULATION
-DESIGNED WITH INTENT TO MEET UL SPEC NO.UL-583 LATEST EDITION FOR TYPE 'K'SIZE' INDUSTRIAL ELECTRIC TRUCK
-FINISH FRAME-BLACK ENAMEL
END HEADS-NATURAL ALUMINUM
-FOR ENCLOSED MOTOR USE WT NO.X01-4002
-DESIGNED TO OPERATE IN C.C.W. ROTATION -FORWARD VEHICLE OPERATION
-PERFORMANCE TO CURVES C-44
-VENTILATED ROTOR WITH FAN
-MOTOR WEIGHT -62 lbs
OUTLINE DIMENSIONS ARE NOMINAL UNLESS TOLERANCES ARE SPECIFIED
3/8-16UNC-2A THD 4 TERMINALS
3/8-16UNC-2B THD 12.7 [.50] DP EQUALLY SPACED ON A 146.1 [5.63] DIA B.C.
5/16 [.125] FULL DEPTH OF KEYWAY
5/16-18UNC-2B THREAD 25.4 [1.00] DEEP
DETAIL "A" SCALE-#1
-NAMEPLATE, STAMPED WITH ADVANCED PART NO. AND 72/100 VOLT
-CODE DATE STAMPED ON FRAME NEAR NAMEPLATE.
-U.L. ID. NO. AU 2500 AND CURRENT RATE STAMPED IN RATING BOX
THERMAL SENSOR RATING 120°C NORMALLY OPENED LEADS EXTEND APPROX. 76" FROM HOLE IN FRAME
HEADEND MATERIAL ALUMINUM
5/16-18 UNC-2B THD 12.7 [.50] DP 4-HOLES ON A 152.4 [6.00] DIA B.C.
ROTATION - REVERSIBLE
C.W.DE
CONNECT S-1 TO ONE BATTERY TERMINAL
CONNECT S-2 TO A-1
CONNECT A-2 TO OTHER BATTERY TERMINAL
C.C.W.DE
CONNECT S-1 TO ONE BATTERY TERMINAL
CONNECT S-2 TO A-2
CONNECT A-1 TO OTHER BATTERY TERMINAL
CENTERLINE OF "S" TERMINALS
CENTERLINE OF "A" TERMINALS
VIEW "B-B" SCALE-#2
1/4-20 THD 12.8 [.701 DP.
DETAIL "B" SCALE-#1
WIRING DIAGRAM

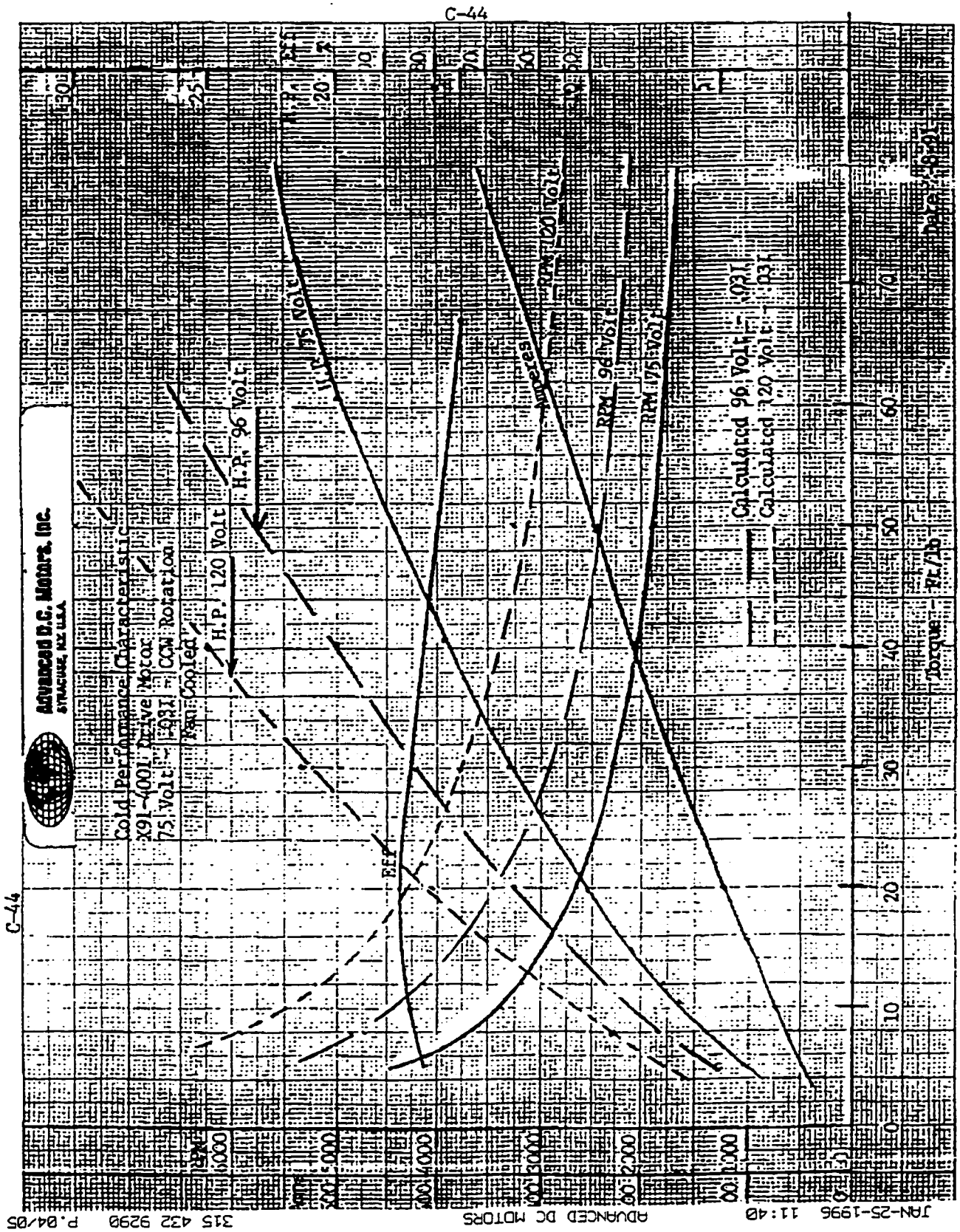
C-44
Advanced D.C. Motors, Inc.
SYRACUSE, NY U.S.A.
Cold Performance Characteristic
X91-4001 Drive Motor
75 Volt - 6231 - CCW Rotation
Fan Cooled
H.P. 120 Volt
H.P. 96 Volt
H.P. 75 Volt
Amperes
RPM 120 Volt
RPM 96 Volt
RPM 75 Volt
Calculated 96 Volt - 6231
Calculated 120 Volt - 6231
Torque - Ft/Lb
JAN-25-1996 11:40
ADVANCED DC MOTORS
315 432 9290 P.04/05
C-44

CURTIS PMC

DATA

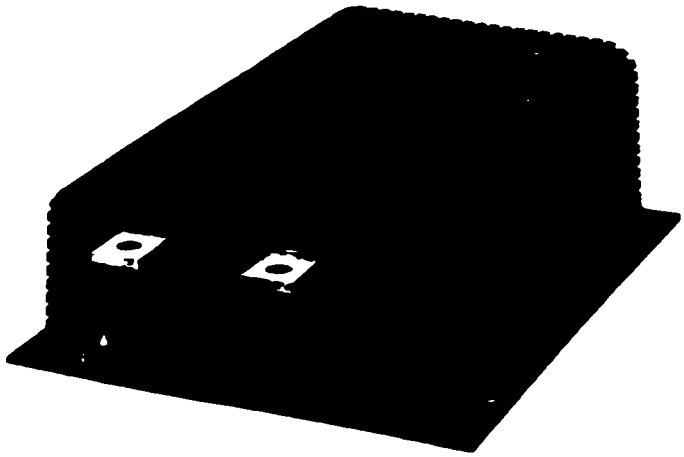

CURTIS PMC MODEL 1209/1221

HIGH POWER ELECTRONIC
MOTOR SPEED CONTROLLER

The **Curtis PMC 1209&1221** are high power electronic motor speed controllers designed to provide smooth, silent, efficient and cost effective speed and torque control for a wide variety of industrial electric vehicle applications. The **1209/1221** combines proven Curtis PMC 1204 power MOSFET controller technology with extended operating features and power ranges. Typical applications include industrial trucks, airport equipment, tow tractors, personnel carriers, forklift applications, on-road vehicles, scissors lift and boom trucks, etc.

FEATURES:

- High frequency switching and ultra low voltage drops provides very high efficiency, silent operation. Costs, heatsinking requirements and motor and battery losses are reduced. Low end torque, range and battery life are increased.
- Total environmental protection provided by epoxy sealed (factory serviceable) rugged anodized aluminum extrusion housing. Simple mounting and wiring with push-on type connectors for control signals. Large solid copper buses used for all power connections.
- Thermal protection and compensation circuit provides undertemperature cutback, constant current limit over operating range and linear rollback in overtemperature. No sudden loss of power under any thermal conditions.
- Adjustable acceleration rate, current limit (protected against exceeding controller rating) and plugging current limit. Adjustments are accessed through sealed screws on side of housing.
- Variable plugging current feature provides throttle position control over braking to improve driveability.
- Full fault detect circuitry monitors power supply, throttle connections, output transistors, etc., to prevent runaway. Neutral start option requires that throttle be returned to neutral before output is allowed. Static return-to-off option requires that F/R selector be returned to neutral before output is allowed.
- Arcless contactor switching for F/R contacts and bypass contacts (if opened below controller current limit).
- Delayed bypass (1A) output drives optional bypass contactor, after throttle reaches 90% and bypass delay times out. Short circuit protected F/R and bypass contactor drivers. (These features only for models ≤36 volts)

WARRANTY : One year from date of delivery, subject to conditions of warranty.

CURTIS PMC • A ... ION OF CURTIS INSTRUMENTS, INC., • 6591 SIERRA LANE • DUBLIN, CA 94568 (415) 828-5001
CURTIS INSTRUMENTS, INC., • 200 KISCO AVENUE • MT. KISCO, NY 10549 • (914) 666-2971 • FAX (914) 666-2188

SPECIFICATIONS:

MODEL NUMBER	INPUT VOLTAGE (volts)	CURRENT LIMIT (amps)	2 MIN RATING (amps)	5 MIN RATING (amps)	1 HOUR RATING (amps)	VOLTAGE DROP@ 100 A	UNDER-VOLTAGE CUTBACK (volts)
1209-46xx	24-36	500	500	350	225	<.15V	16
1209-55xx	36-48	450	450	300	200	<.30V	21
1209-64xx	48-72	400	400	275	175	<.30V	32
1209-62xx	48-72	275	275	200	125	<.45V	32
1209-61xx	48-72	175	175	125	75	<.70V	32
1209-72xx	72-120	275	275	175	100	<.70V	48
1221-48xx	24-36	600	600	425	250	<.10V	16
1221-57xx	36-48	550	550	375	225	<.25V	21
1221-66xx	48-72	500	500	350	200	<.25V	32
1221-74xx	72-120	400	400	250	150	<.50V	48

Frequency of operation: 15 kHz
Standby Current: <20 ma
Standard Throttle Input: 0-5KΩ (others available)
Weight: 1209=8.8 lb, 1221=10.8 lb

DIMENSIONS :

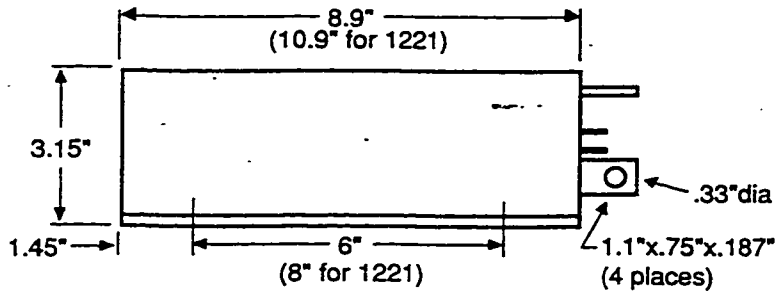

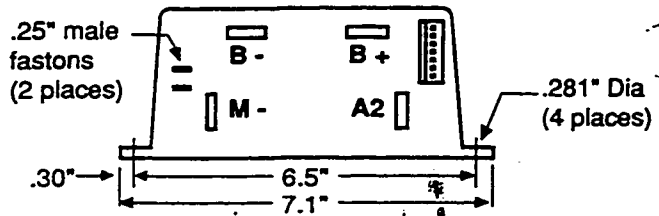

TYPICAL INSTALLATION :

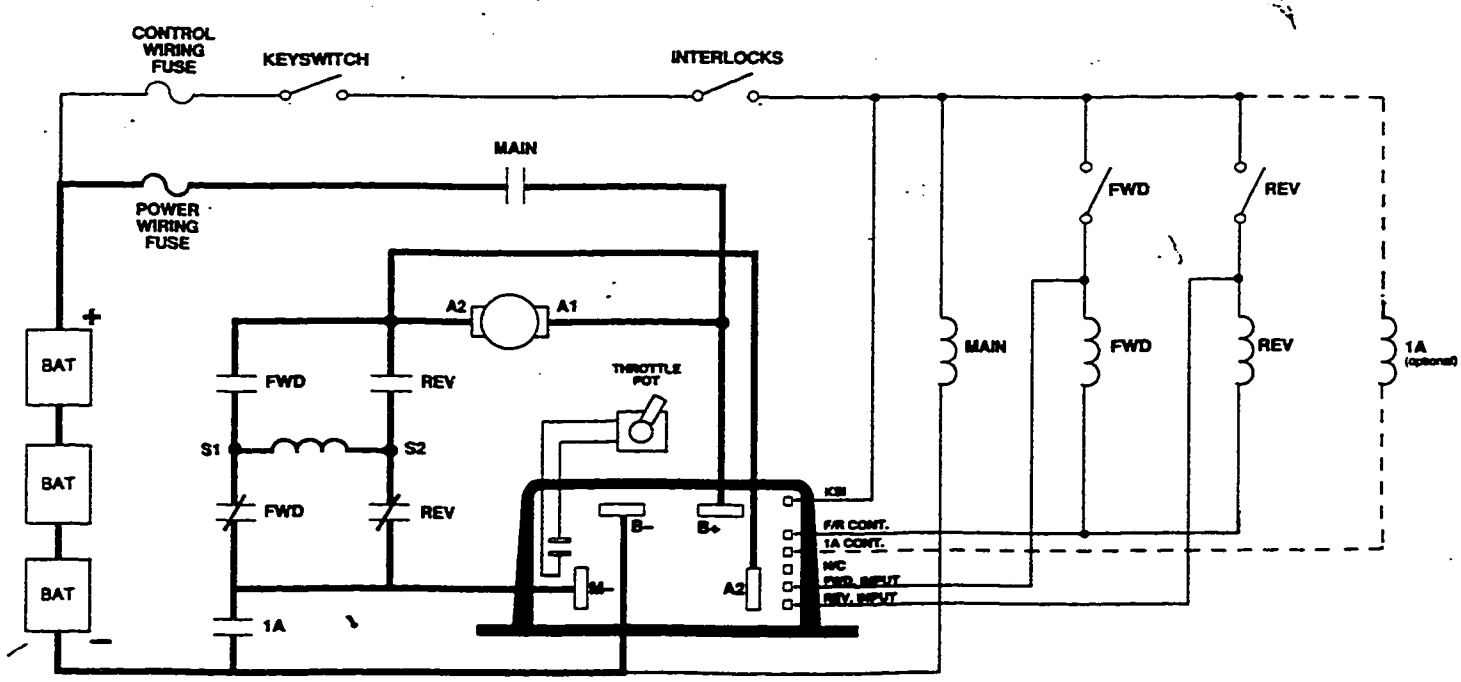

CURTIS PMC

State-of-the-Art
(continued)

Greater Switching Speed

The very fast switching capabilities of transistors permit operation of CURTIS/PMC controllers at very high frequencies with no harmful overheating of components. The result is lower ripple currents, nearly 100% efficiency in all modes of operation and quiet operation, in most cases beyond the audible range.

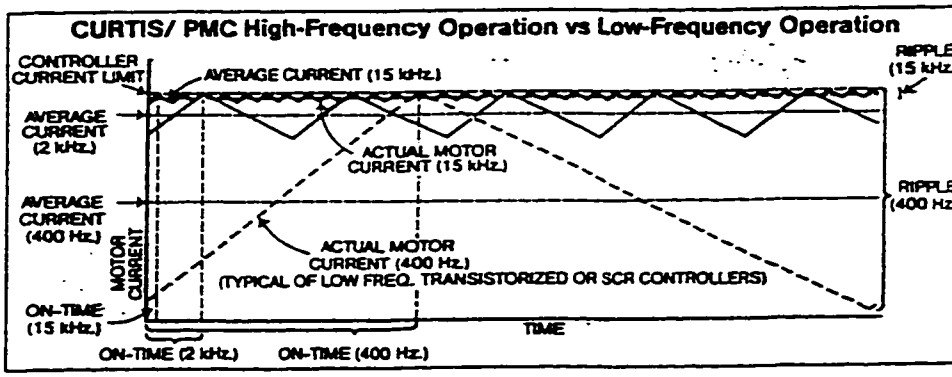

High ripple currents keep average current levels unnecessarily far below the peak current—torque is reduced. With low ripple currents the motor stall current is kept close to the controller current limit to privide higher stall torque and optimize efficiency.

Smooth Speed Control

Transistors permit varying speed smoothly from zero to full, resulting in total and precise control of motor speed and torque. Vehicles equipped with a CURTIS/PMC controller can climb a ramp at any desired speed—no lurching starts.

Electrical Characteristics and Features

Current Limiting

With a CURTIS/PMC controller motor current is limited to a preset maximum value to protect the controller and to reduce the possibility of motor winding or battery terminal burnout that can occur with vehicle abuse.

Current Multiplication

During acceleration or reduced speed operation CURTIS/PMC controllers act as DC transformers. More current flows to the motor than flows out of the battery. Range per battery charge is increased.

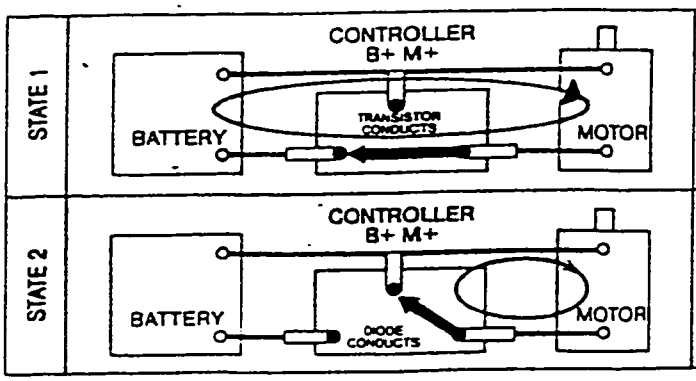

	BATTERY CURRENT	MOTOR CURRENT
STATE 1	X	X
STATE 2	0	X
	TOTAL X	TOTAL 2X

The controller operates by switching from State 1 to State 2 at a rapid rate. The ratio of the time spent in State 1 to the total time is the duty cycle. When the duty cycle is less than the unity, the current in the motor is always greater than the current out of the battery. In the case above, where the duty cycle is equal to 50% (i.e., motor voltage = one-half battery voltage), the motor current is twice the battery current.

Table A.1 American Wire Gage Conductor Selection.

AWG Size	Cir Mils	AWG Size	Cir Mils Area
18	1 820	4	41 740
16	2 680	3	52 820
14	4 110	2	66 360
12	6 630	1	83 690
10	10 380	I/0	106 600
8	16 610	I/00	133 100
6	26 240	I/000	187 800

$$CMA = \frac{I_{max} \cdot LF \cdot K \cdot n}{AVD} \tag{A.1}$$

where:

I_{max} is the maximum current in the conductor,
LF is the conductor loop length (m),
K is a copper constant (36.1),
AVD is the allowable voltage drop for the maximum drain in amperes (3),
CMA is the Cir Mils Area,
n is the safety factor (1.25).

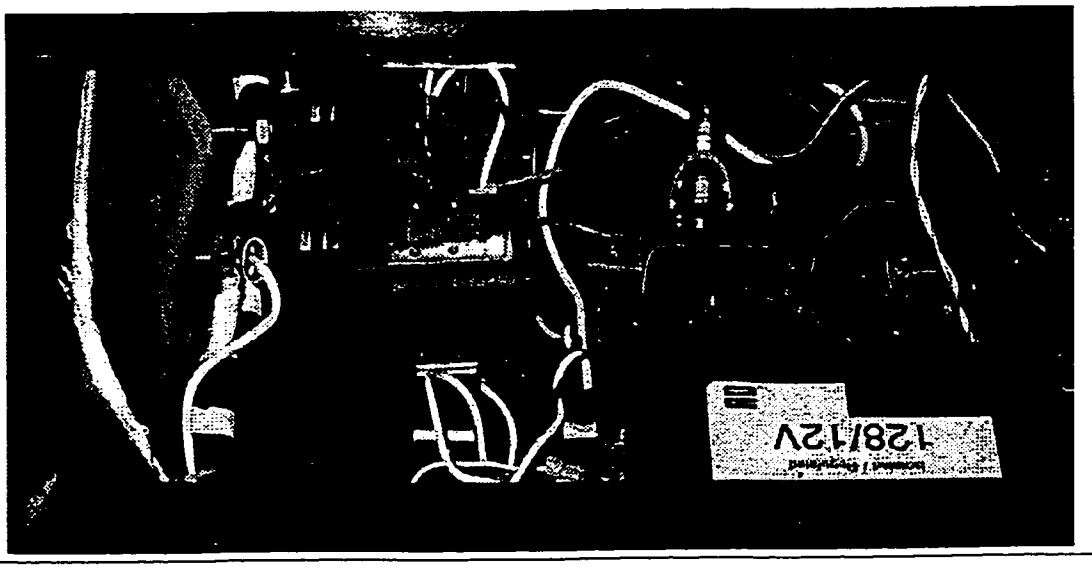

Figure A.2 Placement of Contactors and DC-DC Converter.

SW200 SERIES OF D.C. CONTACTORS

UNIQUE RANGE

The SW200 series of contactors has been designed for direct current loads, particularly motors as used on larger electric vehicles such as industrial trucks, airport tractors, etc.

They have double breaking main contacts with silver alloy contact tips, which are weld resistant, hard wearing and have excellent conductivity.

The range comprises: Single Pole, on/off types (SW200), Single Pole normally closed types (SW210), paired version of these for motor reversing (SW202) and derivatives of these types to give various combinations and configurations.

COMPACT SIZE

The contactors are compact in size and are fully serviceable, with a full range of spare parts available.

EASY INSTALLATION

Mounting is by means of 5mm tapped holes in the switch frame together with a range of mounting brackets complete with screws and washers.

Coil connections are by means of 6mm spades of which two are supplied per terminal.

Contactor types SW202, SW204, SW205, SW208, SW213 and SW214 are supplied as an assembly which includes a mounting bracket as a standard feature.

Mounting attitudes are detailed in the drawings on the following pages.

OPERATING COILS

Coil voltages ranging from 6 to 240 are available and these are wound for D.C. operation.

However coils can be fitted with a bridge rectifier for use from A.C. supplies.

Coils are normally wound for intermittent duty (up to 70% "on" time) but continuous duty version (100%) are also available.

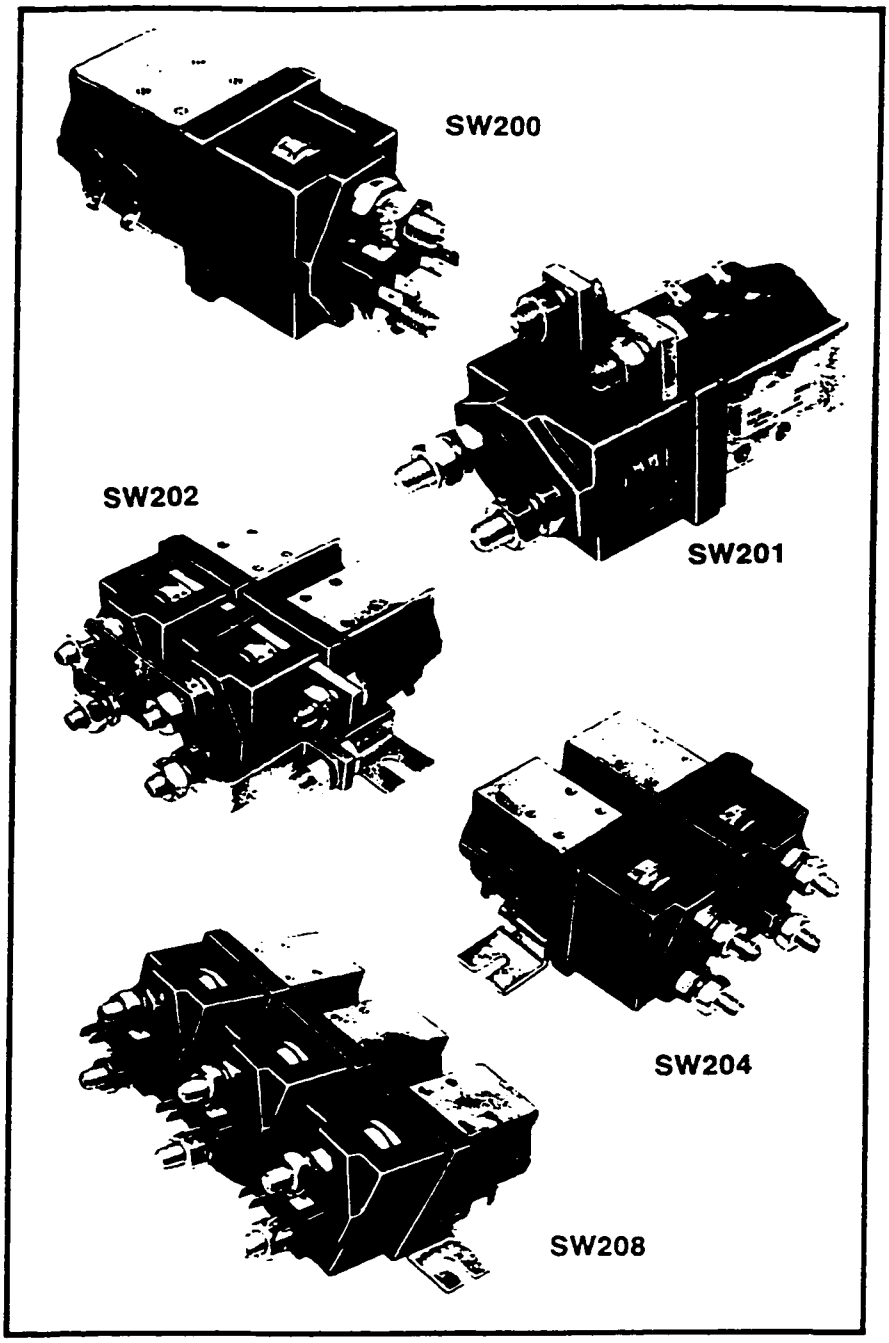

CONTACTORS

SW200	SINGLE POLE SINGLE THROW	SW205	2xSW201 ON DOUBLE BRACKET
SW201	SINGLE POLE DOUBLE THROW	SW208	3xSW200 ON TRIPLE BRACKET
SW202	PAIRED SINGLE POLE DOUBLE THROW ON DOUBLE BRACKET (for motor reversing)	SW210	SINGLE POLE SINGLE THROW (normally closed)
		SW213	3xSW210 ON TRIPLE BRACKET
SW204	2xSW200 ON DOUBLE BRACKET	SW214	2xSW210 ON DOUBLE BRACKET

PERFORMANCE DATA

Thermal current rating (100%)	250 Amperes
Intermittent current rating	
30% duty	450 Amperes
40% duty	390 Amperes
50% duty	360 Amperes
60% duty	320 Amperes
70% duty	300 Amperes
Typical fault currents which can be ruptured (5ms time constant)	
SW200N and SW210N	1500 Amperes at 48V D.C.
SW200 and SW210	1500 Amperes at 96V D.C.
SW201N * and SW202N *	600 Amperes at 48V D.C.
SW201 * and SW202 *	1500 Amperes at 96V D.C.
* *Normally open contacts, not normally closed contacts.*	
Maximum recommended contact voltages	
SW200N and SW210N	48V D.C.
SW200 and SW210	96V D.C.
SW201N and SW202N	48V D.C.
SW201 and SW202	96V D.C.
Typical voltage drop across contacts per 100 Amperes	
SW200 and SW210	40mV
SW201 and SW202 (normally open contacts)	40mV
SW201 and SW202 (normally closed contacts)	40mV
Mechanical life	> 5 x 10^6
Coil power dissipation	
Intermittently rated types	30-60 Watts
Continuously rated types	13-21 Watts
Maximum pull-in voltage (coil at 20°C)	
Intermittently rated types	60%V
Continuously rated types	66%V
Typical drop-out voltage	10-20%V
Typical pull-in time (n/o contacts to close)	40ms
Typical drop-out time (n/o contacts to open)	
Without suppression	10ms
With diode suppression	100ms
With diode and resistor (depending on value)	30ms
Typical main contact changeover time (SW201 and SW202)	
Normally closed to normally open	14ms
Normally open to normally closed	8ms
Typical contact bounce period	3ms
Auxiliary contact thermal current rating	5 Amperes
Auxiliary contact switching capacities (resistive load)	5A at 24V D.C. 2A at 48V D.C. 0.5A at 240V D.C.

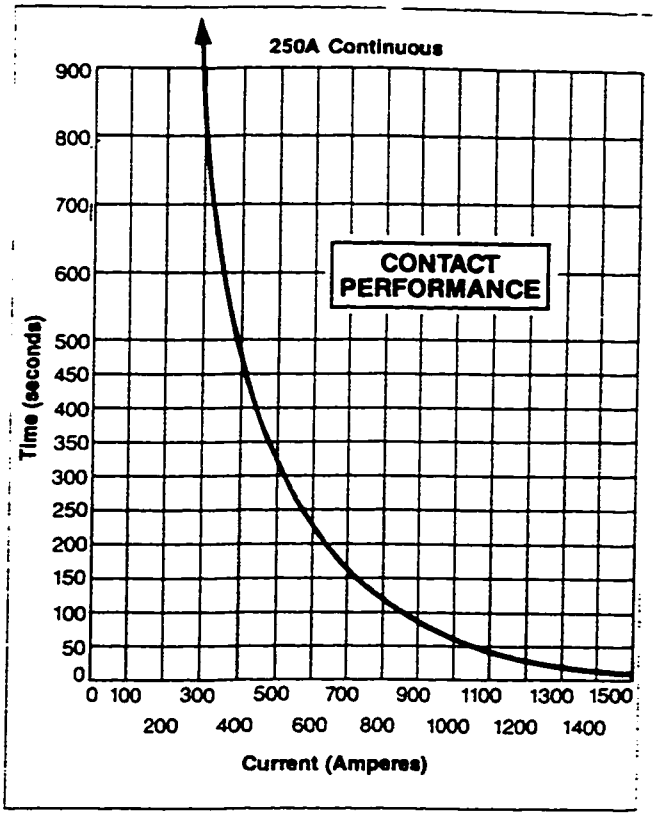

All the above figures should be used as a guide only. Some derating may be necessary according to type and application.

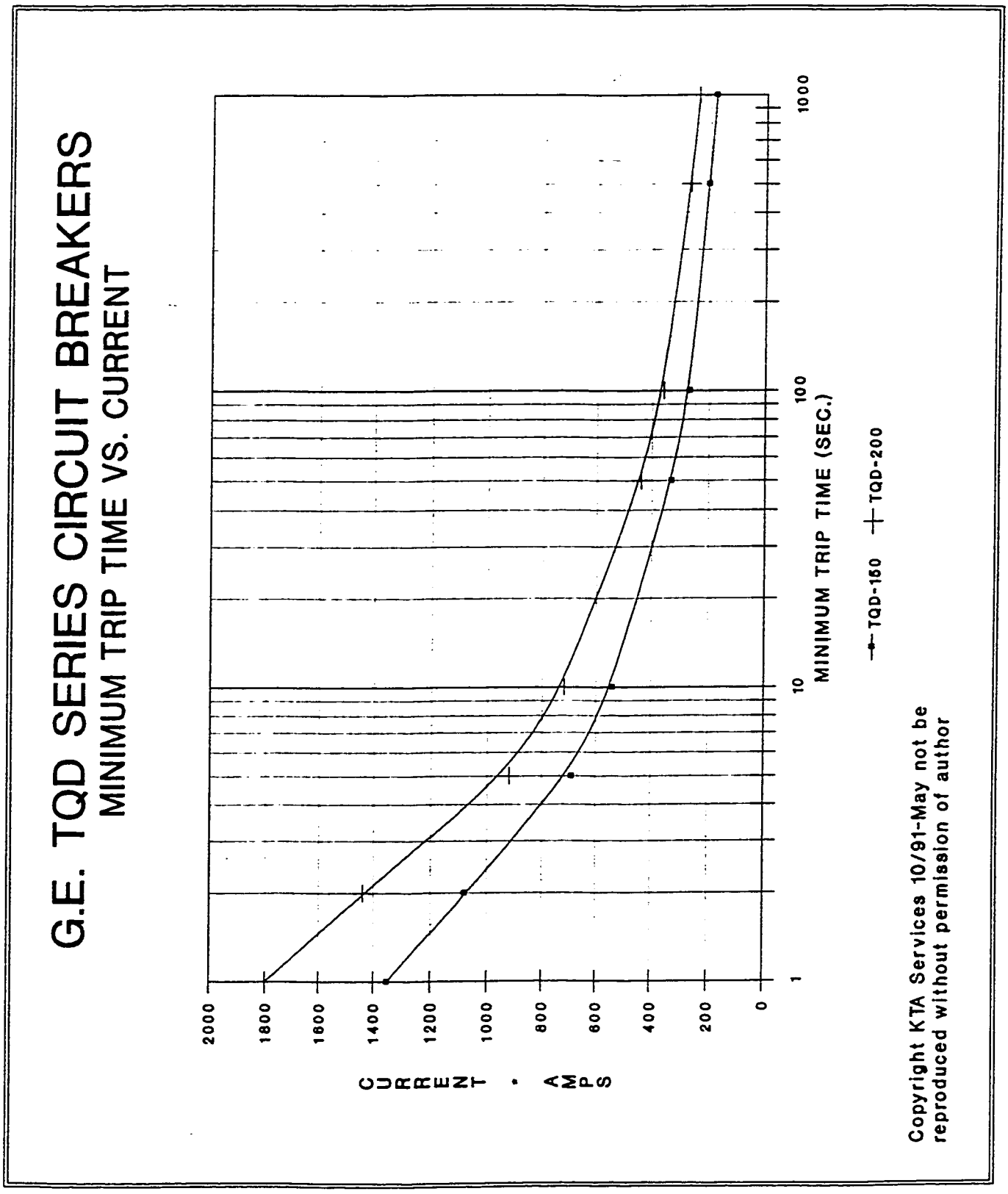
G.E. TQD SERIES CIRCUIT BREAKERS
MINIMUM TRIP TIME VS. CURRENT
CURRENT - AMPS
2000
1800
1600
1400
1200
1000
800
600
400
200
0
1
10
100
1000
MINIMUM TRIP TIME (SEC.)
TQD-150
TQD-200
Copyright KTA Services 10/91-May not be reproduced without permission of author

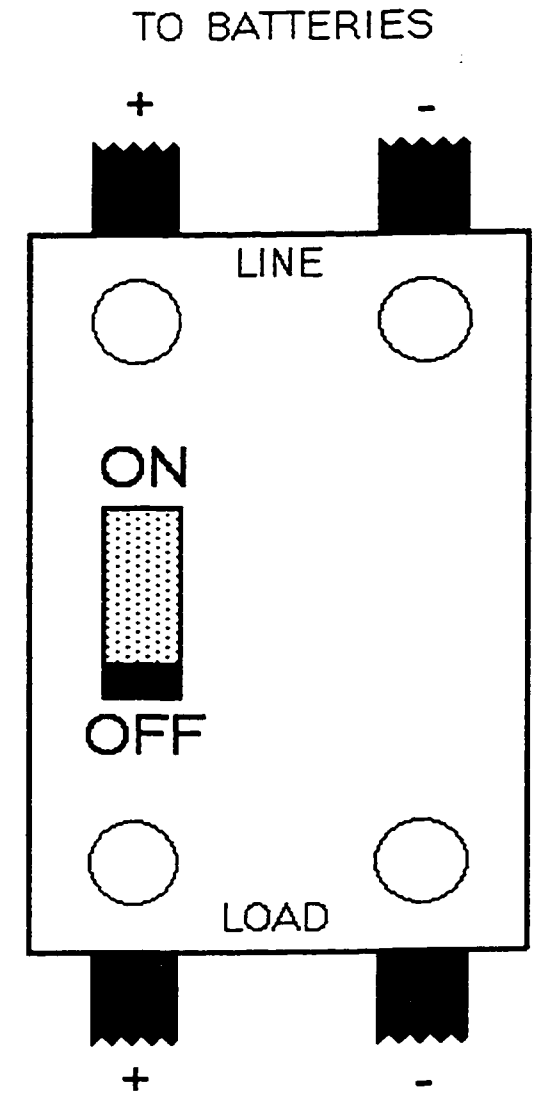

KTA SERVICES

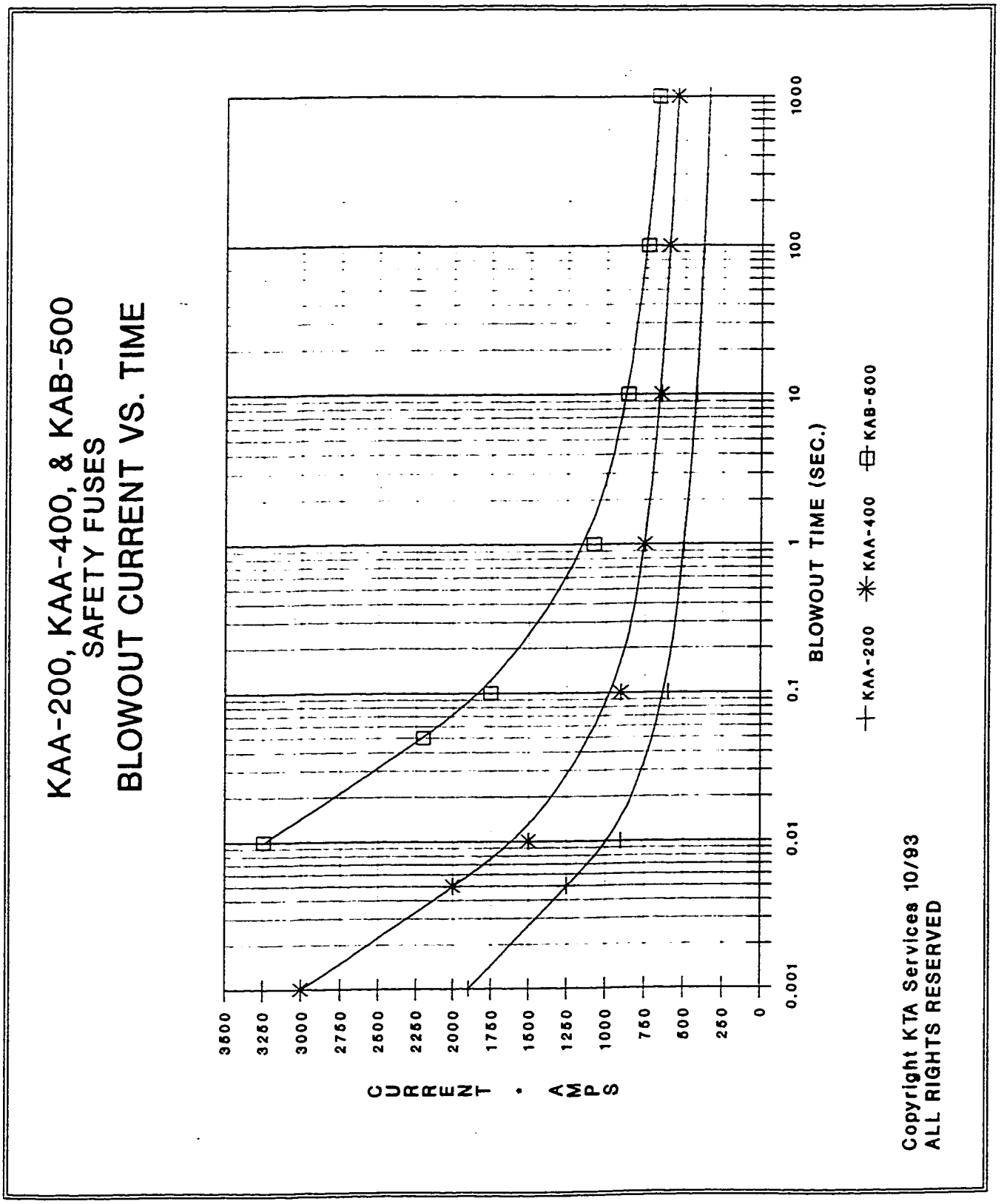
KAA-200, KAA-400, & KAB-500
SAFETY FUSES
BLOWOUT CURRENT VS. TIME
CURRENT - AMPS
3500
3250
3000
2750
2500
2250
2000
1750
1500
1250
1000
750
500
250
0
0.001
0.01
0.1
1
10
100
1000
BLOWOUT TIME (SEC.)
KAA-200
KAA-400
KAB-500
Copyright KTA Services 10/93
ALL RIGHTS RESERVED

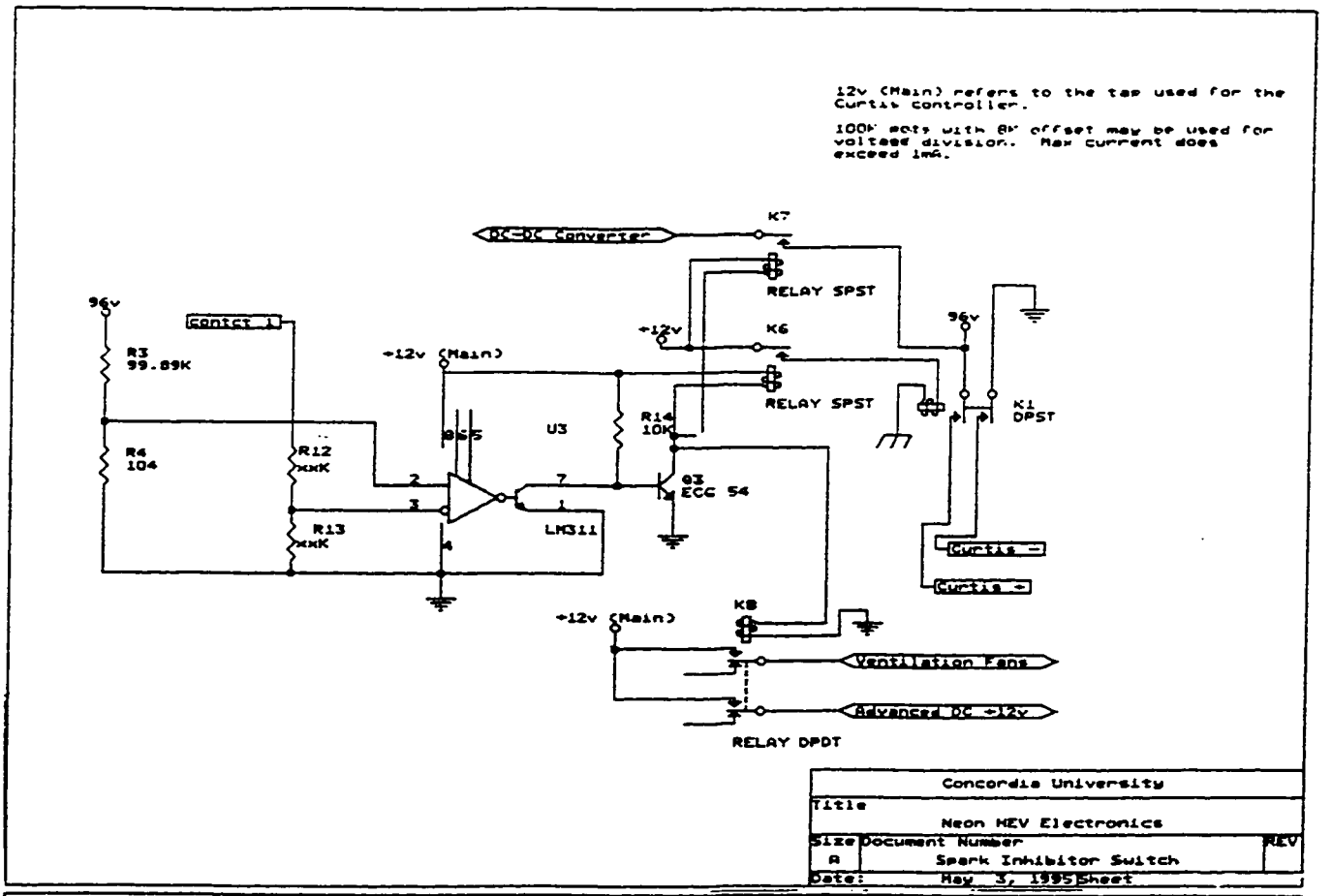

Concordia University		
Title: Neon MEV Electronics		
Size: A	Document Number: Spark Inhibitor Switch	REV:
Date: May 3, 1995	Sheet	

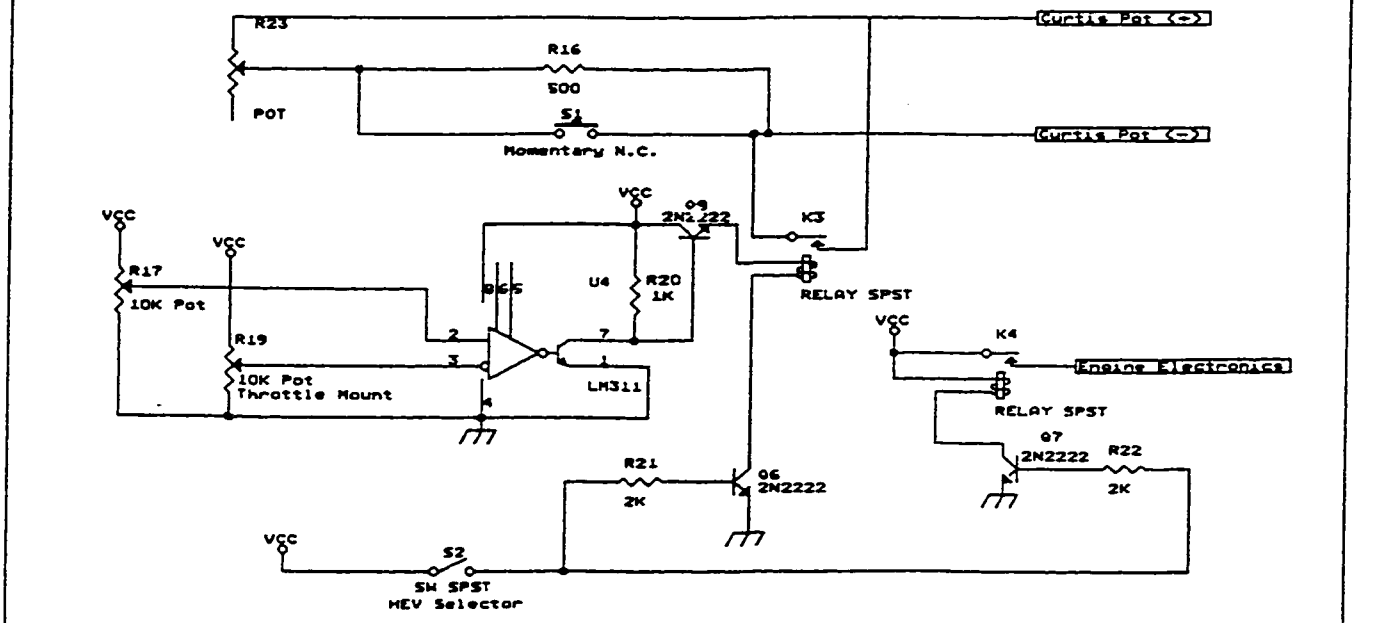

Concordia University		
Title: Neon MEV Electronics		
Size: A	Document Number: General Control Layout	REV:
Date: May 3, 1995		

COMPRESSOR

10PA17

■ SPECIFICATIONS

Compressor	Model	10PA17
	Bore, mm	29.5
	Stroke, mm	26.0
	No. of Cylinders	10
	Piston Displacement, cm³/rev	178
	Air Tightness, MPa {kgf/cm²}	3.14 {32} (High press. side)
		1.67 {17} (Low press. side)
	Max. Speed, r/min	9,000
	Lubrication Oil	ND-OIL 8, 100cm³
	Mass, kg	4.4
Magnetic Clutch	Model	L50
	Rated Voltage, V	12
	Torque, N·m (kgf·m)	53 (5.4) Min.
	Power Consumption, W	40 Max.
	Max. Speed, r/min	9,000
	Belt	POLY-V-belt, PK4
	Pulley Effective Dia., mm	125
	Mass, kg	2.25

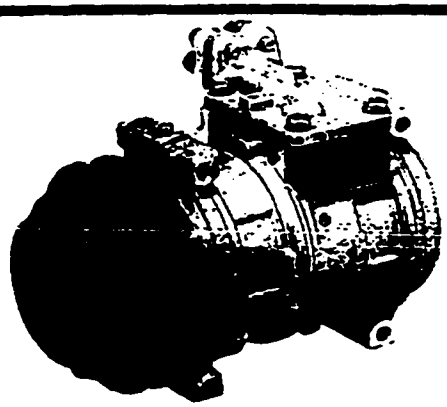

■ PERFORMANCE CURVES

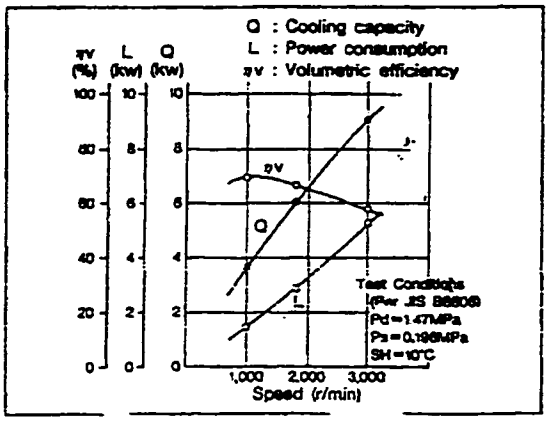

■ OVERALL DIMENSIONS

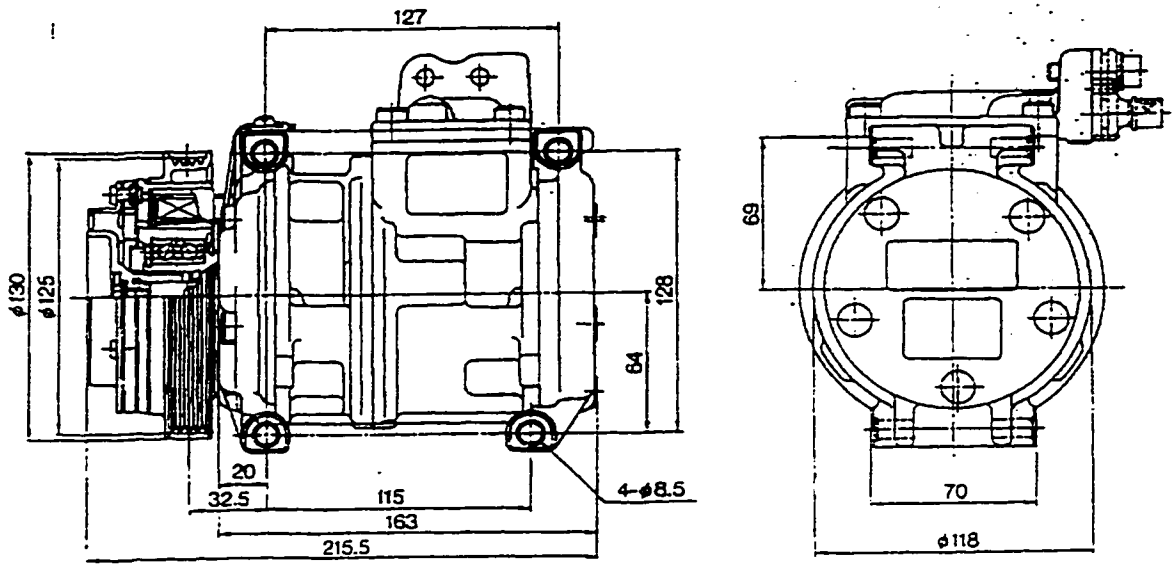

CURTIS DATA

CURTIS 900R BATTERY "FUEL" GAGE

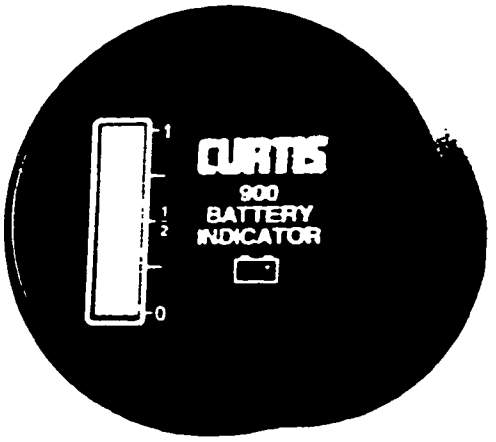

FEATURES:

The CURTIS 900R Battery "Fuel" Gage is a low-cost, easily-installed "fuel" gage that has been specifically designed for battery-powered equipment and electric vehicles not requiring lift lockout.

The CURTIS 900R has been derived from the CURTIS 933/3 "Fuel" Gage and Battery Controller technology used on electric fork lift trucks worldwide.

The CURTIS 900R comes in a one-piece package containing all electronics and is installed via a simple 2-wire connection.

The unit features:

- A digital, multi-colored 10-LED display of state-of-charge.
- A flashing light "energy reserve" alarm at 75% depth of discharge.
- A double flashing light "empty" alarm at 80% depth of discharge.
- Improperly charged battery recognition.

APPLICATION OPTIONS:

CURTIS 900R units have been designed specifically for the two major classes of lead acid battery-powered vehicles not served by the CURTIS 933/3:

- The CURTIS 900R **HG** unit is for industrial/recreational electric vehicles that **remain connected** to their batteries during the charge cycle.
- The CURTIS 900R **BN** unit is for electric fork lift equipment and electric vehicles that can be either **disconnected** from or **remain connected** to their batteries during the charge cycle.

  BN units have undefeatable memory that remembers the state-of-charge of the battery when disconnected.

SYSTEM VOLTAGES:

HG units: 12V, 24V, 36V, 48V, 72V, 80V

BN units: 12V, 24V, 36V, 48V, 72V, 80V

Non-standard voltages available.

WARRANTY:

One year from date of delivery. Replacement without charge.

CURTIS INSTRUMENTS, INC., • 200 Kisco Avenue, Mt. Kisco, N.Y. 10549 • Tel. (914) 666-2971 • FAX (914) 666-2188

5900R-858 7/93 REV A

DIMENSIONS:

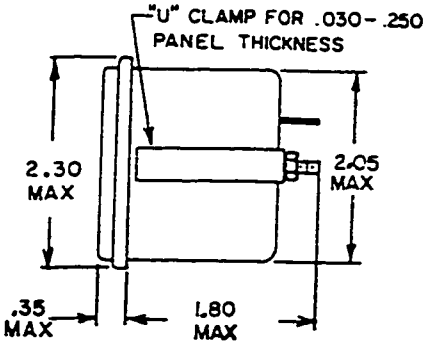

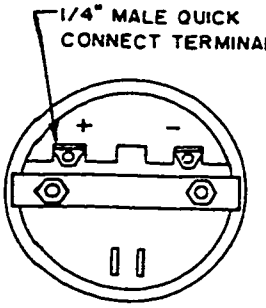

MODEL ENCODEMENT:

900R **B** **24** **B** **N** **A** **A** **O**

- **B** — Black Bezel
- **24** — VOLTAGE: 12, 24, 36,48 72, 80 VDC
- **B** — RESET LEVEL: B – with memory, 2.09 v/c; H – no memory, 2.35 v/c
- **N** — DISCHARGE PROFILE: N = 2.04 v/c at full to 1.73 v/c at empty; G = 1.97 v/c at full to 1.75 v/c at empty; A = Adjustable; range of 1.56 to 1.82 v/c at empty; B = Light duty adjustable; range of 1.71 to 1.93 v/c at empty
- **A** — OPTION: A = no option
- **A** — OPTION: A = no option; B = audible alarm
- **O** — OEM CODE: O = CURTIS logo

INSTALLATION:

CURTIS 900R "Fuel" Gage positive (+) terminal to battery positive (+) bus; gage negative (–) terminal to battery negative (–) bus.

HOW THE 10-LED STATE-OF-CHARGE DISPLAY WORKS:

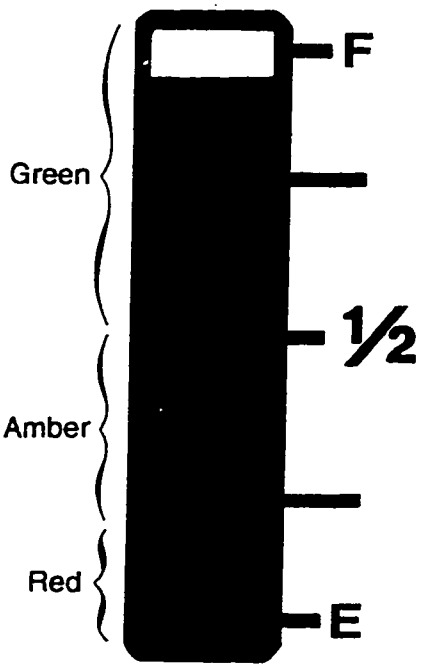

The battery is properly charged only when the top LED is illuminated.

As the battery's state-of-charge decreases successive LEDs light up: ONLY the LED indicating the state-of-charge is illuminated.

At this point, the LED flashes, indicating "energy reserve" (70% depth of discharge).

At this point, both bottom LEDs alternately flash, indicating "empty" (80% depth of discharge).

APPLICATIONS:

H units are suited to personnel carriers, cargo (burden) carriers, tractors, sweepers, golf cars, etc.

B units are suited to pallet jack walkies, walkies, transpallets, scissor lifts, etc.

REGULATED DC/DC CONVERTER

Output Voltage Fully Isolated from Primary Power Source

The new Generation II Sevcon Regulated DC/DC Converter is a "power supply" designed to give a stable high power, low voltage DC supply for vehicle accessories such as lights, horns, wipers and radios, thus eliminating the need for battery taps and fragile, expensive high voltage components. The output voltage is isolated from the primary power source and conforms to U.L. standard 583 section 9.16. In addition, the output voltage is regulated to a constant 13.5 volts. This ensures full lamp brightness regardless of load current or state of battery charge.

- ☐ Voltage In: 72 and 128 Volts DC.
- ☐ Current: Maximum 25 Amps.

Technical Features

- — Output supply isolated.
- — Nominal voltage inputs 72 and 128 Volts.
- — Output nominal 13.5 Volts regulated.
- — 330 watts continuous output.
- — Short circuit protection.
- — Overload protection.
- — Reverse polarity protection.
- — Transient protection.
- — Double isolation of power components.

Other Features

- — Inaudible operation.
- — Robust construction.
- — Designed to operate with motor controllers.
- — Designed to U.L. and F.E.M. standards.

[illegible]

Sevcontrol Tech/Ops

Specifications continued on reverse

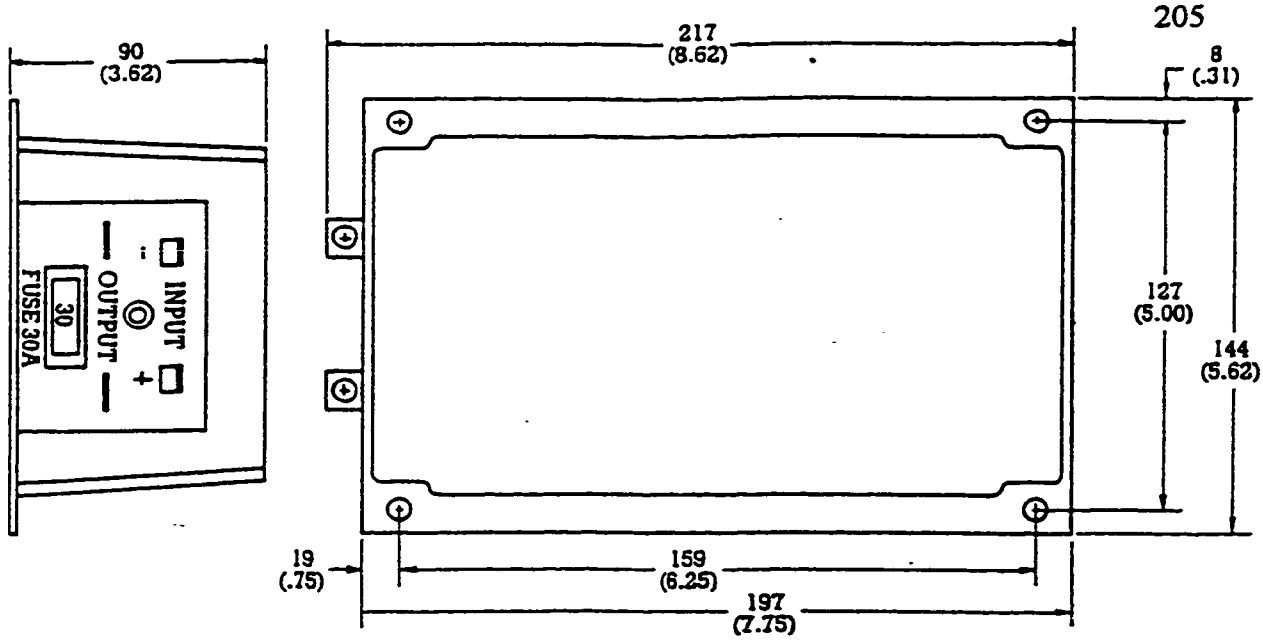

OUTLINE SPECIFICATION:

Input voltage:	2 models available for 72 or 128 volt applications. Operating range 60% to 110% of nominal battery voltage.
Output voltage:	Nominal 13.5 volts (Regulated).
Output:	Up to 330 watts continuous.
Ambient Temperature Range:	Operating: –20°C + 40°C. Storage: –30°C + 70°C.
Customer Light Wiring Connector:	M4 thru holes (8/32 Screw)
Customer Heavy Wiring Connector:	M6 thru holes (1/4 Screw)
Weight:	4 lbs.

Note: This product bulletin is an outline specification only. For specific application data the full engineering specifications available from Tech/Ops should be used.

Tech/Ops is constantly striving to improve its products and reserves the right to alter specifications without notice.

SEVCON Tech/Ops

Tech/Ops Sevcon, Inc.
Burlington, Mass.
U.S.A. 01803
Tel: (617) 272-3612
Telex: (232) 00130

Tech/Ops Ltd.
Gateshead
England NE11 0QA
Tel: (09) 487-8516
Telex: 53328

Tech/Ops S.A.
Paris
France 95100
Tel: (3) 410 9545
Telex: 698505

APPENDIX 3

Specifications and Information Relative to Chapter 6

POWER SOURCE™

BATTERY CHARGER/POWER SUPPLY

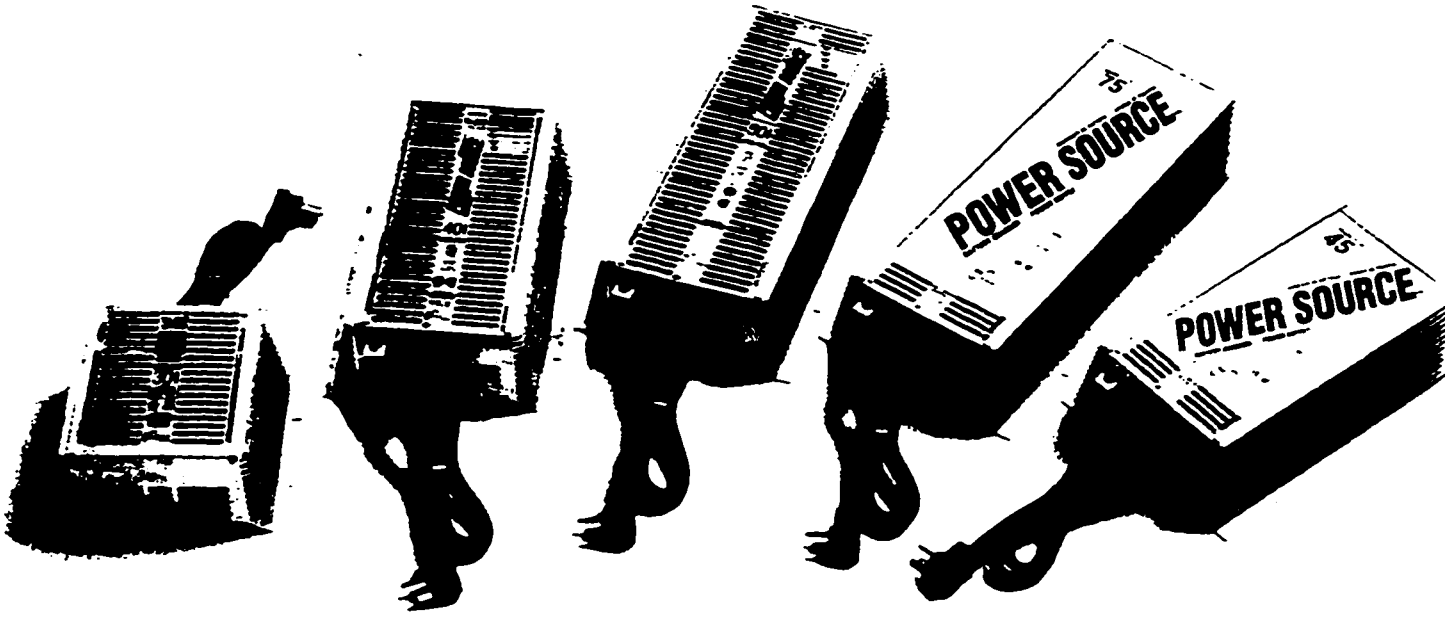

LISTED

LR 98322 TO 386465170

BATTERY CHARGING

TOTALLY FILTERED AND REGULATED OUTPUT. "Locked in" at 14 volts, the entire output is PURE DC, and totally battery compatable.

NATURAL CHARGING™! Flawless charging as natural as water running down hill. No more overcharging or undercharging.

TURBO-CHARGING™! Total charger capacity means battery recovery in **hours** instead of days.

FILTERED POWER SUPPLY

CONSTANT VOLTAGE PURE DC OUTPUT! Works perfectly with RV load; appliances run at the right speed even in RV park "brown outs." No ripple to cause early bulb burnout, excess motor heat.

PURE FLOATING OPERATION! Works equally well with or without a battery. Charges the battery and carries the load; works with or without, **never instead of,** the battery.

ENGINEERING LANDMARKS

SILENT OPERATION! Makes less noise than your bedside clock.

LIGHT WEIGHT! It takes FIVE 30 amp Power Source™ units to equal ONE 30 amp competitor's massive weight!

SUBCOMPACT SIZE! It takes THREE 30 amp Power Source™ units to equal ONE 30 amp competitor's hulking size.

LESS HEAT! Power Source™ generates almost no heat until approx. **70% LOAD!** A competitor's generates almost full temperature at **NO LOAD!** Cooler Power Source™, cooler coach, cooler customer. . .

EASY INSTALLATION! Three exterior wiring lugs, and plug it in. Designed for the electrician, by an electrician!

REPUTATION/SERVICE! Designed and built by the company with a reputation for supplying comparable premium quality electrical components to the RV manufacturers for over ten years:
Todd Engineering Sales, Inc. Impeccable!

ENGINEERING SALES INC.

(602) 889-9333
TUCSON, AZ

(219) 293-8633
ELKHART, IN

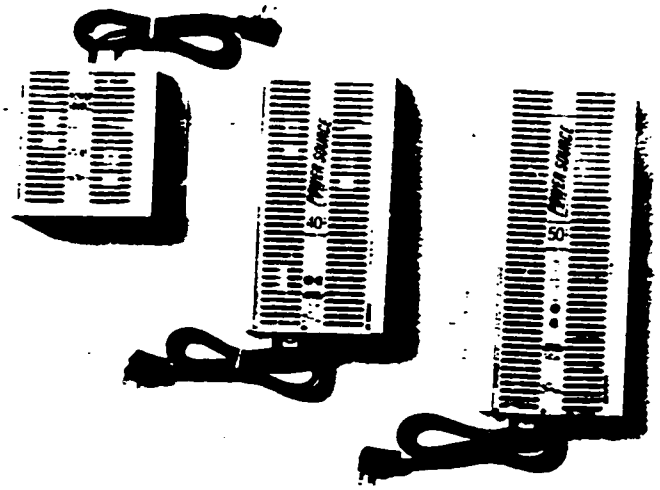

BATTERY CHARGING

PURE DC OUTPUT - Totally filtered output works perfectly with RV batteries; no ripple current to cause battery "cooking". No need to engineer one special "filtered" output circuit while all the other circuits remain unprotected; the entire output is pure DC.

REGULATED OUTPUT VOLTAGE - Output voltage is "locked in" at 14 volts for connection to RV batteries; it is not only flawless for charging, it is also highly desirable for long term direct-connected operation as it cannot overcharge a sound battery.

NATURAL CHARGING™ - With a pure DC output locked in at 14 volts, safe battery charging is now simply a matter of charger voltage vs. battery voltage. If the battery voltage is lower (discharged) than the charger voltage, then the electrical current flows naturally to the battery. The greater the difference in voltage between the charger and the battery the faster the current flow; the smaller the difference between the two the slower the flow (or taper charge) until the battery reaches the same voltage level as the charger, at which point there is no flow at all (except an ongoing replacement of any future discharge); the battery in now charged! . . .a Natural Charge™!

TURBO-CHARGING™ - Unlike most RV converters where only one small circuit is filtered enough to allow connection to the battery, and where that trickle of current can take days to recover the battery when it is discharged; the entire output of the Power Source™ is battery compatable. Since this entire output is available to the battery as it is needed, recovery time is greatly speeded. Recharge is now hours instead of days. We call this Turbo-charging™.

FILTERED POWER SUPPLY

PURE DC OUTPUT - Totally filtered output works perfectly with RV load; lights, appliances, fans, pumps, electronic PC boards in monitor panels, refrigerator and hot water heater circuits, etc. No ripple voltage to cause early light bulb burnout, or fan and pump motor heat buildup. No special "filtered" circuit for the stereo radio while all other circuits operate on raw ripple output.

CONSTANT VOLTAGE OUTPUT - Lights, fans, pumps, etc. now run at the right speed even in the back of the park on the crowded weekends when "the 110 ain't 110". Whether the input voltage is 125V or whether it's 95V the Power Source™ sends out a voltage level regulated so tightly that you can't see the needle move on a 4" volt meter. Due to sophisticated controls in its system the output voltage level "locks" on 14V and stays there from NO LOAD to about 85% FULL LOAD at which point the output level gradually drops to 12V at 100% full load. The voltage never exceeds 14VDC under any conditions.

PURE FLOATING OPERATION - The Power Source™ works equally well with or without an RV battery. Since most people have, or plan on someday having an RV battery or bank of batteries in their coach, it should be helpful to understand how they operate in conjunction with each other. In short, they work together. THE POWER SOURCE™ NEVER SWITCHES AN EXISTING BATTERY OUT OF THE SYSTEM! As 12V load is turned on in the coach, the current is drawn from the TEAM of battery and power supply working together; the Power Source™ provides the power across the terminals of the battery to the RV load. Additionally, in those infrequent times when more load is turned on than the Power Source™ can supply, the excess comes from the battery, until its voltage gradually drops from its 14V floating level to the operating level of the Power Source™, probably somewhere between 14V and 12V. Then, as load is ultimately turned off the output voltage of the Power Source™ climbs back to 14V and current flows back into the battery until its voltage catches up. Again, Power Source™ and battery working together; a Natural Charge™.

ENGINEERING LANDMARKS

SILENT OPERATION - The Power Source™ makes as much noise as this piece of paper. Gone forever is the infernal "midnight hum" that has haunted the operation of other units for years. Now the Power Source™ can be mounted "under the bed" if desired without concerns of a distracting noise byproduct from its operation. Even with the models having a cooling fan, the reduced load during night time operation renders the fan virtually silent while you sleep. Essentially, the fan sleeps when you do.

LIGHT WEIGHT - 30A Power Source™ is approximately **one fifth** the weight of its competition; even the powerful 75A Power Source™ weighs only **one third** that of its rival. Clearly solid state engineering has generated a weight savings which allows easier handling, enhanced installation options, and an ultimately lighter finished coach.

SUBCOMPACT SIZE - Several years ago another manufacturer downsized its models, offering a compact unit to the industry. The Power Source™ battery charger/power supply comes in a package so compressed it is clearly *subcompact*. The 30A Power Source™ measures **two thirds** smaller than a competing model; the 75A (our largest) is still **one third** smaller. Subcompact size means increased installation options; once again the customer benefits.

LESS HEAT - Subcompact size and lighter weight alone would not solve the engineering challenges without the third parameter of the Power Source™ design; lower heat emission. From no load to approximately 70% full load it operates at a temperature so low that it is hard to tell if it is on by touching it with a hand. Even at full load it is cooler than its competing predecessor in degrees F., and with lighter weight, smaller size.

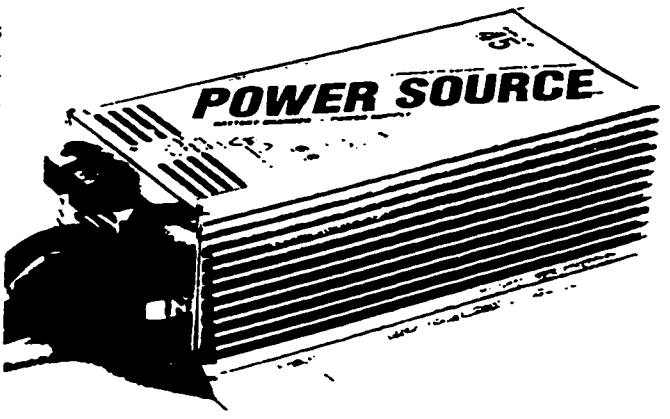

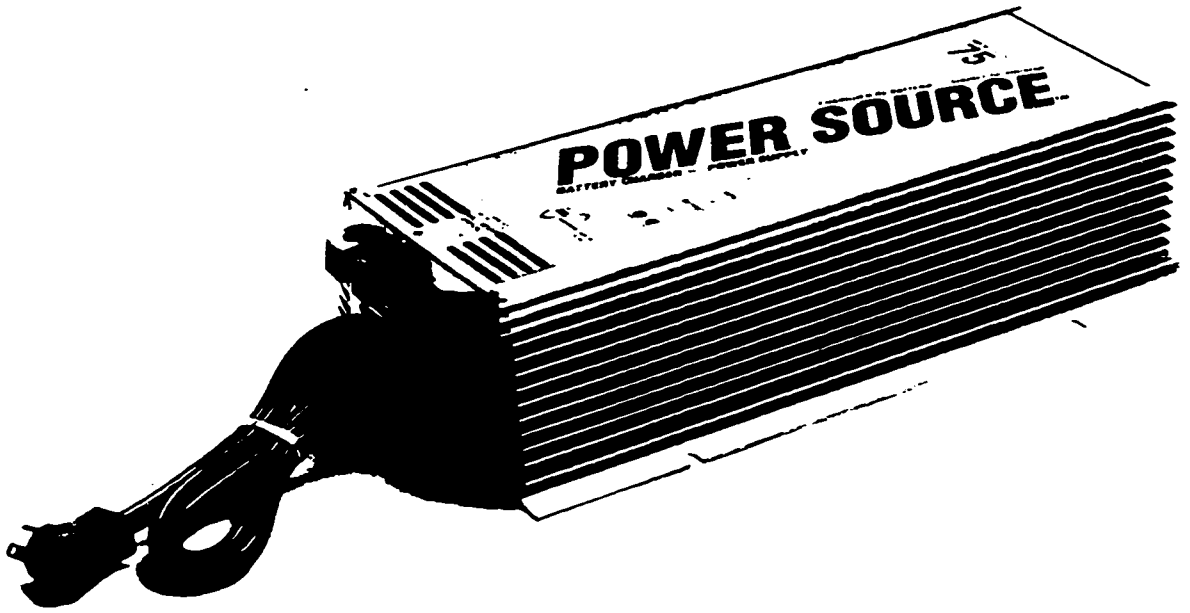

and less mass, **overall heat emissions are significantly lower.** Visualize a huge bonfire and a tiny bonfire. Each fire is about the same temperature, but the small fire gives off less heat. The Power Source™ is the same; because of its reduced weight, size, and temperature, it generates fewer BTU's. This translates into a cooler dinette seat when the Power Source™ is mounted underneath. RVs have always been plagued with nasty converter heat emission problems; they need no more.

FORCED AIR COOLING - The 45A and 75A Power Source™ models have a two speed automatic fan included to insure that the electronics never exceed a temperature range condusive to maximum operating efficiency. The fan allows the Power Source™ to be **mounted in virtually any position** because it force-cools internal components whose life expectancies consequently can be extended by as much as ten times. Air sounds and vibration generated by the cooling fan are far reduced from that of competing models. It is only one fourth the size of other units and is designed with electronic motor regulation, roller bearings, and a seven bladed fan, all of which eliminate both noise and wear. It is rated to run on high speed for 60,000 hours non-stop.

The OFF-LOW-HIGH automatic feature engineered with the fan insures **audibly invisible operation.** The fan remains OFF during light load conditions such as night time operation. Depending on installation air space and ambient temperature the fan switches to LOW around 25% load, or medium conditions. It only switches to HIGH when load remains for some time at approximately 90% or more, and it then usually runs only intermittently.

In terms of **RV liveability**, this is how it sounds to your ears: With light loads the Power Source™ is totally silent. With sustained moderate loads the fan emits a whisper so quiet is is comparable to a person breathing. Even with full load the high speed fan goes totally unnoticed compared to other daytime noises. And at night, due to reduced load during sleeping hours, the fan is virtually always off. Basically, when you go to bed, the fan does too. Sweet silent dreams . . .

INSTALLATION/SERVICE - The Power Source™ has been designed so that wiring connections are simple and direct. Three wires to connect (positive, negative, and chassis ground), and three box lugs to receive them. One 120V AC three foot grounded cord to plug into a receptacle. Fasten it down, and all done. Service is as simple. The red and white lugs offer convenient trouble shooting points should they ever be needed and the replacement of a Power Source™ consists of the same three lug connections and 120V AC plug in. A complete change-out in minutes.

WARRANTY

The POWER SOURCE™ battery charger/power supply is manufactured in the USA by Todd Engineering Sales, Inc. It is warranteed to be free from defects in material and workmanship for one year (12 months) from the date of retail purchase, or for the duration of the RV new vehicle warranty if it was factory installed, whichever is longer. Coverage does not include electrical or physical misuse or abuse, including improperly tightened terminals, or damage from improper RV hi-pot testing. The Power Source™ has no user servicable components inside, however it is designed so that it can be removed/ replaced rapidly thus saving substantial time, cost, labor, etc. For service or repair, in or out of warranty, contact dealer or manufacturer, or Todd Engineering directly. Power Source™ units returned for inspection/repair may be subject to a $9.50 charge to cover postage and handling costs. Proof of purchase may also be required.

SPECIFICATIONS

	MODEL	PC-30	PC-40	PC-45	PC-50	PC-75
INPUT	VOLTS	100-130 VAC				
	WATTS*	415	565	620	706	1040
	HERTZ	30–80 HZ				
OUTPUT	VOLTS	13.8 VDC 0-APPROX 85% LOAD 12 VDC @ FULL LOAD (SEE AMPS)				
	AMPS	30	40	45	50	75
PHYSICAL	FAN	NO	NO	YES	NO	YES
	WEIGHT	4.0	6.0	6.5	8.5	9.0
	SIZE (INCHES)	7.25 WIDE X 4.0 HIGH				
	LENGTH	6.75	11.25	11.25	14.25	15.50

* (.7 Power Factor)

ALL MODELS:
Integral overcurrent protection
Internal overtemperature protection

INSTALLATION INSTRUCTIONS

1. Disconnect RV battery HOT wire at battery before connecting Power Source™ battery charge/power supply to prevent short circuits during installation.
2. Select location to mount Power Source™. This may be on any interior (out of direct weather) surface. An ideal location would be a verticle surface (wall mount) so that the Power Source™ terminals are on the bottom, allowing maximum air flow through cooling fins. Allow also 1" minimum space top and bottom for adequate air flow. Power Source™ may also be floor mounted as required. Convenient locations might be:

   A. Near RV batteries, and connected directly to them by means of appropriate fuse/breaker protection.
   B. Near the 12V circuit distribution panel, and connected to that panel.

   Mounting location is determined by physical space and related needs; Power Source™ will function equally well as both a battery charger and a filtered power supply in either installation. When mounting location is inside a cabinet or compartment, care should be taken that:
   A. Compartment is large enough to allow sufficient space for dissipation of heated air, and
   B. Compartment will not be used for storage of flammable liquids. See CAUTION below.

   Location chosen should be accessible for service after installation!
3. Mount Power Source™ using notches provided in legs. Unit should be firmly screwed to a wood, metal, fiberglass, etc. member strong enough to support its weight during vehicle operation. Converter Model PC30 should preferably be wall mounted vertically with wiring connections UP. Converter Models PC40 and PC50 should preferably be wall mounted vertically with wiring connections DOWN. Models PC45 and PC75 may be mounted in any position desired, but will operate most efficiently when wall mounted with wiring connections DOWN.
4. Determine electrical connections. Diagram A shows a basic battery-circuit panel loop. This is the route in an RV for all 12V power from the battery to the circuit panel where power is divided into smaller circuits throughout the coach. Diagram B shows this basic supply loop with the Power Source™ installed at the battery. Diagram C shows the Power Source™ installed at the circuit panel. In both B and C the Power Source™ is connected pos. to pos. and neg. to neg. Both installations work equally well.
5. Attach electrical wiring. Red lug is pos. (+), white lug is neg. (−). Insert wire(s) into each output connecting lug and tighten. Insert an 8 ga. bare copper wire into the Power Source™ lug marked CHASSIS GROUND and connect directly to RV chassis. Plug the 120V AC input cord into an appropriate receptacle.
6. Reconnect HOT terminal at battery following installation.

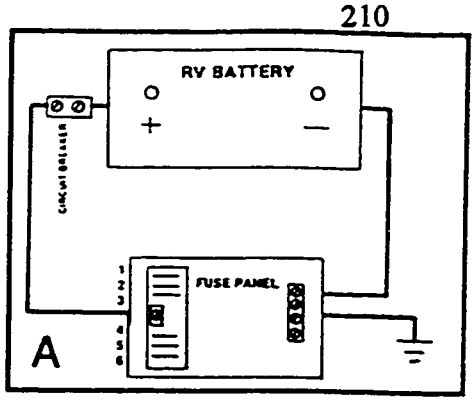

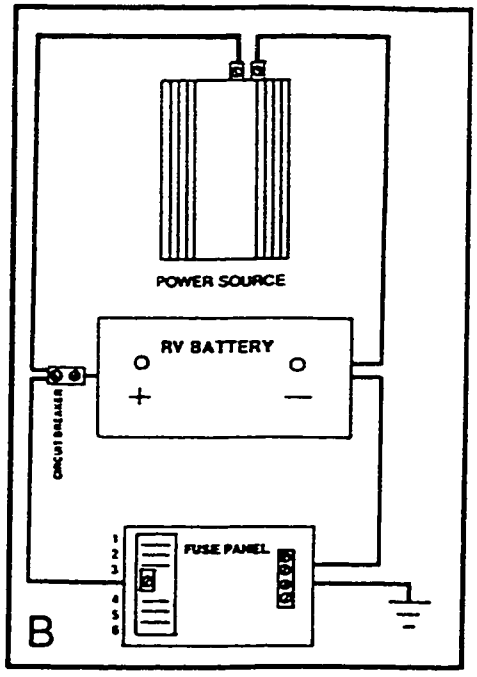

COMMON SENSE DEPARTMENT

NOTE: Loosely tightened connections can quickly cause overheated wires, melted insulators, and ultimately hazard of fire. ALWAYS TIGHTEN CONNECTIONS SECURELY!
NOTE: Always use proper wire gauge. Correct size is governed by output capacity of Power Source™ model selected. EX: A 30 amp unit should have 10 gauge wire.
NOTE: The Power Source™ battery charger/power supply is current limiting by design, and therefore does not require overcurrent protection; however an RV battery has a tremendous current capacity; therefore the positive battery wire should always be protected from overcurrent by a fuse or breaker (preferably a breaker). This protection should be installed within 18" of the battery in almost all situations. When installing the Power Source™ at the RV battery always connect it to the "downstream" side of the breaker from the battery.

HI-POT TESTING

(MANUFACTURING COMPANIES ONLY)

RV coach hi-pot testing should only be done in the following manner:
1. Unplug the converter 120 V AC input cord.
2. disconnect the hot wire from the Power Source at the red lug on the end of the unit.
3. hi-pot the coach.
4. reconnect the hot wire and plug in the input cord.

CAUTION:

Do not install this or any electrical accessory in a compartment capable of storing flammable liquids such as gasoline, etc., whose fumes are explosive and can cause injury and death. There are no components in the Power Source™ which in their normal operation cause arcs or sparks, however, the simple act of **unplugging the cord** on any electrical appliance can cause a spark, and consequently an explosion from gasoline or other vapor.
NEVER STORE EXPLOSIVE LIQUIDS INSIDE A COMPARTMENT CONTAINING ANY ELECTRICAL DEVICE.

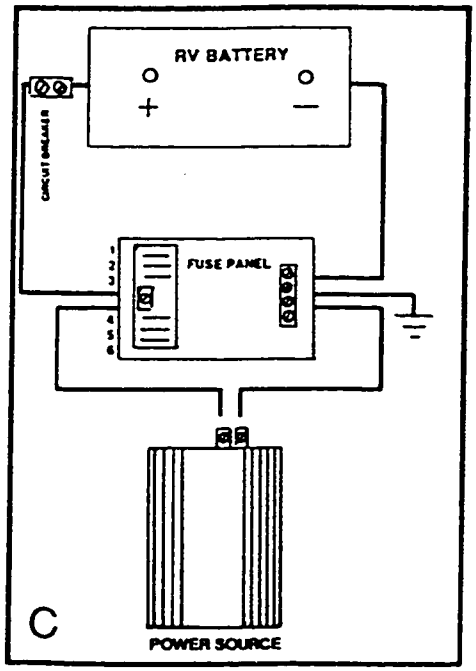

Calculations for a Battery Box Impact

- Battery box construction :

Aluminum angle	- (t_w) wall thickness: 0.25" (0.635 cm)
	- Aluminum, S_{ultAl} : 70 MPa.
Fasteners	- Bolts: (d) diameter: $^5/_{16}$" (0.794 cm)
	- (N) number of bolts per box: 14
	- Grade 8 bolt, S_{ultb}: 1033 MPa.

- Mass of one battery box (incl. batteries) : 65 kg.
- Maximum permissible mass of HEV: 1686 kg.
- Impact occurs with a very large stationary object.

CASE 1

Deceleration : 10g $a = -98.1$ m/s^2

$F = m_{tray} \cdot a = 6376.5$ N

Bearing Stress of Aluminum Angle : $\sigma_B = {}^F/_{2\, t_w\, dN} = 4.52$ MPa

Safety Factor: $FS = S_{ultAl} / \sigma_B = 15.5$

Bolts: Shear Stress: $\tau = {}^F/_{N¼\pi d^2} = 9.2$ MPa

Bolts: Shear Stress Safety Factor: $FS_{sf} = S_{ultb}/2\tau = 56.15$

CASE 2

Deceleration : 30g $a = -294.3$ m/s^2

$F = m_{tray} \cdot a = 19129.5$ N

Bearing Stress of Aluminum Angle : $\sigma_B = {}^F/_{2\, t_w\, dN} = 10.54$ MPa

Safety Factor: $FS = S_{ultAl} / \sigma_B = 6.65$

Bolts: Shear Stress: $\tau = {}^F/_{N¼\pi d^2} = 27.6$ MPa

Bolts: Shear Stress Safety Factor: $FS_{sf} = S_{ultb}/2\tau = 18.7$

APPENDIX 4

Specifications and Information Relative to Chapter 7

Brusa Elektronik
CH-9473 Gams
Tel. 081-771 36 08
Fax 081-771 46 55

Antriebe und Komponenten für Elektro-Fahrzeuge und -Boote

Electric drives and components for vehicles and boats

BRUSA

Me[illegible]mes

vorgegeb. Werte			gemessene Werte				
Schlupf	Drehzahl	Mom	Batt spg	Batt strom	eta	Mot-Temp	AMC-Temp
[Hz]	[U/min]	[Nm]	[V]	[A]	[%]	[°C]	[°C]
AMC 320 mit Thien GT 20							
	0	74					
0	1002,77	73,95	143,97	87,34	61,75	27,83	26,37
0	2004,54	74,05	144,24	144,87	74,39	29,05	30,52
0	3000,26	73,71	143,55	202,72	79,58	27,1	29,3
0	4000,02	71,7	143,9	251,36	83,03	30,52	29,79
0	4998,76	51,71	143,9	221,51	84,92	27,1	29,3
0	5998,51	38,51	143,92	197,65	85,05	31,01	29,3
0	7000,28	29,72	143,93	179,09	84,51	31,01	28,81
0	8003,05	23,68	143,94	164,84	83,65	31,25	28,81
0	8992,74	19	143,95	152,47	81,5	31,25	27,59
0	10024,71	15,58	143,95	142,02	79,99	31,25	28,56
0	11026,47	12,55	143,96	131,65	76,46	31,49	27,83
0	12031,26	10,46	143,97	123,92	73,85	31,74	28,81
0	13003,83	8,97	143,97	117,27	72,35	31,98	30,52
AMC 220 mit Thien GT 20							
	0	48,4					
0	1026,94	48,26	144,03	52,9	68,11	23,93	25,63
0	2001,52	48,38	144,05	89,58	78,58	24,66	28,32
0	3001,27	48,34	143,97	127,11	83,02	25,15	29,3
0	3995,99	48,05	143,97	163,08	85,63	25,39	27,1
0	5000,78	43,31	143,96	182,08	86,53	26,12	31,01
0	6010,6	35,68	143,78	182,47	85,6	26,37	29,79
0	6994,24	29,09	143,76	177,6	83,46	27,83	26,12
0	8003,05	23,98	143,89	169,95	82,2	28,08	28,56
0	9003,81	19,47	143,9	157,61	80,94	28,32	29,05
0	10019,67	15,9	143,91	146,25	79,26	28,56	29,3
0	10983,18	13,09	143,92	135,72	77,1	28,81	27,1
0	12049,38	10,58	143,93	126,7	73,2	29,05	29,05
0	13133,71	8,74	143,92	118,16	70,67	29,3	29,3

Digitalsteuerung

24.8.94

Brusa Elektronik
Tel. 081-771 36 08
Fax 081-771 46 55

Antriebe und Komponenten für Elektro-Fahrzeuge und -Boote

Electric drives and components for vehicles and boats

BRUSA

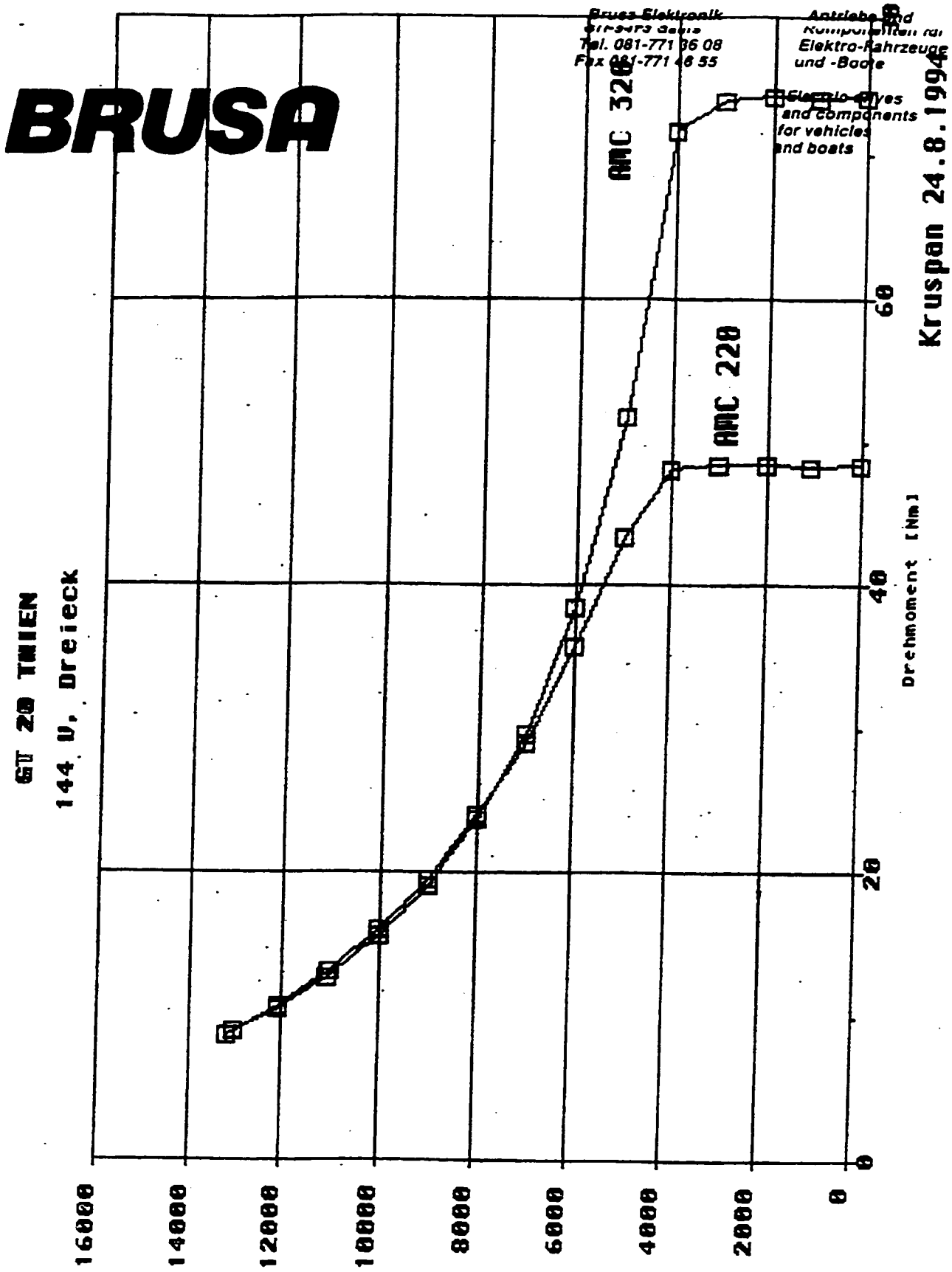

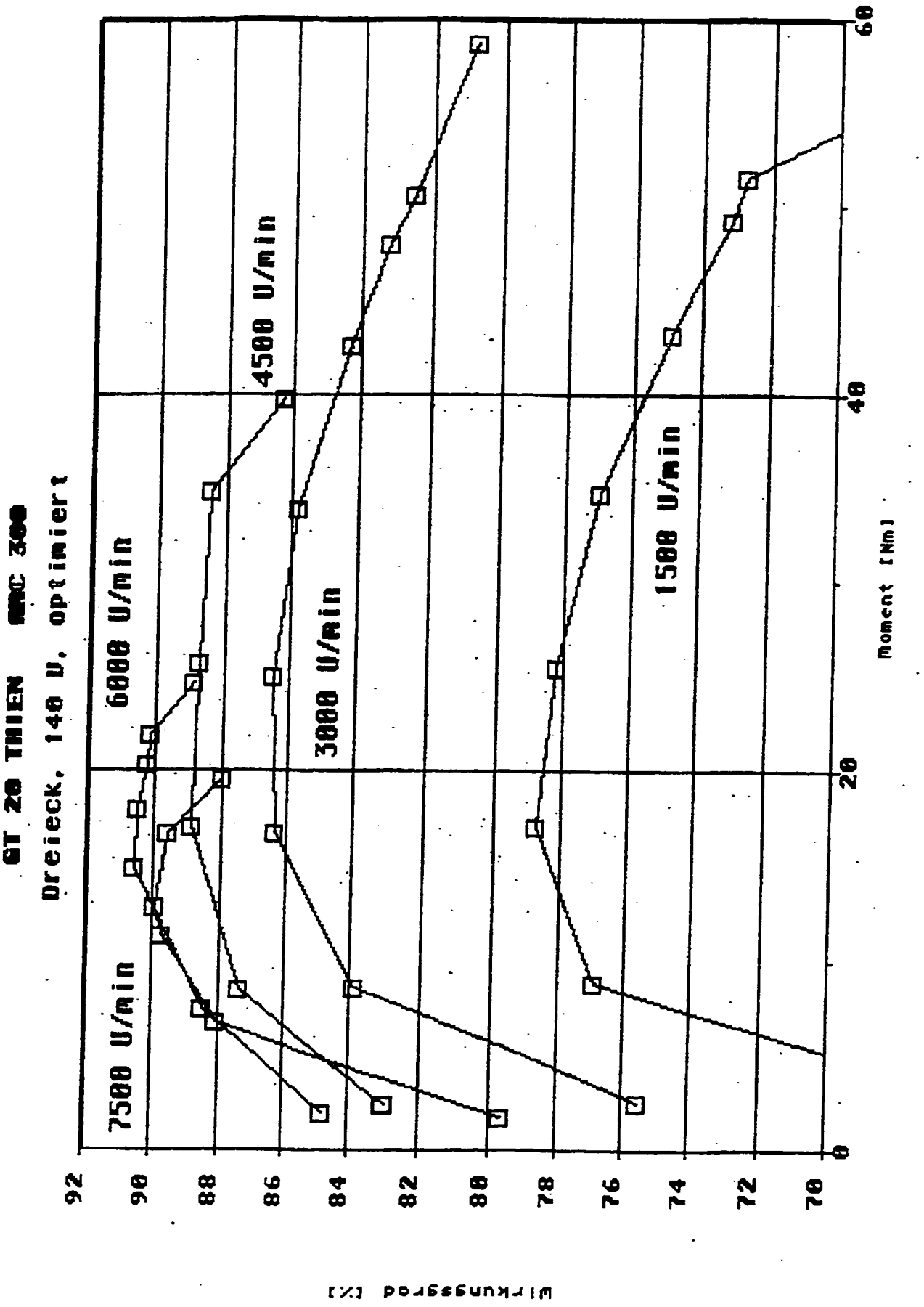
GT 20 THIEN
Dreieck, 140 V, optimiert
7500 U/min
6000 U/min
4500 U/min
3000 U/min
1500 U/min
Moment [Nm]
Wirkungsgrad [%]
92
90
88
86
84
82
80
78
76
74
72
70
60
40
20
0

SOLECTRIA

ELECTRIC VEHICLE COMPONENTS

Effective April 1996

Drive Systems

AC Induction - high efficiency, with control wiring, pot box and regenerative braking

Model	Battery Current (Max.)	Battery Voltage (Nominal)	Efficiency (peak)	Price
UMOC340 Controller	210A	204-252V	98%	$4370
AC320 Controller	240A	120-144V	99%	$5885
AC325 Controller	240A	156-180V	99%	$6480
ACgtx20 Motor (28 HP)			91%	$1800
ACgu20 (28 HP)			91%	$1800
AC30 Motor (34 HP)			90%	$2390

DC Brush Permanent Magnet and DC Brushless (with regenerative braking)

DC20 Controller (non-regen)	20A	150 or 228V	98%	$450
DC20 Controller (non-regen)	20A	320V	98%	$750
UMOC225 Controller	160A	96- 144V	98%	$3670
BPM3 Motor (3 HP cont.)	40A (@72V)	48, 72, 120, or 216V	86%	$850
BPM6 Motor (6 HP cont.)	80A (@60V)	60V, 120V	88%	$950
BPM8 Motor (8.5 HP cont.)	54A	120V	89%	$1070
BRLS8 (8HP cont.)	280/140A	60/120V	95%	$2450
BRLS11 (11 HP cont.)	200A	120V	95%	$2980

Ampere-Hour & Watt-Hour Counters

AH100 Ampere-hour Counter (99% accurate, digital display; use with SH100 shunt)	$449
WH100 Watt-hour Counter (99% accurate, digital display; use with SH100 shunt)	$499
SH100 Shunt, 100A, 60mV	$39
SH60 Shunt, 60A, 60mV	$39
SH200 Shunt, 200A, 60mV	$78

Maximum Power Trackers

	Solar	Battery	Efficiency (Peak)	
MPT150N	9-170V, 6A max.	180V max.	99%	$698
MPT150HN	9-170V, 15A max.	180V max.	99%	$950

DC-DC Converters, 12V Output

Provides 12V from main battery, 85-90% efficient. Input voltage must be specified when ordering; available voltage inputs are 100-200V or 200-400V.

DC-DC200	200W output (12V output up to 16A)	$329
DC-DC380	380W output (12V output up to 32A)	$395
DC-DC575	575W output (12V output, up to 46A)	$589
DC-DC750	750W output (12V output up to 60A)	$790

Battery Chargers

Compact, lightweight, micro-processor based, for on-board or off-board use.

Model	Weight	Input Voltage	Power Output	Volt. Range	Efficiency	
BC1000	8.2 lb.	120 or 208-240VAC	1000W	100-270V DC	91-92%	$1250
BC3300	14.5 lb	208-240VAC	3000W	100-400V DC	93-94%	$3870
BC1600*		120V AC	1600W	120-180V DC	90-92%	$1490
BC6600	14.5 lb	208-240V AC	6000W	100-400V DC		$6890

* Available in May 1996.

Gearboxes

AT600 w/ACgtx20 motor (used w/ AC220 or AC320 Controller)	$3420
AT1200 w/ ACgu20, ACgtx20 or AC30 motor (used w/ AC325 Controller)	$3880

Accelerator/Brake Controller

5 kΩ potentiometer with integrated spring return, compatible with all Solectria Motor Controllers.

ABC-1	$40

Standard turnaround time on all component orders is approximately eight to twelve weeks maximum. Expedited turnaround and volume discounting may be available. All prices and specifications are subject to change. Please contact the Solectria Component Department if you have further questions.

SOLECTRIA CORPORATION
68 INDUSTRIAL WAY
WILMINGTON, MA 01887
USA

508-658-2231
FAX 508-658-3224